

STUDY ON THE EXPERIMENTAL THERMAL PARAMETERS OF BUILDING ENVELOPE COMPONENTS UNDER THE TROPICAL CLIMATIC CONDITIONS AND COMPARING THE RESULTANT BUILDING COOLING LOAD WITH THOSE OBTAINED FROM GLOBALLY AVAILABLE DIFFERENT SIMULATION TOOLS

By Debasish Chowdhury

**STUDY ON THE EXPERIMENTAL THERMAL PARAMETERS OF
BUILDING ENVELOPE COMPONENTS UNDER THE TROPICAL
CLIMATIC CONDITIONS AND COMPARING THE RESULTANT
BUILDING COOLING LOAD WITH THOSE OBTAINED FROM
GLOBALLY AVAILABLE DIFFERENT SIMULATION TOOLS**

75
**THESIS SUBMITTED FOR THE DEGREE OF
DOCTOR OF PHILOSOPHY (ENGINEERING)
OF
JADAVPUR UNIVERSITY**

BY
DEBASISH CHOWDHURY
81
M. TECH. (ENERGY SCIENCE & TECHNOLOGY)

**SCHOOL OF ENERGY STUDIES
JADAVPUR UNIVERSITY
KOLKATA – 700032
INDIA**

2022

**JADAVPUR UNIVERSITY
KOLKATA – 700032, INDIA**

INDEX NO. D-7/ISLM/34/15

1. Title of the thesis:

“STUDY ON THE EXPERIMENTAL THERMAL PARAMETERS OF BUILDING ENVELOPE COMPONENTS UNDER THE TROPICAL CLIMATIC CONDITIONS AND COMPARING THE RESULTANT BUILDING COOLING LOAD WITH THOSE OBTAINED FROM GLOBALLY AVAILABLE DIFFERENT SIMULATION TOOLS”

2. Name, Designation & Institution of Supervisors:

Dr. Subhasis Neogi, Former Professor, School of Energy Studies, Jadavpur University.

3. List of Publications:

- (i) **“Thermal performance evaluation of traditional walls and roof used in tropical climate using guarded hot box”**, Construction and Building Materials, Elsevier Publications, Vol. 218 (2019), pg. 73-89.
- (ii) **“Process control strategy and its impact on performance of the cold box of guarded hot box test facility for U-value measurement”**, International Journal of Energy Technology & Policy, Vol 12, No. 2, 2016.
- (iii) **“Performance evaluation of a chilled storage-based cooling system for Guarded Hot Box facility”**, International Journal of Emerging Technology and Advanced Engineering, Volume 3, Special Issue 3: ICERTSD (International Conference on Energy Resources & Technologies for Sustainable Development) 2013, Feb 2013, pages 394-399.

4. List of Patents: Nil

5. List of Presentations in National / International Conferences / Workshops

- (i) **“Study in impact of varying air velocity rates on the overall heat transfer through walls using Guarded Hot Box.”**, Proceedings of International Conference on Energy and Sustainable Development 2020 (ICESD – 2020, Feb 14 -15, 2020) Jadavpur University.
- (ii) **“Thermal characterization of building wall fabrics using Guarded Hot Box Testing: A Review.”**, e-Proceedings of International Conference on Advancements in Mechanical Engineering (ICAME 2020), Aliah University, Kolkata, 16-18 January 2020.

CERTIFICATE FROM THE SUPERVISORS

This is to certify that the thesis entitled “**STUDY ON THE EXPERIMENTAL THERMAL PARAMETERS OF BUILDING ENVELOPE COMPONENTS UNDER THE TROPICAL CLIMATIC CONDITIONS AND COMPARING THE RESULTANT BUILDING COOLING LOAD WITH THOSE OBTAINED FROM GLOBALLY AVAILABLE DIFFERENT SIMULATION TOOLS**”, submitted by Shri Debasish Chowdhury, who got his name registered on 16.04.2015 for the award of **Ph.D.(Engineering)** degree of Jadavpur University is absolutely based upon his own work under the supervision of Dr. Subhasis Neogi, Former Professor, School of Energy Studies, Jadavpur University and that neither his thesis nor any part of the thesis has been submitted for any degree / diploma or any other academic award anywhere before.

Subhasis Neogi
19/12/2022

(Dr. Subhasis Neogi)
Signature of the Supervisor
& Date with Office Seal

Subhasis Neogi
Former Professor
School of Energy Studies
Jadavpur University
Kolkata - 700 032

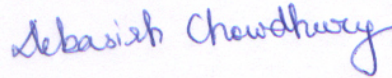
STATEMENT OF ORIGINATILY

I Debasish Chowdhury registered on 16.04.2015 do hereby declare that this thesis entitled **“STUDY ON THE EXPERIMENTAL THERMAL PARAMETERS OF BUILDING ENVELOPE COMPONENTS UNDER THE TROPICAL CLIMATIC CONDITIONS AND COMPARING THE RESULTANT BUILDING COOLING LOAD WITH THOSE OBTAINED FROM GLOBALLY AVAILABLE DIFFERENT SIMULATION TOOLS”**, contains literature survey and original research work done by the undersigned candidate as part of Doctoral studies.

All the information in this thesis have been obtained and presented in accordance with existing academic rules and ethical conduct. I declare that, as required by these rules and conduct, I have fully cited and referred all the materials and results that are not original to this work.

I also declare that I have checked this thesis as per the “Policy on Anti Plagiarism, Jadavpur University, 2019”, and the level of similarity as checked by iThenticate software is 6%.

Signature of Candidate:



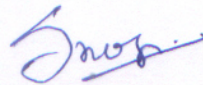
Date

:

19/12/2022

Certified by

:



Dr. Subhasis Neogi

Former Professor, School of Energy Studies, Jadavpur University

ACKNOWLEDGEMENT

I feel honoured to express my deepest respect, reverence, indebtedness and heartiest gratitude to my respected guide **Dr. Subhasis Neogi** (Former Professor, School of Energy Studies, Jadavpur University) for his judicious guidance, constant inspiration, and help during the entire period of execution of present work.

I would like express my thanks to Jadavpur University for providing me the financial assistance under State Government Departmental Fellowship Scheme.

I am also grateful to **Prof. Biswajit Ghosh** (Former Professor, School of Energy Studies, Jadavpur University), **Prof. Tushar Jash** (Professor, School of energy Studies) and **Dr. Ratan Mandal** (Director School of Energy Studies, Jadavpur University) for their support and encouragement during the period of work. I would also like to expresses my thanks to **Dr. Avijit Ghosh** (Principal Technical Officer, Central Glass & Ceramic Research Institute) for his valuable suggestion, advice and constant motivation while carrying out my study.

I like to mention about the help and active support received from my fellow research scholar **Mrs. Amrita Ghosh**. I would also like to express my gratitude to the non-teaching staff of the School of Energy Studies, Jadavpur University for their support during the course of my work.

Lastly, I would like to thank my family members who silently co-operated and supported me in every moment of my life.

Date: 19.12.2022

Place: Jadavpur University

Debasish Chowdhury
Debasish Chowdhury

Dedicated to
My Parents
&
my Wife

CONTENTS

NOMENCLATURE	i – iii
LIST OF FIGURES	iv – xi
LIST OF TABLES	xii – xvi
CHAPTER 1 – GENERAL INTRODUCTION	1 – 39
1.1 Background – Energy Scenario	1
1.1.1 Introduction	1
1.1.2 Building Energy Scenario	4
1.1.2.1 Building Types	5
1.1.2.1.1 Residential Buildings Scenario	5
1.1.2.1.1 Commercial Buildings Scenario	7
1.2 National Climates – Five Climatic zones	8
1.2.1 Climate of Kolkata (Warm & humid) & Variation of climatic parameters in Kolkata	9
1.3 Objective and Scope of work	11
1.4 Review of Earlier Work	13
CHAPTER 2 – GUARDED HOT BOX TESTING SET-UP	40 – 70
2.1 Introduction	40
2.1.1 Guarded Hot Box	40
2.1.2 Metering Box	43
2.1.3 Guard Box	43
2.1.4 Cold Box	44
2.1.5 Surround Panel or Mask Wall	45
2.2 Experimental Boundary Condition Range	46
2.3 Control and Strategy	48
2.3.1 Metering Box and Guard Box Control Strategy	51
2.3.2 Cold Box Control Strategy	52
2.4 Calibration	53
2.4.1 Measurement of Air Velocity of Metering Box and Cold Box	54

2.4.2 Measurement of Extraneous Heat Transfer	58
2.4.3 Measurement of Flanking Losses	60
2.5 Performance evaluation of Metering Box and Cold Box	63
2.6 Uncertainty Analysis of U-value Measurement	65
2.7 Conclusion	67
CHAPTER 3 – EVALUATION OF THERMAL PERFORMANCE OF BUILDING ENVELOPE COMPONENTS (OPAQUE WALLS ROOF AND GLAZINGS)	71 – 109
3.1 Introduction	71
3.2 Opaque Walls	72
3.2.1 Sample Construction and Description	73
3.2.2 Experimental Procedure	78
3.2.3 Results	80
3.3 Roof	90
3.3.1 Sample Construction and Description	91
3.3.2 Experimental Procedure	92
3.3.3 Results	93
3.4 Double Glazing Unit (with warm edge spacer)	97
3.4.1 Sample Construction and Description	97
3.4.2 Experimental Procedure	99
3.4.3 Results	100
3.5 Uncertainty Analysis	105
3.6 Conclusion	107
CHAPTER 4 – COOLING LOAD ESTIMATION BY SIMULATION TOOLS	110 – 176
4.1 Introduction	110
4.2 Building Model Description	110
4.2.1 Building HVAC, Schedules and internal details	111
4.3 Simulation Engine	112
4.3.1 DesignBuilder simulation	115
4.3.2 ECOTECH simulation	121
4.3.3 eQUEST simulation	127

4.4 Results	133
4.4.1 DesignBuilder Simulation Results	133
4.4.2 ECOTECT Simulation Results	147
4.4.3 eQUEST Simulation Results	160
4.5 Conclusion	173
CHAPTER 5 - RESULTS AND DISCUSSIONS	177 – 189
CHAPTER 6 – CONCLUSION AND FUTURE SCOPE OF WORK	190 – 192
ANNEXURE A	193 – 196
PAPERS PUBLISHED	197 – 201

NOMENCLATURE

SYMBOL	MEANING	
MB	Metering box	
CB	Cold Box	
GB	Guard Box	
\dot{Q}	Heat flow rate	[W]
\dot{Q}_{extra}	Extraneous heat transfer	[W]
$\dot{Q}_{Heaters}$	Power Input from Heaters in Metering Box	[W]
\dot{Q}_{Fans}	Power Input from Fans in Metering Box	[W]
$\dot{Q}_{Heat I/P}$	Total power input from heaters and fans installed in the metering box	[W]
$\dot{Q}_{MB Wall Loss}$ $\dot{Q}_{MB Avg Wall Loss}$	Total metering box wall loss	[W]
\dot{Q}_{Sample}	Heat flow through sample	[W]
$\dot{Q}_{sample,measured}$	Measured heat flow through sample experimentally	[W]
$\dot{Q}_{sample Calc}$	Calculated heat flow though sample	[W]
\dot{Q}_{SurPnl}	Heat flow rate through surround panel	[W]
\dot{Q}_{Fl}	Flanking loss, heat flow rate	[W]
$T_{MB Air}$	Average metering box air temperature	
$T_{CB Air}$	Average cold box air temperature	
k	Thermal conductivity	[W/(m.K)]
xps	Extruded polystyrene sheet	
A	Area	[m ²]
δt	Differential temperature	[°C]
δt_{air}	Differential air temperature between metering box and cold box	[°C]

δx	Thickness	[m]
Samp	Sample	
A_{Samp}	Sample surface area	[m ²]
A_{SurPnl}	Surround panel surface area	[m ²]
$A_{metering\ box\ wall}$	Total surface area of metering box walls	
$\delta x_{metering\ box\ wall}$	Thickness of metering box wall	
$\dot{Q}_{MB\ to\ CB}$ calculated	Calculated heat flow from metering box to cold box	[W]
$\dot{Q}_{MB\ to\ CB}$ measured	Measured heat flow from metering box to cold box	[W]
RCC	Reinforce cement concrete	
U	Overall heat transfer coefficient	[W/m ² .K]
$u_{MB\ Air}$	Metering box fan velocity	[m/s]
$u_{CB\ Air}$	Cold box fan velocity	[m/s]
h_1, h_2	Surface coefficient of hot and cold faces of specimen	[W/(m ² .K)]
h_{ce}, h_{ci}	Convective heat transfer coefficient due to external and internal environments	[W/(m ² .K)]
h_{re}, h_{ri}	Convective heat transfer coefficient due to external and internal environments	[W/(m ² .K)]
l_i	Thickness of individual layers of specimen	[m]
A	Area of specimen perpendicular to the heat flux direction	[m ²]
N	No of layers of different materials in case of composite material	
T_{in}	Air temperature on indoor side	[°C]
T_{out}	Air temperature on outdoor side	[°C]
h_{in}	Surface heat transfer coefficient on the indoor side	[W/(m ² .K)]
h_{out}	Surface heat transfer coefficient on the outdoor side	[W/(m ² .K)]
$h_{int,c}$	Convective heat transfer coefficient on the indoor side	[W/(m ² .K)]
$h_{out,c}$	Convective heat transfer coefficient on the outdoor side	[W/(m ² .K)]

MB1 to MB9	Thermocouple locations on baffle in the metering box	
CB1 to CB9	Thermocouple locations on baffle in the cold box	
A1,A2,A3	Thermocouple locations for air temperature measurements in metering box	
S1 to S5	Thermocouple locations on sample surface facing metering box	
S6 to S9	Thermocouple locations on sample surface facing cold box	
$T_{\text{SurPnl Temp Hot Face, Avg}}$	Surround panel hot side surface average temperature	[°C]
$T_{\text{SurPnl Temp Cold Face, Avg}}$	Surround panel cold side surface average temperature	[°C]
$\Delta T_{\text{SurPnl Surface}}$	Differential surface temperature of surround panel	[°C]
$\Delta T_{\text{Samp Surface}}$	Differential surface temperature of sample	[°C]
$T_{\text{Samp Temp Hot Face, Avg}}$	Sample hot side surface average temperature	[°C]
$T_{\text{Samp Temp Cold Face, Avg}}$	Sample cold side surface average temperature	[°C]

LIST OF FIGURES

CHAPTER 1 – GENERAL INTRODUCTION

Sl. No.	Description	Page no.
1.1	World's primary energy (sector-wise) consumption for 2021	2
1.2	India's primary energy (sector-wise) consumption for 2021	3
1.3	Total GHG emissions (Gt CO ₂ eq./yr) by economic sectors	4
1.4	Sector CO ₂ emissions in the year 2020	5
1.5	Residential Sector Energy Consumption in India	7
1.6	Sector wise breakup of energy consumption in commercial sector	8
1.7	Five Climatic Zones of our Country	9
1.8	Variation of daily average direction radiation and diffuse radiation for Kolkata	11
1.9	Variation of daily average wind speed and direction for Kolkata	11
1.10	Sector wise breakup of energy consumption in commercial sector	12

CHAPTER 2 - GUARDED HOT BOX TESTING SET-UP

Sl. No.	Description	Page no.
2.1	Schematic set-up of Guarded Hot Box Testing Facility	40
2.2	Guarded Hot Box Test set-up installed at laboratory	41
2.3	Guarded Hot Box Test set-up in open condition.	41
2.4	Metering Box and Guard Box	43
2.5	Cold Box	43
2.6	Surround Panel	44
2.7	Close up view of the aperture in surround panel	44
2.8	K-type thermocouple sensor used for temperature measurements	48
2.9	Constant temperature oil bath	48
2.10	Location of air temperature sensors (A1, A2 & A3) in the metering box	49

2.11	Temperature sensors placed on the surround panel and sample surface	49
2.12	Interface for Agilent VEE Software	50
2.13	Heat Exchanger Fan Coil unit along with rotameter based flow control mechanism.	51
2.14	Sub-zero dilute calcium chloride based chilled storage unit	52
2.15	Hot wire anemometer (HTC AVM-08)	53
2.16	Hot wire anemometer setup for measuring air velocity	53
2.17	Section of guarded hot box showing air velocity locations in metering box and cold box	54
2.18	Air velocity profile at P4 under varying input voltage to fan in metering box.	55
2.19	Air velocity profile at P1 under varying input voltage to fan in cold box.	55
2.20	Air velocity profile at P5 under varying input voltage to fan in metering box.	55
2.21	Air velocity profile at P2 under varying input voltage to fan in cold box.	55
2.22	Air velocity profile at P6 under varying input voltage to fan in metering box	56
2.23	Air velocity profile at P3 under varying input voltage to fan cold box.	56
2.24	Variation of air velocity with input fan voltage for at different positions.	56
2.25	Variation of fan velocity with input fan voltage for different sample thickness	57
2.26	Schematic heat flow regime at interface of metering box wall and guard box wall with surround panel	57
2.27	Variation of extra heat transfer with differential air temperature	58
2.28	Variation extraneous heat transfer with fan velocity	58
2.29	50mm extruded polystyrene sample mounted inside surround panel of GHBC	59
2.30	Effect of δt_{air} on variation of flanking loss with sample thickness	60
2.31	Variation of flanking loss with sample thickness for varying metering box fan velocity (a) and cold box velocity (b) at $\delta t_{\text{air}} = 30^{\circ}\text{C}$	60

2.32	Variation of flanking loss with sample thickness for varying MB fan velocity (c) and CB velocity (d) at $\delta t_{\text{air}} = 20^{\circ}\text{C}$	61
2.33	Variation of hot box temperature profile with time	63
2.34	Variation of cold box temperature profile with time	63
2.35	Variation of metering box wall losses with time	63

CHAPTER 3 – EVALUATION OF THERMAL PERFORMANCE OF BUILDING ENVELOPE COMPONENTS (OPAQUE WALLS ROOF AND GLAZINGS)

3.1	Sample holding frame	73
3.2	Burnt clay brick	74
3.3	Masonry wall being built inside the sample holding frame	74
3.4	Sample WI – 125mm brick wall with 0.5 inches plaster inside sample holding frame	74
3.5	Sample WI loaded into sample holding aperture	74
3.6	Sample WII	75
3.7	Sample WIII loaded onto surround panel	75
3.8	Sample surfaces prepared for spectrophotometry	76
3.9	Solar spectral response of coloured surfaces	77
3.10	Variation of air and surface temperature in metering box and cold box for Sample WI.	81
3.11	Fluctuations in air temperature in Metering Box	82
3.12	Variation of air and surface temperature in metering box and cold box for Sample WII	84
3.13	Variation of air and surface temperature in metering box and cold box for Sample WIII	86
3.14	Variation of U-value with differential air temperature for Sample WI & WII	87
3.15	Variation of U-value with differential air temperature for Sample WIII	87
3.16	Effect of variation of metering box and cold box air velocity on U-value for Sample WII.	89
3.17	Side view of the RCC roof slab (Sample WIV).	91
3.18	Cross-sectional view of the slab showing the layout of the steel reinforcements.	91

3.19	100 mm RCC roof (Sample WIV) mounted on surround panel with thermocouple sensors placed on the surface.	92
3.20	Variation of U-value with differential air temperature for Sample WIV	93
3.21	Variation of air and surface temperature in metering box and cold box for Sample WIV	95
3.22	Variation of Metering box wall heat transfer with time.	95
3.23	Warm-edge spacers and corner keys	97
3.24	DGU placed in wooden frame.	97
3.25	Schematic view of the frame on which glazing units are mounted	98
3.26	Sample WV placed in the surround panel with thermocouple sensors mounted.	99
3.27	Variation of U-value with differential air temperature for Sample WV	100
3.28	Variation of air and surface temperature in metering box and cold box for Sample WV	101
3.29	Real-time view of the variation of the various temperature profile as recorded in Agilent VEE program.	102
3.30	Variation of U-value with differential air temperature for conventional aluminium spacer based double glazing unit.	103

CHAPTER 4 – COOLING LOAD ESTIMATION BY SIMULATION TOOLS

Sl. No.	Description	Page no.
4.1	Plan of the simulated building	112
4.2	Schematic view of the different orientations	114
4.3	AutoCAD plan as imported in DesignBuilder interface	115
4.4	Surface Azimuth angle of Window is 180° (N0) in DesignBuilder (North facing)	117
4.5	Surface Azimuth angle of Window is 0° (S0) in DesignBuilder (South facing)	117
4.6	Surface Azimuth angle of Window is 270° (E0) in DesignBuilder (East facing)	118
4.7	Surface Azimuth angle of Window is 90° (W0) in DesignBuilder (West facing)	118
4.8	Surface Azimuth angle of Window is 225° (NE45) in DesignBuilder	118

4.9	Surface Azimuth angle of Window is 135° (NW45) in DesignBuilder	119
4.10	Surface Azimuth angle of Window is 330° (SE30) in DesignBuilder	119
4.11	Surface Azimuth angle of Window is 315° (SE45) in DesignBuilder	119
4.12	Surface Azimuth angle of Window is 300° (SE60) in DesignBuilder	120
4.13	Surface Azimuth angle of Window is 30° (SW30) in DesignBuilder	120
4.14	Surface Azimuth angle of Window is 45° (SW45) in DesignBuilder	120
4.15	Surface Azimuth angle of Window is 60° (SW60) in DesignBuilder	121
4.16	AutoCAD plan as imported in ECOTECH interface	122
4.17	Surface Azimuth angle of Window is 0° (N0) in ECOTECH (North facing)	123
4.18	Surface Azimuth angle of Window is 180° (S0) in ECOTECH (South facing)	123
4.19	Surface Azimuth angle of Window is 90° (E0) in ECOTECH (East facing)	123
4.20	Surface Azimuth angle of Window is -90° (W0) in ECOTECH (West facing)	124
4.21	Surface Azimuth angle of Window is 135° (NE45) in ECOTECH	124
4.22	Surface Azimuth angle of Window is -135° (NW45) in ECOTECH	124
4.23	Surface Azimuth angle of Window is -30° (SE30) in ECOTECH	125
4.24	Surface Azimuth angle of Window is -45° (SE45) in ECOTECH	125
4.25	Surface Azimuth angle of Window is -60° (SE60) in ECOTECH	125
4.26	Surface Azimuth angle of Window is 30° (SW30) in ECOTECH	126
4.27	Surface Azimuth angle of Window is 45° (SW45) in ECOTECH	126
4.28	Surface Azimuth angle of Window is 60° (SW60) in ECOTECH	126
4.29	AutoCAD plan as imported in eQUEST interface	128
4.30	Surface Azimuth angle of Window is 180° (N0) in eQUEST (North facing)	129
4.31	Surface Azimuth angle of Window is 0° (S0) in eQUEST (South facing)	129
4.32	Surface Azimuth angle of Window is 270° (E0) in eQUEST (East facing)	130

4.33	Surface Azimuth angle of Window is 90° (W0) in eQUEST (West facing)	130
4.34	Surface Azimuth angle of Window is 225° (NE45) in eQUEST	130
4.35	Surface Azimuth angle of Window is 135° (NW45) in eQUEST	131
4.36	Surface Azimuth angle of Window is 30° (SW30) in eQUEST	131
4.37	Surface Azimuth angle of Window is 45° (SW 45) in eQUEST	131
4.38	Surface Azimuth angle of Window is 60° (SW 60) in eQUEST	132
4.39	Surface Azimuth angle of Window is 330° (SE 30) in eQUEST	132
4.40	Surface Azimuth angle of Window is 315° (SE 45) in eQUEST	132
4.41	Surface Azimuth angle of Window is 300° (SE 60) in eQUEST	133
4.42	Monthly variation of Cooling Demand for orientation N0 in DesignBuilder (North facing)	134
4.43	Monthly variation of Cooling Demand for orientation S0 in DesignBuilder (South facing)	135
4.44	Monthly variation of Cooling Demand for orientation E0 in DesignBuilder (East facing)	136
4.45	Monthly variation of Cooling Demand for orientation W0 in DesignBuilder (West facing)	137
4.46	Monthly variation of Cooling Demand for orientation NE45 in DesignBuilder	138
4.47	Monthly variation of Cooling Demand for orientation NW45 in DesignBuilder	139
4.48	Monthly variation of Cooling Demand consumption for orientation SE30 in DesignBuilder	140
4.49	Monthly variation of Cooling Demand consumption for orientation SE45 in DesignBuilder	141
4.50	Monthly variation of Cooling Demand consumption for orientation SE60 in DesignBuilder	142
4.51	Monthly variation of Cooling Demand for orientation SW30 in DesignBuilder	143
4.52	Monthly variation of Cooling Demand for orientation SW45 in DesignBuilder	144
4.53	Monthly variation of Cooling Demand for orientation SW60 in DesignBuilder	145
4.54	Monthly variation of Cooling Demand for orientation N0 in ECOTECH (North facing)	148

4.55	Monthly variation of Cooling Demand for orientation S0 in ECOTECT (South facing)	149
4.56	Monthly variation of Cooling Demand for orientation E0 in ECOTECT (East facing)	150
4.57	Monthly variation of Cooling Demand for orientation W0 in ECOTECT (West facing).	151
4.58	Monthly variation of Cooling Demand for orientation NE45 in ECOTECT	152
4.59	Monthly variation of Cooling Demand for orientation NW45 in ECOTECT	153
4.60	Monthly variation of Cooling Demand for orientation SE30 in ECOTECT	154
4.61	Monthly variation of Cooling Demand for orientation SE45 in ECOTECT	155
4.62	Monthly variation of Cooling Demand for orientation SE60 in ECOTECT	156
4.63	Monthly variation of Cooling Demand for orientation SW30 in ECOTECT	157
4.64	Monthly variation of Cooling Demand for orientation SW45 in ECOTECT	158
4.65	Monthly variation of Cooling Demand for orientation SW60 in ECOTECT	159
4.66	Monthly variation of cooling Demand for orientation N0 in eQUEST (North facing)	161
4.67	Monthly variation of Cooling Demand for orientation S0 in eQUEST (South facing)	162
4.68	Monthly variation of Cooling Demand for orientation E0 in eQUEST (East facing)	163
4.69	Monthly variation of cooling Demand for orientation W0 in eQUEST (West facing)	164
4.70	Monthly variation of Cooling Demand for orientation NE45 in eQUEST	165
4.71	Monthly variation of Cooling Demand for orientation NW45 in eQUEST	166
4.72	Monthly variation of Cooling Demand for orientation SE30 in eQUEST	167
4.73	Monthly variation of Cooling Demand for orientation SE45 in eQUEST.	168
4.74	Monthly variation of Cooling Demand for orientation SE60 in eQUEST.	169

4.75	Monthly variation of Cooling Demand for orientation SW30 in eQUEST	170
4.76	Monthly variation of Cooling Demand for orientation SW45 in eQUEST	171
4.77	Monthly variation of Cooling Demand for orientation SW60 in eQUEST	172

LIST OF TABLES

Chapter 2 - GUARDED HOT BOX TESTING SET-UP

Sl. No.	Description	Page no.
2.1	Various environmental conditions consolidated from various standards for measurement/calculation of U-value	46
2.2	Tabular representation of instrument/probe used with accuracy, precision, response time of thermocouple sensor.	49
2.3	Tabular representation of instrument/probe used with accuracy, precision, response time of Hot Wire Anemometer.	54
2.4	Maximum fluctuations of air temperatures in metering box and cold box.	65

CHAPTER 3 – EVALUATION OF THERMAL PERFORMANCE OF BUILDING ENVELOPE COMPONENTS (OPAQUE WALLS ROOF AND GLAZINGS)

Sl. No.	Description	Page no.
3.1	Detailed description of the wall samples	77
3.2	Reflectance and absorptance of sample surfaces calculated over visible spectrum	78
3.3	Variation in extraneous heat transfer.	80
3.4	Testing report for Sample WI	81
3.5	Fluctuations in air temperature and standard deviation of U-value for Sample WI	81
3.6	Testing report for Sample WII	84
3.7	Fluctuations in air temperature and standard deviation of U-value for sample WII.	85
3.8	Testing report for Sample WIII	86
3.9	Fluctuations in air temperature and standard deviation of U-value for Sample WIII	87
3.10	Variation of U-value of Sample WII with change in metering box and cold box air velocity respectively	89

3.11	Testing report for Sample WIV	94
3.12	Fluctuations and standard deviations of air temperatures for Sample WIV	95
3.13	Testing report for Sample WV	100
3.14	Fluctuations and standard deviations of air temperatures for Sample WV	101
3.15	Test Report for DGU Air filled with conventional aluminium spacer	103
3.16	Comparative analysis of overall heat transfer coefficient of aluminium spacer based double glazing unit and warm-edge spacer based.	104
3.17	Measurement results and uncertainty analysis	106

CHAPTER 4 – COOLING LOAD ESTIMATION BY SIMULATION TOOLS

Sl. No.	Description	Page no.
4.1	Construction details of building block material	110
4.2	General simulation inputs	111
4.3	Details of various orientation used in simulation	114
4.4	Overall heat transfer values comparison using DesignBuilder	117
4.5	Overall heat transfer values comparison using ECOTECH	122
4.6	Overall heat transfer values comparison using eQUEST (eQUEST uses imperial unit system)	129
4.7	Monthly Cooling Demand in kWh for orientation N0 by Experimental value and ASHRAE value in DesignBuilder. (North facing)	134
4.8	Monthly Cooling Demand in kWh for orientation S0 by Experimental value and ASHRAE value in DesignBuilder. (South facing)	135
4.9	Monthly Cooling Demand in kWh for orientation E0 by Experimental value and ASHRAE value in DesignBuilder (East facing).	136
4.10	Monthly Cooling Demand in kWh for orientation W0 by Experimental value and ASHRAE value in DesignBuilder (West facing).	137

4.11	Monthly Cooling Demand in kWh for orientation NE45 by Experimental value and ASHRAE value in DesignBuilder.	138
4.12	Monthly Cooling Demand in kWh for orientation NW45 by Experimental value and ASHRAE value in DesignBuilder.	139
4.13	Monthly Cooling Demand in kWh for orientation SE30 by Experimental value and ASHRAE value in DesignBuilder.	140
4.14	Monthly Cooling Demand in kWh for orientation SE45 by Experimental value and ASHRAE value in DesignBuilder.	141
4.15	Monthly Cooling Demand in kWh for orientation SE60 by Experimental value and ASHRAE value in DesignBuilder.	142
4.16	Monthly Cooling Demand in kWh for orientation SW30 by Experimental value and ASHRAE value in DesignBuilder.	143
4.17	Monthly Cooling Demand in kWh for orientation SW45 by Experimental value and ASHRAE value in DesignBuilder.	144
4.18	Monthly Cooling Demand in kWh for orientation SW60 by Experimental value and ASHRAE value in DesignBuilder.	145
4.19	Monthly Cooling Demand in kWh for orientation N0 by Experimental value and ASHRAE value in ECOTECH (North facing).	147
4.20	Monthly Cooling Demand in kWh for orientation S0 by Experimental value and ASHRAE value in ECOTECH (South facing).	148
4.21	Monthly Cooling Demand in kWh for orientation E0 by Experimental value and ASHRAE value in ECOTECH (East facing).	149
4.22	Monthly Cooling Demand in kWh for orientation W0 by Experimental value and ASHRAE value in ECOTECH (West facing).	150
4.23	Monthly Cooling Demand in kWh for orientation NE45 by Experimental value and ASHRAE value in ECOTECH.	151
4.24	Monthly Cooling Demand in kWh for orientation NW45 by Experimental value and ASHRAE value in ECOTECH.	152
4.25	Monthly Cooling Demand in kWh for orientation SE30 by Experimental value and ASHRAE value in ECOTECH.	153
4.26	Monthly Cooling Demand in kWh for orientation SE45 by Experimental value and ASHRAE value in ECOTECH.	154

4.27	Monthly Cooling Demand in kWh for orientation SE60 by Experimental value and ASHRAE value in ECOTECT.	155
4.28	Monthly Cooling Demand in kWh for orientation SW30 by Experimental value and ASHRAE value in ECOTECT.	156
4.29	Monthly Cooling Demand in kWh for orientation SW45 by Experimental value and ASHRAE value in ECOTECT.	157
4.30	Monthly Cooling Demand in kWh for orientation SW60 by Experimental value and ASHRAE value in ECOTECT.	158
4.31	Monthly Cooling Demand in kWh for orientation N0 by Experimental value and ASHRAE value in eQUEST (North facing).	160
4.32	Monthly Cooling Demand in kWh for orientation S0 by Experimental value and ASHRAE value in eQUEST (South facing).	161
4.33	Monthly Cooling Demand in kWh for orientation E0 by Experimental value and ASHRAE value in eQUEST (East facing).	162
4.34	Monthly Cooling Demand in kWh for orientation W0 by Experimental value and ASHRAE value in eQUEST (West facing).	163
4.35	Monthly Cooling Demand in kWh for orientation NE45 by Experimental value and ASHRAE value in eQUEST.	164
4.36	Monthly Cooling Demand in kWh for orientation NE45 by Experimental value and ASHRAE value in eQUEST.	165
4.37	Monthly Cooling Demand in kWh for orientation SE30 by Experimental value and ASHRAE value in eQUEST.	166
4.38	Monthly Cooling Demand in kWh for orientation SE45 by Experimental value and ASHRAE value in eQUEST.	167
4.39	Monthly Cooling Demand in kWh for orientation SE60 by Experimental value and ASHRAE value in eQUEST.	168
4.40	Monthly Cooling Demand in kWh for orientation SW30 by Experimental value and ASHRAE value in eQUEST.	169
4.41	Monthly Cooling Demand in kWh for orientation SW45 by Experimental value and ASHRAE value in eQUEST.	170
4.42	Monthly Cooling Demand in kWh for orientation SW60 by Experimental value and ASHRAE value in eQUEST.	171

Chapter 5 - Results & Discussions

Sl. No.	Description	Page no.
5.1	Thermal properties of building materials used	182
5.2	Theoretical U-value of Sample W1	183
5.3	Theoretical U-value of RCC roof (Sample WIV)	183
5.4	Cooling energy difference range for entire year	185
5.5	Annual cooling energy difference w.r.t. experimental value	186

CHAPTER 1 – GENERAL INTRODUCCION

1.1 Background – Energy Scenario

1.1.1 Introduction

Energy is an indispensable part of every activity of life. Energy is one of the key components for any nation's economic progress. As per *BP Statistical Review of World Energy* (Table 1.1), the total primary energy consumption of world including renewable energy for the year 2021 was 595.14 EJ while for India it was 35.44 EJ. From Fig 1.1 and Fig 1.2, it is evident that fossil fuel-based resources are still the primary energy consumption for industrial, transportation, commercial and residential uses. India's energy consumption is 5.95% of world's energy consumption, is expected to grow by 4.2% each year (faster than all major economies in the world).

Table 1.1 – Primary energy consumption statistics from various fuel resources.

	World primary energy (sector-wise) consumption for 2021 (ExaJoules)	India primary energy (sector-wise) consumption for 2021 (ExaJoules)
Oil	184.21 (30.95%)	9.41 (26.55%)
Gas	145.35 (24.42%)	2.24 (6.32%)
Coal	160.10 (26.90%)	20.09 (56.69%)
Nuclear	25.31 (4.25%)	0.40 (1.13%)
Hydro	40.26 (6.76%)	1.51 (4.26%)
Renewables	39.91 (7.71%)	1.79 (5.05%)
Total	595.14 (100%)	46.47 (100%)

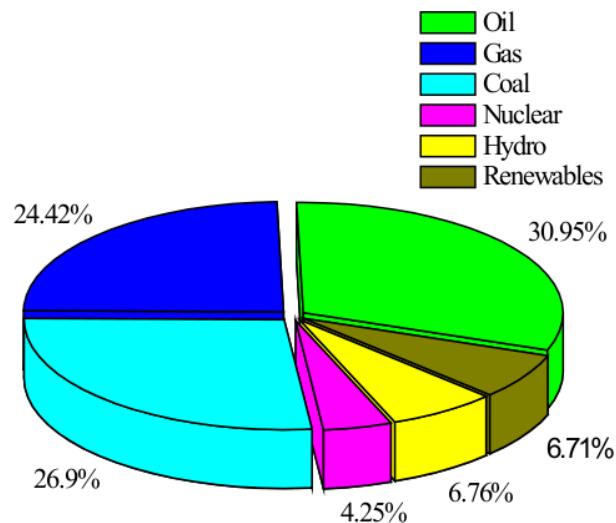


Fig. 1.1 World's primary energy (sector-wise) consumption for 2021

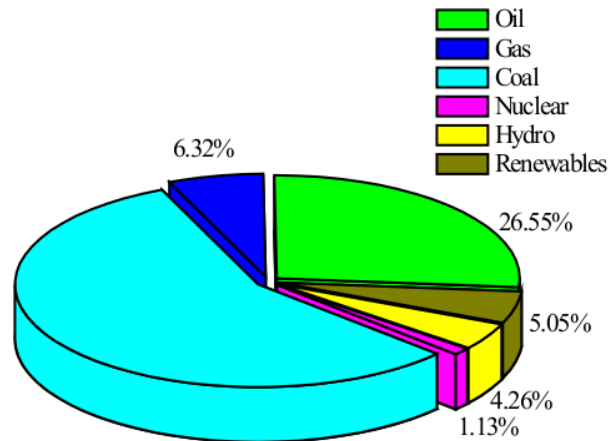


Fig. 1.2 India's primary energy (sector-wise) consumption for 2021

Electricity has become quintessential part of life of human beings. We rely on electricity for everyday needs such as: mobility, cooking, lighting, heating and cooling. According to *A Report On Energy Efficiency And Energy Mix In The Indian Energy System (2030)*, the total energy demand which was 804 TWh in 2012 would increase to around 4,487 TWh (in absence of energy efficiency measures). This report used NITI Ayog's energy sector planning tool - *IESS, 2047* for generating the projections. Out of four levels in *IESS, (2047)* level 2 (determined effort scenario) and the GDP was assumed to have grown at a CAGR of 7.4% from the base year i.e., 2012 to 2047. Table 1.2 shows the electricity demand for various sectors. From the table 1.2, it is evident that electricity demand in building sector (Residential and commercial) which was second highest would ultimately overtake the industry sector demand to become the sector with highest electricity demand by 2047. As per the report, the total installed power capacity is expected to increase from 193 GW in 2011-12 to 1,112 GW by 2047.

Table 1.2 - Sector-wise electricity demand in TWh.

Sector	Year - 2012	Year - 2047
Industry	336	1366
Residential	152	1565
Commercial	86	768
Agriculture	136	501
Others	93	287
Total	804	4487

As per IPCC (2014), total global emissions of greenhouse gases in 2010 was 49 GtCO₂ eq emissions (Fig. 1.3). Among it around 33% of total GHG emissions was released from industry sector followed by 19% from building sector. India's total GHG emissions stood at 3.202 Gt CO₂ eq. which is around 6.5% of world's total emission.

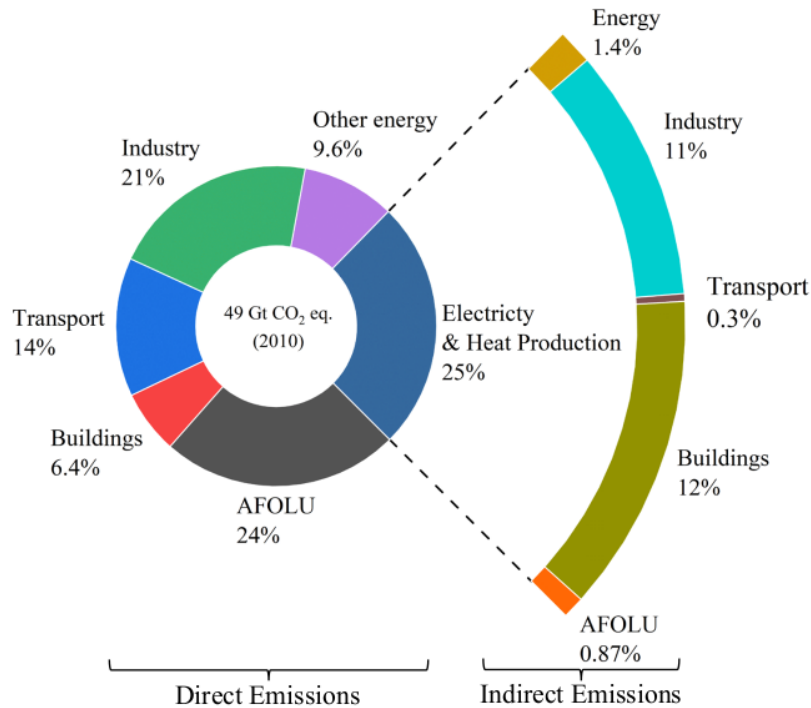


Fig 1.3 Total GHG emissions (Gt CO₂ eq./yr) by economic sectors

As of year 2020, (UNEP 2021) global building's operations and construction sector was responsible for 36% of global energy consumption at 149EJ. Among it, 127 EJ of energy was attributed to building operations while 22% was attributed to manufacturing of building construction materials. The total energy related emissions from building construction and operations during that phase stood at 11.7 gigatons of CO₂ and represented 37% of global CO₂ emissions (Fig. 1.4).

As part of the Paris Agreement, over 200 countries have agreed to cooperate to bring down greenhouse gas emissions and mitigate climate change. In accordance with the agreement, global warming is to be restricted to well below 2°C, and preferably to 1.5°C, as compared to pre-industrial levels. India via its Nationally Determined Contribution (NDC) has pledged three primary targets. One of its targets is to reduce the emission intensity of its GDP by 33-35% by 2030 from its 2005's levels.

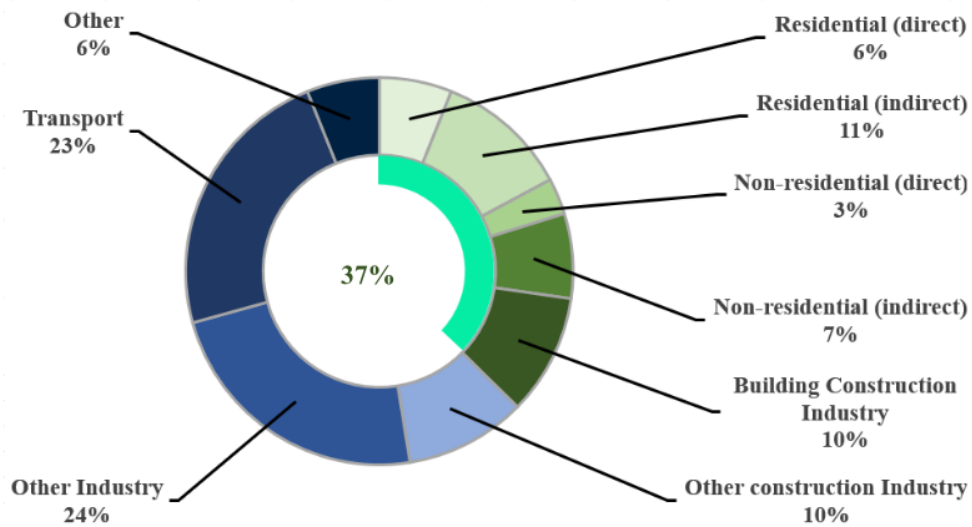


Fig. 1.4 Sector CO₂ emissions in the year 2020.

From the above scenario, it can be seen that overall building sector plays a key role in the future energy demand as well as greenhouse gas emissions. Driven by increased population and quest for improved quality of life, the energy demand and greenhouse emissions are expected to rise. In the next section, overall scenario in the building scenario has been highlighted.

1.1.2 Building Energy Scenario

According to *World Population Prospects (2022)*, population of world which stands at 7.9 billion is anticipated to reach 8.5 billion by 2030. India with a population of 1.4 billion which stands second after China in 2022 is projected to surpass China by 2030. As per *IEA India Energy Outlook 2021*, by the year 2040, India's urban population is expected to increase by 270 million. Consequently, the demand for energy-intensive building materials would increase significantly. The *PMAY-Urban* was launched on June 25th 2015 to provide housing for all in urban areas by 2022. This mission seeks to build affordable housing and deliver them at an affordable house within the stipulated time. Based on data from a report by *Ministry of Statistics and Programme Implementation (2019)*, the building sector in India is the second largest consumer of electricity, after industry. It accounts for close to 33% of the total electricity consumption, 9% of which comes from the commercial sector and 24% from the domestic sector. According to *Energy Statistics India (2021)*, buildings contributed to around 33% of the total electricity consumption of 1291 TWh in 2019-20 in India. According to *V. Chaturvedi et al. (2014)*, the final energy demand of the Indian building

sector will eventually grow over five times by the end of this century due to rapid economic growth and population growth in India.

1.1.2.1 Building Types

The type of building plays a key role on the energy consumption of the building and the related greenhouse gas emissions. According to type of occupancy *NBC (2016)* buildings can be categorised into following groups: Group A – Residential, Group B – Educational, Group C – Institutional, Group D – Assembly, Group E – Business, Group F – Mercantile, Group G – industrial Group H – Storage and Group J – Hazardous. A Residential building is one in which sleeping accommodation is provided for normal residential purposes. They can be further classified into Lodging or rooming houses, one or two-family private dwellings, Dormitories, Apartment houses (flats), Hotels, Hotels (Starred). According to *IPCC AR6 WGIII (2022)*, buildings can be grouped into residential and non-residential buildings. Residential buildings can be classified as single-family house, slums and multi-family house or apartment/flats building. Single-family house can be further sub-divided into single-family detached (cottages, house barns, etc.) and single-family attached (or small multi-family, terrace house etc.).

Non-residential buildings are cultural buildings (such as theatres and performance, museums, libraries, and cultural centres), educational buildings (for e.g. kindergarten, schools, research centre, and laboratories), healthcare buildings, sports, hospitality (hotel, casino, lodging, restaurants and bars), commercial buildings and offices (like institutional buildings, markets, office buildings, retail, and shopping centres), public buildings (for e.g, government buildings, military and security buildings), religious buildings, and industrial buildings (such as data centres, factories, warehouses, energy plants, agricultural and transportation buildings).

Building energy consumption depends upon its end use (whether residential, industrial or commercial), type of building (whether npn-air-conditioned or air conditioned), and the climate in which it is located.

1.1.2.1.1 Residential Buildings Scenario

The residential building sector in India accounts to 79.9% of total housing stock (*CensusInfo 2011*). A study made by Central European University (CEU) reported that by 2050, 85% of floor space area will be for residential use while rest 15% would be used for commercial floor area. Electricity consumption in residential sector which was 295 TWh (15.16% of total electricity consumption) in FY 1989-90 has risen to 24% i.e. 308 TWh in FY 2019-20

(CEA, 2021). It is the second highest consuming sector in India after industrial sector at 533 TWh (43%). The annual electricity use per household is expected to increase from 650 kWh in 2012 to 2750 kWh by 2050, under business-as-usual scenario (GBPN, 2014). Sector wise energy consumption in residential sector is shown in Fig. 1.5 (Climate Works Foundation, 2010). It can be seen from the energy consumption distribution in that HVAC in residential sector, amounts to about 45% of total energy consumed.

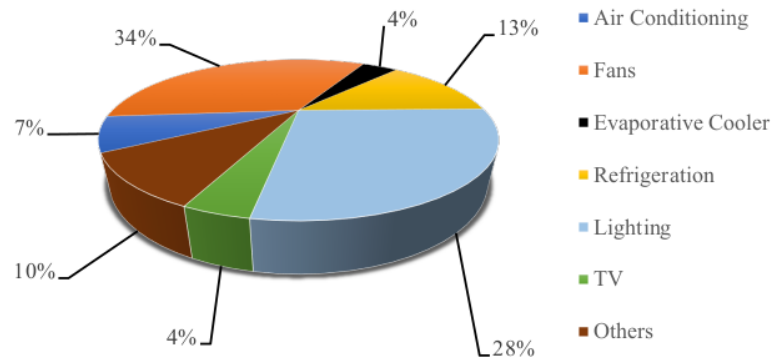


Fig. 1.5 Residential Sector Energy Consumption in India.

From the overall annual energy consumption for space cooling in buildings (S. Kumar et al, 2018), it was found that the non-refrigerant based cooling technologies i.e., fans and air-coolers together represent almost 40% of the cooling energy consumption. This is significantly more than Chillers, VRF and DX based cooling systems based used in commercial sector.

Several studies have found that residential air conditioning (AC) accounts for 20-40% of the annual electricity consumption of urban dwellings, and it is likely to be tripled by 2030.

A recent study conducted across four cities, four hundred surveyed houses and twenty monitored houses showed that air conditioning contributed to 75% of the energy use during summer, spring and even in the autumn season (TERI, 2008). It is expected that the overall penetration of room air conditioners in the sector will increase from 8 percent in 2017-18 to 12 percent by 2022-23 and 21 percent by 2027-28, respectively, with the urban residential stock having approximately 44 percent penetration of room air conditioners in 2027-28 (S. Kachhawa et. al, 2019).

1.1.2.1.2 Commercial Buildings Scenario

The Energy Information Administration defines a 'commercial building' as one that is not used for residential, industrial, or agricultural purposes. Commercial buildings include offices, hotels, hospitals, educational institutions, retail malls, etc. As reported by CEA, the commercial sector accounts for approximately 9% of the country's total electricity consumption. As reported in the 17th Electric Power Survey of the Central Electricity Authority, the demand for electricity in 2011-12 is expected to increase by approximately 40% and 175% when compared to 2006-07. NITI Aayog has projected that there will be an increase in electricity consumption for the commercial sector of 7 to 11 times from 2012 to 2047 (IESS, 2047). India's rapid growth in commercial buildings has been primarily driven by a demand for Information Technology services. A study conducted by *McKinsey (2009)* has estimated that present built up area of one billion square meters of commercial buildings that is expected to grow to four billion square meters by 2030. Sector wise energy consumption in commercial sector has been shown in Fig. 1.6 (*CEA's 'Year End Review 2012-13*). From the figure it is evident that, HVAC accounts for about 52% of total energy consumption.

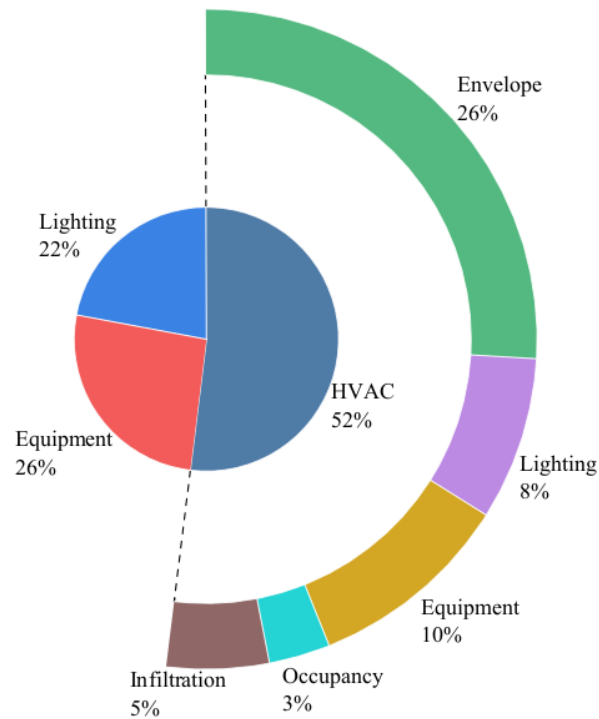


Fig. 1.6 Sector wise breakup of energy consumption in commercial sector.

1.2 National Climates – Five Climatic zones

An individual's physiological and psychological well-being is dependent upon the level of indoor thermal comfort, which is achieved through active heating, cooling, or a combination of both. This is largely determined by the local weather and seasonal changes. Different parts of the country experience different weather conditions. It indicates that, with the exception of a few states in the foothills of the Himalayas, the country has a relatively limited need for heating, both geographically and in terms of duration. As a result, thermal comfort in the country is primarily related to the cooling of buildings. According to *ECBC (2017)*, the country has been divided into five climatic zones (Fig 1.7) namely: Hot and Dry, Cold, Warm and humid, Temperate and Composite.

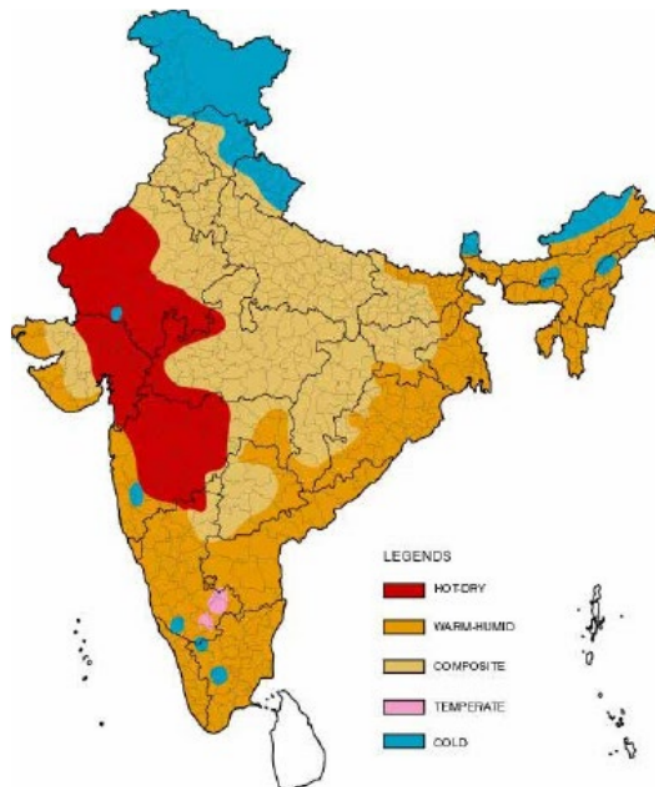


Fig. 1.7 Five Climatic Zones of our Country.

In Hot and Dry type climate, the summer time temperatures vary between 20°C to 45°C and winter time temperatures vary between 0°C to 25°C, while the relative humidity remains around 55%. The individual variation of climatic parameters such as air temperature and relative humidity has been discussed below (*India Cooling Action Plan, 2019*).

In Warm and Humid type climatic, the summer time temperature varies between 25° to 35° and winter time temperature varies between 20°C to 30°C. The relative humidity ranges between 70% to 90%.

In Composite type climate, the summer time temperature varies between 27°C to 35°C and winter time temperature varies between 4°C to 25°C while the relative humidity ranges between 20% to 25% for dry type weather and between 55% to 95% for wet type weather.

In Temperate type climate, the summer time temperature varies between 17°C to 34°C while the winter time temperature varies between 16°C to 33°C. The relative humidity in type of climate is less than 75%.

Lastly, in Cold type climate, the summer time temperature varies between 17°C to 30°C and winter time temperature varies between -3°C to - 8°C while relative humidity varies between 70% to 80%.

Building construction in general should take into account the respective climatic zones in which it would be built, so that we reduce the dependencies on energy intensive measures to provide the appropriate thermal comfort. For example, in a hot and dry region the climate is normally characterised by high daytime temperatures and low night time temperatures. So, use of high thermal capacity materials like mud, stones, thick concrete block can significantly delay the entry of heat into the building so that the building/house can remain cool during daytime and cool during night time. Moreover, the houses may be closely spaced to maximise the building volume while minimising the surface area exposed to the sun. This would result in a considerable reduction in the amount of absorbed solar radiation thereby keeping the interior space cool during the daytime. During the night time majority of the heat stored would be radiated out into the sky and a small amount would warm the indoor space. Similarly, in a warm and humid climatic zone where variations in diurnal temperature is comparatively small, use of materials of low thermal energy storage would be more appropriate. Adequate provisions should be kept for allowing air circulation and air ventilation to avoid stagnation of humid air in the built space.

1.2.1 Climate of Kolkata (Warm & humid) & Variation of climatic parameters in Kolkata

Kolkata is ¹⁰¹ the capital of the West Bengal state in eastern India. Its climate is considerably influenced by the Bay of Bengal. As per ⁷⁰ Köppen climate classification, Kolkata experiences a tropical wet-and-dry climate. It falls under warm & humid climatic zone of the country with an annual mean temperature of 26.8°C and the mean monthly temperatures ranges

between 19°C to 30°C. Summer, monsoon and winter are the three seasons which dominate the climate of Kolkata. Summer (March to June) is hot and humid with maximum temperatures sometimes exceeding 40°C, while winter (December to February) is mild and dry with temperatures ranging between 9°C to 18°C. Rainy season lasts between June to September with an annual rainfall of about 1600mm. October and November i.e., the post monsoon season represents the transition period from monsoon to winter. During these period days are mostly clear and night is comfortable. This season also sometimes experience severe cyclonic storm over the Bay of Bengal. Variation of radiation falling on a horizontal plane for Alipore-Kolkata has been generated using *Climate Consultant 6* and shown in Fig. 1.8. Variation of daily average wind speed (shown as red line) and daily average wind direction (shown as black line) generated using *Climate Consultant 6* and 'Calcutta weather data' is shown in Fig. 1.9. Fig. 1.10 shows the variation of daily average dry bulb temperature, daily average wet bulb temperature and daily average relative humidity as generated using *Climate Consultant 6*.

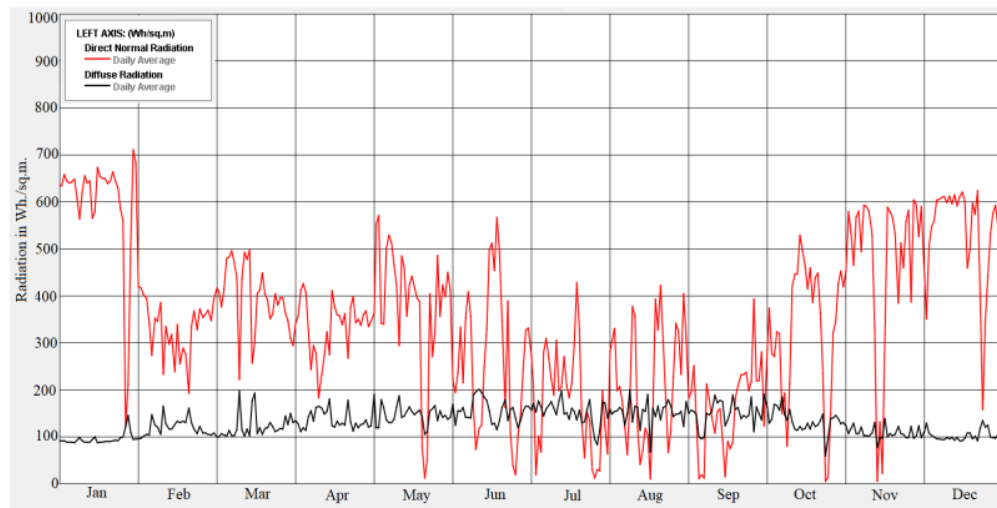


Fig. 1.8 Variation of daily average direction radiation and diffuse radiation for Kolkata

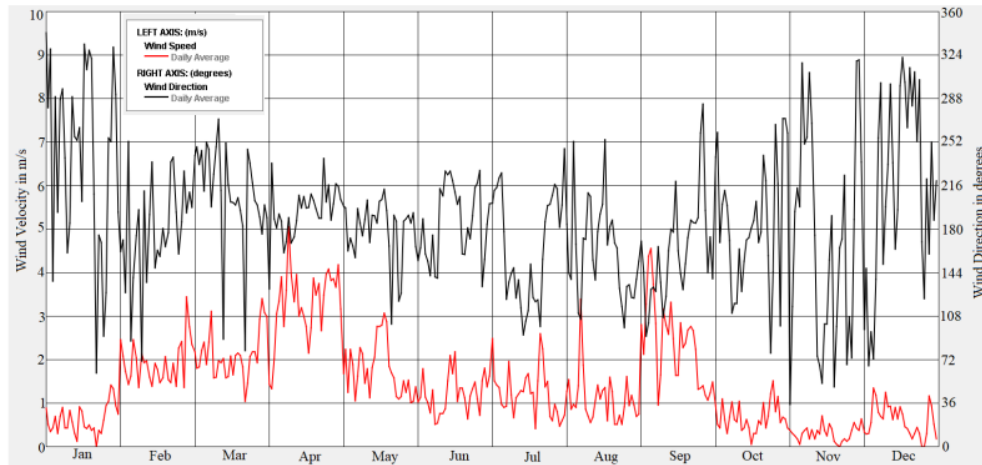
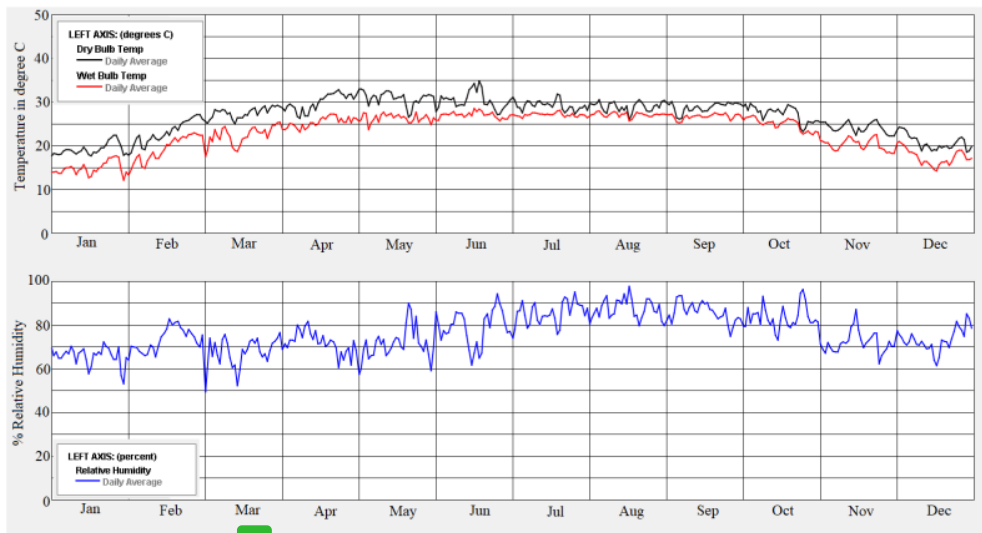


Fig. 1.9 Variation of daily average wind speed and direction for Kolkata



77

Fig. 1.10 Variation of daily average dry bulb temperature, wet bulb temperature and relative humidity for Kolkata

1.3 Objective and Scope of Work

Objective of the Research Work:

Building owners and designers use energy simulation to evaluate a building's energy performance and make necessary modifications in the design before construction to make the building more energy efficient. It is also used to find whether the performance of an existing building is compliant with respect to building energy efficiency codes such as ECBC, ASHRAE 90.1 etc. Computer-based energy simulation programs simulate the visual, thermal, ventilation, and other energy-consuming processes occurring in a building in order

to predict its energy efficiency. It predicts and analyses the energy efficiency of a building by taking into consideration building geometry and orientation, building materials used, façade design and characteristics, indoor environment conditions, climate parameters, functionality, occupant activities and schedules, lighting and HVAC and systems, and other parameters. Among these parameters, building geometry, orientation and the building structural components (Walls, roof, glazing) play a vital role in determining the energy load (heating / cooling loads) of a building.

It is necessary to manually input data such as thermos-physical properties of the building structures, weather data file, lighting, occupancy, equipment related loads and their operational characteristics, the desired air temperature set points, detailed HVAC systems related input, hot water services etc.

The properties of the individual layers of building components have a significant effect on the heat and moisture transfer across that layer and ultimately on the space load. By general convention, the simulation software uses the thermos-physical properties of the building components to analyse the performance of the building fabrics as per some reference standards such as ASHRAE 90.1, CIBSE admittance methods, DOE-2 library etc. ¹⁷ The overall heat transfer coefficient of the building components is also calculated thereof.

The objective of the study is to explore the impact of impregnating experimentally obtained overall heat transfer coefficient values of common building components (such as wall, roof & glazings) directly into simulation software, and comparing the same with software based results, based entirely on embedded library of materials, their properties and resultant U-value thereof.

Among the various methods of experimental evaluation of overall heat transfer coefficient, Guarded Hot Box testing based on BS EN 8990:1996 is the most accurate method, which has been followed in this study with the help of locally available building materials.

The scope of research work involves the following:

- (i) Identification of common building materials used for Energy Efficient Building construction.
- (ii) Extensive Calibration of Guarded Hot box as per BS EN 8990-1996.
- (iii) Study of the various boundary conditions applicable w.r.t. building components for measurement of U-value.
- (iv) Determination of spectral properties of opaque coloured surfaces.
- (v) Impact of varying air velocity on the overall heat transfer coefficient of the Masonry Wall surface.
- (vi) Determination of U-value of Building envelop components like Masonry Wall, Reinforced Cement Concrete Roof and Window glazing using Guarded Hot Box, and Cooling load calculation for the enclosed space considered.
- (vii) Identification of globally available building simulation tools, such as DesignBuilder, ECOTECT and eQUEST, which are recommended for Energy Conservation Building Code 2017 application.
- (viii) Following ASHRAE 2017 Handbook, U-values of envelop components would be calculated by each of the above simulation tool, and resultant cooling load calculated thereof.
- (ix) Comparison of the cooling load obtained from experimental parameter with those using DesignBuilder, ECOTECT & eQUEST. Effect of change in orientation on cooling load also studied by different simulation tools.

***CHAPTER 2 – GUARDED HOT BOX
TESTING SET-UP***

2.1 Introduction

Guarded hot box testing setup is a testing facility for experimental characterisation of steady state overall thermal transmittance or overall heat transfer coefficient or U-value of any specimen. It is one of the laboratory and in-situ non-destructive method of evaluation of thermal transmittance. Other methods involve Heat Flow Meter method (*ISO 9869-1:2014*, *ASTM C1155-95*), Guarded hot plate method (*BS 874-part-2 section 2.1:1986*, *ISO 8302-1991*, *ASTM C1173-13*) and Infrared Thermography (*BS ISO 9869-2:2018+A1:2021*). Guarded hot box testing is conducted as one of the following test standards: *BS-EN-ISO-8990-1996*, *ASTM C1199 – 97*, *ASTM C1363 – 11*.

In the present work, detailed measurement of U-value of typical wall and roof configurations along with DGU with warm edge spacer has been presented.

In present chapter, a detailed overview of the guarded hot box test setup, its calibration procedure and overall strategy of measurement have been presented.

2.1.1 Guarded Hot Box

Overall heat transfer coefficient or thermal transmittance (U-value) plays a pivotal role in the overall thermal performance of a building in terms of both the energy savings throughout its operational phase and the thermal comfort. It gives a quantitative measure of the amount of heat flowing through unit area of any material for every degree differential temperature on either side of the material.

Having a knowledge of the U-value of the elements during the design phase of the building can help optimise the energy demand for maintaining appropriate thermal comfort of the inhabitants. It is also a crucial parameter while performing building energy simulation for optimising the design and configuration of the construction elements so as to reduce the cooling or heating loads.

Laboratory scale measurement of U-value is obtained via two methods: Calibrated Hot Box method and Guarded Hot Box method. The methods are primarily intended for measurement of large, inhomogeneous and homogenous specimens.

Mathematically U-value in general can be defined as:

$$U = \left[\left(\frac{1}{h_{ce} + h_{re}} \right) + \sum_{i=1}^n \frac{l_i}{k_i} + \left(\frac{1}{h_{ci} + h_{ri}} \right) \right]^{-1} \quad (2.1)$$

Guarded Hot Box Test facility is used for experimental evaluation of the U-value under steady state condition. One such facility had been developed at Building Energy Laboratory, School of Energy Studies, Jadavpur University. The testing facility was set up in accordance with BS EN ISO 8990:1996 and BS EN ISO 874: Part 2: Section 3.1: 1987. This testing method is applicable for thermal characterisation of homogeneous or non-homogeneous specimens and building structure (walls, roofs, window glazing, doors etc.). This setup can be used to measure the steady state thermal transmittance of any construction element with thermal transmittance and conductance in the range of $0.1\text{W}/(\text{m}^2.\text{K})$ to $15\text{W}/(\text{m}^2.\text{K})$ for testing within temperature range -10°C to 50°C . Schematic set-up of the same is given in Fig. 2.1 (D. Chowdhury et al, 2016).

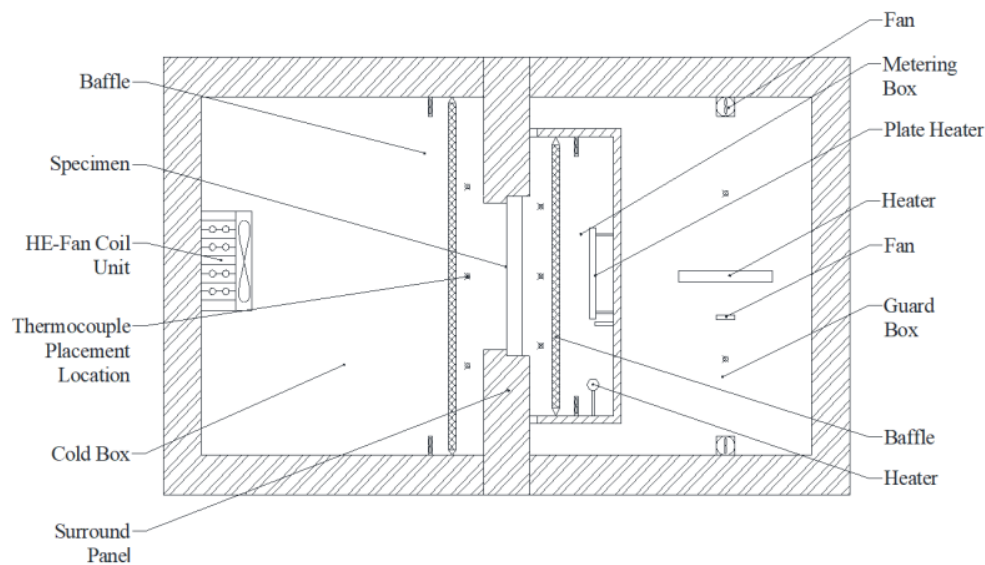


Fig. 2.1 Schematic set-up of Guarded Hot Box Testing Facility

It consists of metering box (MB), guard box (GB), cold box (CB) and surround panel to hold the sample in place between Metering Box and Cold Box. The sample is placed in the sample holding cut-out of surround panel in between metering box and cold box. This cut-out is present in exactly midway from either edge of surround panel. Fig. 2.2 (D. Chowdhury et al, 2019) and Fig. 2.3 show photographic view of Guarded Hot Box Test facility installed at School of Energy Studies, Jadavpur University. The walls of set up is made of 250 mm extruded polystyrene insulation.



Fig. 2.2 Guarded Hot Box Test set-up installed at laboratory (*D. Chowdhury et. al 2019*).



Fig. 2.3 Guarded Hot Box Test set-up in open condition.

The metering box along with guard box and cold box are locked against the surround panel using guy wire and rod assembly as shown in Fig. 2.2 to form air tight chamber. Several standards are available for experimental determination of U-value using guarded hot box and

they have been also compared by *F. Asdrubali et al. (2011)* in their study. Literature survey have shown numerous instances where the above standards and Guarded Hot Box Test facility has been used for thermal characterisation such as in *F. Geola et al. (2009)*, *Y. Fang et al. (2007)*, *P. Blanus et al. (2005)*, *F. Chen and Wittkopf (2012)*. Heat is supplied to the metering box at constant rate which causes the apparatus slowly reaches the desired equilibrium condition. Alternately the temperature in the metering box space may be kept constant by a suitable control of the heat input when thermal equilibrium achieved. When the surface temperature on both face of test specimen and the heat flowing through it are constant, then thermal equilibrium is said to have been achieved. Under such conditions the final measurements are taken and overall heat transfer coefficient is evaluated.

2.1.2 Metering Box

The metering box (MB) (Fig. 2.4) is a five enclosed sided with a rectangular or square cross-section having dimensions of 1840mm by 600mm by 1600mm. The walls of metering box are made of 50mm thick extruded polystyrene sheets (closed cell foam insulation material) with plywood skin on the internal surface.

For thermal transmittance measurements a baffle is fixed in the metering box, parallel to the surface of the test element, in order to provide a radiating surface of near uniform temperature and assist in adjusting the air curtain velocity over the sample surface. The baffle plate extends to the full width of the metering box and have gaps at top and bottom to allow air circulation. For the purpose of maintaining a constant air temperature inside the metering box two tubular heaters 60W (each) and a plate heater of 110W have been installed in the metering box. DC circulating fans are installed inside metering box in order to achieve uniform air flow across the specimen surface.

2.1.3 Guard Box

Guard box as the name suggests surrounds the metering box (Fig. 2.4). The exterior dimension of guard box is made of 250mm thick extruded polystyrene insulation. The purpose of the guard box is to modulate the environment around the metering box so that heat flow through the metering box walls and imbalance heat flow in the surface of the specimen from metered area to guard area is minimized. The system is made so as to restrict the heat transfer from the guard box and metering box within a limit of ten percent of power supplied to the metering box. Two tubular heaters of 120W (each) have been placed on the vertical wall and a tubular heater of 60W has been installed on the floor of the guard box space. Circulating fans are placed for uniform circulation of air and distribution of heat inside the guard box.



Fig. 2.4 Metering Box and Guard Box

2.1.4 Cold Box

Cold box provides a controlled environment opposite to metering chamber. The exterior dimension of the cold box is same as that of guard box (Fig. 2.5). The walls of the cold box are made of 250mm thick extruded polystyrene insulation. This is done in order to reduce the cooling load on the cooling system and also to prevent condensation on the outside of the chamber walls. For thermal transmittance measurements a baffle similar to that used in metering box is installed in cold box. A heat exchanger fan coil unit has been installed to maintaining the appropriate air temperature. Similar to metering box, a baffle has been installed in the cold box chamber parallel to the surround panel surface.



Fig. 2.5 Cold Box

2.1.5 Surround Panel

Surround panel is placed midway between hot side and cold side (Fig. 2.6). The surround panel is made of extruded polystyrene insulation. The outside dimension of the surround panel is equal to that of outside dimensions of cold box and guard box. There is an aperture inside the surround panel where the sample specimen (500mm by 500mm) to be tested is placed. The sample holding aperture of surround panel is shown in Fig. 2.7.

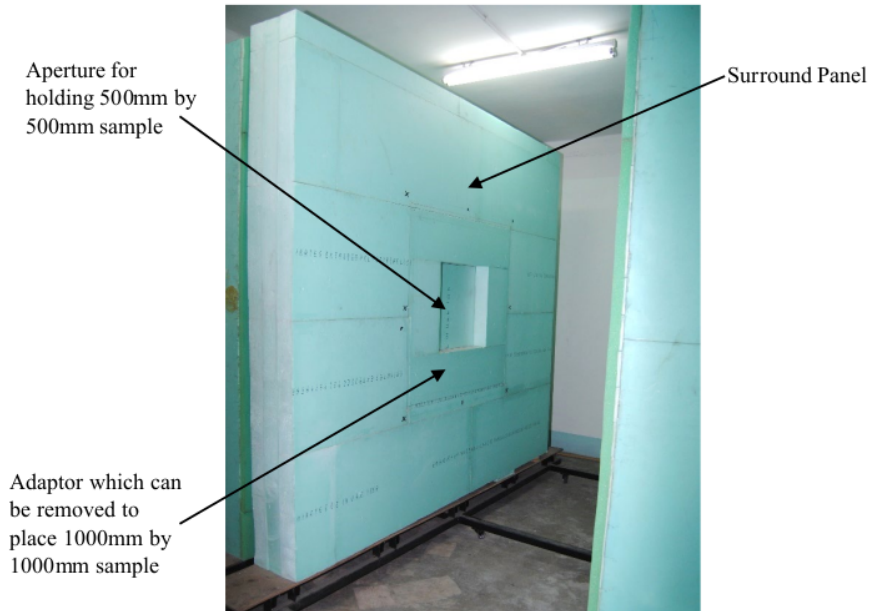


Fig. 2.6 Surround Panel



Fig. 2.7 Close up view of the aperture in surround panel

2.2 Experimental Boundary Condition Range

As per *BS EN ISO 8990*, the environmental in the metering box and cold box were maintained at constant temperatures such that minimum differential air temperature between metering box and cold box was at least 20°C. By varying the operating conditions, the different climatic zones of our country with different temperatures could be replicated. Moreover, by varying the velocity of air over surface of the specimen the magnitude of convective heat transfer coefficient could be altered as well. A tabular representation (Table 2.1) of various operating conditions consolidated from various standards for measurement of U-value is presented below:

Table 2.1 - Various environmental conditions consolidated from various standards for measurement/calculation of U-value

Experimental Methods:	
ASTM C1199-97: Standard Test Method for Measuring the Thermal Transmittance of Fenestration Systems Using Hot Box Methods.	Room side / Indoor conditions: $T_{in} = 21^{\circ}\text{C}$ $h_{in} = 8.3 \text{ W}/(\text{m}^2 \text{ K})$ Weather / Outdoor side: $T_{out} = -18^{\circ}\text{C}$ $h_{out} = 29 \text{ W}/(\text{m}^2 \text{ K})$
ASTM E1423-14: Standard Practice for Determining Steady State Thermal Transmittance of Fenestration Systems	
BS EN ISO 8990:1996 - Thermal insulation — Determination of steady-state thermal transmission properties — Calibrated and guarded hot box.	Test conditions is to be selected based upon the end-use application while taking into account the effect of testing conditions on accuracy. Mean air temperatures of 10°C to 20°C and a air temperature difference of at least 20°C has to be maintained.
BS EN ISO 12567-1:2010 - Thermal performance of windows and doors - Determination of thermal transmittance by the hot-box method. Part 1: Complete	Air velocity on the hot and cold sides would be adjusted according to the purpose of the test.

windows and doors (ISO 12567-1:2010)

Theoretical Calculation Methods:

BS EN ISO 6946: Building components and building elements — Thermal resistance and thermal transmittance — Calculation method	Surface resistance (m ² K/ W)	Direction of heat flow		
		Upwards	Horizontal	Downwards
	R _{si}	0.10	0.13	0.17
	R _{se}	0.04	0.04	0.04

The value for internal surface resistance (R_{si}) is calculated for ε = 0.9 and h_{r0} has been evaluated at 20°C.

The value for external surface resistance (R_{se}) is calculated for ε = 0.9, h_{r0} has been evaluated at 10°C, and for v = 4 m/s.

h_{r0} = Radiative coefficient for a black-body surface. The value for external surface resistance (R_{se}) for wind speeds from 1m/s to 10m/s are tabulated. Moreover, the h_{r0} for mean temperature of -10°C, 0°C, 10°C, 20°C and 30°C are also tabulated.

ISO 15099:2003: Thermal performance of windows, doors and shading devices — Detailed calculations

Unless any specific boundary conditions are specified, the following are advised to be used:

Winter conditions:	Summer conditions:
T _{int} = 20°C	T _{int} = 25°C
T _{ex} = 0°C	T _{ex} = 30°C
h _{cv,int} = 3.6 W/(m ² K)	h _{cv,int} = 2.5 W/(m ² K)
h _{cv,ex} = 20 W/(m ² K)	h _{cv,ex} = 8.0 W/(m ² K)
T _{r,m} = T _{int}	T _{r,m} = T _{ex}

ASHRAE Standard 90.1 -2007 Energy Standard for Buildings Except Low-Rise Residential Buildings

Air Film resistance	Condition
0.03	Exterior surfaces
0.08	Semi-exterior surfaces
0.11	Interior horizontal surfaces, heat flow direction is up

0.17	Interior horizontal surfaces, heat flow direction is down
------	--

0.12	Interior vertical surfaces
------	----------------------------

Exterior surfaces are areas which are exposed to the wind.

Semi-exterior surfaces are protected surfaces with natural or mechanical ventilation such as: face attics, crawlspaces, and parking garages.

Interior surfaces are surfaces which are within enclosed spaces.

As per *ASTM C1199 – 97*, the specimens are to be tested as per the nominal conditions as shown in Table 2.1. These results were derived after inter-laboratory test results comparison on standard tests specimens. But as per BS EN ISO 8990: 1996, the testing boundary conditions would be governed by the actual environmental conditions where the sample is meant to be used.

As of now no standard is available whereby Indian climatic conditions have been highlighted for experimental determination of overall heat transfer coefficient using Guarded Hot Box. *D. Mitra et. al, (2016)* conducted a study whereby the probable set point temperatures to be used for testing of samples using Guarded Hot Box were highlighted.

In present study U-value has been determined with varying differential air temperature across the specimen. The metering box air temperature has been kept fixed at 40°C while cold box air temperature is varied (0°C, 10°C and 20°C). The effect of variation of air velocity on the overall heat transfer coefficient has also been studied.

2.3 Control and Strategy

For the purpose of temperature measurements K-type thermocouples (made of Chromel and Alumel wire) of 0.2mm diameter were used (Fig. 2.8). These thermocouples were made at the laboratory using a spot-welding kit and were calibrated using a constant temperature oil bath (Fig. 2.9). The thermocouple sensors were attached to the surface with an aluminium foil tape to facilitate proper thermal contact with the surface. The details of the temperature sensor is presented in Table 2.2.

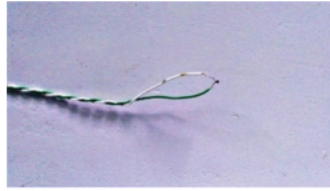


Fig. 2.8 K-type thermocouple sensor used for temperature measurements

Table 2.2 - Tabular representation of instrument/probe used with accuracy, precision, response time etc. are follows:

Instrument/Probe	Parameter measured	Range	Accuracy	Time Response
Class 1 K-type thermocouple sensor	Temperature	100 to 250°C	($\pm 0.15 \text{ C} \pm 0.25\%$)	0.1 s



Fig. 2.9 Constant temperature oil bath

Temperature sensors placed on following locations:

- Sensors distributed over the inner surface walls of metering box and over the outer surface walls of metering box.
- Sensors have also been placed on the each of the baffle plate for hot side and cold side.
- Three sensors haven been placed in the air space between metering box baffle and surround panel (Fig. 2.10) and distributed in the air space between cold box baffle and surround panel.
- Temperature sensors are also placed in the air space in the guard box space behind the metering box and over the surround panel surface facing hot side and cold side.
- Sensors have evenly been spread over the sample surface facing metering box (Fig. 2.11) and cold box.



Fig. 2.10 Location of air temperature sensors (A1, A2 & A3) in the metering box

Agilent 34970A data acquisition system has been used to acquire data from the temperature sensors. The temperature sensors terminals have been fed into 34901A module which has a built-in thermocouple reference junction to eliminate the errors caused due to thermal gradients when measuring thermocouples. Voltage supplied to the plate heater, tubular heater and the circulating fans inside the metering box have also been recorded in the data acquisition system along with the respective currents (measured using DC shunt) flowing through each of them. Using these data, the total instantaneous power input into the metering box from the heaters and fans can be evaluated.



Fig. 2.11 Temperature sensors placed on the surround panel and sample surface (*D.*

Chowdhury et. al 2019)

2.3.1 Metering Box and Guard Box Control Strategy

For the purpose of data acquisition and control an Agilent VEE Software based interface (Fig. 2.12) was developed which interacts with the Agilent 34970A data-logger via Agilent 82357B USB/GPIB Interface Converter. Temperature data from air temperature sensors A1, A2 & A3 (Fig. 2.13) were fed into the software which were averaged to form the average air temperature in the metering box. This served as input signal to the controller. Similarly, data from air temperature sensors G1, G2 & G3 were averaged to form the average air temperature in the guard box. The temperature vs time profile for the air average air temperature, baffle plate surface temperature, surround panel surface temperature and sample surface temperature have also been displayed in the interface.

A fuzzy logic driven virtual PID controller had been developed (*C. Basak et al. 2016*) which used pulse width modulation technique to alter the input voltage duty cycle of the heaters placed in the guard box and metering box. Previously a virtual PID control, on-off logic-based technique was used to control the energy delivered from the heaters (*A. Ghosh et al. 2014*). The output of the controller is calculated using MATLAB based fuzzy logic script from the set point and the averaged value of air temperature. The output from the 34907A multifunction card is used to turn on or off the heaters via an in-house developed control circuitry.

The purpose of the guard box is to maintain a controlled environment outside the metering box such that rate of heat flow via metering box walls is minimum.

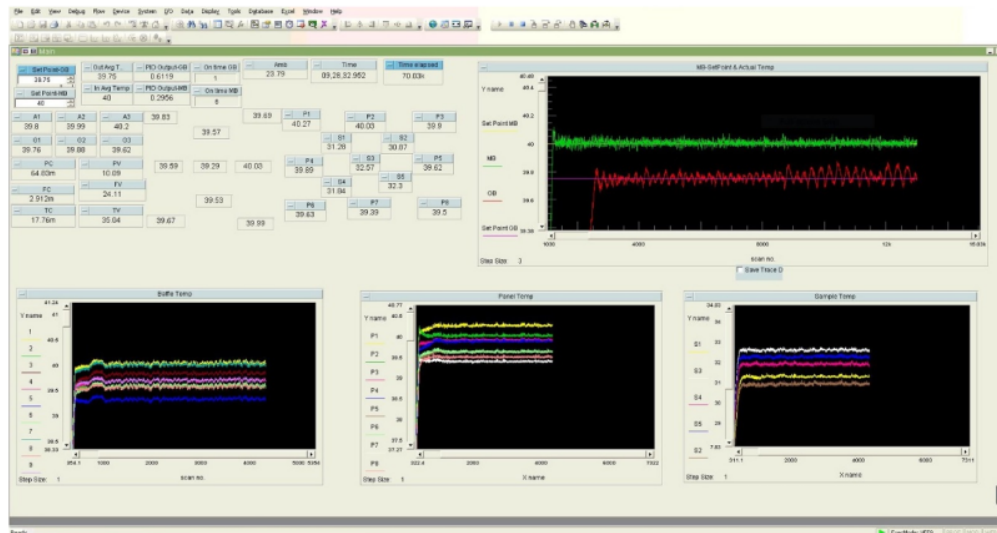


Fig. 2.12 Interface for Agilent VEE Software

Now as per BS EN ISO 8990:1996, this rate of heat flow through the metering box walls should be limited to within 10% of the input power delivered into the metering box. In the guard box, the three air temperature sensors have been distributed evenly in the guard space.

2.3.2 Cold Box Control Strategy

In cold side, chilled calcium chloride solution storage-based system incorporating heat exchanger-fan coil unit (Fig. 2.13, Fig. 2.14) has been setup. *F. Chen et. al (2013)* used guarded calorimetric hot box to evaluate U-value of double glazing where chilled water-based cooling system incorporating PID controller has been used in cold box. A PID controller (SELEC T533) was installed for the purpose of maintaining a constant temperature inside the cold box. Out of the three air temperature sensors placed in the cold box air curtain in front of the baffle, sensor in the middle position was used as input to the PID controller. The output signal drives the circulating pump via an auxiliary relay. A flow control mechanism has been kept to alter the flow rate of the calcium chloride solution.



Fig. 2.13 Heat Exchanger Fan Coil unit along with rotameter-based flow control

The advantage of using such a system is that dead zone of control involved in traditional air conditioning systems is completely eliminated. Thereby precise control of air temperature is possible by use of PID. Moreover, the flow rate of the chilled fluid can be measured via rotameter (Fig. 2.13) Detailed study of the same has been presented by *D. Chowdhury (2013)* in his M. Tech. thesis.

For the purpose data-logging Agilent 34970A data-logger was installed. *D. Chowdhury et. al (2016)* had given a detailed study of the cooling circuit being employed in the cold box of the same guarded hot box facility.



Fig. 2.14 Sub-zero dilute calcium chloride solution based chilled storage unit

2.4 Calibration

The calibration procedure of guarded hot box is of utmost importance to accurately determine the overall heat transfer coefficient of any material. To accurately determine the heat transfer through the sample specimen, it is necessary to isolate and quantify the various losses associated with the metering box. It consists of flanking losses and heat transfer from metering box into ambient through surround panel. For this purpose, calibration panels having known thermal properties and similar to that of surround panel were placed in the sample holding aperture.

As per *ASTM C1363-11*, flanking losses can occur at two locations in a hot box:

- (a) Contact point of metering box wall on surround panel.
- (b) Edge of aperture of surround panel holding a sample smaller than metering box opening.

The first loss occurs from metering box to guard box. This loss coupled with heat transfer from metering box to ambient from surround panel forms the extraneous heat transfer \dot{Q}_{extra} [W] involved with the metering box. The second loss occurs directly from metering box space to cold box space via the surround panel or frame holding the sample. The direction of this heat flow is parallel to the surround panel opening surface skin.

Now as per standards BS 874: Part 3: Section 3.1:1987, calibration tests were carried out using the same temperature and air velocity conditions as that would be used during actual testing of specimen. Thus, prior to carrying out calibration, air velocity needed to be quantified.

2.4.1 Measurement of Air Velocity of Metering Box and Cold Box

Air velocity was measured at various locations in the air curtain between baffle and surround panel in both metering box and cold box using hot wire digital anemometer (Fig. 2.15, Fig. 2.16 & Fig. 2.17). The air velocity was varied by changing the input voltage to the circulating fans keeping the baffle position fixed with respect to the surround panel. The sample used was 300mm extruded polystyrene insulation. Air velocities were measured at a distance of 5mm, 30mm, 60mm and 90mm from surround panel surface at positions P1, P2 and P3 in cold box and P4, P5 & P6 in metering box. P1, P2 and P3 are at distance of 450mm, 850mm and 1250mm respectively from the top edge of cold box opening aperture on surround panel while P4, P5 and P6 are at a distance 303mm, 688mm and 1073mm respectively from top edge of metering box opening projection on surround panel. Detailed specifications of the same given in Table 2.3.

Table 2.3 - Tabular representation of instrument/probe used with accuracy, precision, response time etc. are follows:

Instrument/Probe	Parameter measured	Range	Accuracy	Time Response
Hot Wire Anemometer	Air Velocity	0.1 ~ 25 m s ⁻¹	(±01.5°C	0.8s(approx)
	Air Temperature	0°C ~ 50°C	±0.25%)	0.8s(approx)



Fig. 2.15 Hot wire anemometer (HTC AVM-08)



Fig. 2.16 Hot wire anemometer setup for measuring air velocity

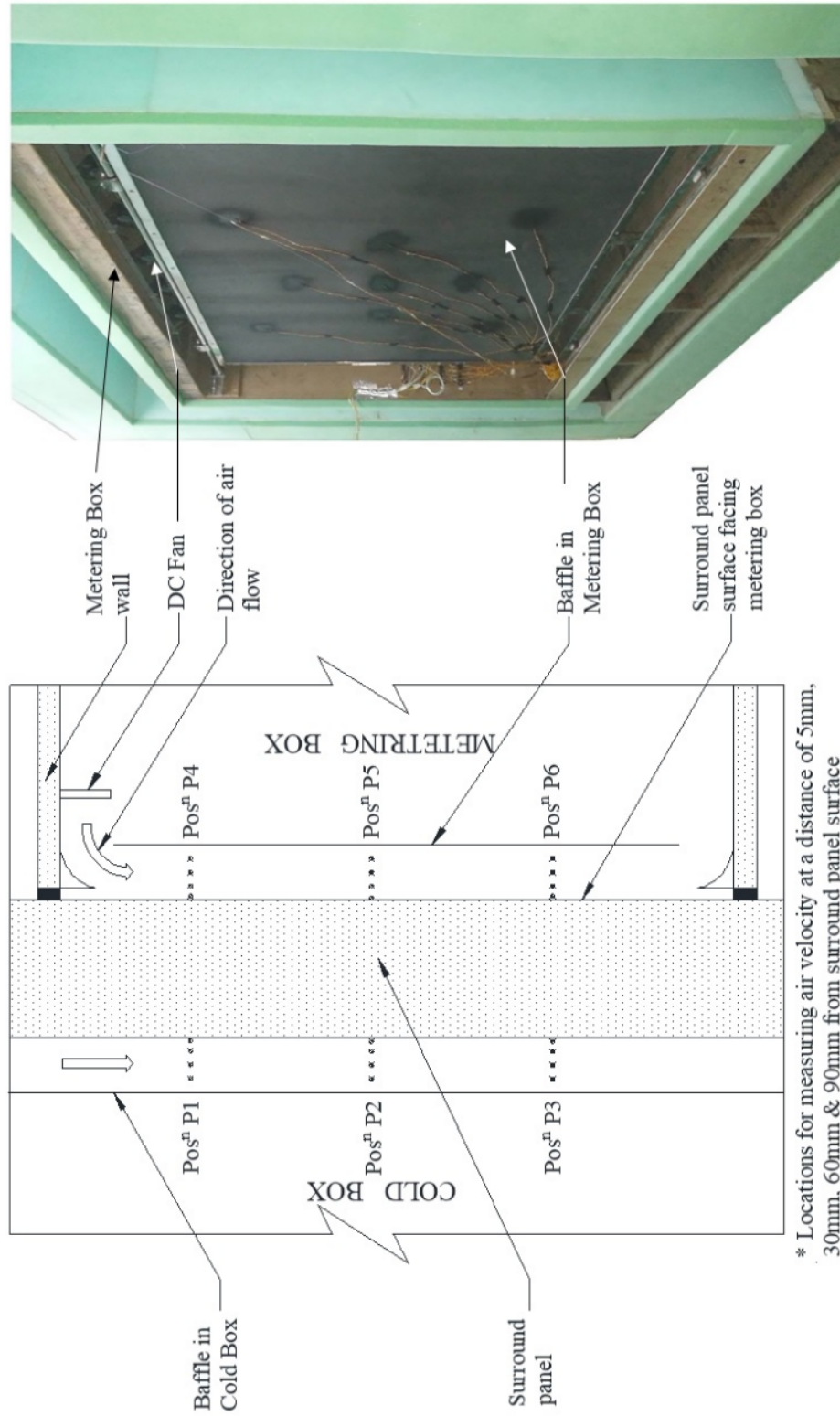


Fig. 2.17 Section of guarded hot box showing air velocity locations in metering box and cold box (D. Chowdhury et. al 2019)

Detailed air velocity profiles at various positions of metering box and cold box air are shown in Fig. 2.18 to Fig. 2.23. The Y-axis represents the vertical surround panel surface.

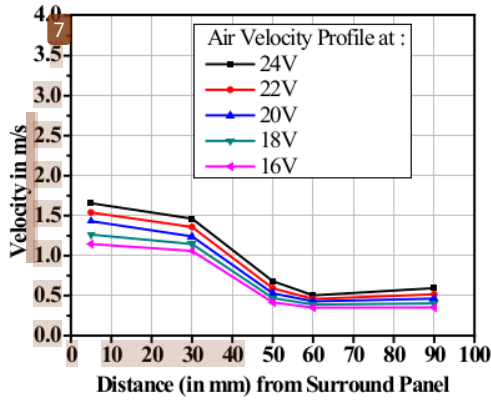


Fig. 2.18 Air velocity profile at P4 under varying input voltage to fan in metering box.

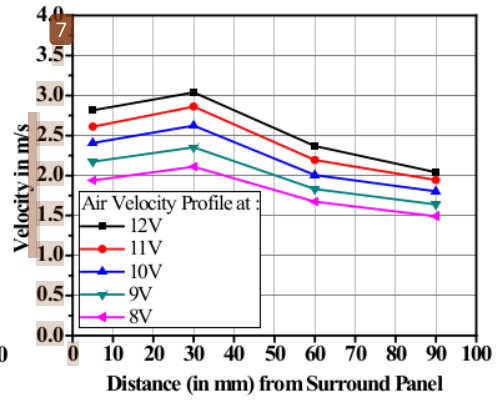


Fig. 2.19 Air velocity profile at P1 under varying input voltage to fan in cold box.

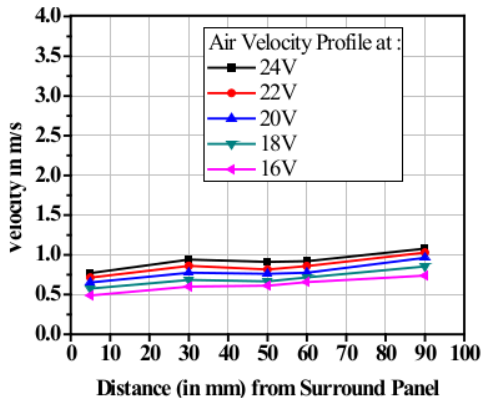


Fig. 2.20 Air velocity profile at P5 under varying input voltage to fan in metering box.

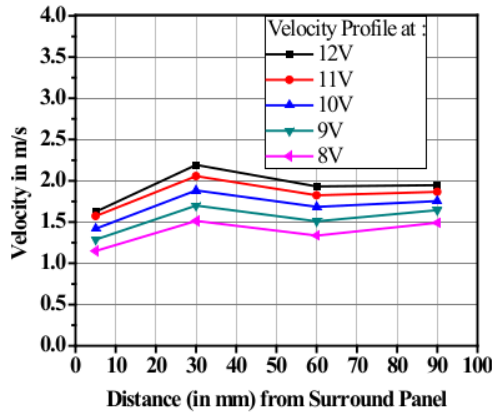


Fig. 2.21 Air velocity profile at P2 under varying input voltage to fan in cold box.

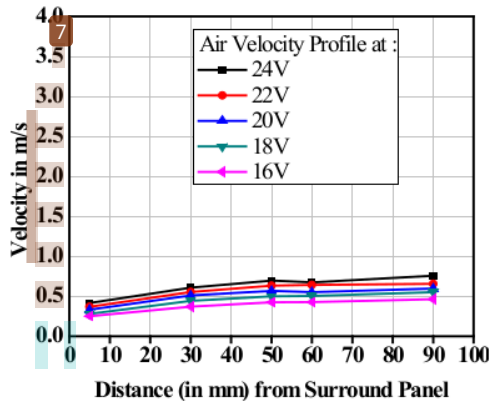


Fig. 2.22 Air velocity profile at P6 under varying input voltage to fan in metering box.

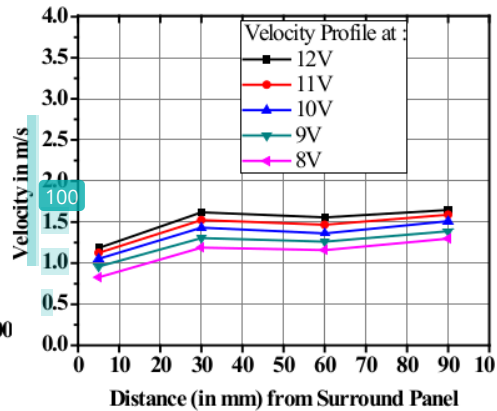


Fig. 2.23 Air velocity profile at P3 under varying input voltage to fan cold box.

Now as per BS EN ISO 12567-1:2010, which is based on BS EN ISO 8990:1996, the air velocity sensors should be aligned in the centre of the parallel flow. In the present setup the baffle plate was placed at distance of 120mm from the surround panel and the velocity at the location of 60mm from the baffle plate was be considered for calibration and testing. Fig. 2.24 shows the variation of metering box and cold box air velocity with input fan voltage.

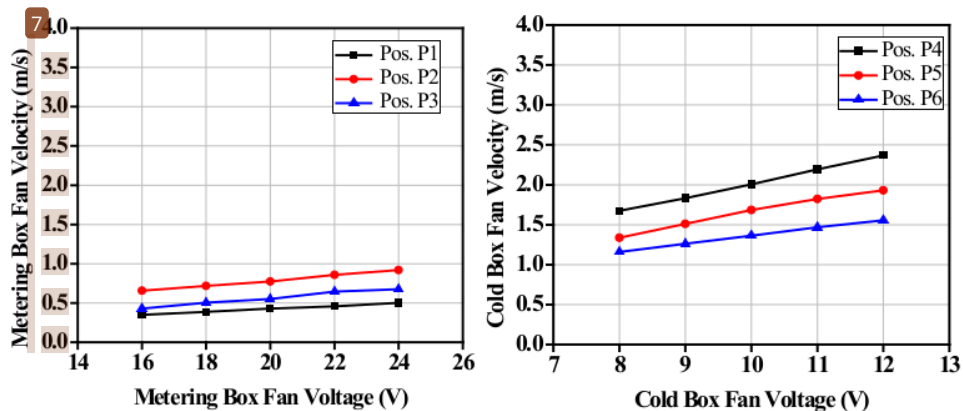


Fig. 2.24 Variation of air velocity with input fan voltage for at different positions.

94

Studies were also conducted to investigate the impact of sample thickness on the metering box and cold air velocity. Fig. 2.25 shows that sample thickness seemed to have almost no impact on the air velocity of metering box and cold box.

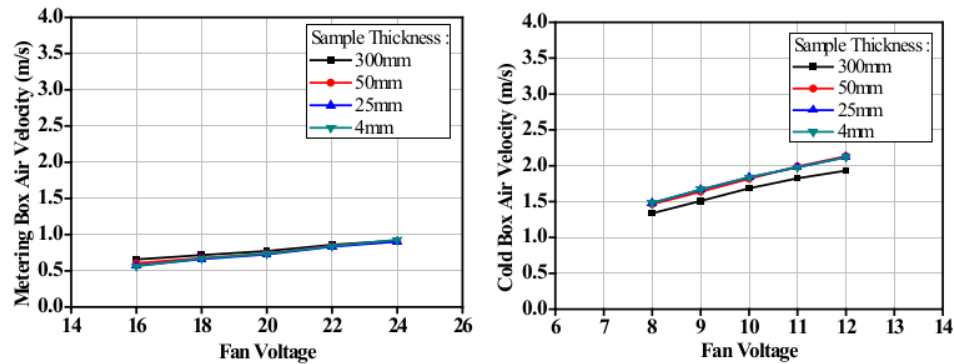


Fig. 2.25 Variation of fan velocity with input fan voltage for different sample thickness

2.4.2 Measurement of Extraneous Heat Transfer

The extraneous heat transfer, \dot{Q}_{Extra} mainly includes heat transfer occurring between the guard box and the metering box along contact point of metering box wall and the surround panel. It also includes the heat flow from metering box to ambient via surround panel (Fig. 2.26).

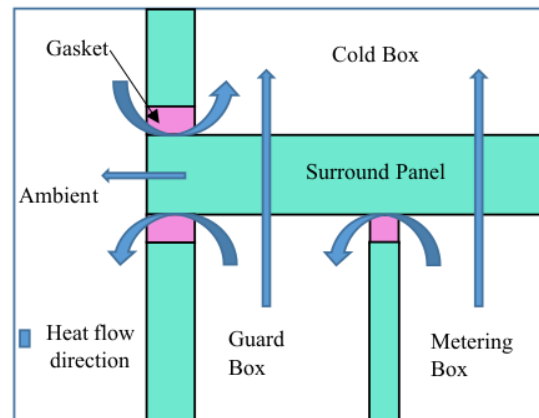


Fig. 2.26 Schematic heat flow regime at interface of metering box wall and guard box wall with surround panel (D. Chowdhury et. al 2019).

The extra heat transfer (\dot{Q}_{Extra}) is calculated as: Actual heat input into metering box ($\dot{Q}_{Heat\ I/P}$) – total metering box wall loss ($\dot{Q}_{MB\ Wall\ Loss}$) – calculated heat flow through surround panel (\dot{Q}_{SurPnl}) – Heat flow through sample (\dot{Q}_{Sample}).

For evaluation of \dot{Q}_{Extra} , sample made of extruded polystyrene insulation and having thickness 300mm was inserted in the sample holding aperture of the surround panel.

The test was performed with varying differential air temperature across the surround panel while keeping metering box fan velocity at 0.920 m/s and that of cold box fan velocity at

1.931 m/s. The metering box air temperature was held constant at 40°C while the cold box air temperature was varied from -5°C to 20°C (-5°C, 0°C, 10°C, 20°C). Subsequently tests were also carried out at fixed differential air temperature of 30°C (metering box air temperature at 40°C and cold box air temperature at 0°C) and at varying the fan velocity of metering box and cold box one at time.

From Fig. 2.27, it is evident that \dot{Q}_{Extra} increased with the increase in differential air temperature between metering box and cold box in a linear fashion. But change in air velocity of metering box and cold box seemed to have little impact on \dot{Q}_{Extra} (Fig. 2.28).

This can be due to the fact that with increase in differential air temperature, the total heat flow from metering box to cold box also increases proportionately resulting in an increased extra heat transfer. Detailed dataset with a sample calculation has been shown in Annexure A.

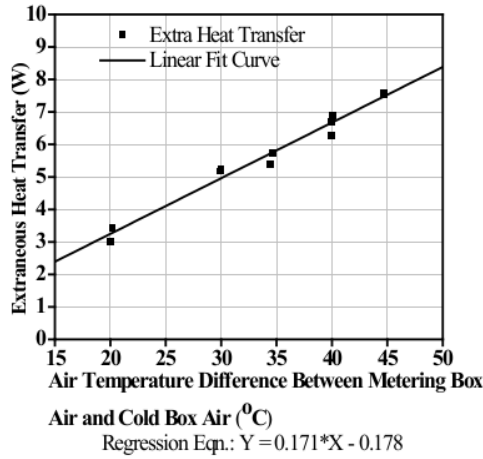


Fig. 2.27 Variation of extra heat transfer with differential air temperature.

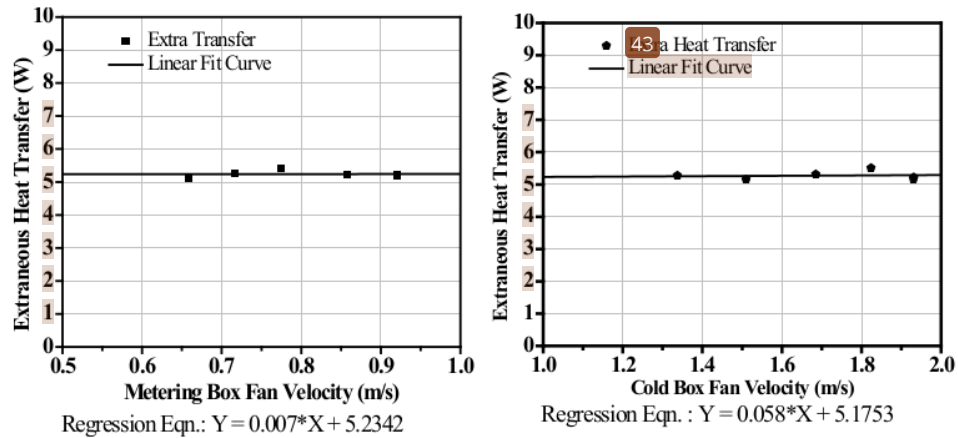


Fig. 2.28 Variation extraneous heat transfer with fan velocity

2.4.3 Measurement of Flanking Losses

Flanking loss, \dot{Q}_{Fl} occurs at the opening where the surround panel thickness is different from the specimen thickness (Fig. 2.29). This flanking loss is a function of sample thickness δx , the differential air temperature between metering box and cold box δt_{air} and the air velocities of metering box $u_{MB\ Air}$ and cold box $u_{CB\ Air}$ respectively.

Experientially it is determined by following equations (*BS EN ISO 8990: 1996*):

$$\dot{Q}_{Fl} = \dot{Q}_{Heat\ I/P} - \dot{Q}_{MB\ Wall\ Loss} - \dot{Q}_{Sur\ Pnl} - \dot{Q}_{Extra} - \dot{Q}_{Sample} \quad (2.2)$$

$$\dot{Q}_{Sample} = k_{xps} * A_{Sample} * \delta t_{Surface} / \delta x \quad (2.3)$$

where, $\delta t_{Surface}$ is differential temperature across sample surface,

k_{xps} is thermal conductivity of extruded polystyrene (0.033 W/m°C)

A_{Sample} is area of sample.



Fig. 2.29 50mm extruded polystyrene sample mounted inside surround panel of GHBC

To evaluate the effect of sample thickness on flanking loss, extruded polystyrene of thickness 25mm, 50mm and 100mm having dimensions of 500mm by 500mm have been used as samples. After placing the interface of edge of the sample and the surround panel aperture surface was properly sealed by applying silicon sealant. This was done to prevent any air leakages through the edge of the sample. For each sample, flanking loss is evaluated at δt_{air} of 40°C, 30°C & 20°C (Fig. 2.30). Calculation of flanking loss for δt_{air} equal to 20°C has been shown in Annexure A.

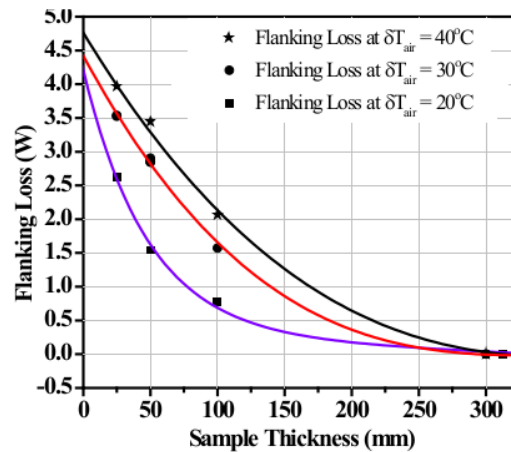


Fig. 2.30 Effect of δT_{air} on variation of flanking loss with sample thickness.

The metering box air temperature was kept fixed at 40°C for all cases, while the cold box air temperature was set at 0°C , 10°C and 20°C respectively. Similar study was conducted by *A. G. Lavine et al. (1983)* on a calibrated hot box system. Thereafter effect of varying metering box and cold box fan velocity on flanking loss vs sample thickness profile was also studied. The air temperatures inside the metering box and the cold box were at 40°C and 10°C respectively while the metering box fan velocity was varied and vice-versa. Similar tests were also conducted with metering box air temperature at 40°C and cold box air temperature at 10°C . Results are presented in Fig. 2.31 and Fig. 2.32.

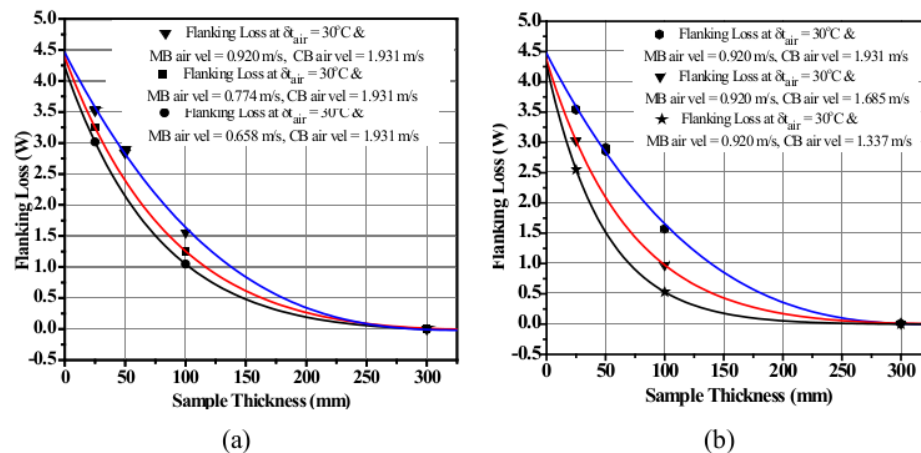


Fig. 2.31 Variation of flanking loss with sample thickness for varying metering box fan velocity (a) and cold box velocity (b) at $\delta T_{air} = 30^{\circ}\text{C}$.

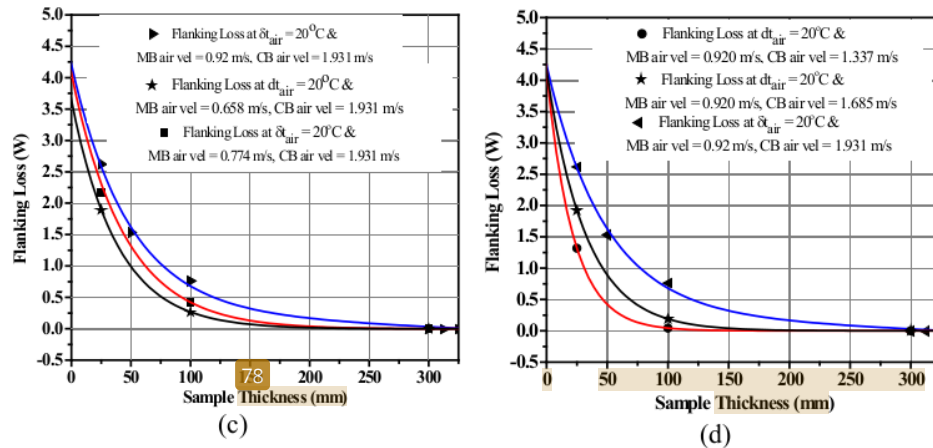


Fig. 2.32 Variation of flanking loss with sample thickness for varying MB fan velocity (c) and CB velocity (d) at $\delta t_{air} = 20^\circ\text{C}$.

Following gives equations of variation of flanking loss (Φ_{Fl}) with sample thickness (δx) with change in δt_{air} at fixed $u_{MB Air}$ (0.920 m/s) and $u_{CB Air}$ (1.931 m/s):

Flanking Loss at $\delta t_{air} = 40^\circ\text{C}$:

$$Y = 4.764 - 0.0329 * X + 0.000071 * X^2 - 0.000000045 * X^3 \quad (2.4)$$

Flanking Loss at $\delta t_{air} = 30^\circ\text{C}$:

$$Y = 4.420 - 0.0369 * X + 0.0001 * X^2 - 0.00000009 * X^3 \quad (2.5)$$

Flanking Loss at $\delta t_{air} = 20^\circ\text{C}$:

$$Y = 3.9274 * \exp(-X/47.89) + 0.2845 - 0.000843 * X \quad (2.6)$$

Following gives equations of variation of flanking loss (Φ_{Fl}) with sample thickness (δx) for varying metering box fan velocity and cold box fan velocity with δt_{air} fixed at 30°C :

Flanking Loss at $u_{MB Air} = 0.920$ m/s, $u_{CB Air} = 1.685$ m/s:

$$Y = 4.5714 * \exp(-X/71.7963) - 0.2228 + 0.0005 * X \quad (2.7)$$

Flanking Loss at $u_{MB Air} = 0.920$ m/s, $u_{CB Air} = 1.337$ m/s:

$$Y = 4.3075 * \exp(-X/48.7822) - 0.0324 + 0.00008 * X \quad (2.8)$$

Flanking Loss at $u_{MB Air} = 0.774$ m/s, $u_{CB Air} = 1.931$ m/s:

$$Y = 4.9612 * \exp(-X/93.772) - 0.5886 + 0.0013 * X \quad (2.9)$$

Flanking Loss at $u_{MB Air} = 0.658$ m/s, $u_{CB Air} = 1.931$ m/s:

$$Y = 4.5501 * \exp(-X/80.055) - 0.3296 + 0.0007 * X \quad (2.10)$$

Following gives equations of variation of flanking loss (Φ_{Fl}) with sample thickness (δx) for varying metering box and cold box air velocity with δt_{air} fixed at 20°C :

Flanking Loss at $u_{MB Air} = 0.920$ m/s, $u_{CB Air} = 1.685$ m/s:

$$Y = 4.1555 \cdot \exp(-X/32.4621) - 0.0015 + 0.0000038 \cdot X \quad (2.11)$$

Flanking Loss at $u_{MB \text{ Air}} = 0.920 \text{ m/s}$, $u_{CB \text{ Air}} = 1.337 \text{ m/s}$:

$$Y = 4.1287 \cdot \exp(-X/21.898) - 0.0000178 + 0.00000004585 \cdot X \quad (2.12)$$

Flanking Loss at $u_{MB \text{ Air}} = 0.774 \text{ m/s}$, $u_{CB \text{ Air}} = 1.931 \text{ m/s}$:

$$Y = 4.0785 \cdot \exp(-X/44.651) - 0.0177 + 0.00004375 \cdot X \quad (2.13)$$

Flanking Loss at $u_{MB \text{ Air}} = 0.658 \text{ m/s}$, $u_{CB \text{ Air}} = 1.931 \text{ m/s}$:

$$Y = 3.6426 \cdot \exp(-X/38.4969) - 0.0055 + 0.00001385 \cdot X \quad (2.14)$$

From the variation of flanking loss with fan velocity, it can be observed that the span of the graph is much wider for variation of flanking loss with cold box air velocity ($u_{CB \text{ Air}}$) as compared to that of metering box air velocity ($u_{MB \text{ Air}}$). This means that variation of cold side air stream velocity had a more dominant effect on flanking loss heat transfer as compared to hot side air stream. Moreover, for differential air temperature of 30°C, the flanking loss was much more as compared to that at 20°C. This could be attributed to the fact that under reduced differential air temperature across the sample, the total heat flow from metering chamber to cold box reduces. As a result, flanking loss had also reduced proportionately.

2.5 Performance evaluation of Metering Box and Cold Box

300mm extruded polystyrene insulation was inserted in the sample holding aperture such that entire surround panel achieves a uniform thickness. The set-point of metering box was kept at 40°C and the cold box air temperature had been varied (0°, 10°, and 20°C). The test was conducted for a minimum of eight to ten hours.

Now as per BS EN ISO 8990:1996, under steady state, the controllers should keep any random temperature fluctuations and long-term drifts within one percent of the air-to-air temperature difference over the specimen over a period of eight hours.

Table 2.4 shows the maximum fluctuations of air temperatures in metering box and cold box. All the calculations were made after the air temperatures and surface temperatures in the metering box, cold box and guard box had reached their respective set points and stabilised (Fig. 2.33, Fig. 2.34). Fig. 2.35 shows the metering box wall loss. It is evident from the results that the fluctuations were very much within the prescribed limits.

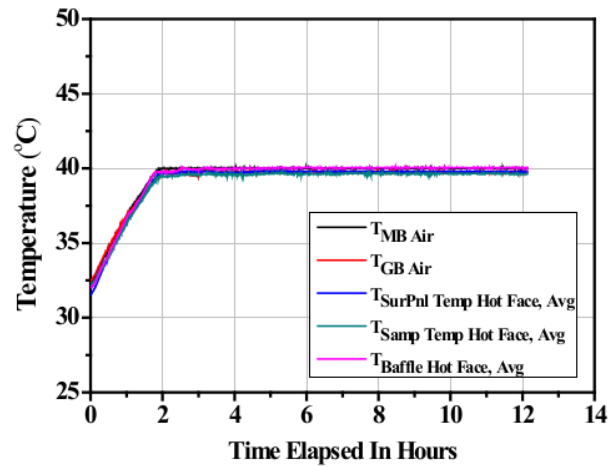


Fig. 2.33 Variation of hot box temperature profile with time

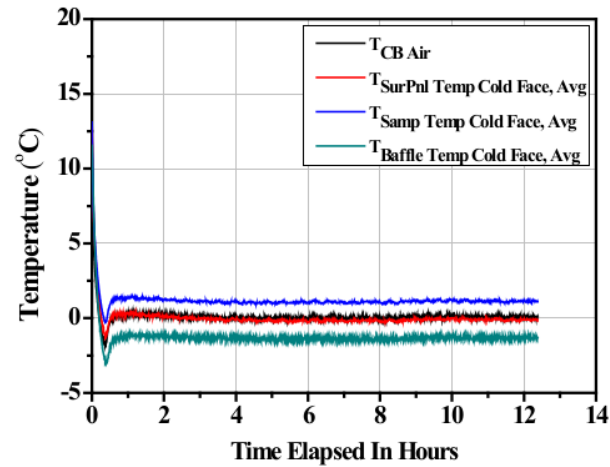


Fig. 2.34 Variation of cold box temperature profile with time

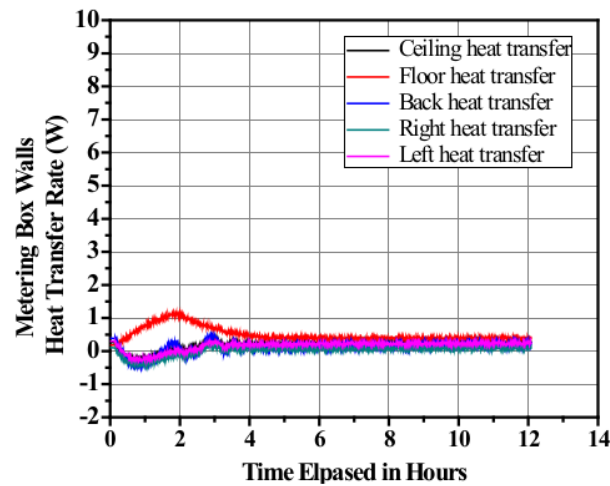


Fig. 2.35 Variation of metering box wall losses with time

Table 2.4 - Maximum fluctuations of air temperatures in metering box and cold box

Differential Air Temperature between Metering Box and Cold Box [°C]	1% of the air-to-air temperature difference across the sample [°C]	Steady State Average air temperature of Metering Box [°C]	Absolute Maximum Fluctuation in air temperature of MB [°C]
40.10	0.40	40.02	0.0499
29.99	0.30	40.00	0.0563
20.16	0.20	40.01	0.0762
Differential Air Temperature between Metering Box and Cold Box [°C]	1 % of the air-to-air temperature difference across the sample [°C]	Steady State Average air temperature of Metering Box [°C]	Absolute Maximum Fluctuation in air temperature of CB [°C]
40.10	0.40	-0.17	0.2034
29.99	0.30	10.11	0.1790
20.16	0.20	19.90	0.2286

2.6 Uncertainty Analysis of U-value Measurement

Uncertainty analysis involves estimating the extent to which uncertainties in individual measurements influence the calculated results.

The combined uncertainty in U-value or overall heat transfer coefficients measurement can be analysed using law of propagation of uncertainty as per GUM method (*JCGM 100:2008*). The combined variance $u_c^2(y)$ can be represented as sum of variances of each term associated with output.

$$\text{In other words, } u_c^2(y) \equiv \sum_{i=1}^n u_i^2(y) \quad (2.15)$$

$$\text{Now we know, } U = \emptyset_{\text{Sample}} / (A * \delta t_{\text{air}}) = \emptyset_{\text{Sample}} / \{A * (T_{\text{MB Air}} - T_{\text{CB Air}})\}. \quad (2.16)$$

$$\text{So as per GUM Method the combined uncertainty is expressed as,} \quad (2.17)$$

$$u_c^2(U) = u_c^2(\emptyset_{\text{Sample}}) + u_c^2(A) + u_c^2(\delta t_{\text{air}}) \quad (2.18)$$

$$u_c^2(\delta t_{\text{air}}) = u_c^2(T_{\text{MB Air}}) + u_c^2(T_{\text{CB Air}}) \quad (2.19)$$

$$u_c^2(\emptyset_{\text{Sample}}) = u_c^2(\emptyset_{\text{Heat I/P}}) + u_c^2(\emptyset_{\text{MB Wall Loss}}) + u_c^2(\emptyset_{\text{extra}}) + u_c^2(\emptyset_{\text{FI}}) + u_c^2(\emptyset_{\text{SurPnl}}) \quad (2.20)$$

Now, the measurements of air temperature and surface temperatures were done using temperature sensors which were thoroughly calibrated using a constant temperature oil

bath and proper cold junction compensation were provided for thermocouples during calibration procedure.

Overall system calibration was performed during estimation of \emptyset_{extra} whereby a calibration panel of same thickness and material as that of surround panel was used. This further reduces the uncertainty of measurements. Moreover, during all calibration and thermal transmittance runs, at least three to four data acquisitions were made to check for repeatability of the results. The measurements of length and breadth of the sample were made a number of times to reduce any chance error during measurement. The uncertainty in measurement of area of sample can be considered as zero.

In this section uncertainty analysis in estimation of \emptyset_{extra} has been presented.

$$\emptyset_{extra} = \emptyset_{MB \text{ to } CB \text{ measured}} - \emptyset_{MB \text{ to } CB \text{ calculated}} \quad (2.21)$$

$$\emptyset_{MB \text{ to } CB \text{ measured}} = \emptyset_{Heaters} + \emptyset_{Fans} - \emptyset_{MB \text{ Avg Wall Loss}} \quad (2.22)$$

$$\emptyset_{MB \text{ to } CB \text{ calculated}} = k * A * \Delta T / \delta x \quad (2.23)$$

$$u_c^2(\emptyset_{extra}) = u_c^2(\emptyset_{Heaters}) + u_c^2(\emptyset_{Fans}) + u_c^2(\emptyset_{MB \text{ Avg Wall Loss}}) + u_c^2(\Delta T) \quad (2.24)$$

$$u_c^2(\emptyset_{Heaters}) = u_c^2(TV) + u_c^2(TC) + u_c^2(PV) + u_c^2(PC) \quad (2.25)$$

$$u_c(\emptyset_{Heaters}) = \sqrt{(0.000848^2 + 0.000001^2 + 0.0001319^2 + 0.000005^2)} \quad (2.26)$$

$$= 8.5 * 10^{-4} \quad (2.27)$$

$$= 0.00085 \quad (2.28)$$

$$u_c^2(\emptyset_{Fans}) = \sqrt{(0.000013^2 + 0.00000026^2)} \quad (2.29)$$

$$= 1.30026 * 10^{-5} \quad (2.30)$$

$$u_c(\emptyset_{Fans}) = 0.000013 \quad (2.31)$$

$$u_c^2(\emptyset_{MB \text{ Avg Wall Loss}}) = 0.002507685 \quad (2.32)$$

$$u_c^2(\Delta T) = u_c^2(\Delta T_{SurPnl \text{ Surface}}) + u_c^2(\Delta T_{Samp \text{ Surface}}) \quad (2.33)$$

$$= u_c^2(T_{SurPnl \text{ Temp Hot Face, Avg}}) + u_c^2(T_{SurPnl \text{ Temp Cold Face, Avg}}) \quad (2.34)$$

$$+ u_c^2(T_{Samp \text{ Temp Hot Face, Avg}}) + u_c^2(T_{Samp \text{ Temp Cold Face, Avg}}) \quad (2.35)$$

$$u_c(\Delta T) = \sqrt{(0.000342^2 + 0.000728^2 + 0.001457^2 + 0.001228^2)} \quad (2.36)$$

$$= 0.00207 \quad (2.37)$$

So,

$$u_c(\emptyset_{extra}) = \sqrt{(0.00085^2 + 0.000013^2 + 0.002507685^2 + 0.00207^2)} \quad (2.38)$$

$$= 0.00332 \quad (2.39)$$

2.6 Conclusion

In this chapter detailed description ⁹¹ of the guarded hot box test setup has been presented. A detailed overview of the control strategy implemented in the metering box and cold box has been explained. The metering box wall loss was within ten percent of the power input to the metering box. The fluctuations in air temperature in metering box and cold box were well within the prescribed limits (one percent) as per BS EN 8990:1996. Then after the extraneous heat transfer and flanking losses have been estimated for the test setup. The extraneous heat transfer seemed to have increased linearly with increase in differential air temperature whereas change in air velocity of metering box and cold box fan seemed to have little impact over the extraneous heat transfer.

Using these values, the overall heat transfer coefficient of any specimen can be accurately determined. Thereafter detailed description of uncertainty analysis has been presented as well.

***CHAPTER 3 – EVALUATION OF
THERMAL PERFORMANCE OF
BUILDING ENVELOPE COMPONENTS
(OPAQUE WALLS, ROOF AND
GLAZINGS)***

3.1 Introduction

Primary function of a building is to protect the users from the influence of outside weather or environment and provide desired thermal comfort. The building space may be controlled or uncontrolled. Controlled means ¹⁰² the temperature and relative humidity within the space is maintained with the help of some form of air conditioning system and uncontrolled meaning no temperature or humidity control is done. The building envelope acts as a filter and allows for some desirable aspect of environment to come in such as natural sunlight, natural ventilation but at the same time cuts off or reduces the heat radiation, excess temperature, moisture ingress, glare etc. As per *Model Building Bye-Laws (2016)*, based on the end use activity buildings can be categorised as: Residential Building, Institutional ²³ Building, Educational Building, Assembly Building, Mercantile Building, Business Building, Industrial Building, Hazardous Building, Storage Building, Mixed Land Building and Wholesale Establishment. Buildings can also be classified based on design and height as: Detached Building, Multi-storeyed Building or High Rise Building and Semi-detached Building. Building envelope includes doors, windows, roof, foundation, floor and all the components such as structural masonry and insulation. In this chapter, we mainly focus our study on typical residential building constructions. Building envelope mainly regulates indoor thermal comfort. So thermal performance evaluation of building envelope is of utmost importance. This chapter involves experimental evaluation of thermal properties of building envelopes such as masonry walls, roofs and glazing over entire range of differential temperature as experienced by building in various climatic zones. Overall heat transfer coefficient or U-value is determined for various configurations of masonry wall, roof and glazing. Estimation of the U-value of the opaque components is a crucial parameter for estimating the heating or cooling demand for maintaining appropriate thermal comfort for any climatic zones. It is an important tool while conducting building energy simulation studies.

Now U-value of building envelope components can be determined by several methods:

(a) In situ thermal transmittance measurements as per *BS ISO 9869:2014* and *ASTM C1155* wherein the overall heat transfer coefficient ⁶¹ can be determined by measuring the heat-flow through the element with the help of heat-flow meter and the air temperature ²⁸ on both sides of the sample under steady state conditions. Calculations are based on average values of heat flow rate and air temperatures averaged over a reasonably long duration of time in order to get a fairly estimate of the steady-state condition (*D. J. Harris, 2012*).

(b) Analytical calculation methods using *EN ISO 6946:2007* which requires the knowledge of thickness, thermal conductivity of each layer of wall elements. (F. Asdrubali et. al, 2014).

(c) Overall thermal transmittance of building walls can also be determined in-situ by infrared thermography (B. Tejedor et. al 2017, P. A. Fokaodes et. al 2011, R. Albatici et. al 2010).

(d) Experimentally it can be determined by Guarded Hot Box in accordance with *BS EN ISO 8990:1996* and Calibrated Hot Box in accordance with *BS EN 874 – 3.2:1990*.

Among these methods, only Hot Box Testing methods gives in true sense steady state overall heat transfer coefficient. The Guarded Hot Box Testing method provides a higher degree of accuracy and is more flexible in comparison to calibrated hot box. Since constructions used in traditional buildings are typically non-homogeneous, therefor determination of U-value using guarded hot box is accurate and reliable.

Three different typical wall envelope configurations and a typical roof system generally used in traditional residential buildings are selected for study. Study is also conducted on a double-glazing unit incorporated with warm edge spacer.

3.2 Opaque Walls

Opaque wall components are the vertical structures which isolates the interior space from the outer environment or partitions the interior spaces. It generally covers the four sides of a typical building. Broadly a building wall can be classified as load bearing wall and non-load bearing wall. Load bearing wall is a structural component of a building which supports the weight of the roof and upper floors of a building. It supports structural members like beams, slab and walls on above floors above. Put simply, it is designed to cater the vertical load. A non-load bearing wall on the other hand doesn't cater the structural load of a building and holds up only itself. Non-load bearing walls may include interior partition walls whose function is to divide the structure into rooms. Opaque wall may be generally in either or combination following forms as follows: Precast Concrete Wall, Retaining Wall, Masonry Wall, Pre-Panelised Load Bearing Metal Stud Walls, Brick Wall, Stone Wall, Hollow Concrete Block, Hollow Bricks etc.

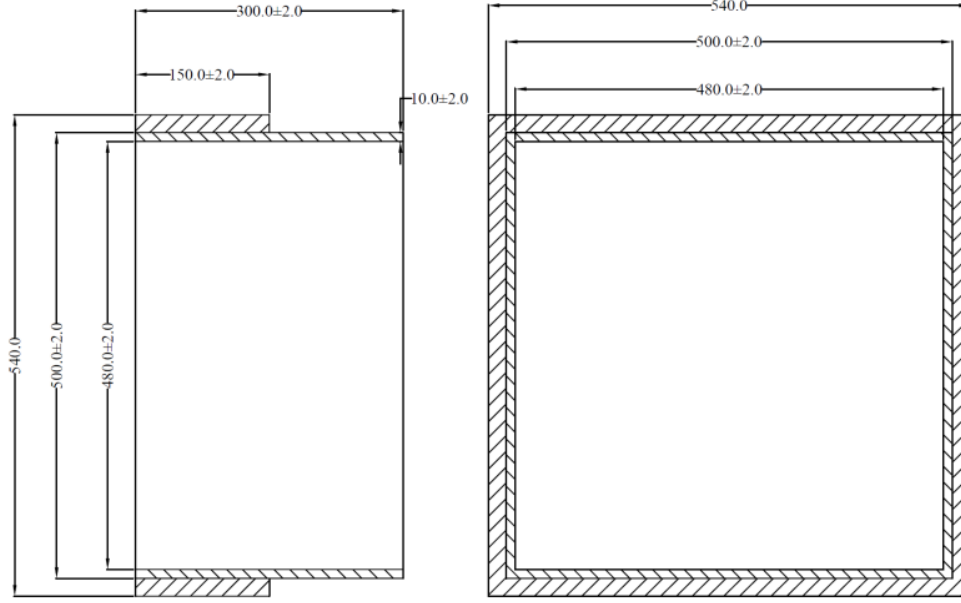
In the present study we concentrate upon brick wall made of burnt red clay bricks. In conventional residential households in India, walls are generally made of brick, mortar, plaster and layer of putty and paint on the outside and inside. According to Bureau of Indian Standards 1077:1992, standard modular size of common building bricks is 190mm(L) x 90mm(W) x 90mm(H) or 40mm(H) and that of non-modular bricks are 230mm(L) x

110mm(W) x 70mm(H) or 30mm(H). But practically in sites 230mm(L) x 110(H) x 110(W) or 230mm(L) x 100mm(W) x 75mm(H) is used normally. In a city like Kolkata average brick size is approximately 230mm(H) x 125(W) x 75mm(H). It has been a common practice to use 230mm brick wall with 12.5mm cement plaster on either side for outside walls and 125mm brick wall with 12.5mm cement plaster on either side for partition walls. Nowadays, use of 125mm brick wall having 12.5mm cement plaster on either side for outside walls and 75mm brick wall with 12.5mm cement plaster as inner partition walls have also become common practice. Present work is directed towards determining the thermal performance of conventional 125mm brick walls, roof and double-glazing unit.

3.2.1 Sample Construction and Description

For carrying out Guarded hot box testing of masonry walls and roof, a wooden sample holding frame was constructed (Fig. 3.1). The frame was treated to make it impervious to moisture as much as possible. Wooden guides were also provided so that the masonry sample could be built right in the centre position.

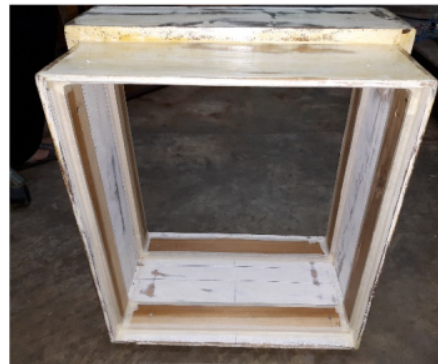
125mm masonry wall (with using stretcher bonds for bricks) was built inside the frame itself using 125mm thick burnt red clay brick (Fig. 3.2) and cement mortar bought from locally available vendor. ⁵⁰ Commercially available Portland Pozzolana Cement (PPC) conforming to *IS 1489 Part 1 (1991, Reaffirmed 2005)* was used. Then after 12.5mm or 0.5 inches cement plaster was applied on both sides (Fig. 3.3). Requisite amount of water was added for proper curing. The whole wall assembly was left to cure for at least two and half weeks. This was the reference Sample WI (Fig. 3.4). After curing, the frame along with the sample was loaded into the surround panel (Fig. 3.5) for testing. The composition of plaster and mortar was cement and sand in the ratio of 1:6 (*IS 2250 - 1981*). Area of the masonry constructed in the sample holding frame is 480mm by 480mm. The interface between wooden sample holding frame and the surround panel was sealed with silicone sealant and masking tape to form an air tight seal so that there was no direct leakage of heat from metering box to cold box.



Sectional side view and front view of the frame



Front View



Back View

Fig. 3.1 Sample Holding Frame



Fig. 3.2 Burnt clay brick



Fig. 3.3 Brick wall being built inside the sample holding frame.



Fig. 3.4 Sample WI – 125mm brick wall with 12.5mm plaster inside sample holding frame



Fig. 3.5 Sample WI loaded into sample holding aperture

Plastered surface was properly smoothed and prepared for application of primer. Two coats of acrylic cement primer were applied on both the sides and left to dry. This was Sample WII (Fig. 3.6). Sample WIII was made from sample WII by applying two coats of water based plastic paint (magenta colour) on side which would face metering box (Fig. 3.7). The other side of the wall was left unchanged. Table 3.1 gives a brief description of all the wall samples.

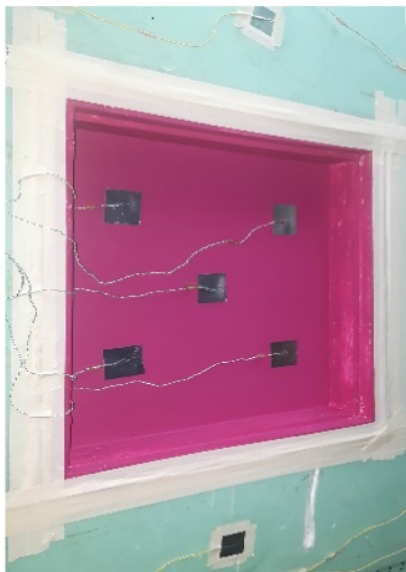


(a) Sample WII prepared from Sample WI



(b) Sample WII mounted on surround panels

Fig. 3.6 Sample WII



(a) Side of sample facing metering box.



(b) Side of sample facing cold box.

Fig. 3.7 Sample WIII loaded onto surround panel.

Table 3.1 - Detailed description of the wall samples

Sl. No.	Sample Description	Sample Surface facing Metering Box	Sample Surface facing Cold Box	Identification
1.	12.5mm cement plaster + 125mm brick wall + 12.5mm cement plaster	Cement plaster	Cement plaster	WI
2.	Acrylic cement primer + WI + Acrylic cement primer	Cement primer	Cement primer	WII
3.	Water based plastic paint (magenta colour) + WII	Plastic paint	Cement primer	WIII

For better understanding of the results, spectrophotometric tests (of various textured surfaces Fig. 3.8) were conducted to study the solar reflectance characteristics of the sample surfaces. Measurement of reflectance spectra was conducted using Perkin Elmer make UV-Vis-NIR spectrophotometer LAMDA 950 which has a wavelength range of 190 – 3200 nm (Central Glass & Ceramic Research Institute). The spectrophotometric test of diffuse reflectance was carried out using 150 mm integrating sphere for the range 250 nm to 2500 nm. From the results obtained and using the equation $\alpha + \rho + \tau = 1$, solar absorptance characteristics of the surfaces are obtained (Fig. 3.9) where α is absorptance, ρ is reflectance and τ is transmittance. Using *ASTM E903-93*, reflectance and absorptance over visible spectrum (Table 3.2a) and over entire solar spectrum (Table 3.2b) has been calculated.

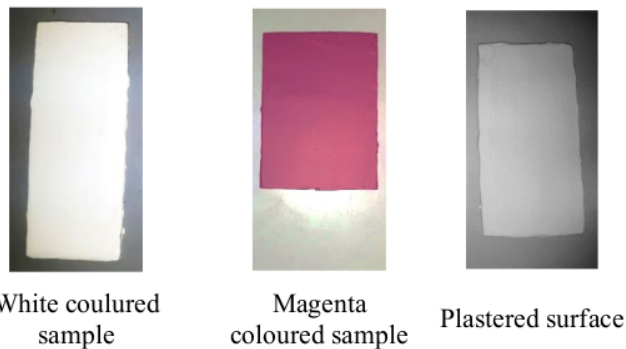


Fig. 3.8 Sample surfaces prepared for spectrophotometry

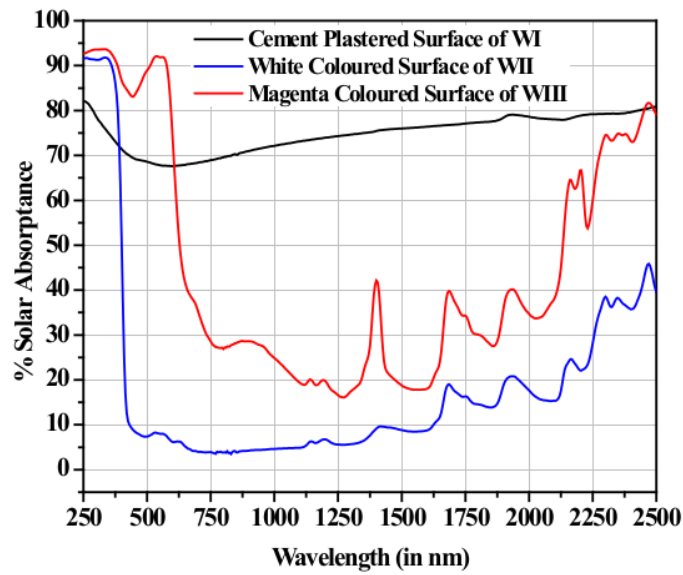


Fig. 3.9

Table 3.2a - Reflectance and absorbance of sample surfaces calculated over visible spectrum.

Sample Name	% ρ	%α
Cement Plastered Sample Surface of WI	31.39	68.61
White Coloured Sample Surface of WII	90.50	9.50
Magenta Coloured Sample Surface of WIII	32.54	67.46

Table 3.2b - Reflectance and absorbance of sample surfaces calculated over entire spectrum.

Sample Name	% ρ	%α
Cement Plastered Sample Surface of WI	29.23	70.77
White Coloured Sample Surface of WII	88.84	11.16
Magenta Coloured Sample Surface of WIII	49.29	50.71

3.2.2 Experimental Procedure

After the samples had been properly mounted and sealed in the sample aperture, ³² the surround panel was sandwiched between the hot side and cold side. Appropriate set points of metering box and cold box were set in the Agilent VEE based interface software. The

distance between baffle plate surface and surround panel surface was kept fixed at 120mm in both metering box and cold box.

As per *BS EN ISO 8990:1996*, steady state is said to have been achieved when average measurements of U-value, $\dot{Q}_{Heat\ I/P}$ (total heat input to metering box), temperature of metering box air and cold box air ($T_{MB\ Air}$, $T_{CB\ Air}$) along with surface temperatures of samples and $\dot{Q}_{MB\ Wall\ Loss}$ (Metering box wall loss) from two successive periods of at least three hours after near stability, vary within one percent. In present study, variation of overall heat transfer coefficient of the samples with varying differential air temperature (δt_{air}) was studied. The metering box air temperature was set at 40°C while that of cold box air temperature was varied at 0°C, 10°C & 20°C so as to maintain a minimum δt_{air} at 20°C as per standard. Therefore, at steady state the temperature fluctuations were also calculated to ensure that the fluctuations in air temperature did not exceed one percent of δt_{air} . For each set point, repeated number of tests were conducted to check the consistency of the test setup results and it exhibited similar tendency. The air velocity in metering box was kept constant at 0.920 m/s while in cold box the air velocity was kept constant at 1.931 m/s. The standard deviation of the results was also calculated.

Before conducting study on actual wall sample, the impact of wooden sample holding frame on the overall heat transfer coefficient of the sample needed to be studied. For this purpose, the sample holding frame wall completely filled with 300mm extruded polystyrene insulation. The sample holding frame filled with insulation was loaded on to the sample holding aperture. Then the test was conducted with environmental conditions similar to that would be during actual testing of the samples. The difference in heat flow through the surround panel (along with the wooden frame) and surround panel with 300mm extruded polystyrene insulation was calculated.

Additional studies were also conducted to study the impact of varying convective heat transfer rate on overall heat transfer coefficient of the masonry walls. The experiment was conducted at 30°C and 20°C differential air temperature across the sample. For each differential air temperature, air velocity was also varied in the metering box and cold box respectively.

In first condition, metering box air set point was kept at 40°C, while cold box air set point was kept at 10°C. Keeping this differential temperature fixed, U-value of the sample was determined at metering box air velocity of 0.920 m/s, 0.658 m/s and 0.774 m/s while cold box fan velocity was kept constant at 1.931 m/s. U-value was also determined at cold box fan velocity of 1.931 m/s, 1.685 m/s and 1.337 m/s while keeping metering box fan velocity

at 0.920 m/s at same differential air temperature. The minimum test setup run time was about twelve hours. Air velocity was varied in the metering chamber and cold box by varying the supply voltage to the circulation fans installed in the metering box and cold box. In second condition, metering box air set point was kept at 40°C, while cold box air set point was kept at 20°C. Keeping this differential temperature fixed, U-value of the sample was determined again at varying velocities of metering box and cold box air velocity similar to above condition.

3.2.3 Results

Comparative analysis of difference in extraneous heat flow (\dot{Q}_{extra}) through the surround panel structure with and without sample holding frame inserted are presented in Table 3.3. From the results it is evident that effect of frame on heat transfer through the surround panel is very less.

Table 3.3 - Variation in extraneous heat transfer.

Test no.	δt_{air} (°C)	\dot{Q}_{extra} with 300mm xps insulation placed in wooden frame used as sample (W)	\dot{Q}_{extra} with 300mm xps insulation placed as sample (W)	Variation in extra heat transfer (%)
1.	39.91	6.666	6.657	0.14
2.	39.75	6.679	6.629	0.75
3.	29.70	4.981	4.908	1.47
4.	29.67	4.958	4.904	1.09
5.	20.02	3.276	3.251	0.76
6.	19.93	3.274	3.235	1.19

The overall heat transfer coefficients (U-value) of the sample W1 along with the other detailed parameters such as total heat input to metering box ($\dot{Q}_{Heat\ I/P}$), flanking loss associated with the sample (\dot{Q}_{Fl}), total metering box wall loss ($\dot{Q}_{MB\ Wall\ Loss}$), actual heat flow occurring from metering box to cold box ($\dot{Q}_{MB\ to\ CB,\ measured}$), sample heat flow rate (\dot{Q}_{Sample}), extraneous heat transfer (\dot{Q}_{Extra}) are represented in Table 3.4, 3.5. The testing was conducted with metering box air velocity and cold box air velocity held constant at 0.920 m/s and 1.931 m/s.

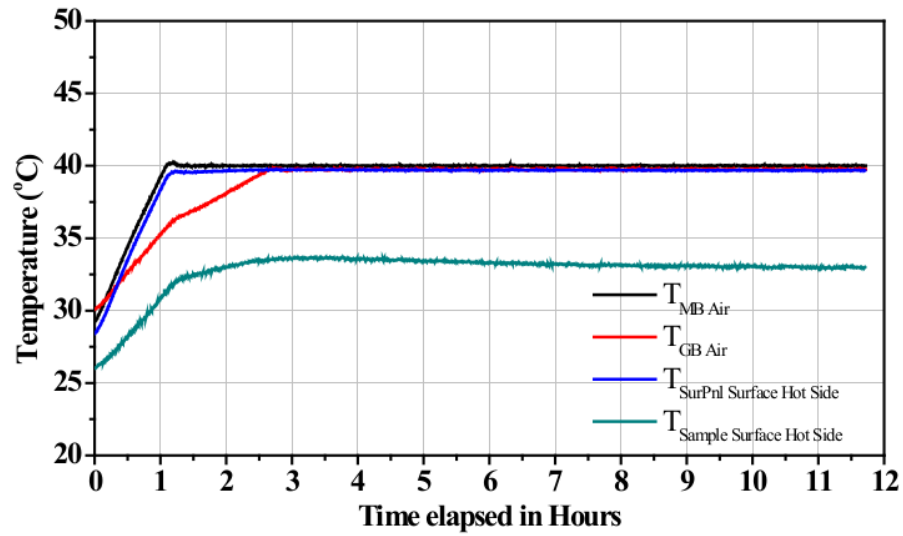
Table 3.4 - Testing report for Sample WI

Test no	$T_{MB\ Air}$ (°C)	$T_{CB\ Air}$ (°C)	δt_{air} (°C)	$\dot{Q}_{Heat\ IP}$ (W)	$\dot{Q}_{MB\ Wall\ Loss}$ (W)	$\dot{Q}_{MB\ to\ CB,\ measured}$ (W)	\dot{Q}_{FI} (W)	\dot{Q}_{Extra} (W)	$\Delta T_{Sur-Pnl\ Surface}$ (°C)	$\Delta T_{Samp\ Surface}$ (°C)	\dot{Q}_{Sample} (W)	U-value (W/m ² K)
1.	40.01	0.01	40.0	41.26	1.39	39.86	1.28	6.67	39.9	26.51	21.5	2.330
2.	40.01	-0.09	40.1	41.11	1.24	39.87	1.28	6.69	40.0	26.74	21.4	2.321
3.	40.01	-0.09	40.1	41.16	1.22	39.94	1.28	6.69	40.0	26.74	21.5	2.328
4.	40.01	10.11	29.9	31.65	1.40	30.25	0.87	4.94	29.7	19.94	16.7	2.417
5.	40.01	10.13	29.9	31.52	1.37	30.15	0.87	4.94	29.7	20.02	16.6	2.405
6.	40.01	19.96	20.0	21.71	1.37	20.34	0.34	3.26	19.8	13.49	11.6	2.503
7.	40.01	19.95	20.1	21.56	1.35	20.21	0.34	3.26	19.8	13.48	11.4	2.473

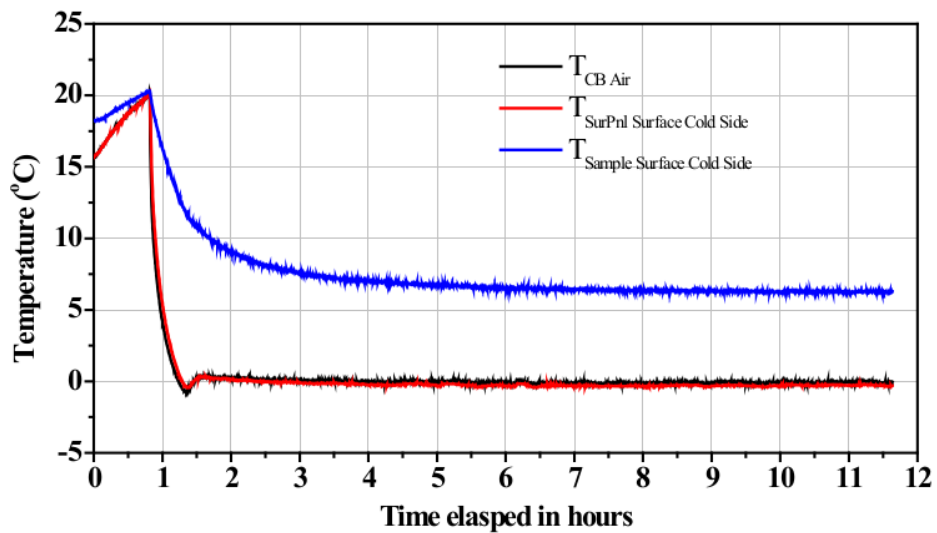
Table 3.5 - Fluctuations in air temperature and standard deviation of U-value for Sample WI

Test no	δt_{air} (°C)	U-value (W/m ² K)	Maximum fluctuations allowed as per BS EN ISO 8990:1996 (°C)	Maximum random fluctuations in air temperature (°C)		Average U-value (W/m ² K)	Standard deviation
				$T_{MB\ Air}$	$T_{CB\ Air}$		
1.	40.00	2.330	0.40	0.043	0.058		
2.	40.10	2.321	0.40	0.042	0.127	2.326	0.0048
3.	40.10	2.328	0.40	0.044	0.101		
4.	29.90	2.417	0.30	0.050	0.134	2.411	0.0082
5.	29.90	2.405	0.30	0.053	0.120		
6.	20.00	2.503	0.20	0.057	0.140	2.424	0.0209
7.	20.10	2.473	0.20	0.054	0.148		

Fig. 3.10 shows the variation of air temperature, sample surface temperature for sample WI having metering box air set point at 40°C and cold box air set point at 0°C. Fig. 3.11 shows the fluctuation in metering box air temperature and cold box air temperature is within 0.4°C.

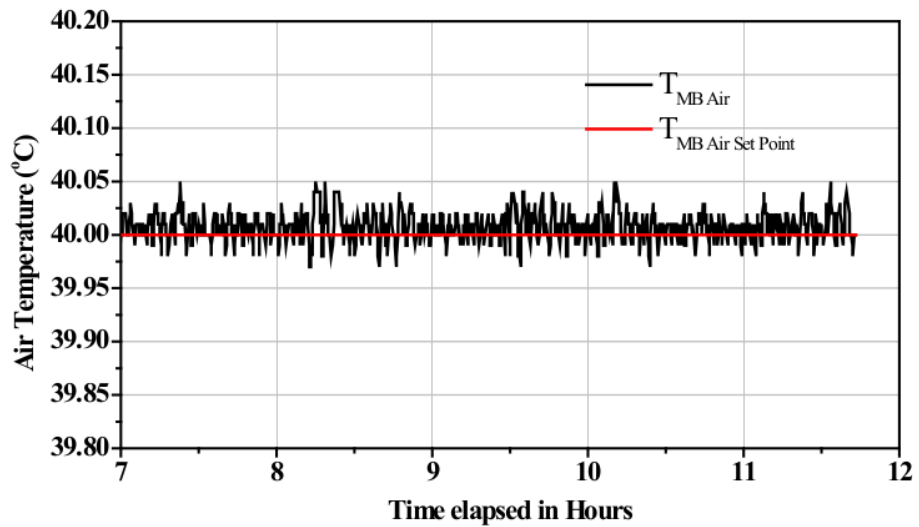


(a) Hot box temperature profiles for Sample WI

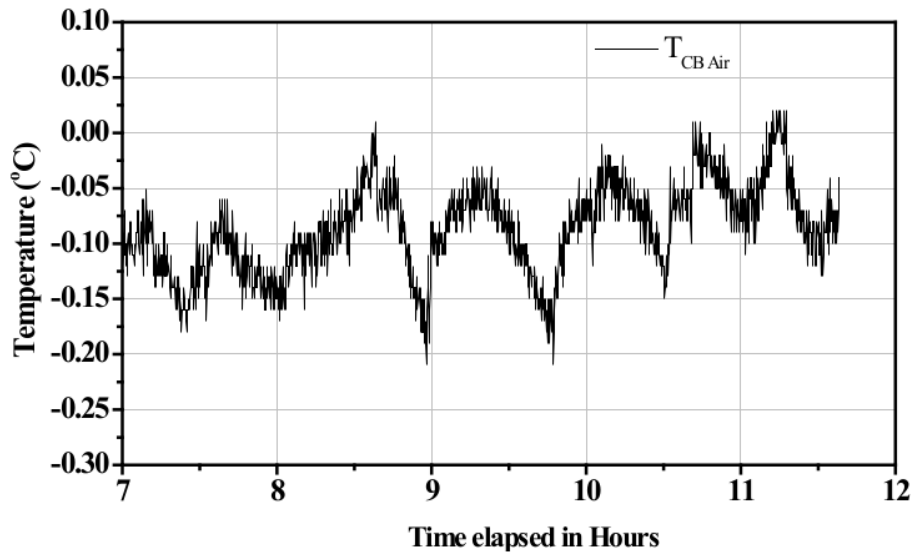


(b) Cold box temperature profiles for Sample WI

Fig. 3.10 Variation of air and surface temperature in metering box and cold box for Sample WI.



(a) Fluctuation in metering box air temperature with time during steady state for Sample WI



(b) Fluctuation in cold box air temperature with time during steady state for Sample WI

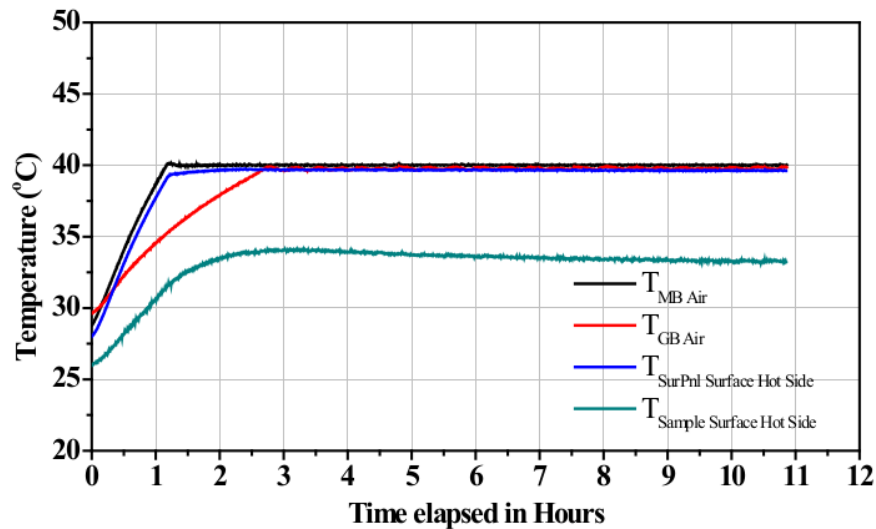
Fig. 3.11 Fluctuations in air temperature in Metering Box.

The overall heat transfer coefficients (U-value) of the sample WII along with the other detailed parameters as obtained from testing are represented in Table 3.6, 3.7. The testing was conducted with metering box air velocity and cold box air velocity held constant at 0.920 m/s and 1.931 m/s. Fig. 3.12 shows the variation of air temperature, sample surface

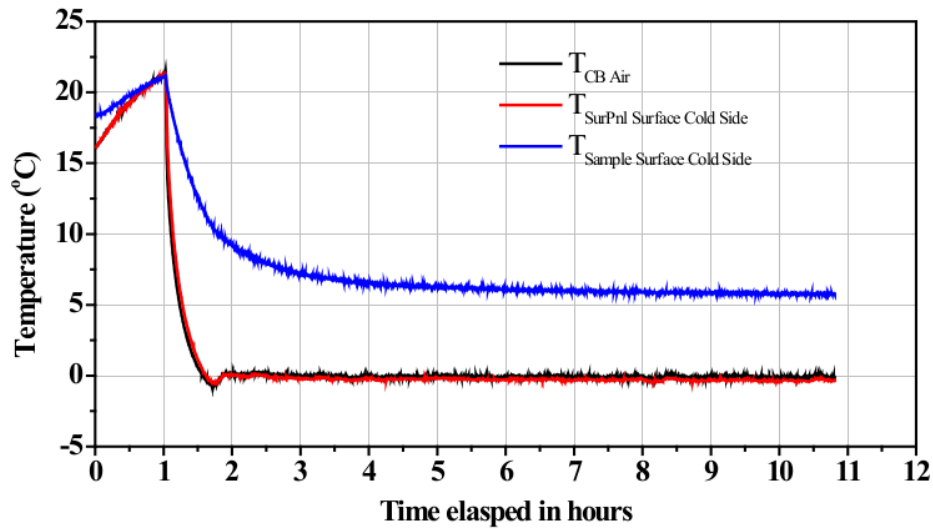
temperature for sample WI having metering box air set point at 40°C and cold box air set point at 0°C.

Table 3.6 - Testing report for Sample WII

Test no	$T_{MB\ Air}$ (°C)	$T_{CB\ Air}$ (°C)	δt_{air} (°C)	$\Phi_{Heat\ I/P}$ (W)	$\Phi_{MB\ Wall\ Loss}$ (W)	$\Phi_{MB\ to\ CB,\ measured}$ (W)	Φ_{FI} (W)	Φ_{Extra} (W)	$\Delta T_{SurPnl\ Surface}$ (°C)	$\Delta T_{Samp\ Surface}$ (°C)	Φ_{Sample} (W)	U-value (W/m ² K)
1	40.01	-0.20	40.21	39.77	0.95	38.83	1.28	6.71	40.00	27.68	20.37	2.199
2	40.01	-0.09	40.10	39.63	0.85	38.79	1.28	6.69	39.94	27.51	20.37	2.205
3	40.01	-0.07	40.08	39.50	0.88	38.62	1.28	6.69	39.94	27.49	20.21	2.188
4	40.01	10.10	29.91	23.62	7.01	30.63	0.99	29.63	0.87	4.94	16.03	2.327
5	40.01	10.14	29.88	23.94	7.00	30.94	1.21	29.74	0.87	4.94	16.14	2.345
6	40.01	10.17	29.84	23.29	7.00	30.29	1.01	29.28	0.87	4.93	15.71	2.285
7	40.01	19.96	20.00	21.71	1.37	20.34	0.34	3.26	19.8	13.49	11.6	2.503
8	40.00	19.95	20.10	21.56	1.35	20.21	0.34	3.26	19.8	13.48	11.4	2.473



(a) Hot box temperature profiles for Sample WII



(b) Cold box temperature profiles for Sample WII

Fig. 3.12 Variation of air and surface temperature in metering box and cold box for Sample WII

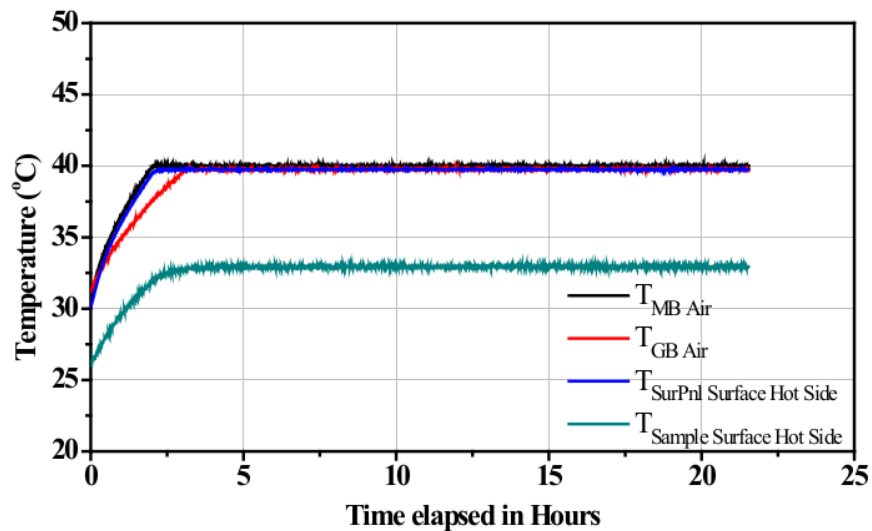
Table 3.7 - Fluctuations in air temperature and standard deviation of U-value for Sample WII

Test no.	δt_{air} (°C)	U-value (W/m ² K)	Maximum fluctuations allowed as per BS EN ISO 8990:1996 (°C)	Maximum random fluctuations in air temperature (°C)		Average U-value (W/m ² K)	Standard deviation
				$T_{MB Air}$	$T_{CB Air}$		
1.	40.21	2.199	0.40	0.054	0.116	2.197	0.0067
2.	40.10	2.205	0.40	0.048	0.107		
3.	40.08	2.188	0.40	0.058	0.196		
4.	29.91	2.327	0.30	0.057	0.233	2.319	0.0253
5.	29.88	2.345	0.30	0.067	0.157		
6.	29.84	2.285	0.30	0.080	0.145		
7.	20.00	2.503	0.20	0.064	0.145	2.440	0.0901
8.	20.10	2.473	0.20	0.074	0.165		

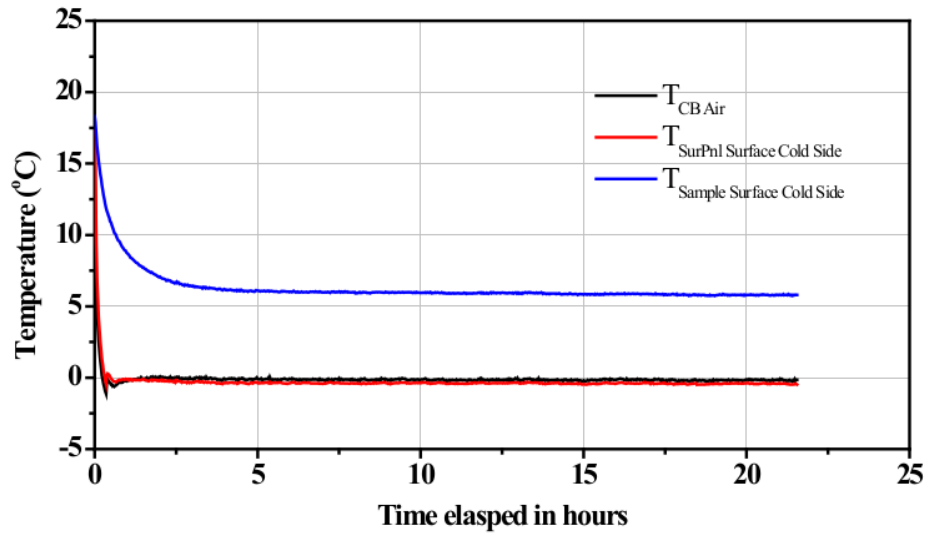
The overall heat transfer coefficients (U-value) of the sample WIII along with the other detailed parameters as obtained from testing are represented in Table 3.8, 3.9. The testing was conducted with metering box air velocity and cold box air velocity held constant at 0.920 m/s and 1.931 m/s. Fig. 3.13 shows the variation of air temperature, sample surface temperature for sample WIII having metering box air set point at 40°C and cold box air set point at 0°C.

Table 3.8 - Testing report for Sample WIII

Test no	$T_{MB\ Air} (^{\circ}C)$	$T_{CB\ Air} (^{\circ}C)$	$\delta t_{air} (^{\circ}C)$	$\phi_{Heat\ LP} (W)$	$\phi_{MB\ Wall\ Loss} (W)$	$\phi_{MB\ to\ CB,\ measured} (W)$	$\phi_{FI} (W)$	$\phi_{Extra} (W)$	$\Delta T_{SurPnl\ Surface} (^{\circ}C)$	$\Delta T_{Samp\ Surface} (^{\circ}C)$	$\phi_{Sample} (W)$	U-value (W/m^2K)
1	40.01	0.20	39.81	39.99	1.50	38.49	1.28	6.64	39.75	26.79	20.17	2.199
2	40.01	-0.17	40.18	40.27	1.18	39.10	1.28	6.70	40.09	27.12	20.62	2.228
3	40.01	0.26	39.74	39.73	1.22	38.51	1.28	6.63	39.68	26.86	20.22	2.208
4	40.01	10.06	29.95	29.46	1.41	28.05	0.87	4.95	29.76	20.10	14.44	2.092
5	40.01	10.27	29.74	29.05	1.08	27.97	0.87	4.92	29.53	19.87	14.46	2.110
6	40.01	10.13	29.88	29.31	1.20	28.10	0.87	4.94	29.72	20.02	14.52	2.109
7	40.01	19.85	20.16	19.66	1.23	18.42	0.34	3.28	19.96	13.54	9.59	2.064
8	40.01	19.87	20.14	19.86	1.50	18.35	0.34	3.27	19.77	13.64	9.57	2.062



(a) Hot box temperature profiles for Sample WIII



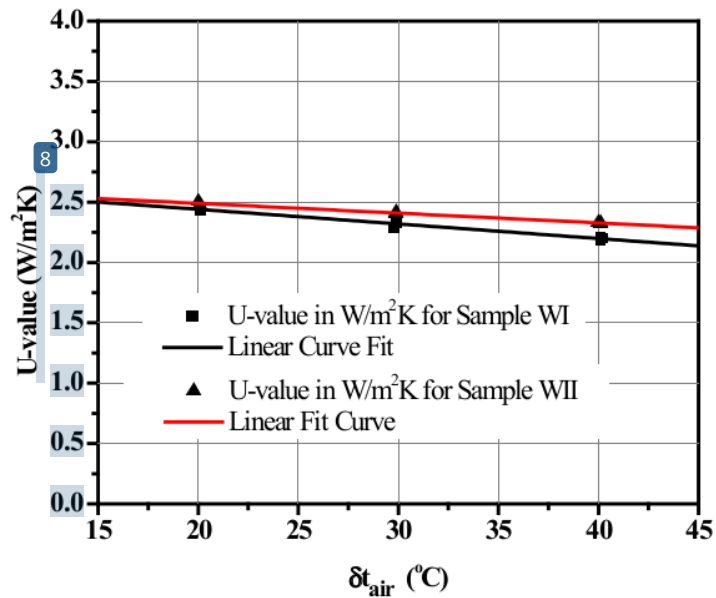
(b) Cold box temperature profiles for Sample WIII

Fig. 3.13 Variation of air and surface temperature in metering box and cold box for Sample WIII

Regression plot for the variation of U-value with δt_{air} for Sample WI and Sample WII is presented in Fig. 3.14 while for Sample WIII is presented in Fig. 3.15

Table 3.9 - Fluctuations in air temperature and standard deviation of U-value for Sample WIII

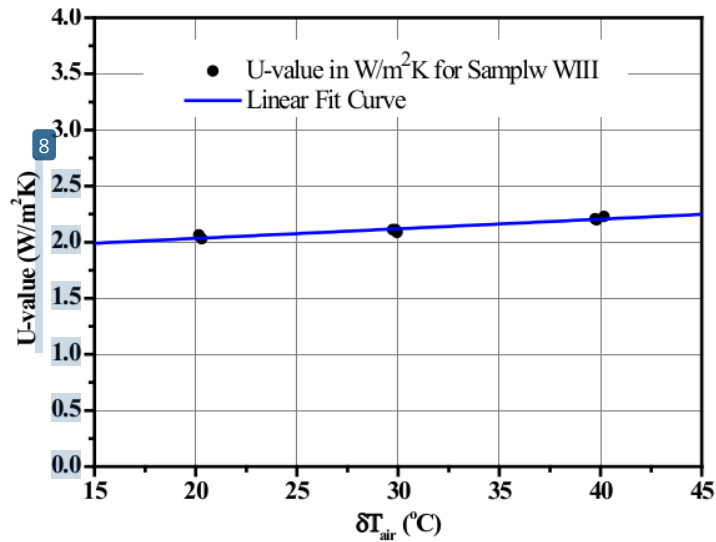
Test no.	δt_{air} (°C)	U-value (W/m ² K)	Maximum fluctuations allowed as per BS EN ISO 8990:1996 (°C)	Maximum random fluctuations in air temperature (°C)		Average U-value (W/m ² K)	Standard deviation
				T _{MB Air}	T _{CB Air}		
1.	39.81	2.199	0.40	0.064	0.123	2.212	0.01205
2.	40.18	2.228	0.40	0.056	0.121		
3.	39.74	2.208	0.40	0.058	0.134		
4.	29.95	2.092	0.30	0.075	0.166	2.104	0.00798
5.	29.74	2.110	0.30	0.066	0.154		
6.	29.88	2.109	0.30	0.053	0.156		
7.	20.16	2.064	0.20	0.088	0.133	2.063	0.00101
8.	20.14	2.062	0.20	0.077	0.173		



Regression Eqn. for Sample WI: $Y = -0.012105 * X + 2.682339$

Regression Eqn. for Sample WII: $Y = -0.008096 * X + 2.651288$

Fig. 3.14 Variation of U-value with differential air temperature for Sample WI & WII



Regression Eqn. for Sample WIII: $Y = 0.008580 * X + 1.86189$

Fig. 3.15 Variation of U-value with differential air temperature for Sample WIII

From Fig. 3.14, it was observed that U-value of Sample WI having cement plastered surface was always greater than that of surface of sample WII which had white coloured surface. This can be attributed to the fact that surface of the sample WI has a higher absorption coefficient as compared to that of sample WII (as evident from Table 3.2). In other words,

radiative heat transfer component has been reduced for sample WII as compared to sample WI. Moreover, it can be also observed that U-value in both the cases increased with decrease in δt_{air} across the sample. This is probably due to the fact that sample surfaces were hygroscopic in nature. As a result, the moisture content of the overall sample changed with δt_{air} . In other words, lower the δt_{air} , higher was the moisture content of the sample and higher the U-value of the sample obtained.

From variation of U-value with δt_{air} of sample WIII, it can be observed that contrary to the nature of variation of U-value for samples WI & WII, U-value in case of sample WIII increased with increase in δt_{air} . This nature can be attributed to presence of silicon in the paint which has water repellent properties. As a result, the hygroscopic nature of the sample surface was changed and the moisture content of the sample hardly changed. The increasing trend of U-value with δt_{air} may be due to increase in thermal properties (such as thermal conductivity) with increase in δt_{air} .

For the purpose of studying the impact of varying convection rates on the overall heat transfer coefficient, sample WII was selected. The results of variation of overall heat transfer coefficient (U-value) for Sample WII with air velocity for δt_{air} equal to 30°C and 20°C is presented in Table 3.10 and graphical representation of the same is shown in Fig. 3.16.

Table 3.10 - Variation of U-value of Sample WII with change in metering box and cold box air velocity respectively.

MB Fan Voltage (VDC)	MB Fan velocity (m/s)	U-value at $\delta t_{air} = 30^{\circ}\text{C}$, CB Fan Velocity at 1.931 m/s	U-value at $\delta t_{air} = 20^{\circ}\text{C}$, CB Fan Velocity at 1.931 m/s	CB Fan Voltage (VDC)	CB Fan velocity (m/s)	U-value at $\delta t_{air} = 30^{\circ}\text{C}$, MB Fan Velocity at 0.920 m/s	U-value at $\delta t_{air} = 20^{\circ}\text{C}$, MB Fan Velocity at 0.920 m/s
24.1	0.92	2.31	2.42	11.8	1.931	2.42	2.31
24.1	0.92	2.33	2.43	11.8	1.931	2.43	2.33
20.0	0.774	2.25	2.32	10.0	1.685	2.21	2.22
20.2	0.774	2.26	2.3	10.0	1.685	2.18	2.13
16.0	0.658	2.16	2.25	7.9	1.337	2.10	2.02
16.0	0.658	2.16	2.27	8.0	1.337	2.11	1.98

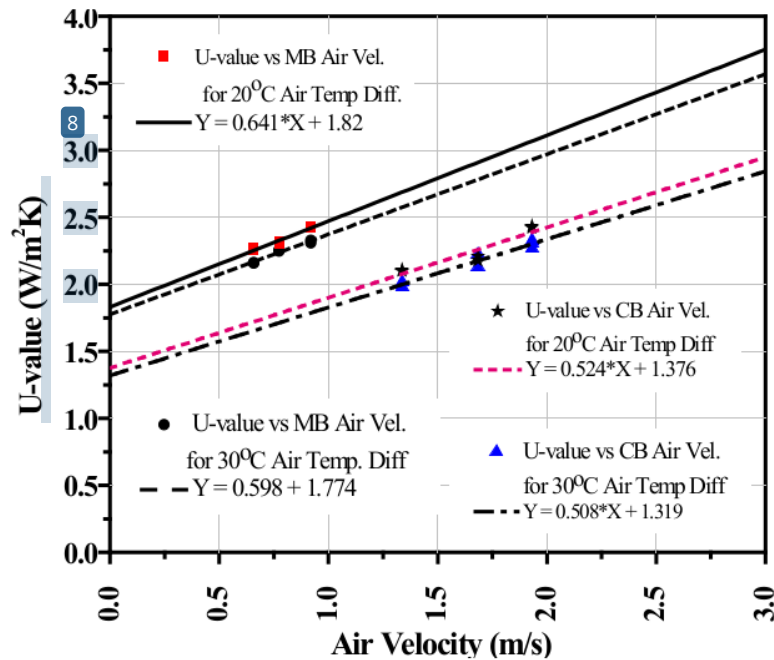


Fig. 3.16 Effect of variation of metering box and cold box air velocity on U-value for Sample WII.

3.3 Roof

Roof is the uppermost component of a building structure. The primary function of the roof is to enclose the space and to protect it from the effects of rain, wind, sun, heat and snow. Roof (especially horizontal flat roof) receives direct solar radiation for the maximum time of the day throughout the year. The choice of the type of roof construction is dependent upon the climatic conditions, shape of building, availability of materials etc. Some of the common roof types used in India are as follows: Thatched roofs, flat roof, parapet roof, gable roof, hip roof, skillion roof and combination roof.

In this chapter we concentrate upon flat roof construction as it's a very common and simplest form of construction used in residential households in India. Flat roofs have a slight slope in order to facilitate drainage of water. Flat roofs are generally avoided in places where there are heavy rainfall or snowfall. Different types of flat roofs include Reinforced Cement Concrete Roof, Precast concrete Roof, Jack Arch Roof, mud terrace roof, Madras Terrace Roof etc. Among these reinforced cement concrete roof flat roofs are conventionally used. It is most durable as compared to other types of flat roof.

In the summer season, flat roofs of buildings are exposed to the intense heat of the sun for the entire duration of the day except during sunrise and sunset. Now concrete being a very dense material has a high thermal mass. As such once it gets heated it retains the heat for a very long time. This stored heat is then radiated into the rooms during the night when the surroundings are getting cool. Due to the stillness of air just under the roof, the air in the room also gets heated up. Moreover, the rotating ceiling fan below the roof pushes the warm air down, thereby increasing the discomfort of the occupants.

Traditionally, “Surkhi”, which is a mixture of brick bat, lime, maravajra (natural adhesive) and Antvalakai (gum fruit) was used in the past as a weatherproof layer in order to prevent the roof from getting heated. Nowadays weather-proof clay panels (having tube like holes within them) are commonly used for insulation. It is placed over the concrete roof with cement mortar. Bituminous sheets having silver coating on the outer side are also used for insulating the roof. They reflect heat and prevents damage to the roof from water seepage.

In this chapter a conventional RCC roof used in typical residential house in India has been fabricated and its thermal performance has been evaluated.

3.3.1 Sample Construction and Description

A traditional reinforced cement concrete (RCC) roof (Sample WIV) used in traditional rooftops in residential household had been constructed. The thickness of the RCC roof and the concrete mix had been done as per *IS 456:2000*. The concrete mix used here was 1:1.5:3 i.e. 1 part of cement 1.5 part of fine aggregate/coarse sand and 3 parts of 20mm down stone aggregate. It had been reinforced by 8 mm steel bars at a spacing of 150mm c/c. The sample size was 480mm by 480mm. Adequate amount of water was added for curing. The whole assembly was cast inside a separate frame and left to cure for 28 days before loaded on to the sample holding frame. After curing process was complete the roof slab was inserted into the sample holding frame and placed midway. One side of the roof surface was plastered (12.5mm thick) with mortar having mix 1:6. The plastered side was properly smoothed and prepared and then two coats of cement primer was applied on it. Self-adhesive bituminous member had been applied on the other surface. Fig. 3.17 shows the side view of the RCC roof slab. Cross-sectional view of the slab showing the layout of the steel reinforcements is shown in Fig. 3.18.

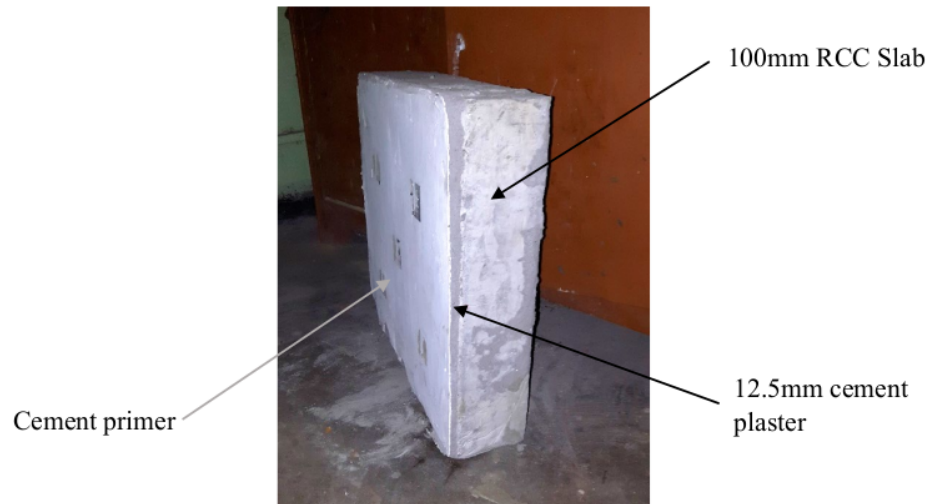


Fig. 3.17 Side view of the RCC roof slab (Sample WIV).

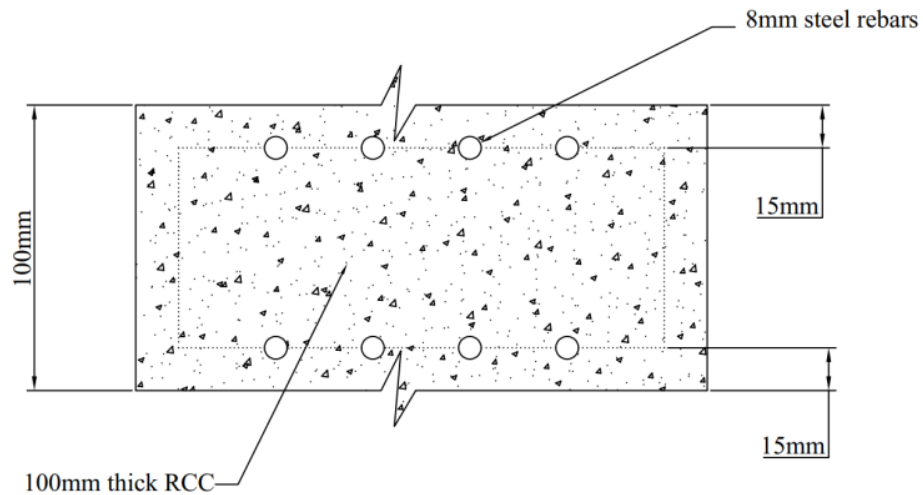


Fig. 3.18 Cross-sectional view of the slab showing the layout of the steel reinforcements.

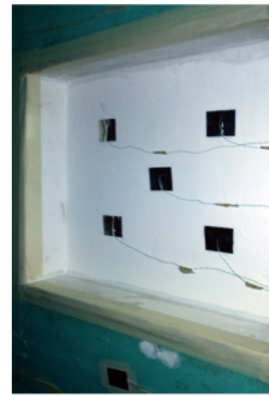
3.3.2 Experimental Procedure

The Sample WIV along with the sample holding frame was mounted on the sample holding aperture frame of the surround panel. The interface between the sample and sample holding frame was properly sealed with silicone sealant. The interface between the sample holding frame and the surround panel was also sealed in similar fashion. Fig. 3.19 show the sample WIV placed on the sample holding frame and mounted on the surrounding panel with thermocouple sensors mounted on both the surfaces. The side having bituminous layer was

facing the metering box chamber while side coated with cement primer was facing the cold box chamber.



Waterproofing membrane applied surface facing metering box



Plastered surface with cement primer applied facing cold box.

Fig. 3.19 100 mm RCC roof (Sample WIV) mounted on surround panel with thermocouple sensors placed on the surface.

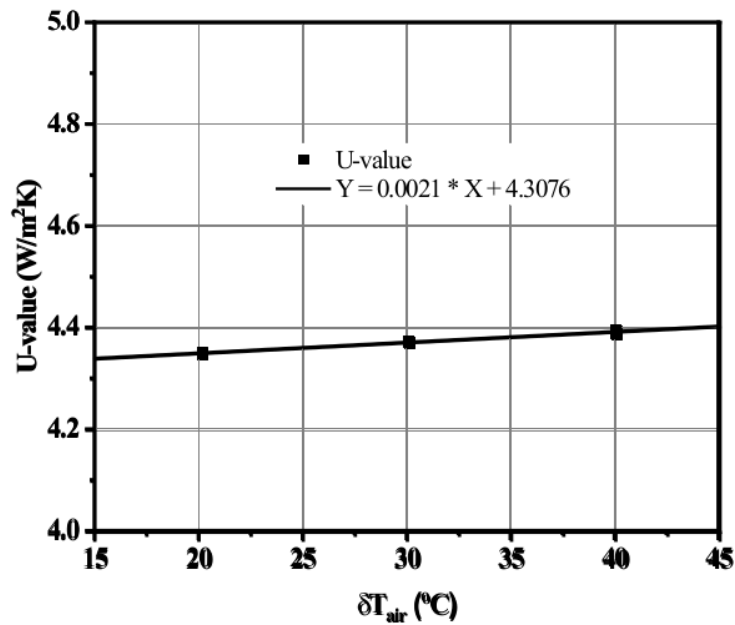
The rest of the testing procedure was similar as described in section 3.2.2. The metering box air velocity was kept constant at 0.920 m/s and cold box air velocity was kept constant at 1.931 m/s while the horizontal distance between baffle surface and surround panel surface was kept at 120mm in both the metering box and cold box.

3.3.3 Results

The results of variation of overall heat transfer coefficient with differential air temperature as well as other parameters are presented in Table 3.11. Regression plot of the same is presented in Fig. 3.20. The standard deviation along with the maximum fluctuations of air temperature are presented in Table 3.12. The variation of air and surface temperature in metering box, cold box, sample surface and surround panel surface are presented in Fig. 3.21. The variation of total heat transfer rate with time occurring through all the five metering box walls from metering box to guard box for Sample WIV is presented in Fig. 3.22.

Table 3.11 - Testing report for Sample WIV

Test no	$T_{MB, Air} (^{\circ}C)$	$T_{CB, Air} (^{\circ}C)$	$\delta t_{air} (^{\circ}C)$	$\phi_{Heat\ IP} (W)$	$\phi_{MB\ Wall\ Loss} (W)$	$\phi_{MB\ to\ CB, measured} (W)$	$\phi_{FI} (W)$	$\phi_{Extra} (W)$	$\Delta T_{Surf\ Int\ Surface} (^{\circ}C)$	$\Delta T_{Surf\ Ext\ Surface} (^{\circ}C)$	$\phi_{Sample} (W)$	U-value (W/m ² K)
1	40.00	-0.08	40.08	59.54	1.71	57.83	0.14	6.69	40.04	15.09	40.52	4.388
2	40.00	-0.05	40.06	59.59	1.76	57.83	0.14	6.68	39.93	15.14	40.56	4.395
3	40.01	9.89	30.11	44.46	1.29	43.17	0.04	4.98	29.86	11.84	30.34	4.372
4	40.00	9.87	30.13	44.90	1.69	43.21	0.04	4.98	29.91	11.98	30.36	4.373
5	40.00	9.86	30.14	44.96	1.74	43.22	0.04	4.98	29.95	12.07	30.35	4.371
6	40.01	19.82	20.19	30.64	1.91	28.73	0.08	3.28	19.67	8.10	20.23	4.347
7	40.01	19.83	20.19	30.67	1.91	28.76	0.08	3.28	19.74	8.25	20.24	4.352

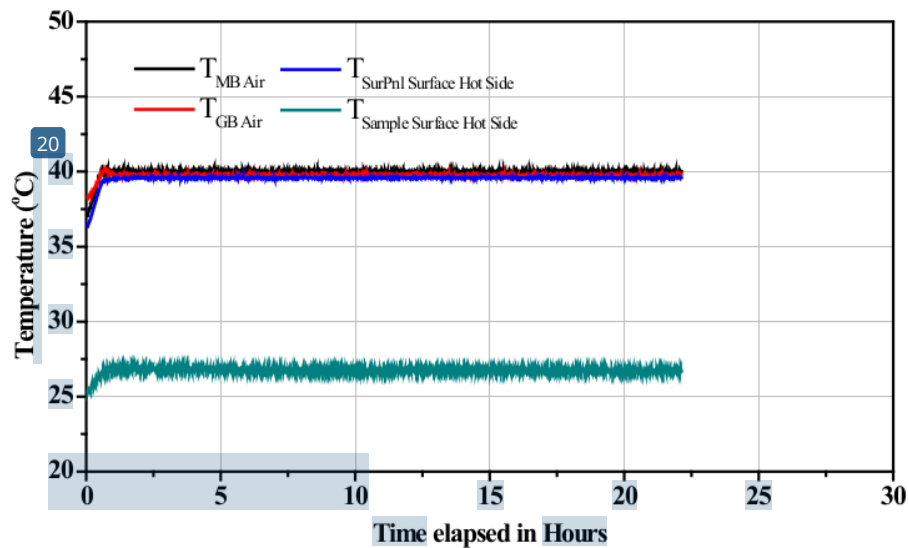


Regression equation for Sample WIV: $Y = 0.0021 * X + 4.3076$

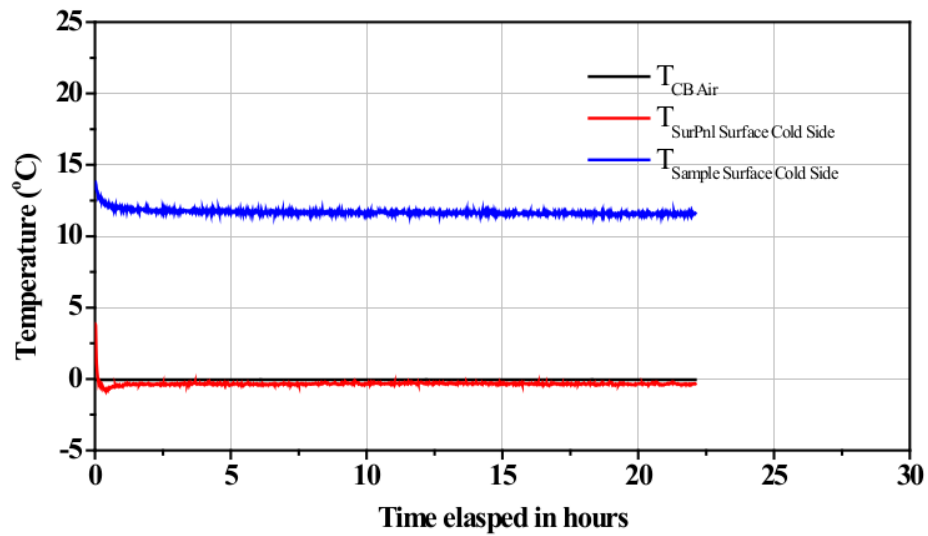
Fig. 3.20 Variation of U-value with differential air temperature for Sample WIV

Table 3.12 - Fluctuations and standard deviations of air temperatures for Sample WIV

Test no.	δt_{air} (°C)	U-value (W/m ² K)	Maximum fluctuations allowed as per BS EN ISO 8990:1996	Maximum random fluctuations in air temperature		Average U-value (W/m ² K)	Standard deviation
				$T_{MB\ Air}$	$T_{CB\ Air}$		
1	40.08	4.388	0.40	0.059	0.112	4.391	0.00341
2	40.06	4.395	0.40	0.061	0.100		
3	30.11	4.372	0.30	0.077	0.146	4.372	0.00109
4	30.13	4.373	0.30	0.075	0.166		
5	30.14	4.371	0.30	0.077	0.164		
6	20.19	4.347	0.20	0.076	0.168	4.349	0.00201
7	20.19	4.352	0.20	0.081	0.170		



(a) Hot Box temperature profile for Sample WIV



(b) Cold Box temperature profile for Sample WIV

Fig. 3.21 Variation of air and surface temperature in metering box and cold box for Sample WIV

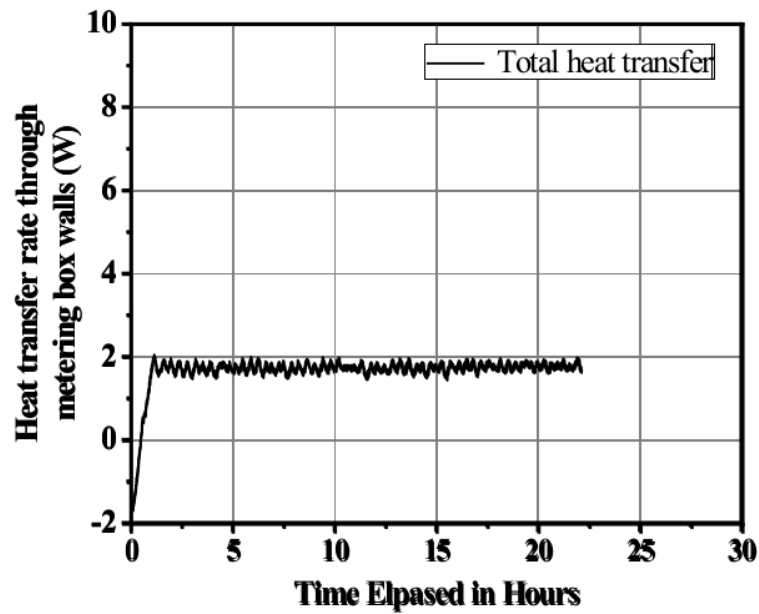


Fig. 3.22. Variation of Metering box wall heat transfer with time.

For the roof sample WIV, the bituminous waterproofing membrane acts as a moisture barrier thereby preventing any change in moisture content of the sample. As a result, U-

value increases with increase in δt_{air} (Fig. 3.20) similar to that in sample WIII. Moreover, the U-value of the roof sample is almost double than that of the wall samples.

3.4 Double Glazing Unit (with warm edge spacer)

Fenestration is a general term which refers to windows, skylight and doors in a building. It can be either fixed or operable. It influences the building energy use via four basic mechanisms: heat transfer, solar heat gain, air leakage or ventilation and daylighting. Components of fenestration include glazing material (which may be glass, plastic or acrylic), framing, insulation dividers and opaque door slabs. In a tropical climate such as India, design, location and configuration of glazing is of prime importance when it comes to aesthetics and energy use of a building. In this section we are mainly focusing upon typical double-glazing unit. A typical double-glazing unit (DGU) not only provides improved thermal insulation but also improved acoustic insulation as compared to single glazing unit. A DGU consists of two glazing layers that are held apart by an edge seal. The most common glazing material is clear float glass. The gap between the two glass panes is generally filled with air. However, argon, krypton gases are also used to reduce the convective heat transfer across the cavity. The edge seal comprises of spacer, primary and secondary sealant along with desiccant. Normally spacers used are made up of metal (for e.g., aluminium, steel). As a result, conductive heat transfer through the edge of double-glazing system is much higher than at its centre. To minimise this heat flow, warm-edge spacers made of materials of lower thermal conductivity such as polymers, foamed silicone etc. are used. The function of the primary seal is to adhere the spacer to the glazing and minimise moisture ingress and gas escape while that of secondary seal is to provide structural integrity to the glazing. The secondary seal is generally made of silicone or polyurethane. The purpose of desiccants is to absorb the trapped moisture within the cavity during the assembly phase or which gradually through the seal. Desiccants include silica gel or molecular sieve or a combination of both. The present study examines the thermal performance of a typical double-glazing unit incorporating warm-edge spacers.

3.4.1 Sample Construction and Description

Double glazing unit incorporating warm-edge spacer was built in the laboratory itself. Two 4mm Modiguard make clear float glass of dimension 505mm by 505mm were thoroughly rinsed and cleaned by using acetone and iso-propanol. The warm-edge spacers (Swispacer Ultimate) samples were supplied by SWISSPACER, Vetrotech Saint-Gobain (International),

Switzerland (Fig. 3.23). The spacers are 14.5mm in width and the height of the same is 6.5mm. The spacer bars were joined by corner keys (which were also supplied by SWISSPACER). Four spacers were joined using corner keys to form a rectangular box whose inner dimension was 490mm by 490mm. Before forming a grid, adequate amount silica gel was placed in the spacer bars. The spacers had an adhesive layer which acted as a primary sealant. The secondary sealant used here was silicone sealant (black coloured). After the sealant had cured properly the double-glazing unit (Sample VI) was placed in a wooden frame (Fig. 3.24). The total thickness of the double-glazing unit was 23mm.

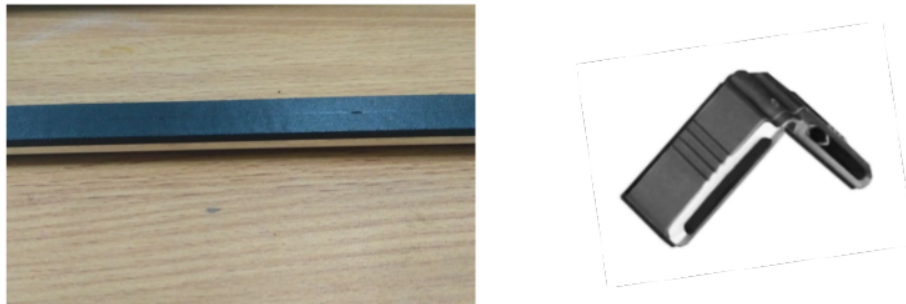


Fig. 3.23 Warm-edge spacers and corner keys



Fig. 3.24 DGU placed in wooden frame.

Similarly, another DGU made of 4mm clear float glass using traditional aluminium 14.5mm thick spacers was also constructed for comparative study. Sectional view of the wooden frame has been shown in Fig. 3.25. The frame was fabricated in the laboratory for the

purpose of carrying out of testing of glazing samples. This frame was also treated to make it impervious to moisture as much as possible.

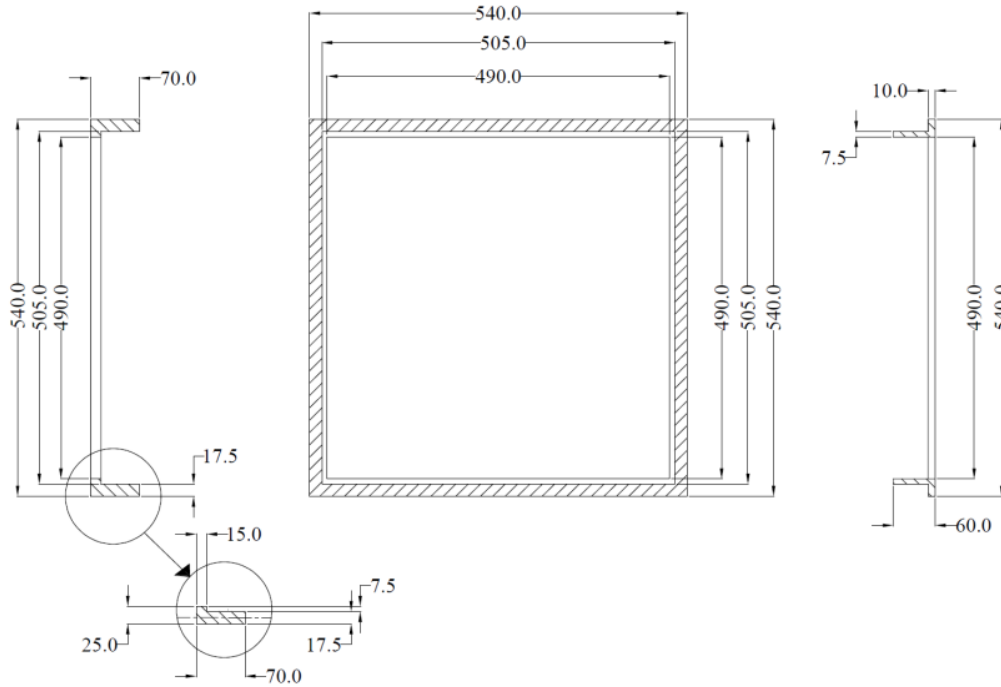


Fig. 3.25 Schematic view of the frame on which glazing units are mounted.

3.4.2 Experimental Procedure

The warm-edge spacer based double glazing unit inserted in wooden frame (Sample WV) was placed in the sample holding aperture in the surround panel (Fig. 3.26). Thermocouple sensors were placed on both the surfaces facing metering box and cold box. The interface between wooden frame and surround panel was properly sealed off to ensure no air leakage occurs from metering box to cold box.

The rest of the testing procedure was similar as described in section 3.2.2. The metering box air velocity was kept constant at 0.920 m/s and cold box air velocity was kept constant at 1.931 m/s while the horizontal distance between baffle surface and surround panel surface was kept at 120mm in both the metering box and cold box.



Fig. 3.26 Sample WV placed in the surround panel with thermocouple sensors mounted.

3.4.3 Results

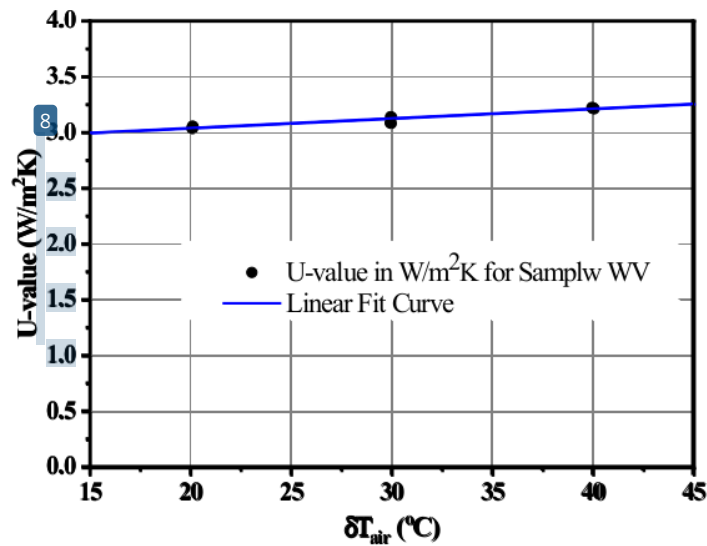
The overall heat transfer coefficients (U-value) of the sample WV along with the other detailed parameters as obtained from testing have been represented in Table 3.13, 3.14. Fig. 3.27 shows the regression plot of variation of U-value with respect to δt_{air} . Fig. 3.28 shows the real-time view of the variation of the various temperature profile for metering box set point of 40°C and cold box set point of 0°C. Fig. 3.29 shows the real-time variation of temperature profile of metering box air, baffle surface, glazing sample surface as being recorded in Agilent VEE program. Table 3.15 shows the test report for conventional double-glazing unit (air filled) with conventional aluminium spacer. Table 3.16 shows the comparative analysis of overall heat transfer coefficient for warm edge spacer based double glazing unit and aluminium spacer based conventional double-glazing unit.

Table 3.13 - Testing report for Sample WV

Test no	$T_{MB\ Air}$ (°C)	$T_{CB\ Air}$ (°C)	δt_{air} (°C)	ϕ_{HeatLP} (W)	$\phi_{MB\ Wall\ Loss}$ (W)	$\phi_{MB\ to\ CB, measured}$ (W)	ϕ_{F1} (W)	ϕ_{Extra} (W)	$\Delta T_{SurPnl\ Surface}$ (°C)	$\Delta T_{Samp\ Surface}$ (°C)	ϕ_{Sample} (W)	U-value (W/m ² K)
1	40.01	-0.02	40.03	55.47	2.21	53.26	2.70	6.68	39.93	18.33	32.17	3.215
2	40.01	0.02	39.99	55.50	2.22	53.28	2.70	6.67	39.87	18.53	32.22	3.223
3	40.01	10.04	29.97	41.86	2.03	39.83	2.70	4.95	29.74	13.72	23.53	3.140
4	40.01	10.06	29.95	40.82	1.51	39.30	2.70	4.95	29.80	13.50	22.99	3.070
5	40.02	19.91	20.11	28.22	1.59	26.63	2.70	3.27	19.87	9.15	15.51	3.085
6	40.01	19.93	20.08	27.85	1.49	26.36	2.70	3.26	19.84	9.12	15.25	3.038

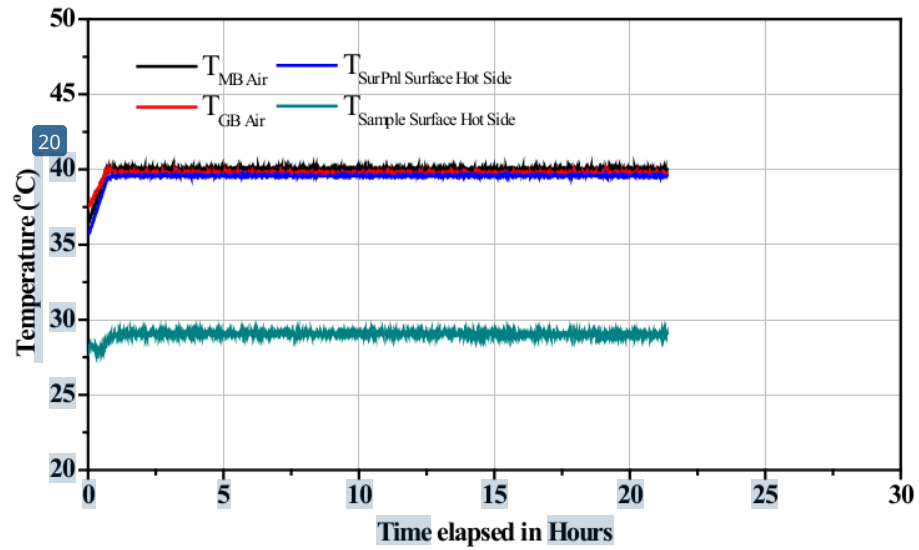
Table 3.14 - Fluctuations and standard deviations of air temperatures for Sample WV

Test no.	δt_{air} (°C)	U-value (W/m ² K)	Maximum fluctuations allowed as per BS EN ISO 8990:1996	Maximum random fluctuations in air temperature		Average U-value (W/m ² K)	Standard deviation
				$T_{MB\ Air}$ (°C)	$T_{CB\ Air}$ (°C)		
1	40.03	3.215	0.40	0.049	0.153	3.219	0.00385
2	39.99	3.223	0.40	0.053	0.153		
3	29.97	3.140	0.30	0.056	0.156	3.112	0.02785
4	29.95	3.070	0.30	0.071	0.169		
5	20.11	3.085	0.20	0.077	0.174	3.047	0.00908
6	20.08	3.038	0.20	0.087	0.134		

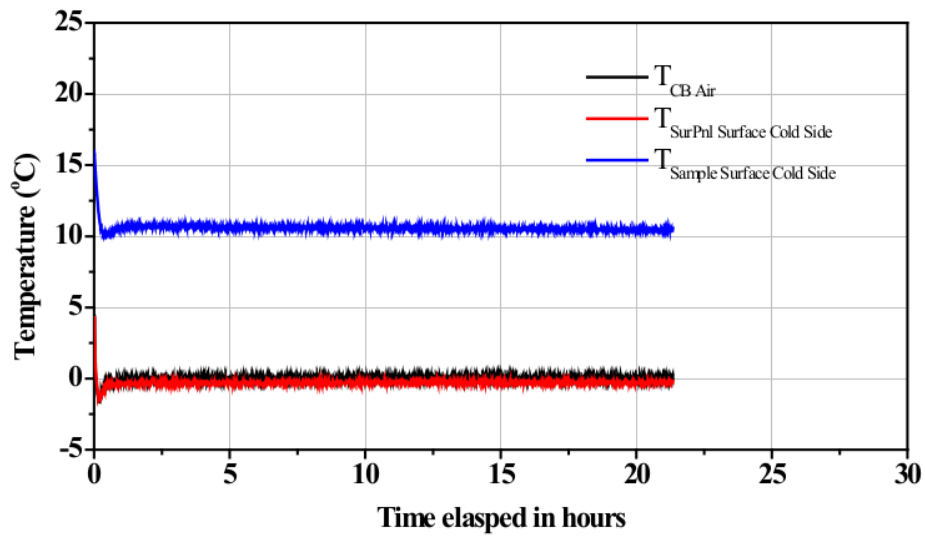


Regression equation for Sample WV: $Y = 0.0087 * X + 2.8659$

Fig. 3.27 Variation of U-value with differential air temperature for Sample WV



(a) Hot Box temperature profile for Sample WV



(b) Cold Box temperature profile for Sample WV

Fig. 3.28 Variation of air and surface temperature in metering box and cold box for Sample

WV

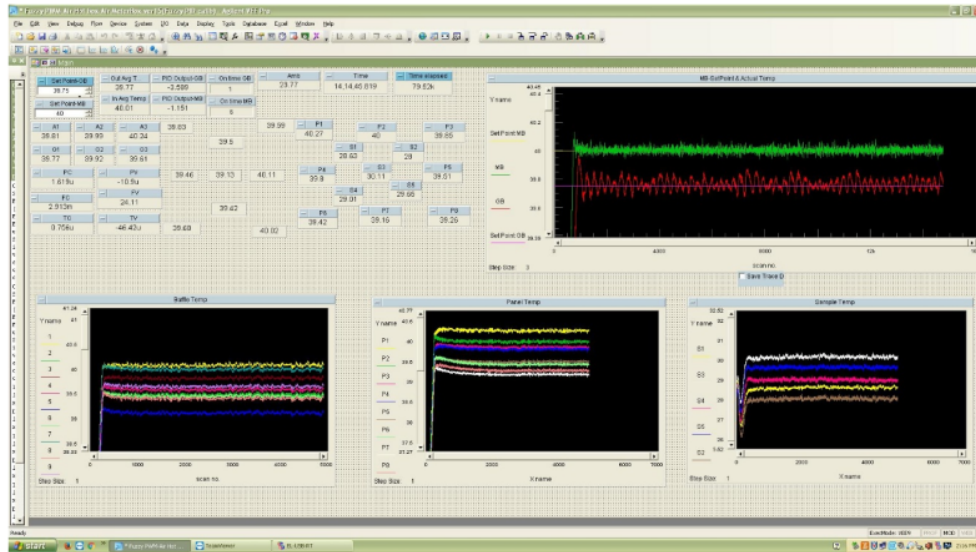
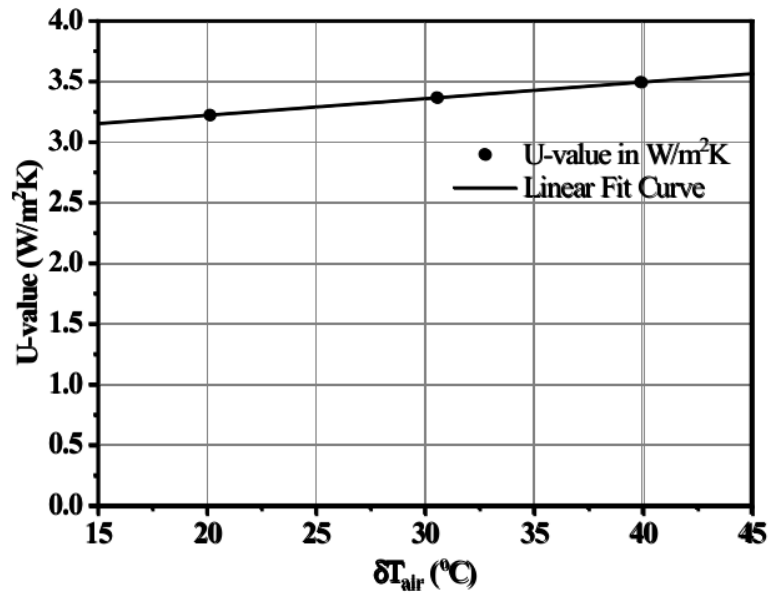


Fig. 3.29 Real-time view of the variation of the various temperature profile as recorded in Agilent VEE program.

Table 3.15 - Test Report for DGU Air filled with conventional aluminium spacer

Test no	$T_{MB\ Air}$ (°C)	$T_{CB\ Air}$ (°C)	δ_{air} (°C)	$\phi_{Heat\ LP}$ (W)	$\phi_{MB\ Wall\ Loss}$ (W)	$\phi_{MB\ to\ CB,\ measured}$ (W)	ϕ_{FI} (W)	ϕ_{Extra} (W)	$\Delta T_{SurPnl\ Surface}$ (°C)	$\Delta T_{Samp\ Surface}$ (°C)	ϕ_{Sample} (W)	U-value (W/m ² K)
1	40.01	0.1	39.91	57.25	1.32	55.94	4.04	4.95	39.98	18.25	34.86	3.494
2	40.02	9.46	30.56	45.27	2.95	42.32	3.63	6.67	30.48	14.3	25.72	3.367
3	40.01	19.84	20.17	28.92	1.23	27.68	2.7	3.28	19.96	9.26	16.53	3.278



Regression equation: $Y = 0.0137 * X + 2.94751$

Fig. 3.30 Variation of U-value with differential air temperature for conventional aluminium spacer based double glazing unit.

Table 3.16 - Comparative analysis of overall heat transfer coefficient of aluminium spacer based double glazing unit and warm-edge spacer based.

Sl no.	δT_{air} (°C)	U-value of DGU with Aluminium spacer (W/m ² K)	U-value of DGU with Warm edge spacer (W/m ² K)	% Reduction in U-value
1	40.01	3.494	3.219	7.87
2	29.96	3.367	3.112	7.56
3	20.10	3.278	3.047	7.06

3.5 Uncertainty Analysis

As per *BS EN ISO 8990:1996* the heat flow through the sample in case of guarded hot box can be summarised as:

$$\dot{Q}_{Sample} = \dot{Q}_{Heat\ I/P} - \dot{Q}_{MB\ Wall\ Loss} - \dot{Q}_{extra} - \dot{Q}_{FI} - \dot{Q}_{SurPnl}$$

where,

$$\dot{Q}_{Heat\ I/P} = \dot{Q}_{Heaters} + \dot{Q}_{Fans}$$

$$\dot{Q}_{Heaters} = TV * TC + PV * PC$$

$$\dot{Q}_{Fans} = FV * FC$$

$$\dot{Q}_{MB\ Wall\ Loss} = k * A_{metering\ box\ wall} * \Delta T_{Surface} / \delta x_{metering\ box\ wall}$$

$$\dot{Q}_{extra} = \dot{Q}_{MB\ to\ CB\ measured} - \dot{Q}_{MB\ to\ CB\ calculated}$$

$$\dot{Q}_{MB\ to\ CB\ measured} = \dot{Q}_{Heaters} + \dot{Q}_{Fans} - \dot{Q}_{MB\ Avg\ Wall\ Loss}$$

$$\dot{Q}_{MB\ to\ CB\ calculated} = k * A_{SurPnl} * \Delta T_{SurPnl\ Surface} / \delta x_{SurPnl} + k * A_{Samp} * \Delta T_{Samp\ Surface} / \delta x_{Samp}$$

$$\Delta T_{SurPnl\ Surface} = T_{SurPnl\ Temp\ Hot\ Face,\ Avg} - T_{SurPnl\ Temp\ Cold\ Face,\ Avg}$$

$$\Delta T_{Samp\ Surface} = T_{Samp\ Temp\ Hot\ Face,\ Avg} - T_{Samp\ Temp\ Cold\ Face,\ Avg}$$

$$U = \dot{Q}_{Sample} / (A * \delta t_{air})$$

The combined uncertainty in measurement of overall heat transfer coefficient can be expressed (as per *GUM Method*) as,

$$u_c^2(U) = u_c^2(\dot{Q}_{Sample}) + u_c^2(A) + u_c^2(\delta t_{air})$$

$$u_c^2(\delta t_{air}) = u_c^2(T_{MB\ Air}) + u_c^2(T_{CB\ Air})$$

$$u_c^2(\dot{Q}_{Sample}) = u_c^2(\dot{Q}_{Heat\ I/P}) + u_c^2(\dot{Q}_{MB\ Wall\ Loss}) + u_c^2(\dot{Q}_{extra}) + u_c^2(\dot{Q}_{FI}) + u_c^2(\dot{Q}_{SurPnl})$$

$$u_c^2(\dot{Q}_{Heat\ I/P}) = u_c^2(\dot{Q}_{Heaters}) + u_c^2(\dot{Q}_{Fans})$$

$$u_c^2(\dot{Q}_{Heaters}) = u_c^2(TV) + u_c^2(TC) + u_c^2(PV) + u_c^2(PC)$$

$$u_c^2(\dot{Q}_{Fans}) = u_c^2(FV) + u_c^2(FC)$$

$$u_c^2(\dot{Q}_{extra}) = u_c^2(\dot{Q}_{Heaters}) + u_c^2(\dot{Q}_{Fans}) + u_c^2(\dot{Q}_{MB\ Avg\ Wall\ Loss}) + u_c^2(\Delta T)$$

$$u_c^2(\Delta T) = u_c^2(\Delta T_{SurPnl\ Surface}) + u_c^2(\Delta T_{Samp\ Surface})$$

$$= u_c^2(T_{SurPnl\ Temp\ Hot\ Face,\ Avg}) + u_c^2(T_{SurPnl\ Temp\ Cold\ Face,\ Avg}) + u_c^2(T_{Samp\ Temp\ Hot\ Face,\ Avg}) + u_c^2(T_{Samp\ Temp\ Cold\ Face,\ Avg})$$

As per JCGM 100: 2008, the uncertainty in measurement can be represented as:

$u = s(\bar{q}) / \sqrt{n}$, where $s(\bar{q})$ is the experimental standard deviation of the mean of n number of observations.

The air and surface temperatures sensors were optimized to give accurate temperature difference. The measurements were done using temperature sensors which were thoroughly calibrated using a constant temperature oil bath and proper cold junction compensation was provided for thermocouples during calibration procedure.

Overall system calibration was performed during estimation of θ_{extra} whereby a calibration panel of same thickness and material as that of surround panel was used. This further reduced the uncertainty of measurements. Moreover, during all calibration and thermal transmittance runs, at least three to four data acquisitions were made to check for repeatability of the results. The measurements of length and breadth of the sample were made a number of times to reduce any chance error during measurement. The uncertainty in measurement of area of sample can be considered as zero. Moreover, the input voltage to the heaters in metering box (TV, PV) and fan voltage (FV) were measured closest to the heaters and fans to minimise the error due to line losses in the leads to the heaters and fans.

The uncertainty in measurements for u-value for walls and roofs are summarised as below (D. Chowdhury et. al 2019).

Table 3.17 - Measurement results and uncertainty analysis.

Sample	δt_{air} (K)	U-value (W/m ² K)	$u_c(\theta_{Sample})$ (W)	$u_c(\delta t_{air})$ (K)	$u_c(A)$ (m ²)	$u_c(U)$ (W/m ² K)
WI	40.06	2.326	0.016	0.025	-	0.030
	29.89	2.411	0.033	0.008	-	0.034
	20.05	2.488	0.045	0.005	-	0.046
WII	40.13	2.197	0.044	0.033	-	0.055
	29.87	2.319	0.039	0.017	-	0.046
	20.10	2.378	0.010	0.024	-	0.026
WIII	39.91	2.212	0.015	0.050	-	0.052
	29.86	2.104	0.019	0.049	-	0.053
	20.20	2.052	0.023	0.041	-	0.047
WIV	40.07	4.391	0.028	0.009	-	0.029
	30.13	4.372	0.028	0.007	-	0.029
	20.16	4.327	0.010	0.025	-	0.027

3.6 Conclusion

This chapter presents a detailed experimental analysis of evaluation of overall heat transfer coefficient of traditional 125mm burnt red clay brick wall-based wall samples. Variation of overall heat transfer coefficient with differential air temperature between metering box and cold box for three types of brick wall configurations: 125mm brick wall with plaster on both sides, 125mm brick wall with plaster and white coloured cement primer applied on both sides and 125mm brick wall with cement primer and magenta colour applied on one side and cement primer on other side. Tests were conducted with metering box fan velocity and cold box air velocity held constant all though the test.

Additional tests were conducted to find the impact of varying metering box fan velocity and cold box fan velocity on overall heat transfer coefficient on 125mm brick wall sample with 12.5mm plaster on both sides.

A conventional 100mm reinforced cement concrete roof sample is constructed with plaster on one side and bituminous layer on another side. Effect of variation of overall heat transfer coefficient with varying differential air temperature between metering box and cold box for this sample was studied.

A double-glazing unit with 4mm clear float glass and warm edge spacer was constructed and the impact of variation of overall heat transfer coefficient with varying differential air temperature between metering box and cold box for this sample was studied. Comparative study between conventional aluminium spacer based double glazing unit and warm-edge spacer based double glazing unit was studied as well.

***CHAPTER 4 – COOLING LOAD
ESTIMATION BY SIMULATION TOOLS***

4.1 Introduction

In this chapter, a three-dimensional model of a building was generated from an AUTOCAD based 2D plan of a building with the simulation software. The building construction details as obtained from *ASHRAE Handbook fundamentals 2017* were used as input to the software. In another scenario, the thermal properties of the building envelope (such as wall, roof and glazing) in form of overall heat transfer coefficient or U-value as obtained from Guarded Hot Box (GHB) testing was used as input in the simulation software. The monthly overall cooling energy consumption (in kWh) or the total cooling load (in kWh) was computed for the above two scenarios using three simulation software: DesignBuilder, ECOTECT and eQUEST. The orientation of the building was changed and its impact on the overall cooling load / energy consumption was observed.

4.2 Building Model Description

A building block of dimension 20' x 20' x 10' or 6.096m x 6.096m x 3.084m was modelled. Window had been placed on south facing wall having window to wall ratio of 40% as per *ECBC (2017)* standards. The area of window is 7.52m² or 80.94sqft. The window was kept closed during all the simulation scenarios. The building was selected for office purpose. 125mm burnt red clay brick wall with 12.5mm cement plaster on both sides was considered as the building wall and 100mm thick reinforced cement concrete with 12.5mm cement plaster on inside and a bituminous waterproofing membrane on outside was considered as roof of the building. Floor consisted of 75mm brick layer over 300mm of soil, covered by 100mm thick plain cement concrete. Ceramic/clay tiles were laid over the concrete layer with 35mm cement concrete screed below it. Window was considered to be air-filled double-glazing unit made of 4mm clear float glass on either side with 14.5mm air gap between the glass panes. No shading or overhang was considered for this study. Details of the building construction materials (*ASHRAE Handbook fundamentals, 2017*) and glass (*Modiguard clear*) as used in simulation have been shown in Table 4.1.

Table 4.1 - Construction details of building block material:

Material / Component	Thermal conductivity (W/mK)	Density (kg/m ³)	Specific Heat Capacity (J/kg.K)
Cement Plaster	0.72	1860	840
Burnt red clay brick	0.81	1920	800
RCC Slab	1.4	2400	800

Modigurad make Clear 4mm float glass	Visible light transmittance (%) -	89	
	Visible light reflectance (%) -	8	
	UV Transmittance (%) -	67	
	Solar Heat Gain Coefficient -	0.85	
	Shading coefficient -	0.98	
Clay tiles	0.85	1900	840
Bitumen layer	0.5	1700	1000
Concrete screed	1.4	2100	350

4.2.1 Building HVAC, Schedules and internal details

The general heating ventilation and air conditioning parameters along with the schedules and various gains used in the simulation have been summarised in Table 4.2.

Table 4.2 – General simulation inputs:

Parameter	Value
Cooling Setpoint	24°C (<i>Kumar et al., 2018</i>)
Heating Setpoint	N.A.
Humidification setpoint	35 (<i>BIS, 2016</i>)
Dehumidification setpoint	65 (<i>BIS, 2016</i>)
Lighting Power Density	9.5 (<i>ECBC, 2017</i>)
Cooling COP	1.8 (<i>BEE, 2016</i>)
Working hours	9AM to 6PM.
Lighting Schedule	9AM to 6 PM
No. of people	4 (2 men, 2 women)
Equipment	4 number of desktop computer 320 W (80W * 4) (<i>ASHRAE Handbook fundamentals, 2017</i>)
Air change rate	0.7 (<i>BEE, 2016</i>)
HVAC	Split no fresh air
Activity	Moderately active office work - 540W (<i>ASHRAE Handbook fundamentals, 2017</i>)

4.3 Simulation Engine

Building energy simulation is an important tool for accurate evaluation of overall energy performance of a building considering the thermal comfort of its inhabitants (A. Ajmal, 2012). Building simulation can help analyse the impact of thermos-physical properties of materials and the performance of various systems under varying external and internal environments. Simulation results help designers compare various options related to building form, system types, energy efficiency at the earliest conceptual design phase. Even post construction of the building, the impact of various energy conservation measures, the cost benefit analysis along with their payback period can be simulated beforehand to determine its effectiveness. Functions of building energy simulation software can be summarised as follows:

- Prediction of thermal behaviour of the building space in relation to the outside environment.
- Evaluation of impact of daylight and artificial lighting in the building space.
- Modelling of the natural ventilation within the building space.
- Estimation of size or capacity of HVAC equipment for meeting the required thermal comfort.
- Evaluation of compliance of building energy performance as per building codes such as ECBC 2017, ECONIWAS SAMHITA 2018 (Part 1), AHRARE 90.1:2007.

Various building energy simulation programs such as Autodesk Green Building Studio, BSim, DesignBuilder, DOE-2, ECOTECT, EnergyPlus, eQUEST, TRNSYS, ESP-r, EnerCAD are available (Harish et al., 2016). Attia et al. (2009), M. Jaric et. al (2013) have made a comparative study of different building performance simulation software in their study.

The present study involves usage of three most commonly used simulation software: DesignBuilder, ECOTECT and eQUEST. The first step in any energy simulation involves creation of a virtual replica of the proposed building or existing building. As such a typical layout of the building (as described in section 4.2) was developed using AutoCAD (Fig. 4.1). This AutoCAD based layout was incorporated into the simulation software and a three-dimensional model of the building was developed. Then the details of the building envelope components such as wall, roof, glazing and floor (Table 4.1), HVAC details (Table 4.2) were given as input into the software as required. The same weather data file of Kolkata had been incorporated in all the simulation software used. Table 4.3 and Fig. 4.2 shows the various orientations of the building taken into consideration for simulation.

Two sets of simulation studies were carried out for each orientation of the building. In one occasion, the details of the building block materials as obtained from ASHRAE Handbook

Fundamentals were used in the simulation software and the resultant cooling load was calculated thereof (**Cooling Energy w.r.t. ASHRAE**). In another occasion, the overall heat transfer coefficient of wall, roof and glazing as obtained from Guarded Hot Box testing results (Chapter 3) were directly given as input to the simulation software and the resultant cooling load was calculated (**Cooling Energy w.r.t. GHB**). The percentage deviation of the results has been calculated as follows:

$$\text{Percentage Deviation (\%)} = \frac{(\text{Cooling Load w.r.t. ASHRAE} - \text{Cooling Load w.r.t. GHB})}{\text{Cooling Load w.r.t. GHB}} * 100 \%$$

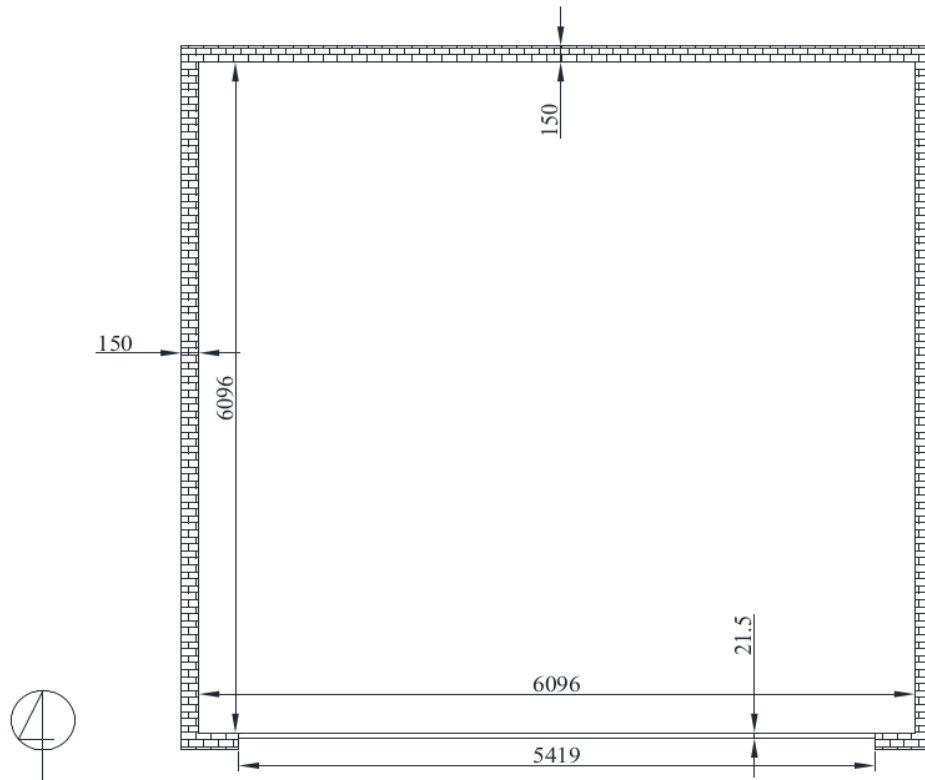


Figure 4.1 Plan of the simulated building.

Table 4.3 - Details of various orientation used in simulation.

Name	Orientation (Surface Azimuth of Window)	Name	Orientation (Surface Azimuth of Window)
N0	North facing (180°)	S0	South facing (0°)
E0	East facing (270°)	W0	West facing (90°)
NE45	North-East facing (-45°)	NW45	North-West facing (45°)
SE30	South-East facing (-30°)	SW30	South-West facing (30°)
SE45	South-East facing (-45°)	SW45	South-West facing (45°)
SE60	South-East facing (-60°)	SW60	South-West facing (60°)

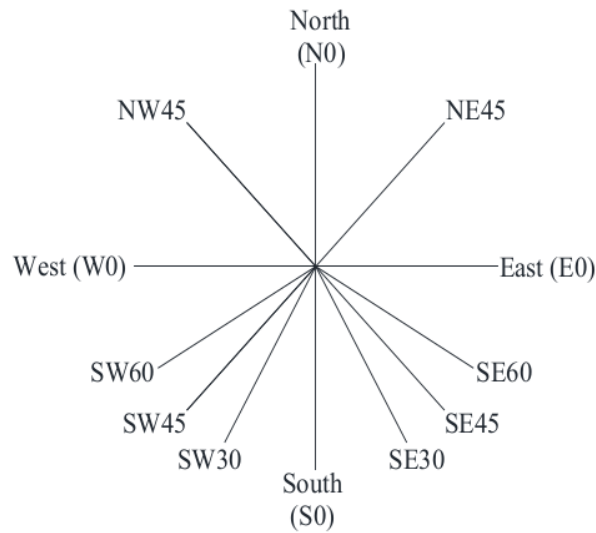


Fig. 4.2 Schematic view of the different orientations

4.3.1 DesignBuilder simulation

DesignBuilder uses the EnergyPlus dynamic thermal simulation engine at its core to generate performance data. EnergyPlus incorporates the capabilities of DOE-2 and BLAST software programs. DesignBuilder software provides a state-of-the-art graphical user interface to generate the three-dimensional model of the building and input various parameters required for simulation. Both naturally ventilated buildings and air-conditioned buildings can be modelled. Users can directly create the three-dimensional model of the building from scratch by importing the .dxf file of the building plan or any .pdf format or picture of the plan and generate the model. Fig. 4.3 shows the imported AutoCAD based layout into the software interface. Building geometry can also be imported from REVIT, ArchiCAD, SketchUP using gbXML file. Supported weather data files includes ASHRAE weather data files, EnergyPlus weather data files such as IWEC (International Weather for Energy Calculations), EPW (EnergyPlus Weather File) and TMY (Typical Meteorological Year) file.

DesignBuilder uses different building blocks to establish different levels and sections of a building. Various thermal zones of a building are represented by blocks. The timestep also known as ‘Zone Timestep’ is used for heat transfer and load calculations. The value entered in the form of “Number of time-steps per hour”. It can be 1, 2, 4, 6, 10, 12, 30 and 60. A Zone Timestep of 6 means an interval of 10 minutes (sixty minutes divided by six) was used for numerical solution of the Zone Heat Balance model. The available weather data is usually hourly data but the EnergyPlus based simulation engine automatically interpolates the weather data as per the time-step.

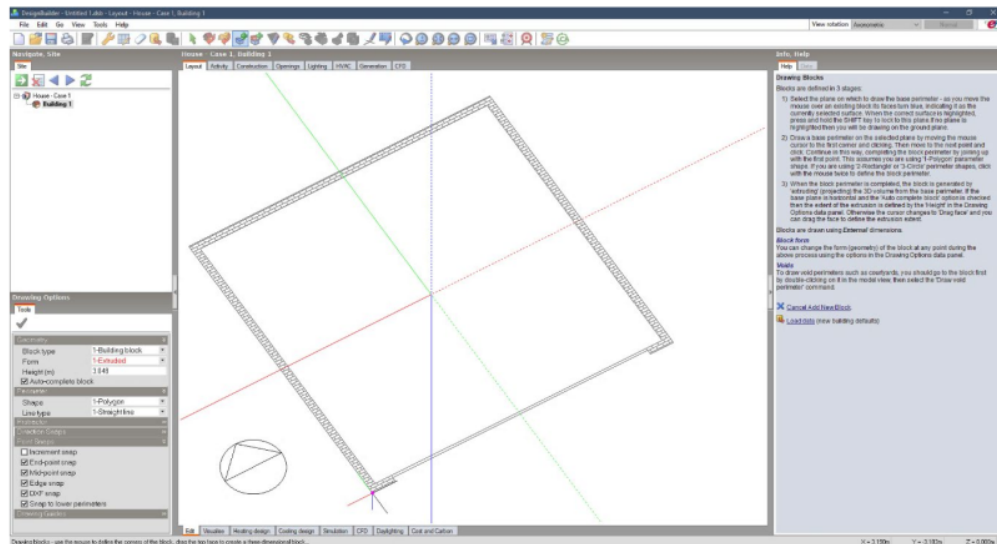


Fig. 4.3 AutoCAD plan as imported in DesignBuilder interface

Moreover, there is also another type of timestamp (which the user has no access) known as HVAC timestamp which governs the driving timestamp for HVAC and plant system modelling. When the HVAC part of simulation begins it uses the 'Zone timestamp' as maximum length but it reduces the time step as necessary to improve the solution. The minimum HVAC time-steps per hour while using Finite Difference solution method is 20. No mechanical ventilation or natural ventilation was considered. The cooling fuel required to generate the cooling energy was selected as '1-Electricity from grid'.

The EnergyPlus (FORTRAN code-based) simulation engine is based on Integrated Solution Manager which is composed of Surface Heat Balance manager, Air Heat Balance manager and Building System's Simulation Manager. The Integrated Solution manager interacts with various in-built program modules (Sky Model Module, Air Loop Module, Shading Module, Zone Equip Module, Daylighting Module, Plant Loop Module, Window Glass Module, Condenser Module, CTF Calculation Module, PV Module and Air Flow Network Module) to calculate energy required for heating and cooling the building. In this EnergyPlus based simulation engine, the building zones, air handling systems and central plant equipment are simulated sequentially and there exists feedback among each other. Here the elements are linked in a simultaneous solution scheme. All the elements are integrated and controlled simultaneously by Integrated Solution Manager. In EnergyPlus, several iterations may be required within each time zone in order to reach a convergent solution. All these factor results in a moderate amount of time being required for simulation. The built in HVAC models are more flexible and robust which can be used to model complex HVAC systems. Modelling of natural ventilation is built in within the EnergyPlus engine whereas in DOE-2, natural ventilation cannot be modelled directly.

The various orientation of the model that had been used in the simulation are shown in Fig. 4.4 to Fig. 4.15. The details of the building envelope components such as wall, roof, glazing and floor were given into the software as per Table 4.1. Table 4.4 shows the comparison between the U-value as computed by the simulation software and that obtained from experimental results of Guarded hot box testing. For calculation of overall heat transfer coefficient using the regression plot obtained from GHB testing (Chapter 3), the average outside air temperature for Kolkata climate was considered as 35°C and the inside ambient air temperature was considered as 24°C. The total monthly cooling electricity consumptions / cooling loads (in kWh) as computed by the software were compared for each condition.

Table 4.4 - Overall heat transfer values comparison using DesignBuilder:

	U-value obtained from GHB testing	U-value as calculated in DesignBuilder	Percentage deviation (%)
Wall	2.549 W/m ² K	2.785 W/m ² K	(+)9.26
Roof	4.332 W/m ² K	4.223 W/m ² K	(-)2.52
Glazing	2.875 W/m ² K	2.705 W/m ² K	(-)5.91

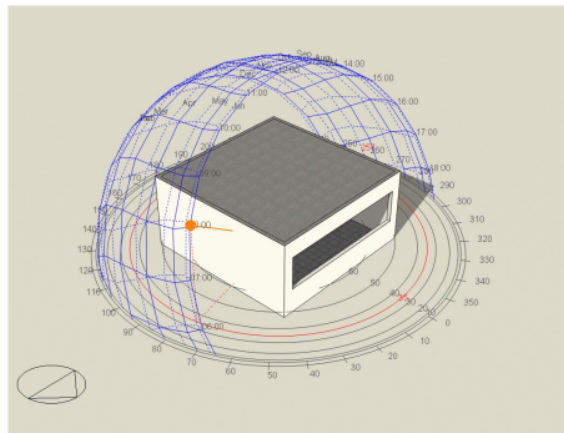


Fig. 4.4 Surface Azimuth angle of Window is 180° (N) in DesignBuilder (North facing)

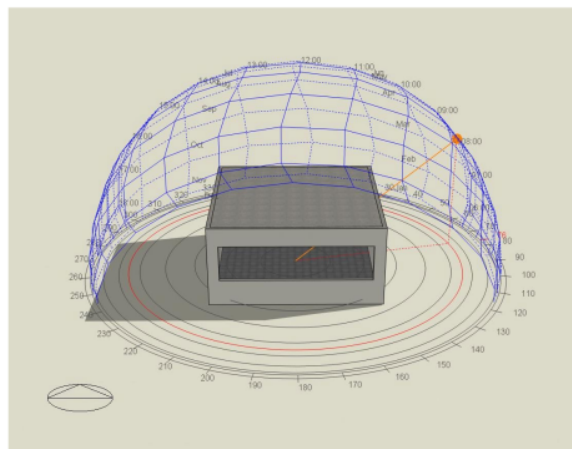


Fig. 4.5 Surface Azimuth angle of Window is 0° (S) in DesignBuilder (South facing)

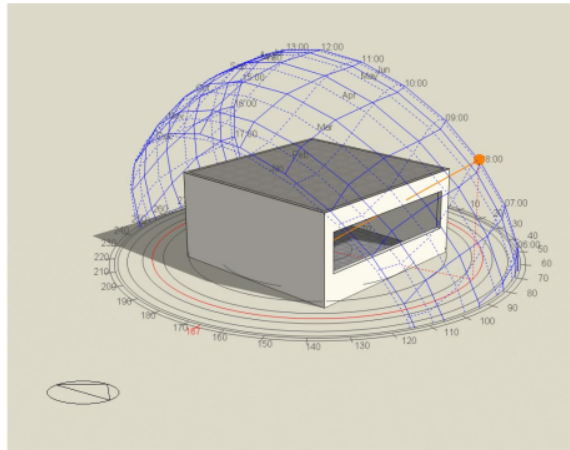


Fig. 4.6 Surface Azimuth angle of Window is 270° (E0) in DesignBuilder (East facing)

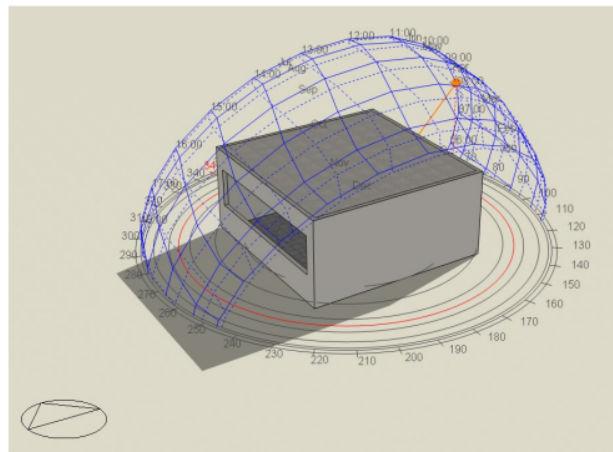


Fig. 4.7 Surface Azimuth angle of Window is 90° (W0) in DesignBuilder (West facing)

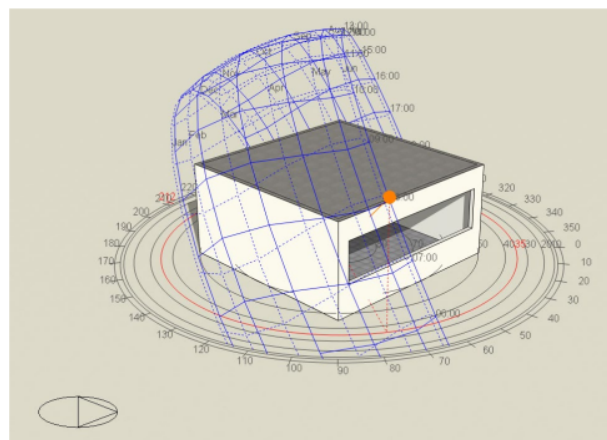


Fig. 4.8 Surface Azimuth angle of Window is 225° (NE45) in DesignBuilder

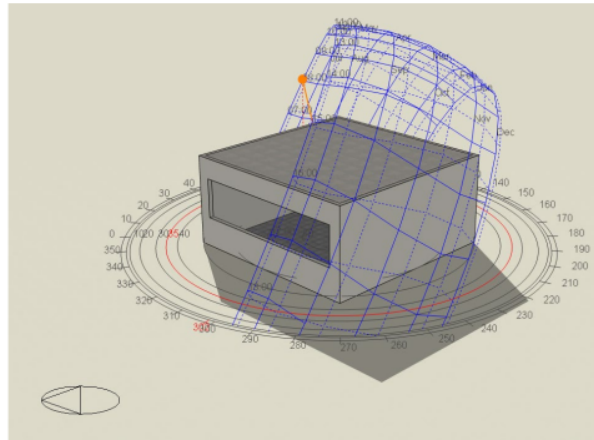


Fig. 4.9 Surface Azimuth angle of Window is 135° (NW45) in DesignBuilder

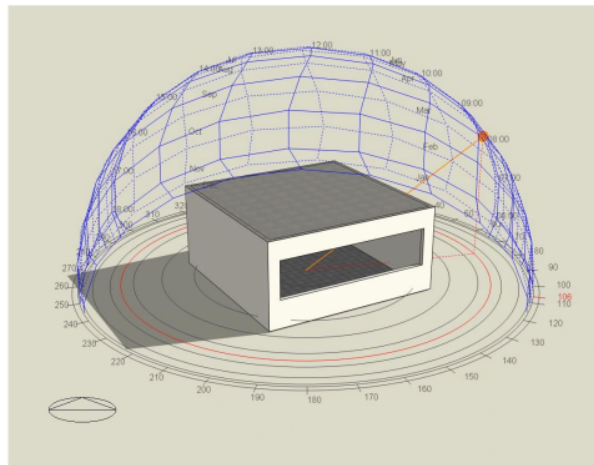


Fig. 4.10 Surface Azimuth angle of Window is 330° (SE30) in DesignBuilder

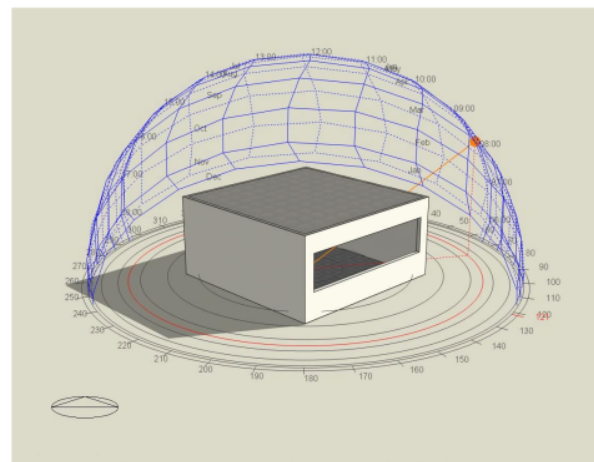


Fig. 4.11 Surface Azimuth angle of Window is 315° (SE45) in DesignBuilder

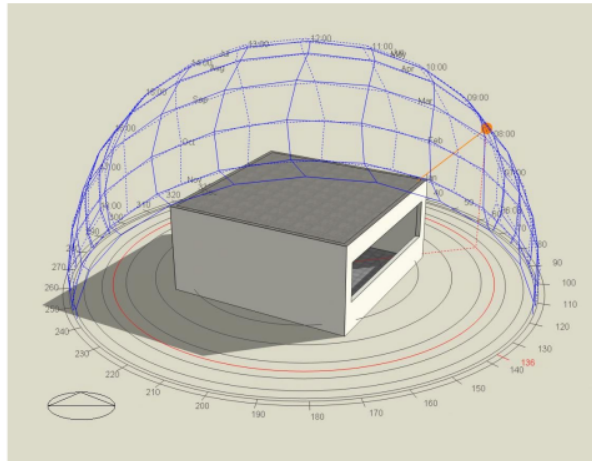


Fig. 4.12 Surface Azimuth angle of Window is 300° (SE60) in DesignBuilder

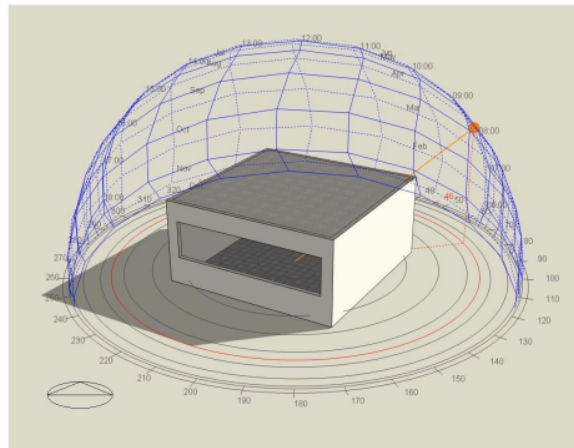


Fig. 4.13 Surface Azimuth angle of Window is 30° (SW30) in DesignBuilder

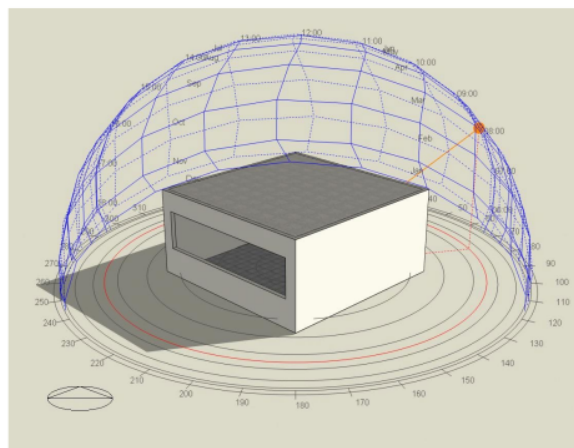


Fig. 4.14 Surface Azimuth angle of Window is 45° (SW45) in DesignBuilder

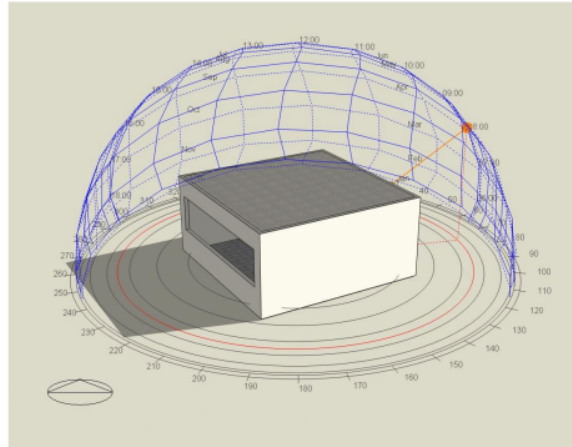


Fig. 4.15 Surface Azimuth angle of Window is 60° (SW60) in DesignBuilder

4.3.2 ECOTECH simulation

ECOTECH analysis is a building energy performance and simulation software developed by Sr. Andrew marsh and Square One Research and owned by Autodesk. It is a complete environmental analysis and building simulation tool which uses 'The Chartered Institute of Building Services Engineers (CIBSE) Admittance Method' at its core to determine internal temperatures and heat loads. The simulation is performed on an hourly basis. In the Admittance Method, the temperature and load calculations are two individual processes. In the first step, the magnitude of hourly potential heat and losses acting on the building fabric are computed in form of load factors. The variation in instantaneous load factor is used to determine the relative thermal stress in each zone which in turn helps in determining the hourly internal temperatures. After this a second calculation is conducted to determine the absolute heating and cooling loads. In the simulation all the calculations are made on hourly basis. Latent heat gains are not included in the internal thermal calculations. This way of computation is similar to that of DOE-2 simulation engine based eQUEST. The Admittance method is not as much accurate as compared to eQUEST or EnergyPlus. Moreover, ECOTECH does not compute the values of thermal decrement and thermal lag of the building structures instead it uses predefined values for the built-in configurations of building masonry structures. However, the user is allowed to manually input these values otherwise the predefined values for the built-in configurations matching to the custom configurations are taken as input. Heat transfer from soil is not considered in ECOTECH. The run time for simulation is least among the three simulation software used in the study.

The .dxf file of the input geometry was imported into the interface (Fig. 4.16) and the three-dimensional model of building was developed. The various orientation of the building models that had been simulated are shown in Fig. 4.17 to Fig. 4.28. Fully air-conditioned mode of HVAC operation was selected without any heating parameter input in the software.

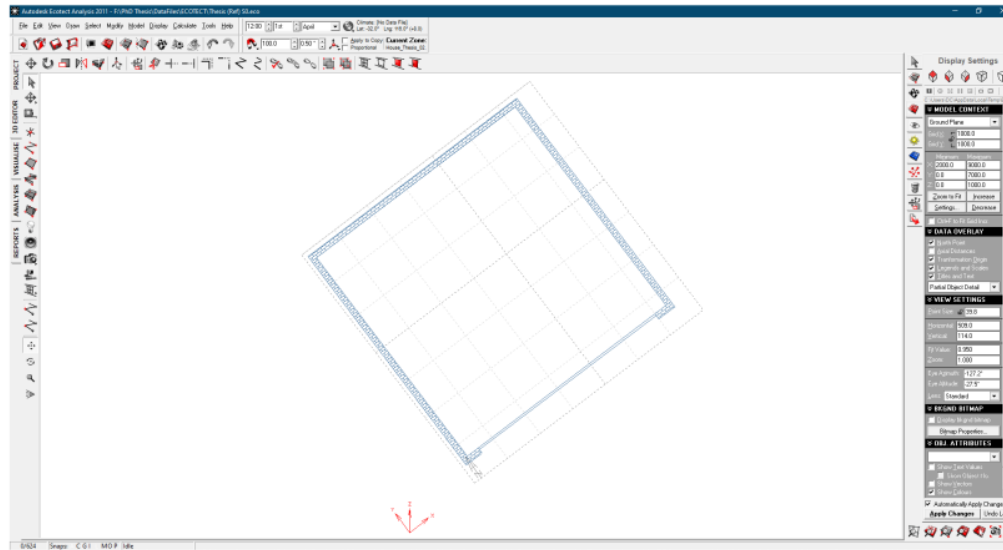


Fig. 4.16 AutoCAD plan as imported in ECOTECT interface

Following parameters were selected among the options available in ECOTECT software.

Clothing – 1.00 Clo (Light Business Suit)

Air speed – 0.3m/s (Barely noticeable)

Lighting Flux - 400 lux (office desk / workshop)

Activity – 65W (Typing)

A comparison of overall heat transfer coefficient values of building components as obtained from guarded hot box testing and as obtained from ECOTECT simulation has been tabulated as Table 4.5.

Table 4.5 - Overall heat transfer values comparison using ECOTECT:

	U-value obtained from GHB testing	U-value as calculated in ECOTECT	Percent deviation (%)
Wall	2.549 W/m ² K	2.720 W/m ² K	(+)6.71
Roof	4.332 W/m ² K	3.640 W/m ² K	(-)19.01
Glazing	2.875 W/m ² K	2.730 W/m ² K	(-)5.04

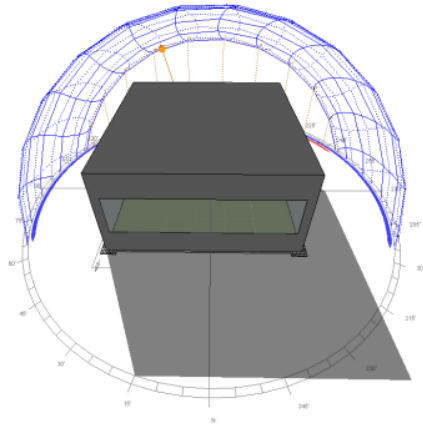


Fig. 4.17 Surface Azimuth angle of Window is 0° (N0) in ECOTECT (North facing)

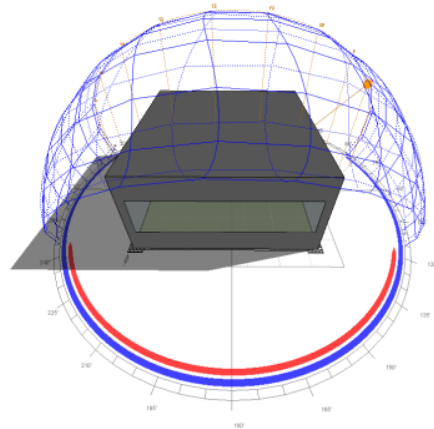


Fig. 4.18 Surface Azimuth angle of Window is 180° (S0) in ECOTECT (South facing)

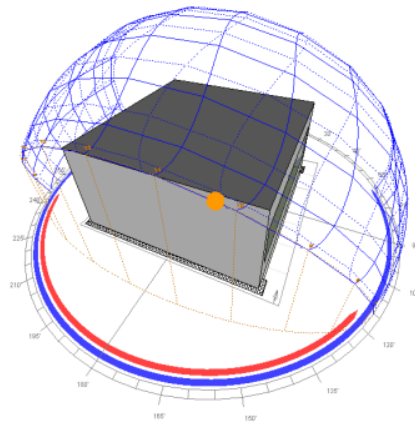


Fig. 4.19 Surface Azimuth angle of Window is 90° (E0) in ECOTECT (East facing)

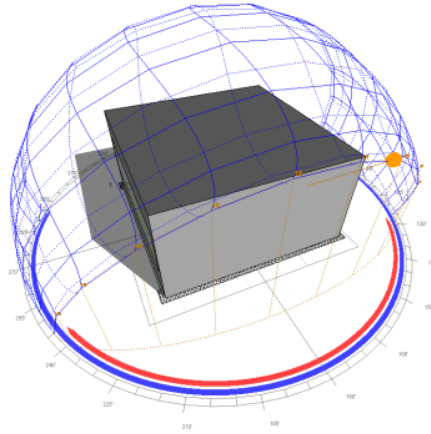


Fig. 4.20 Surface Azimuth angle of Window is -90° (W0) in ECOTECH (West facing)

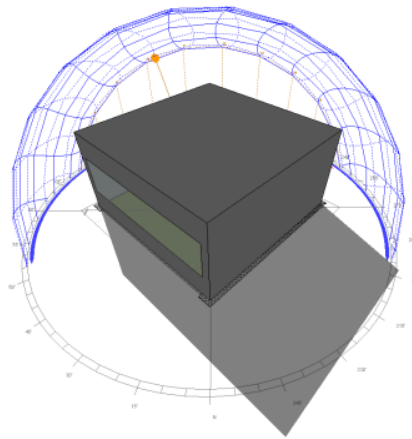


Fig. 4.21 Surface Azimuth angle of Window is 135° (NE45) in ECOTECH

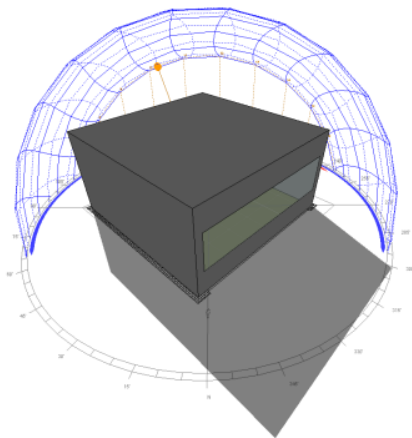


Fig. 4.22 Surface Azimuth angle of Window is -135° (NW45) in ECOTECH

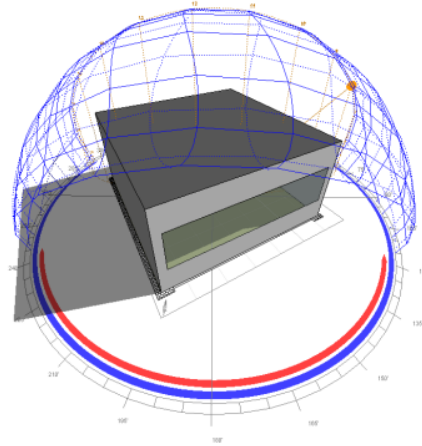


Fig. 4.23 Surface Azimuth angle of Window is -30° (SE30) in ECOTECH

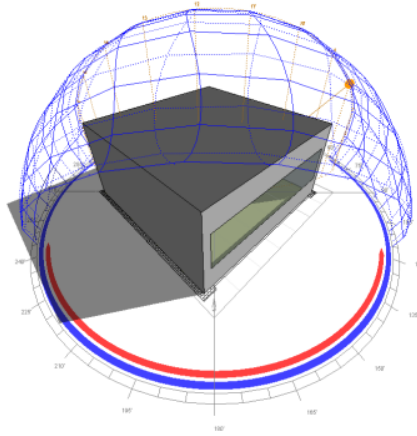


Fig. 4.24 Surface Azimuth angle of Window is -45° (SE45) in ECOTECH

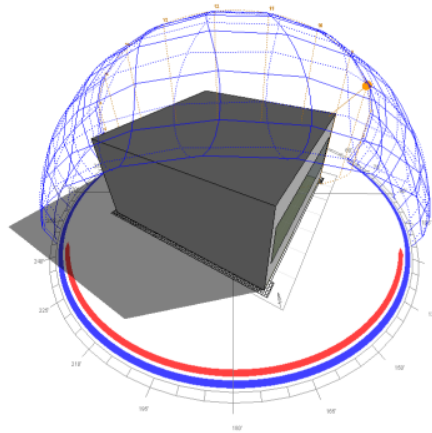


Fig. 4.25 Surface Azimuth angle of Window is -60° (SE60) in ECOTECH

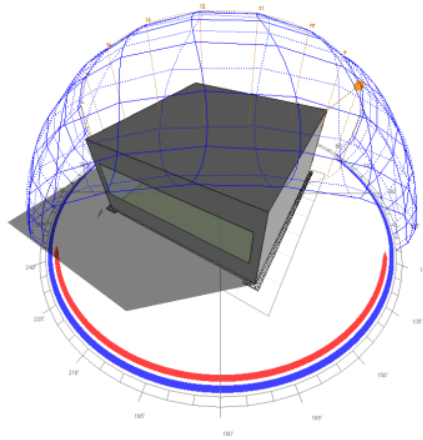


Fig. 4.26 Surface Azimuth angle of Window is 30° (SW30) in ECOTECH

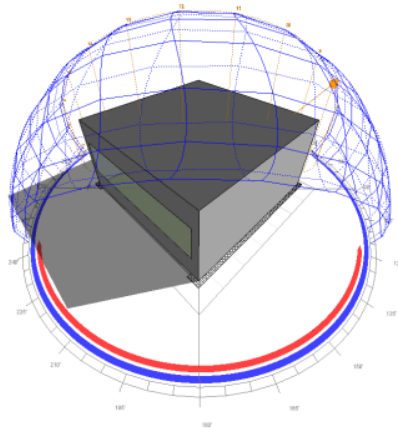


Fig. 4.27 Surface Azimuth angle of Window is 45° (SW45) in ECOTECH

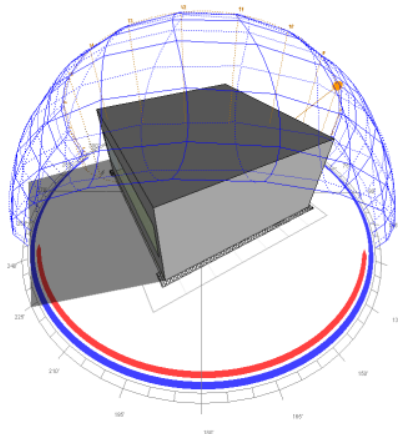


Fig. 4.28 Surface Azimuth angle of Window is 60° (SW60) in ECOTECH

4.3.3 eQUEST simulation

eQUEST or the QUick Energy Simulation Tool is a building energy simulation software from James J. Hirsch and Associates which is based on US Department of Energy or DOE-2.3 from the Lawrence Berkeley National Laboratory. It has a Window-based interface to the DOE-2.3 simulation engine. It performs simulation on an hourly basis. The simulation engine had been designed to study the energy performance of the whole building during the design phase (B. Birdsall *et. al*, 1990). The plan of building geometry was incorporated into the software using AutoCAD based dxf file in ‘building footprint section’. It can also be done using pdf file of the building plan. Proper zoning was done using the built-in tool in eQUEST. From the imported building plan (Fig. 4.29), the thermal zone was traced out. The air conditioning unit was selected as ‘Packaged Terminal AC’ with provision of heating, air economiser, heat recovery, outside ventilation turned off. The condenser was chosen as air cooled. DOE 2.3 within eQUEST performs an hourly simulation of the building based on walls, windows, glazing facades, people, plug loads, and ventilation and simulates the performance of pumps, fans, boilers, chillers and other energy-consuming devices installed in the building. eQUEST uses the concept of shells which is basically a thermal zone. Individual masonry construction data, glazing data were incorporated into the simulation software and the necessary schedules were setup as per Table 4.1 and Table 4.2. The various orientations of the building models that have been used are presented in Fig. 4.30 to Fig. 4.41.

A comparison of overall heat transfer coefficient values of building components as obtained from GHB testing and as calculated within eQUEST simulation has been tabulated as Table 4.6.

The Building Description Language (BDL) processor within the engine transforms this input into a computer readable format which is used by the following subroutines sequentially – LOADS, SYSTEMS, PLANT and ECONOMICS.

The LOADS subroutine computes the hourly cooling and heating loads for thermal zone of a building the BDL description and the weather data. It is a two-step process. Firstly, the heat losses or gains are calculated and then from the space heat losses or gains, the space loads are calculated (the effects of the thermal mass of the space are taken into consideration). The components of the space heat losses or gains include: solar heat gain through windows via transmission radiation, conductive heat transfer through walls, roof, windows and door (which are in contact with outside air), any unintended ventilation through infiltrated air, heat conduction from ground, floors, ceilings and heat gain from occupants, lights, equipment etc.

37

The resulting solutions, called "response factors" are then used in the hourly simulation modulated by the actual indoor and outdoor temperatures.

The SYSTEMS subroutine simply computes the total heating or cooling loads imposed upon the HVAC equipment to meet the defined air temperature set points of the zone.

The PLANT subroutine calculates the fuel requirements of the HVAC in order to meet the calculated performance of the system.

The ECONOMICS subroutine finally computes the costs of energy for the various fuels or utilities used by the equipment.

The DOE-2.3 uses transfer function method at its core which is an approximation of the heat balance method used in EnergyPlus engine of DesignBuilder.

Thus, we can see that DOE-2.3 at first calculates the loads in the thermal zone considering the external and internal loads. Depending upon the temperature difference between the zone in the question and adjacent space, heat transfer is determined while taking the effect of thermal mass. Then the resulting loads are used as an input for HVAC calculations. Thus, the building response to thermal loads is calculated independently of system operation. There is no feedback from HVAC system calculation to load calculation. This may affect the accuracy of the simulation system. However, the runtime of DOE-2.3 based eQUEST simulation is much faster than EnergyPlus based DesignBuilder but slower than ECOTECT. This computational efficiency is due to the sequential software structure which does not simultaneously solve the building thermal dynamics along with HVAC system.

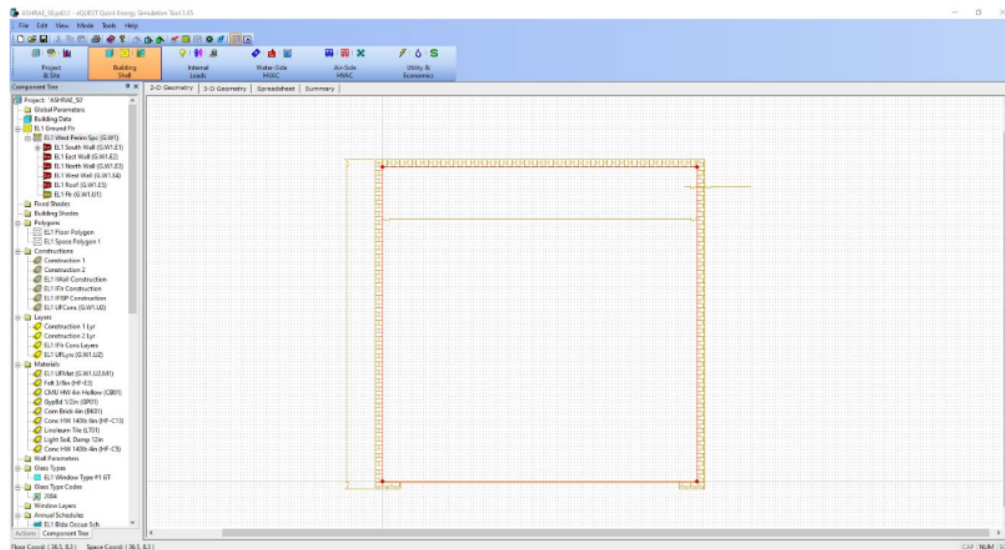


Fig. 4.29 AutoCAD plan as imported in eQUEST interface

Table 4.6 - Overall heat transfer values comparison using eQUEST (eQUEST uses imperial unit system)

	U-value obtained from GHB testing	U-value as calculated in eQUEST	Percent deviation (%)
Wall	0.449 Btu/(hr-ft ² °F) (2.549 W/m ² K)	0.570 Btu/(hr-ft ² °F) (3.278 W/m ² K)	(+)28.6
Roof	0.763 Btu/(hr-ft ² °F) (4.332 W/m ² K)	0.863 Btu/(hr-ft ² °F) (4.622 W/m ² K)	(+)7.62
Glazing	0.507 Btu/(hr-ft ² °F) (2.875 W/m ² K)	0.479 Btu/(hr-ft ² °F) (2.720 W/m ² K)	(-)5.39

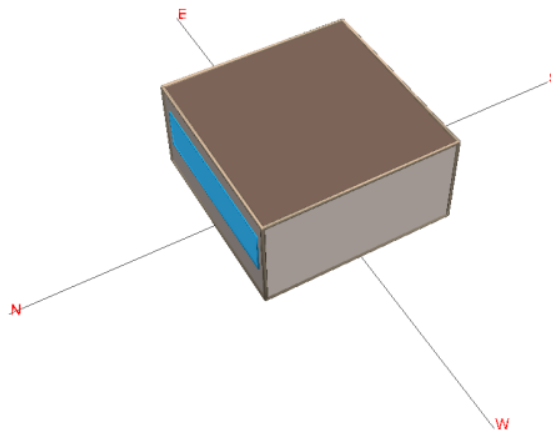


Fig. 4.30 Surface Azimuth angle of Window is 180° (N0) in eQUEST (North facing)

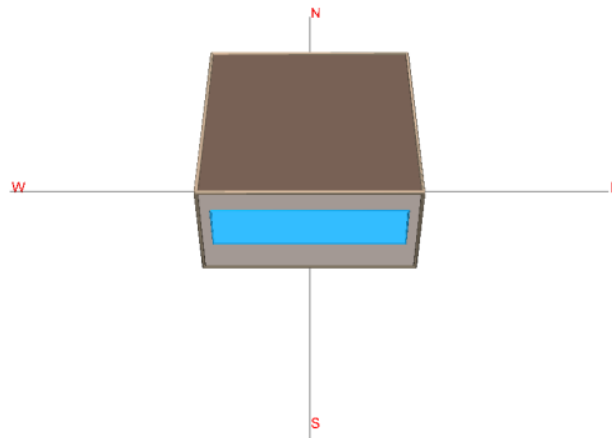


Fig. 4.31 Surface Azimuth angle of Window is 0° (S0) in eQUEST (South facing)

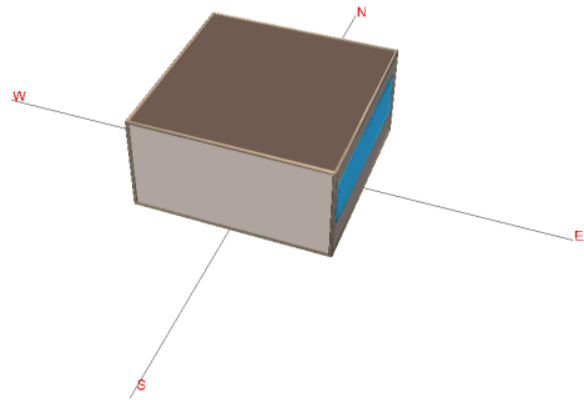


Fig. 4.32 Surface Azimuth angle of Window is 270° (E0) in eQUEST (East facing)

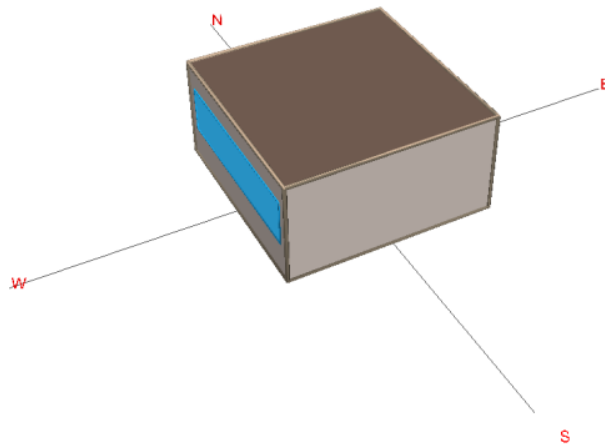


Fig. 4.33 Surface Azimuth angle of Window is 90° (W0) in eQUEST (West facing)

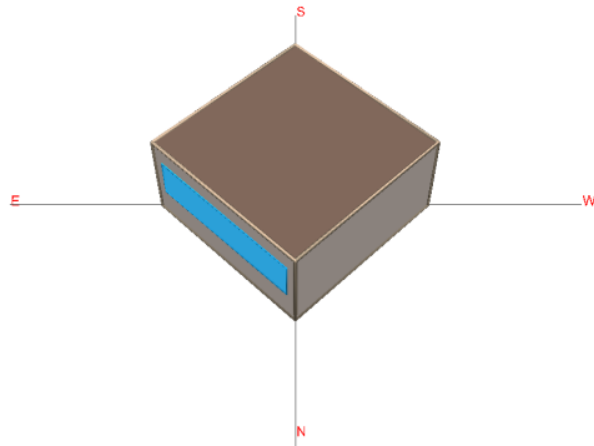


Fig. 4.34 Surface Azimuth angle of Window is 225° (NE45) in eQUEST

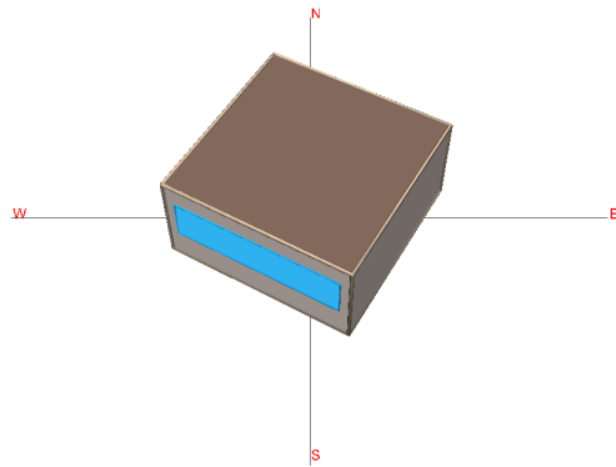
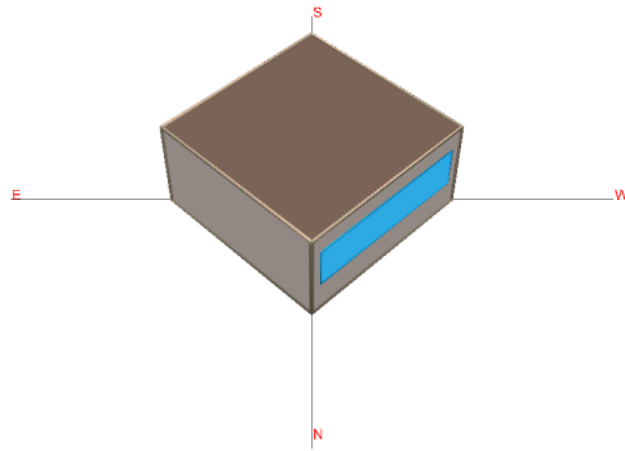


Fig. 4.36 Surface Azimuth angle of Window is 30° (SW 30) in eQUEST

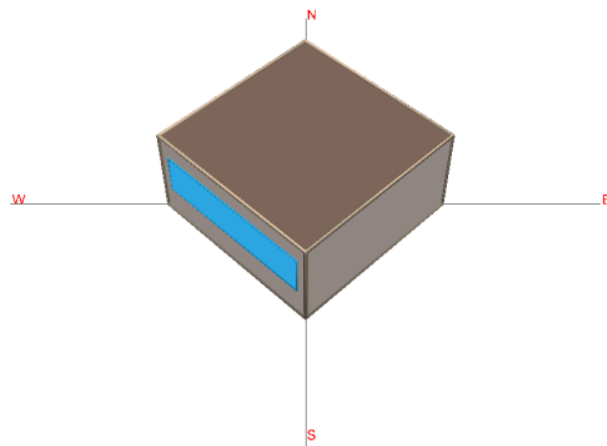


Fig. 4.37 Surface Azimuth angle of Window is 45° (SW 45) in eQUEST

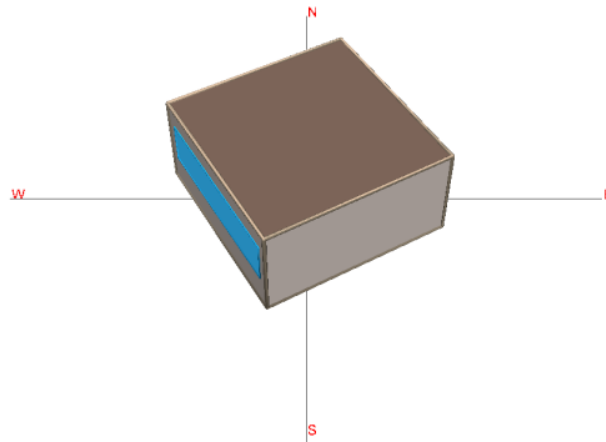


Fig. 4.38 Surface Azimuth angle of Window is 60° (SW 60) in eQUEST

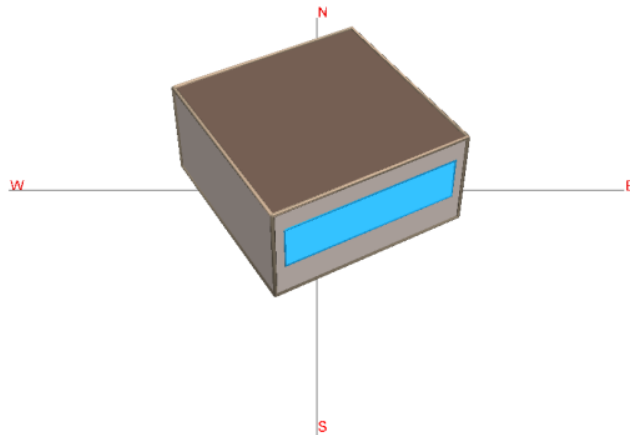


Fig. 4.39 Surface Azimuth angle of Window is 330° (SE 30) in eQUEST

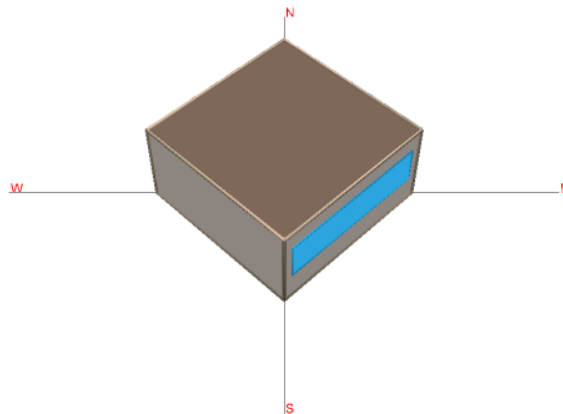


Fig. 4.40 Surface Azimuth angle of Window is 315° (SE 45) in eQUEST

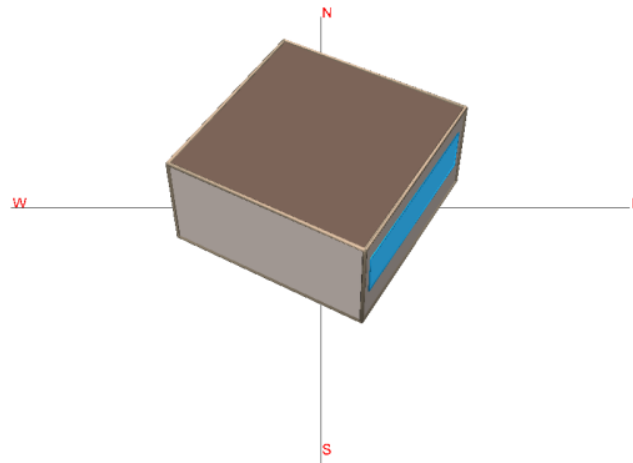


Fig. 4.41 Surface Azimuth angle of Window is 300° (SE 60) in eQUEST

4.4 Results

4.4.1 DesignBuilder Simulation Results

The monthly cooling electrical energy consumptions / cooling load have been tabulated (Table 4.7 to Table 4.18) and presented graphically as well (Fig. 4.42 to Fig. 4.53) for each individual orientation of the building. Here '**Cooling Energy w.r.t. ASHRAE**' refers to the scenario where the simulation was carried out using the thermos-physical properties of the construction materials as per *ASHRAE Handbook Fundamentals, 2017* (Table 4.1). The '**Cooling Energy w.r.t. GHB**' refers to the scenario where the overall heat transfer coefficient values of wall, roof and glazing as obtained from experiment results (Chapter 3) were directly impregnated into the simulation software. The difference in cooling demand between experimental method (**Cooling Energy w.r.t. GHB**) and ASHRAE method scenario has also been calculated and the resultant percentage deviation has also been shown in tables below.

Table 4.7 - Monthly Cooling Demand in kWh for orientation N0 by Experimental value and ASHRAE value in DesignBuilder (North facing).

Month	Cooling Energy w.r.t. GHB (kWh)	Cooling Energy w.r.t. ASHRAE (kWh)	Difference (kWh)	Percentage Deviation (%)
January	138.4	142.6	4.22	(+)3.05
February	162.7	169.5	6.79	(+)4.17
March	365.2	373.5	8.31	(+)2.28
April	433.6	439.8	6.15	(+)1.42
May	612.5	612.1	-0.44	(-)0.07
June	529.9	529.8	-0.06	(-)0.01
July	391.0	391.6	0.55	(+)0.14
August	456.1	457.7	1.61	(+)0.35
September	351.7	356.3	4.66	(+)1.32
October	411.7	415.5	3.78	(+)0.92
November	287.5	292.5	4.93	(+)1.71
December	181.0	185.8	4.77	(+)2.64

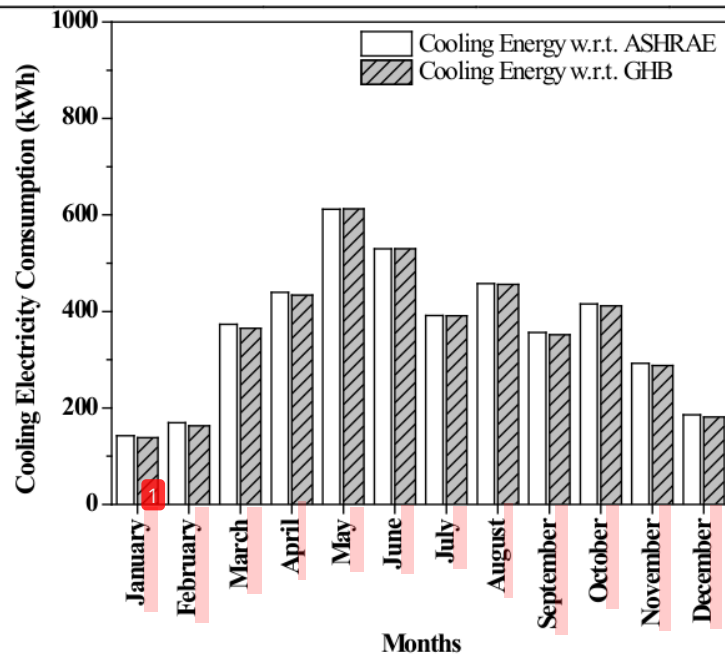


Fig. 4.42 Monthly variation of Cooling Demand for orientation N0 in DesignBuilder (North facing)

Table 4.8 - Monthly Cooling Demand in kWh for orientation S0 by Experimental value and ASHRAE value in DesignBuilder (South facing).

Month	Cooling Energy w.r.t. GHB (kWh)	Cooling Energy w.r.t. ASHRAE (kWh)	Difference (kWh)	Percentage Deviation (%)
January	197.8	197.8	0.00	0.00
February	180.6	185.6	5.00	(+)2.77
March	378.5	385.8	7.30	(+)1.93
April	436.5	442.4	5.90	(+)1.35
May	611.3	610.9	-0.40	(-)0.07
June	526.6	526.9	0.30	(+)0.06
July	389.7	390.4	0.70	(+)0.18
August	458.9	460.2	1.30	(+)0.28
September	356.2	360.1	3.90	(+)1.09
October	443.9	445.4	1.50	(+)0.34
November	348.6	349.6	1.00	(+)0.29
December	245.0	245.4	0.40	(+)0.16

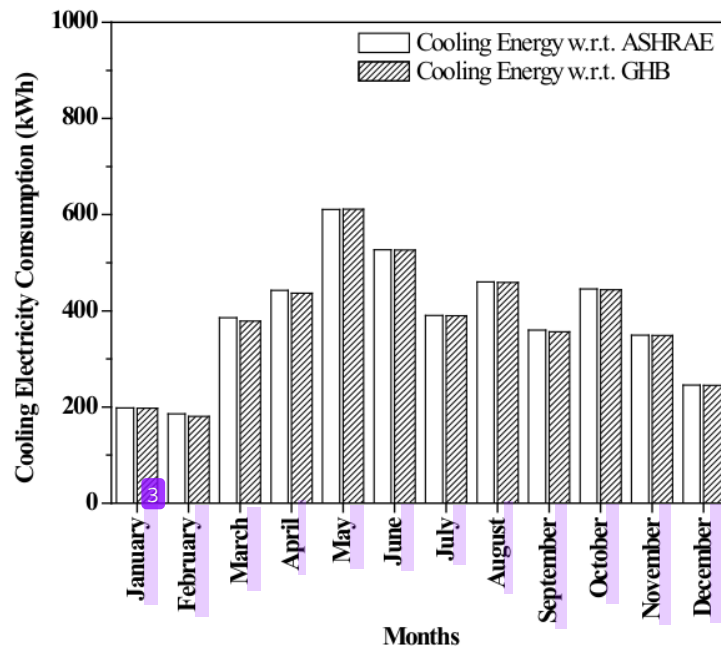


Fig. 4.43 Monthly variation of Cooling Demand for orientation S0 in DesignBuilder (South Facing)

Table 4.9 - Monthly Cooling Demand in kWh for orientation E0 by Experimental value and ASHRAE value in DesignBuilder (East facing).

Month	Cooling Energy w.r.t. GHB (kWh)	Cooling Energy w.r.t. ASHRAE (kWh)	Difference (kWh)	Percentage Deviation (%)
January	149.4	152.2	2.86	(+)1.91
February	188.4	192.6	4.25	(+)2.25
March	408.9	413.5	4.54	(+)1.11
April	474.9	477.6	2.62	(+)0.55
May	639.8	637.7	-2.10	(-)0.33
June	546.9	545.5	-1.45	(-)0.27
July	402.5	402.1	-0.42	(-)0.10
August	473.0	473.4	0.35	(+)0.07
September	386.5	387.9	1.46	(+)0.38
October	429.6	431.6	2.04	(+)0.48
November	305.2	308.5	3.24	(+)1.06
December	194.5	197.8	3.26	(+)1.67

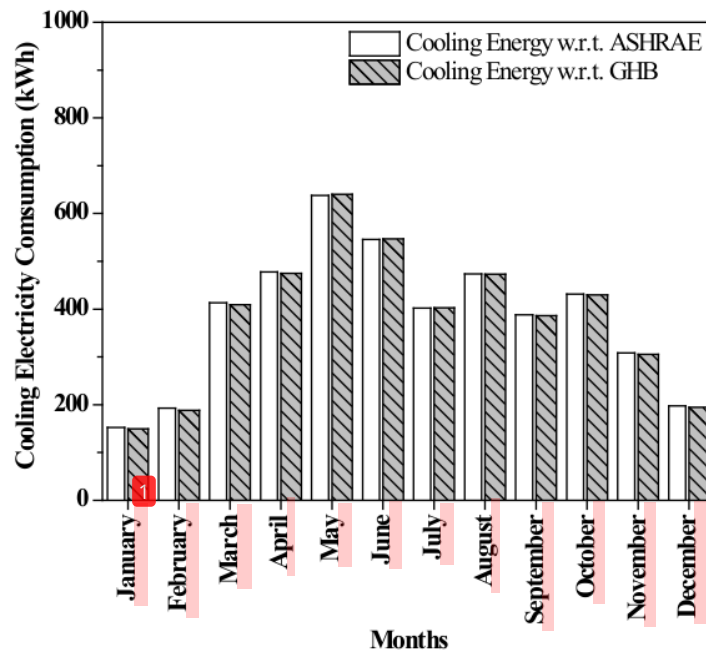


Fig. 4.44 Monthly variation of Cooling Demand for orientation E0 in DesignBuilder (East facing)

Table 4.10 - Monthly Cooling Demand in kWh for orientation W0 by Experimental value and ASHRAE value in DesignBuilder (West facing).

Month	Cooling Energy w.r.t. GHB (kWh)	Cooling Energy w.r.t. ASHRAE (kWh)	Difference (kWh)	Percentage Deviation (%)
January	163.1	166.2	3.15	(+)1.93
February	162.3	168.8	6.54	(+)4.03
March	364.9	372.9	8.03	(+)2.20
April	433.8	439.9	6.11	(+)1.41
May	644.7	642.7	-1.95	(-)0.30
June	550.4	549.5	-0.82	(-)0.15
July	402.3	402.5	0.17	(+)0.04
August	473.6	474.5	0.91	(+)0.19
September	351.7	356.4	4.65	(+)1.32
October	430.4	433.1	2.74	(+)0.64
November	311.2	315.0	3.76	(+)1.21
December	201.7	205.5	3.75	(+)1.86

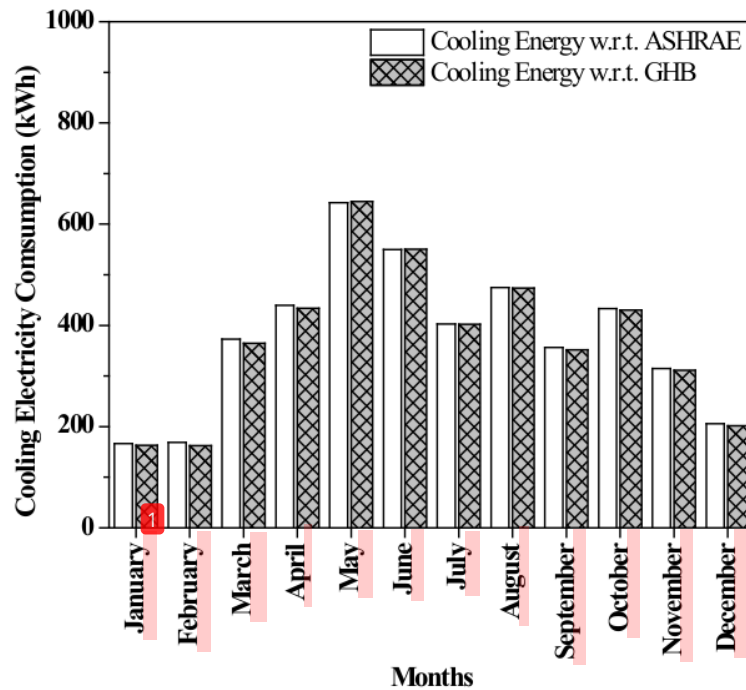


Fig. 4.45 Monthly variation of Cooling Demand for orientation W0 in DesignBuilder (West facing)

Table 4.11 - Monthly Cooling Demand in kWh for orientation NE45 by Experimental value and ASHRAE value in DesignBuilder.

Month	Cooling Energy w.r.t. GHB (kWh)	Cooling Energy w.r.t. ASHRAE (kWh)	Difference (kWh)	Percentage Deviation (%)
January	132.5	136.1	3.57	(+)2.70
February	165.0	170.7	5.65	(+)3.42
March	386.9	394.0	7.03	(+)1.82
April	467.5	472.9	5.35	(+)1.14
May	641.2	639.9	-1.27	(-)0.20
June	548.5	548.6	0.07	(+)0.01
July	402.9	403.3	0.46	(+)0.11
August	470.3	471.6	1.34	(+)0.29
September	381.6	384.9	3.25	(+)0.85
October	412.1	414.8	2.66	(+)0.65
November	281.4	285.3	3.87	(+)1.37
December	174.9	179.0	4.02	(+)2.30

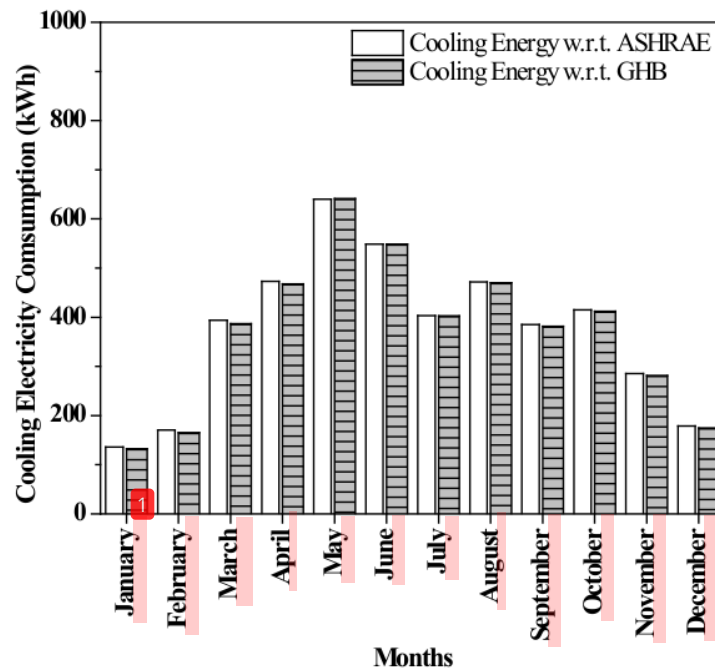


Fig. 4.46 Monthly variation of Cooling Demand for orientation NE45 in DesignBuilder

Table 4.12 - Monthly Cooling Demand in kWh for orientation NW45 by Experimental value and ASHRAE value in DesignBuilder.

Month	Cooling Energy w.r.t. GHB (kWh)	Cooling Energy w.r.t. ASHRAE (kWh)	Difference (kWh)	Percentage Deviation (%)
January	133.7	137.3	3.62	(+)2.71
February	160.4	166.6	6.20	(+)3.86
March	372.1	380.3	8.23	(+)2.21
April	445.0	452.1	7.16	(+)1.61
May	645.3	645.5	0.25	(+)0.04
June	552.2	552.5	0.32	(+)0.06
July	403.5	404.3	0.89	(+)0.22
August	472.1	473.8	1.66	(+)0.35
September	362.8	367.9	5.02	(+)1.38
October	412.7	415.5	2.81	(+)0.68
November	282.2	285.9	3.70	(+)1.31
December	175.4	179.4	4.06	(+)2.32

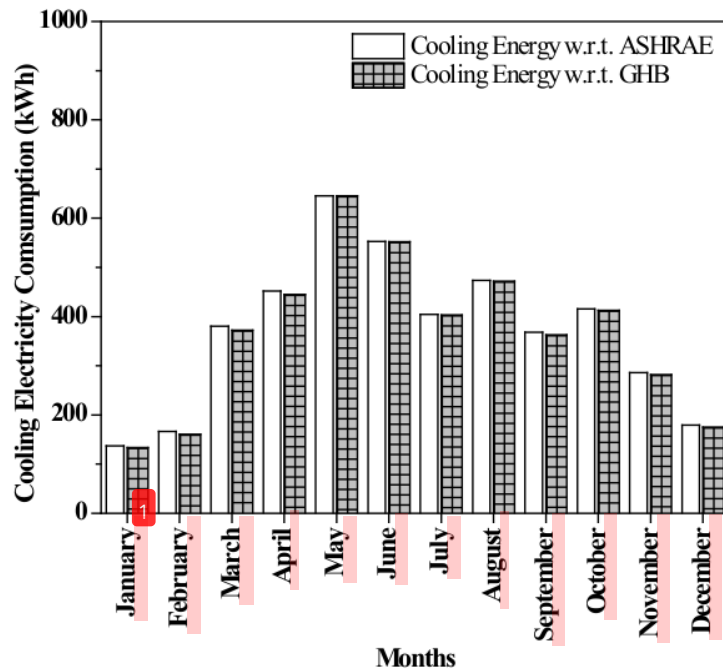


Fig. 4.47 Monthly variation of Cooling Demand for orientation NW45 in DesignBuilder

Table 4.13 - Monthly Cooling Demand in kWh for orientation SE30 by Experimental value and ASHRAE value in DesignBuilder.

Month	Cooling Energy w.r.t. GHB (kWh)	Cooling Energy w.r.t. ASHRAE (kWh)	Difference (kWh)	Percentage Deviation (%)
January	176.5	176.3	-0.20	(-)0.11
February	195.4	199.4	4.00	(+)2.05
March	411.1	417.2	6.10	(+)1.48
April	462.9	468.7	5.80	(+)1.25
May	626.8	626.6	-0.20	(-)0.03
June	533.6	533.9	0.30	(+)0.06
July	395.0	395.4	0.40	(+)0.10
August	468.9	470.3	1.40	(+)0.30
September	382.4	386.4	4.00	(+)1.05
October	441.7	442.9	1.20	(+)0.27
November	331.8	332.7	0.90	(+)0.27
December	226.4	226.6	0.20	(+)0.09

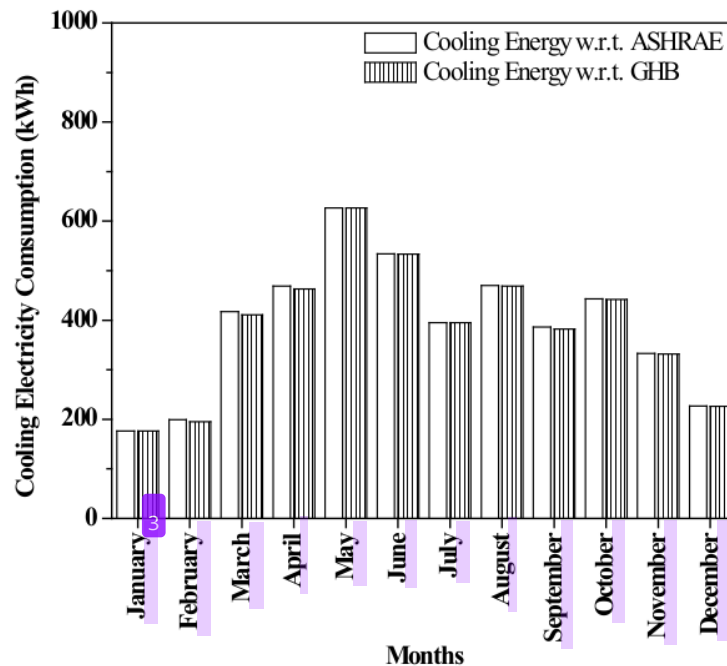


Fig. 4.48 Monthly variation of Cooling Demand for orientation SE30 in DesignBuilder

Table 4.14 - Monthly Cooling Demand in kWh for orientation SE45 by Experimental value and ASHRAE value in DesignBuilder.

Month	Cooling Energy w.r.t. GHB (kWh)	Cooling Energy w.r.t. ASHRAE (kWh)	Difference (kWh)	Percentage Deviation (%)
January	164.8	164.9	0.10	(+)0.06
February	195.0	198.3	3.30	(+)1.69
March	417.5	422.7	5.20	(+)1.25
April	475.4	479.8	4.40	(+)0.93
May	637.8	637.4	-0.40	(-)0.06
June	542.1	542.4	0.30	(+)0.06
July	400.0	400.4	0.40	(+)0.10
August	474.4	475.2	0.80	(+)0.17
September	391.3	393.5	2.20	(+)0.56
October	438.4	439.7	1.30	(+)0.30
November	321.9	322.8	0.90	(+)0.28
December	214.2	214.7	0.50	(+)0.23

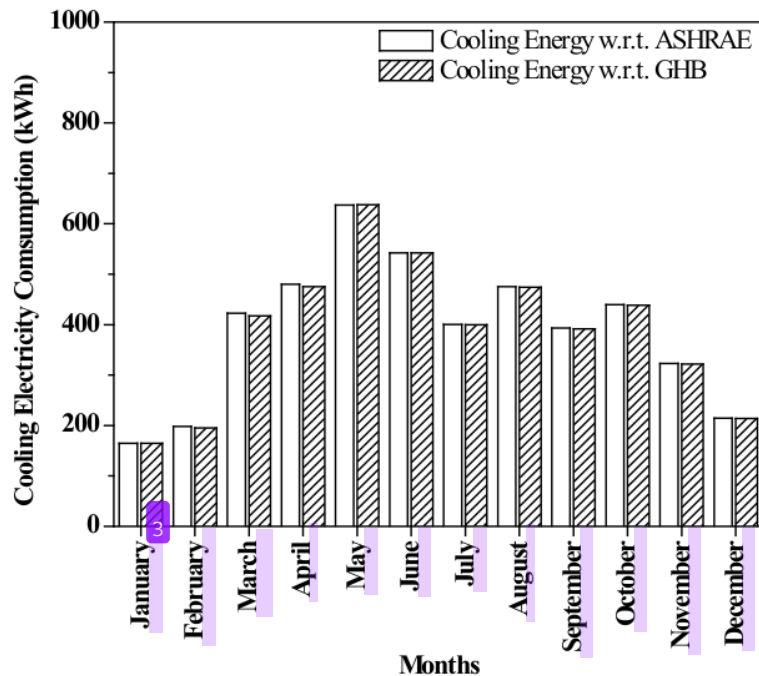


Fig. 4.49 Monthly variation of Cooling Demand for orientation SE45 in DesignBuilder.

Table 4.15 - Monthly Cooling Demand in kWh for orientation SE60 by Experimental value and ASHRAE value in DesignBuilder.

Month	Cooling Energy w.r.t. GHB (kWh)	Cooling Energy w.r.t. ASHRAE (kWh)	Difference (kWh)	Percentage Deviation (%)
January	157.7	158.7	1.00	(+)0.63
February	191.3	194.3	3.00	(+)1.57
March	415.7	419.8	4.10	(+)0.99
April	480.3	484.0	3.70	(+)0.77
May	644.0	642.6	-1.40	(-)0.22
June	546.9	547.3	0.40	(+)0.07
July	402.9	403.3	0.40	(+)0.10
August	476.3	476.9	0.60	(+)0.13
September	393.4	395.4	2.00	(+)0.51
October	434.8	436.0	1.20	(+)0.28
November	315.3	316.7	1.40	(+)0.44
December	206.5	207.8	1.30	(+)0.63

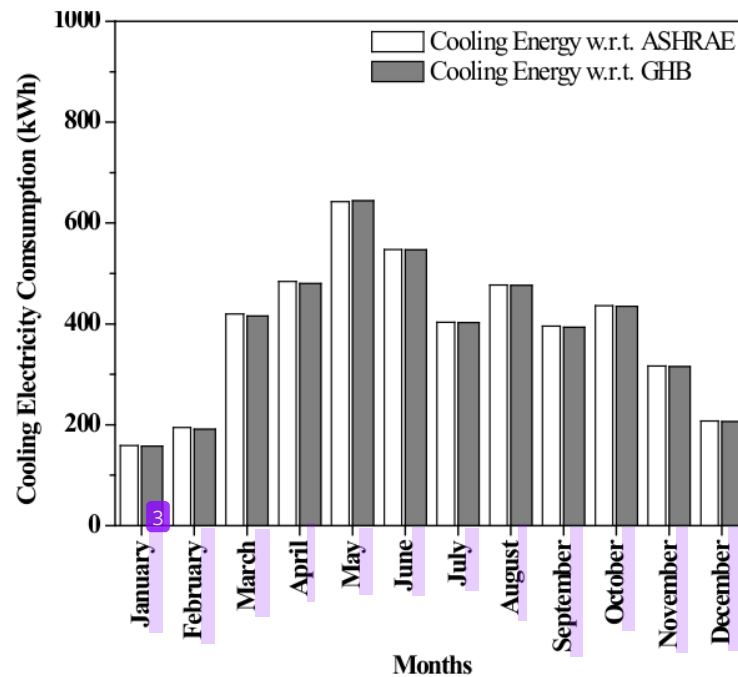


Fig. 4.50 Monthly variation of Cooling Demand for orientation SE60 in DesignBuilder.

Table 4.16 - Monthly Cooling Demand in kWh for orientation SW30 by Experimental value and ASHRAE value in DesignBuilder.

Month	Cooling Energy w.r.t. GHB (kWh)	Cooling Energy w.r.t. ASHRAE (kWh)	Difference (kWh)	Percentage Deviation (%)
January	188.8	189.2	0.40	(+)0.21
February	162.1	168.1	6.00	(+)3.70
March	369.8	377.9	8.10	(+)2.19
April	442.6	449.6	7.00	(+)1.58
May	630.5	630.7	0.20	(+)0.03
June	536.9	537.7	0.80	(+)0.15
July	396.4	397.4	1.00	(+)0.25
August	469.8	471.3	1.50	(+)0.32
September	360.4	365.1	4.70	(+)1.30
October	439.0	440.4	1.40	(+)0.32
November	335.8	337.0	1.20	(+)0.36
December	231.3	232.2	0.90	(+)0.39

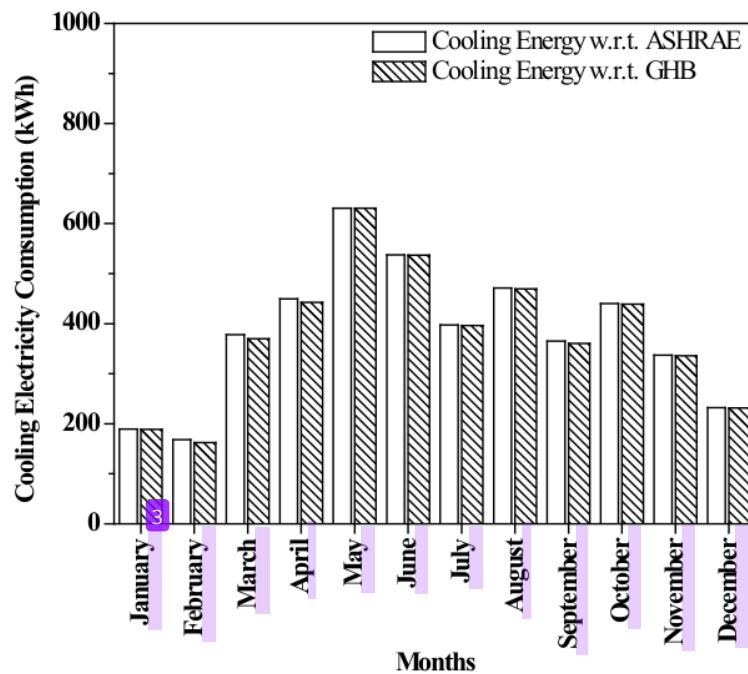


Fig. 4.51 Monthly variation of Cooling Demand for orientation SW30 in DesignBuilder.

Table 4.17 - Monthly Cooling Demand in kWh for orientation SW45 by Experimental value and ASHRAE value in DesignBuilder.

Month	Cooling Energy w.r.t. GHB (kWh)	Cooling Energy w.r.t. ASHRAE (kWh)	Difference (kWh)	Percentage Deviation (%)
January	182.4	183.3	0.90	(+)0.49
February	162.3	168.7	6.40	(+)3.94
March	372.9	381.8	8.90	(+)2.39
April	444.7	451.5	6.80	(+)1.53
May	640.2	640.5	0.30	(+)0.05
June	543.7	544.4	0.70	(+)0.13
July	400.0	400.9	0.90	(+)0.22
August	475.2	476.7	1.50	(+)0.32
September	362.5	367.6	5.10	(+)1.41
October	438.5	440.0	1.50	(+)0.34
November	328.6	330.0	1.40	(+)0.43
December	222.2	223.6	1.40	(+)0.63

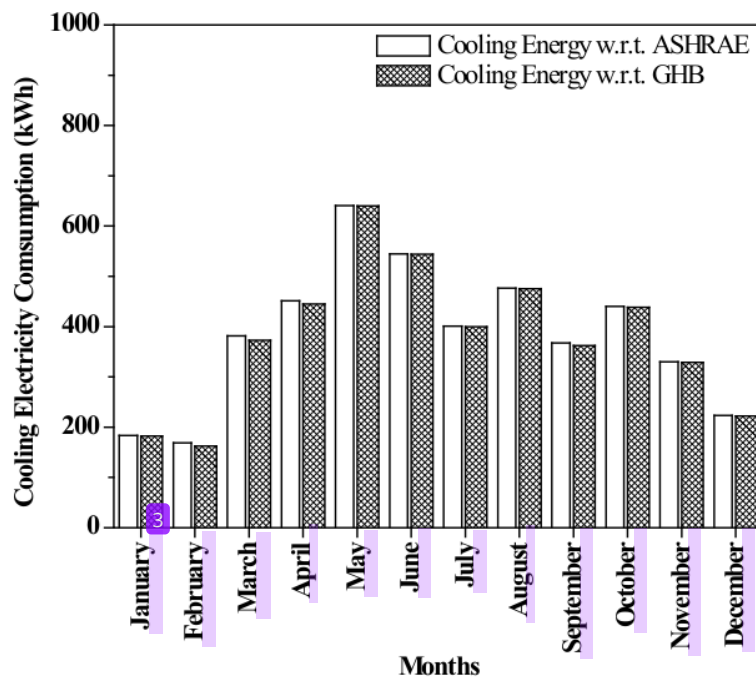


Fig. 4.52 Monthly variation of Cooling Demand for orientation SW45 in DesignBuilder.

Table 4.18 - Monthly Cooling Demand in kWh for orientation SW60 by Experimental value and ASHRAE value in DesignBuilder.

Month	Cooling Energy w.r.t. GHB (kWh)	Cooling Energy w.r.t. ASHRAE (kWh)	Difference (kWh)	Percentage Deviation (%)
January	177.6	179.3	1.70	(+)0.96
February	163.6	170.3	6.70	(+)4.10
March	373.9	382.7	8.80	(+)2.35
April	443.3	450.4	7.10	(+)1.60
May	645.6	645.1	-0.50	(-)0.08
June	547.0	547.3	0.30	(+)0.05
July	401.4	402.1	0.70	(+)0.17
August	477.2	478.4	1.20	(+)0.25
September	361.6	366.8	5.20	(+)1.44
October	437.7	439.5	1.80	(+)0.41
November	323.8	325.9	2.10	(+)0.65
December	216.1	218.3	2.20	(+)1.02

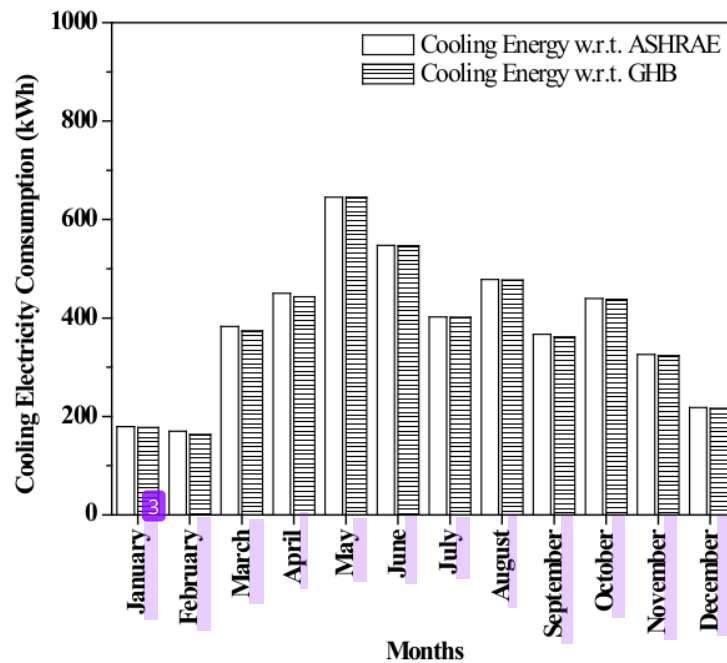


Fig. 4.53 Monthly variation of Cooling Demand for orientation SW60 in DesignBuilder.

From the results (as shown in Table 4.7 to 4.18), it is observed that the percentage deviation of cooling load is lowest in the months of May, June and July (i.e. during Summer months of Kolkata climate) for all the orientations. During these months for orientations North, South, East, West, North-East 45°, South-East 30°, South-East 45°, South-East 60° and South-West 60° the percentage deviation tends to be negative.

For the remaining months, specifically for the months of January, February, November and December (i.e. during winter months of Kolkata climate) the percentage deviation in cooling load is always positive. Moreover, the percentage deviation is also larger in these most for most of the orientations.

The simulated building model has a total wall area of 67.68 m², roof area of 37.16 m² and glazing area of 7.52m².

During peak summer months of May, June and July the zenith angle of the sun is small during solar noon as compared to the winter season when the zenith angle of the sun is higher at solar noon. Thus, for the summer months, impact of roof heat transfer during solar noon is predominant while the impact of East and West wall heat transfer during sunset and sunrise hours is also more. For the winter months, the impact of wall heat transfer is more than that of the roof during solar noon.

Now from the comparative analysis (Table 4.4) of overall heat transfer values obtained from DesignBuilder and Guarded hot box results ⁹³ it can be seen that the overall heat transfer coefficient value of wall as calculated in DesignBuilder is 2.785 W/m²K. It is found to be greater than the experimentally obtained value of 2.549 W/m²K. For the roof material the experimentally obtained U-value is 2.549 W/m²K and that obtained for DesignBuilder is computed to be 4.223 W/m²K.

As such during summer season the impact of roof heat transfer is predominant as compared to wall heat transfer. This results in higher cooling load for experimentally obtained overall heat transfer coefficient induced simulation (Cooling Energy w.r.t. GHB) for the summer seasons. Thus, the percentage deviation during these months tends to be negative.

The U-value of wall obtained from DesignBuilder is found to be higher and when this value is utilised for computing the cooling load through the walls having larger surface area, it results in higher cooling load (Cooling w.r.t. ASHRAE). Thus, for winter season, the percentage deviation of cooling load difference is also higher.

4.4.2 ECOTECT Simulation Results

The monthly cooling loads / cooling demands have been tabulated (Table 4.19 to Table 4.30) and presented graphically as well (Fig. 4.54 to Fig. 4.65) for each individual orientation. Here ‘Cooling Energy w.r.t. ASHRAE’ refers to the scenario where the simulation was carried out using the thermos-physical properties of the construction materials as per *ASHRAE Handbook Fundamentals, 2017* (Table 4.1) and ‘Cooling Energy w.r.t. GHB’ refers to the scenario where the overall heat transfer coefficient values of wall, roof and glazing as obtained from experiment results (Chapter 3) were directly impregnated into ECOTECT simulation software. The difference in cooling loads calculated with respect to the ‘Cooling Energy w.r.t. GHB’ scenario has also been calculated and the resultant percentage deviation has also been shown in tables below.

Table 4.19 - Monthly Cooling Load in kWh for orientation N0 by Experimental value and ASHRAE value in ECOTECT (North facing).

Month	Cooling Energy w.r.t. GHB (kWh)	Cooling Energy w.r.t. ASHRAE (kWh)	Difference (kWh)	Percentage Deviation (%)
January	653.4	613.6	-39.75	(-)6.08
February	761.0	719.2	-41.78	(-)5.49
March	1364.2	1285.5	-78.69	(-)5.77
April	1592.5	1495.0	-97.46	(-)6.12
May	1933.8	1825.2	-108.63	(-)5.62
June	1704.8	1610.2	-94.59	(-)5.55
July	1474.3	1396.3	-77.97	(-)5.29
August	1439.7	1364.4	-75.26	(-)5.23
September	1219.4	1151.5	-67.95	(-)5.57
October	1343.5	1276.5	-67.01	(-)4.99
November	1073.7	1023.8	-49.91	(-)4.65
December	741.1	699.7	-41.40	(-)5.59

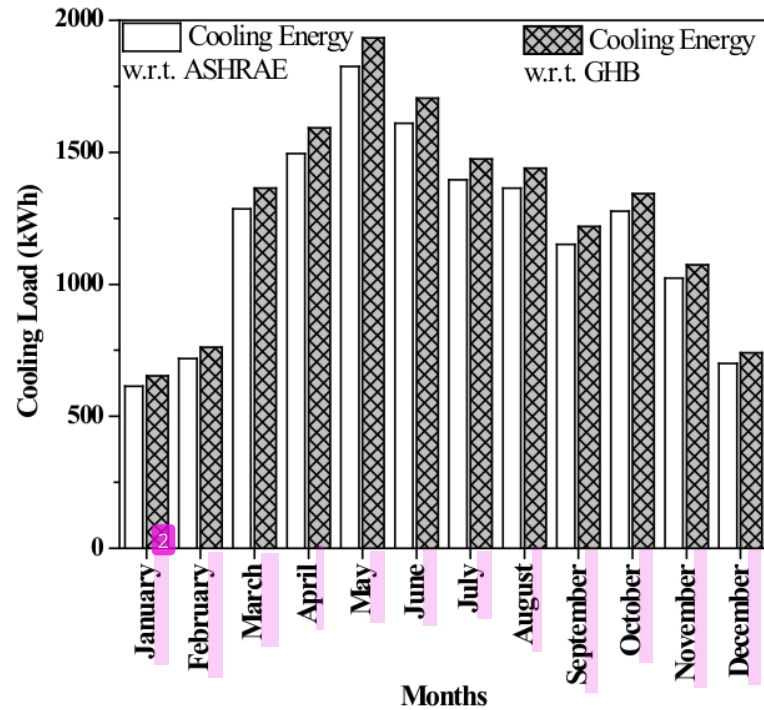


Fig. 4.54 Monthly variation of Cooling Demand for orientation N0 in ECOTECT (North facing).

Table 4.20 - Monthly Cooling Demand in kWh for orientation S0 by Experimental value and ASHRAE value in ECOTECT (South facing).

Month	Cooling Energy w.r.t. GHB (kWh)	Cooling Energy w.r.t. ASHRAE (kWh)	Difference (kWh)	Percentage Deviation (%)
January	679.7	642.1	-37.60	(-5.53)
February	774.7	728.3	-46.40	(-5.99)
March	1375.7	1295.8	-79.90	(-5.81)
April	1593.2	1495.9	-97.30	(-6.11)
May	1934.1	1825.7	-108.40	(-5.60)
June	1699.4	1605.8	-93.60	(-5.51)
July	1471.5	1394.1	-77.40	(-5.26)
August	1444.9	1369.4	-75.50	(-5.23)
September	1221.8	1153.7	-68.10	(-5.57)
October	1379.6	1309.2	-70.40	(-5.10)
November	1138.9	1083.6	-55.30	(-4.86)
December	786.7	739.1	-47.60	(-6.05)

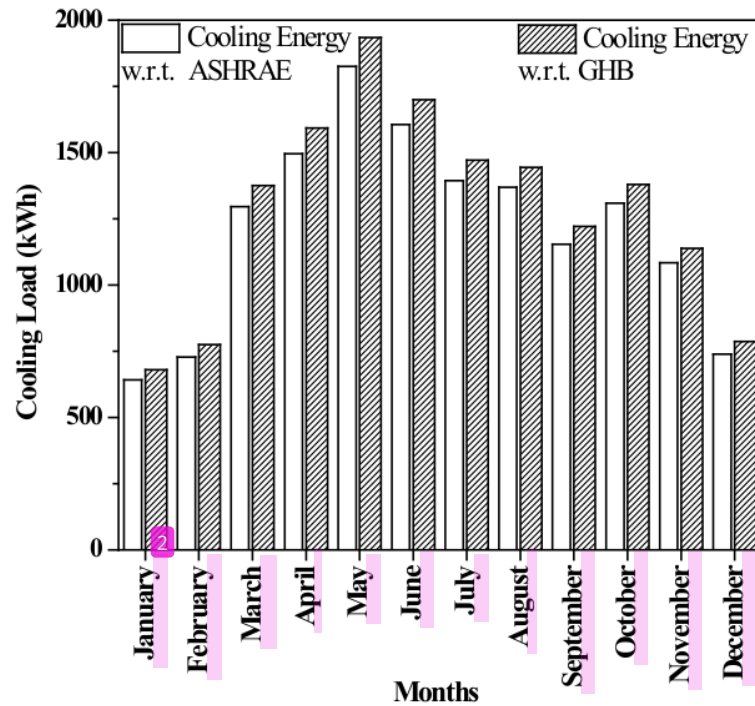


Fig. 4.55 Monthly variation of Cooling Demand for orientation S0 in ECOTECT (South facing).

Table 4.21 - Monthly Cooling Demand in kWh for orientation E0 by Experimental value and ASHRAE value in ECOTECT (East facing).

Month	Cooling Energy w.r.t. GHB (kWh)	Cooling Energy w.r.t. ASHRAE (kWh)	Difference (kWh)	Percentage Deviation (%)
January	635.5	590.7	-44.81	(-)7.05
February	761.6	710.5	-51.05	(-)6.70
March	1380.0	1295.8	-84.20	(-)6.10
April	1607.9	1506.9	-100.94	(-)6.28
May	1939.0	1829.4	-109.56	(-)5.65
June	1705.7	1611.5	-94.19	(-)5.52
July	1476.4	1398.5	-77.92	(-)5.28
August	1443.4	1367.0	-76.45	(-)5.30
September	1230.8	1160.7	-70.02	(-)5.69
October	1352.9	1282.8	-70.09	(-)5.18
November	1083.1	1030.5	-52.58	(-)4.85
December	722.3	680.9	-41.42	(-)5.73

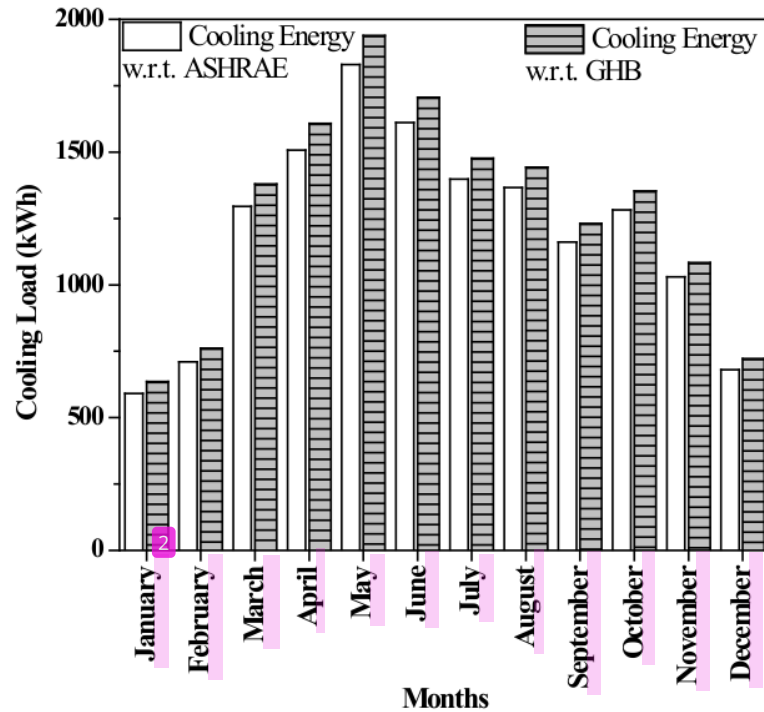


Fig. 4.56 Monthly variation of Cooling Demand for orientation E0 in ECOTECT (East facing).

Table 4.22 - Monthly Cooling Demand in kWh for orientation W0 by Experimental value and ASHRAE value in ECOTECT (West facing).

Month	Cooling Energy w.r.t. GHB (kWh)	Cooling Energy w.r.t. ASHRAE (kWh)	Difference (kWh)	Percentage Deviation (%)
January	696.1	658.6	-37.43	(-)5.38
February	770.4	726.7	-43.68	(-)5.67
March	1363.6	1284.8	-78.84	(-)5.78
April	1585.9	1488.9	-97.03	(-)6.12
May	1965.4	1857.3	-108.18	(-)5.50
June	1722.9	1629.2	-93.67	(-)5.44
July	1485.6	1408.1	-77.49	(-)5.22
August	1457.0	1381.5	-75.42	(-)5.18
September	1216.7	1148.8	-67.86	(-)5.58
October	1364.0	1295.9	-68.13	(-)4.99
November	1101.5	1049.5	-51.96	(-)4.72
December	769.0	727.3	-41.67	(-)5.42

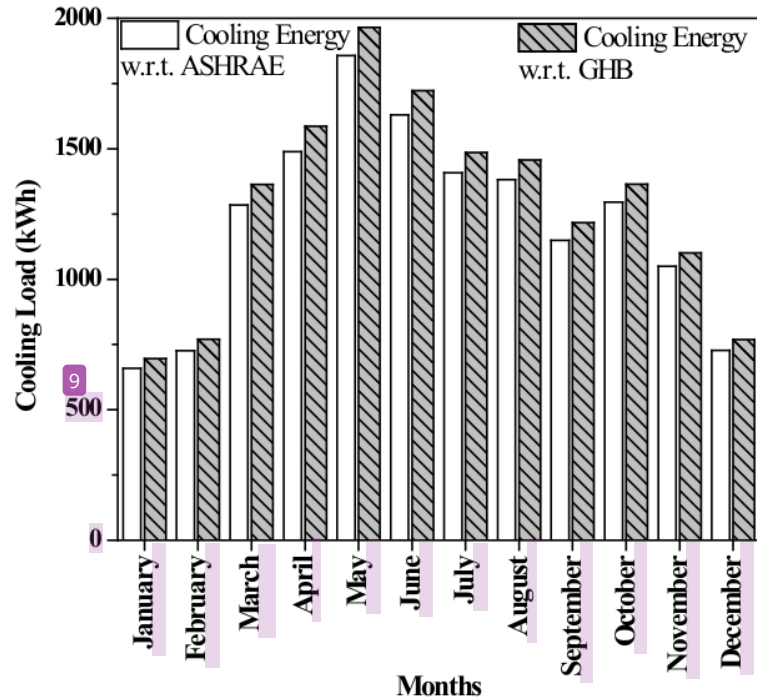


Fig. 4.57 Monthly variation of Cooling Demand for orientation W0 in ECOTECT (West facing).

Table 4.23 - Monthly Cooling Demand in kWh for orientation NE45 by Experimental value and ASHRAE value in ECOTECT

Month	Cooling Energy w.r.t. GHB (kWh)	Cooling Energy w.r.t. ASHRAE (kWh)	Difference (kWh)	Percentage Deviation (%)
January	643.4	601.0	-42.36	(-)6.58
February	751.2	715.4	-35.78	(-)4.76
March	1375.2	1294.2	-81.00	(-)5.89
April	1620.9	1522.4	-98.47	(-)6.08
May	1960.6	1851.8	-108.75	(-)5.55
June	1718.8	1624.5	-94.34	(-)5.49
July	1486.1	1408.3	-77.83	(-)5.24
August	1453.9	1378.5	-75.36	(-)5.18
September	1231.0	1162.3	-68.69	(-)5.58
October	1336.8	1267.8	-69.05	(-)5.16
November	1056.6	1004.3	-52.27	(-)4.95
December	720.1	684.2	-35.89	(-)4.98

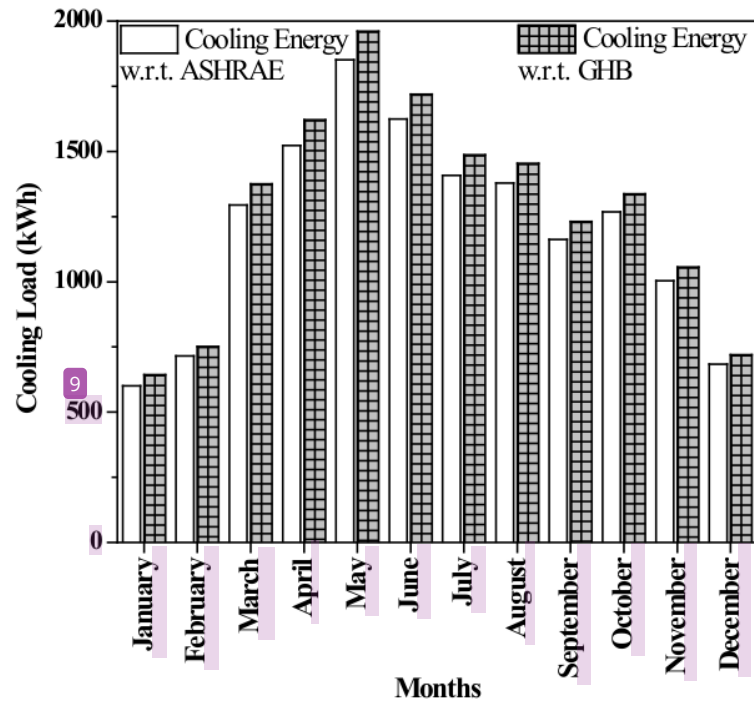


Fig. 4.58 Monthly variation of Cooling Demand for orientation NE45 in ECOTECT.

Table 4.24 - Monthly Cooling Demand in kWh for orientation NW45 by Experimental value and ASHRAE value in ECOTECT.

Month	Cooling Energy w.r.t. GHB (kWh)	Cooling Energy w.r.t. ASHRAE (kWh)	Difference (kWh)	Percentage Deviation (%)
January	644.0	600.4	-43.59	(-6.77)
February	736.1	692.2	-43.99	(-5.98)
March	1365.5	1288.5	-77.04	(-5.64)
April	1599.1	1504.1	-95.07	(-5.94)
May	1979.1	1873.1	-105.95	(-5.35)
June	1732.5	1639.3	-93.21	(-5.38)
July	1493.3	1416.4	-76.89	(-5.15)
August	1461.4	1387.6	-73.77	(-5.05)
September	1220.8	1153.4	-67.33	(-5.52)
October	1337.7	1270.3	-67.45	(-5.04)
November	1057.0	1005.7	-51.24	(-4.85)
December	732.7	690.2	-42.58	(-5.81)

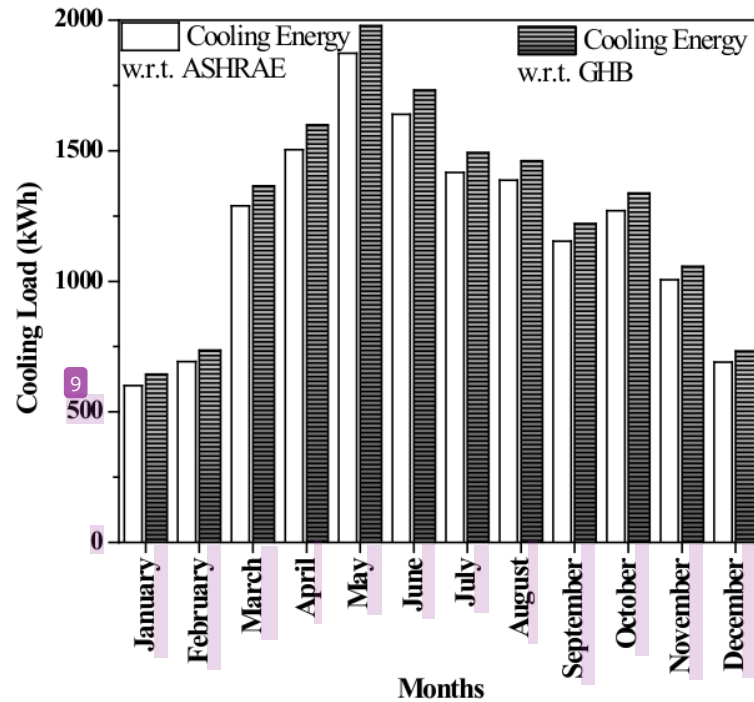


Fig. 4.59 Monthly variation of Cooling Demand for orientation NW45 in ECOTECT.

Table 4.25 - Monthly Cooling Demand in kWh for orientation SE30 by Experimental value and ASHRAE value in ECOTECT.

Month	Cooling Energy w.r.t. GHB (kWh)	Cooling Energy w.r.t. ASHRAE (kWh)	Difference (kWh)	Percentage Deviation (%)
January	634.9	583.5	-51.40	(-)8.10
February	769.6	721.7	-47.90	(-)6.22
March	1392.7	1312.2	-80.50	(-)5.78
April	1616.2	1519.1	-97.10	(-)6.01
May	1955.5	1848.5	-107.00	(-)5.47
June	1710.8	1617.8	-93.00	(-)5.44
July	1480.8	1404	-76.80	(-)5.19
August	1454.4	1379.4	-75.00	(-)5.16
September	1233.1	1164.9	-68.20	(-)5.53
October	1364.6	1294	-70.60	(-)5.17
November	1110.1	1053.6	-56.50	(-)5.09
December	749.3	691.3	-58.00	(-)7.74

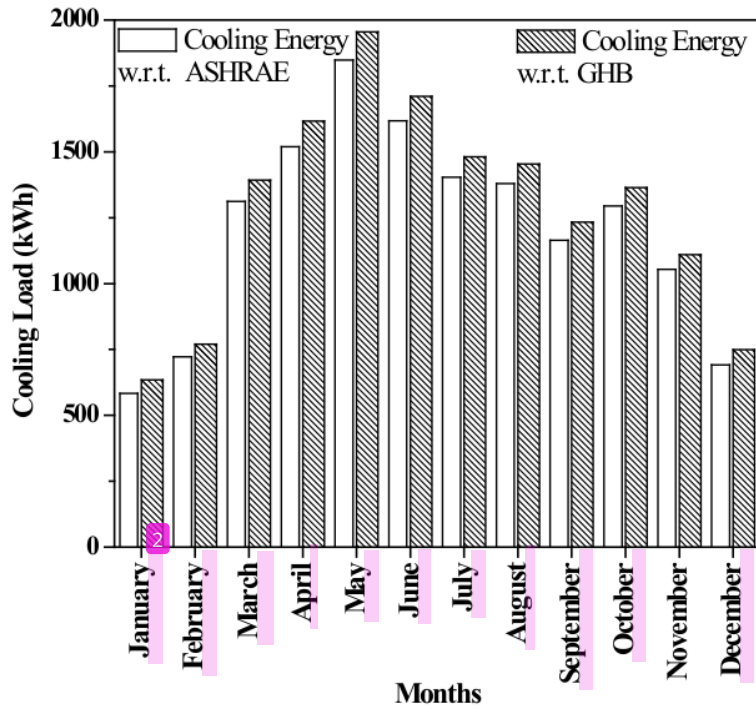


Fig. 4.60 Monthly variation of Cooling Demand for orientation SE30 in ECOTECT

Table 4.26 - Monthly Cooling Demand in kWh for orientation SE45 by Experimental value and ASHRAE value in ECOTECT.

Month	Cooling Energy w.r.t. GHB (kWh)	Cooling Energy w.r.t. ASHRAE (kWh)	Difference (kWh)	Percentage Deviation (%)
January	618.8	561.2	-57.60	(-9.31)
February	758.6	706.3	-52.30	(-6.89)
March	1388.3	1307	-81.30	(-5.86)
April	1621.4	1523.9	-97.50	(-6.01)
May	1960.8	1854	-106.80	(-5.45)
June	1716	1623.4	-92.60	(-5.40)
July	1484.5	1407.7	-76.80	(-5.17)
August	1456.5	1381.8	-74.70	(-5.13)
September	1234.1	1165.6	-68.50	(-5.55)
October	1357.1	1286.8	-70.30	(-5.18)
November	1092.3	1035	-57.30	(-5.25)
December	728.2	674.5	-53.70	(-7.37)

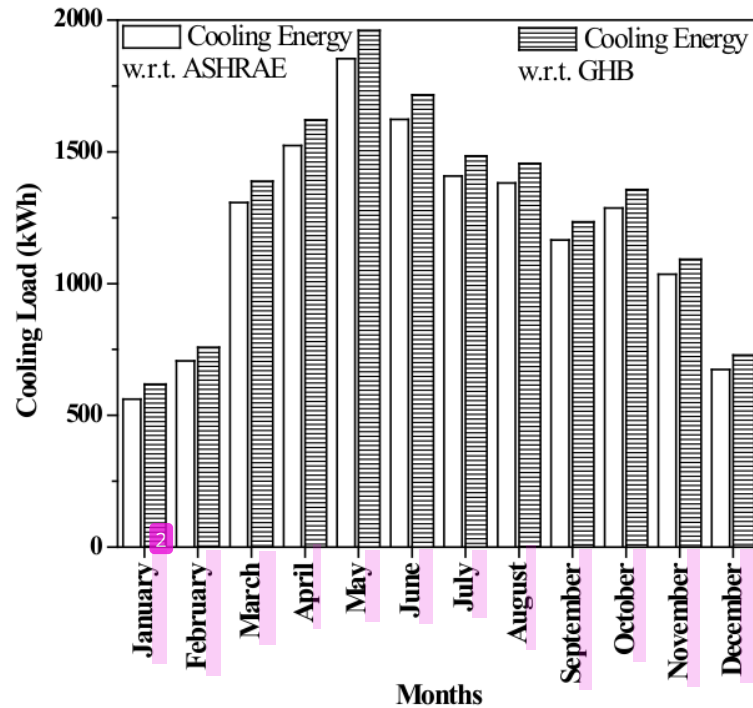


Fig. 4.61 Monthly variation of Cooling Demand for orientation SE45 in ECOTECT

Table 4.27 – Monthly Cooling Demand in kWh for orientation SE60 by Experimental value and ASHRAE value in ECOTECT.

Month	Cooling Energy w.r.t. GHB (kWh)	Cooling Energy w.r.t. ASHRAE (kWh)	Difference (kWh)	Percentage Deviation (%)
January	620.4	566.5	-53.90	(-)8.69
February	742.8	689.9	-52.90	(-)7.12
March	1379.6	1297.3	-82.30	(-)5.97
April	1618.6	1520.4	-98.20	(-)6.07
May	1958	1851.3	-106.70	(-)5.45
June	1715.2	1622.3	-92.90	(-)5.42
July	1484.2	1407.4	-76.80	(-)5.17
August	1453.9	1378.9	-75.00	(-)5.16
September	1231.8	1162.9	-68.90	(-)5.59
October	1352.7	1281.4	-71.30	(-)5.27
November	1084.7	1028	-56.70	(-)5.23
December	725.3	668.4	-56.90	(-)7.85

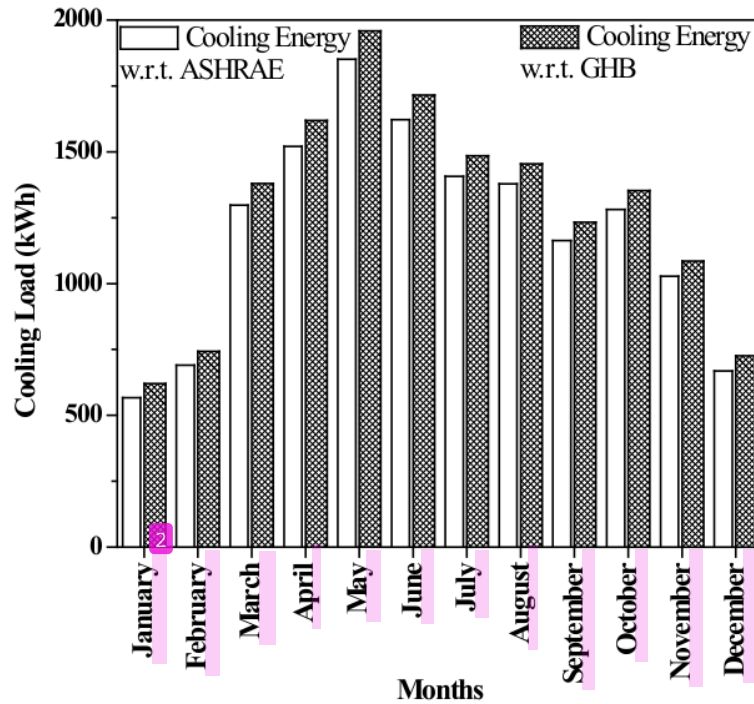


Fig. 4.62 Monthly variation of Cooling Demand for orientation SE60 in ECOTECT

Table 4.28 – Monthly Cooling Demand in kWh for orientation SW30 by Experimental value and ASHRAE value in ECOTECT.

Month	Cooling Energy w.r.t. GHB (kWh)	Cooling Energy w.r.t. ASHRAE (kWh)	Difference (kWh)	Percentage Deviation (%)
January	713.3	670.1	-43.20	(-)6.06
February	760.7	720	-40.70	(-)5.35
March	1366.3	1287	-79.30	(-)5.80
April	1603.8	1507.7	-96.10	(-)5.99
May	1968.3	1860.9	-107.40	(-)5.46
June	1719.6	1626.3	-93.30	(-)5.43
July	1486	1408.9	-77.10	(-)5.19
August	1461.8	1386.8	-75.00	(-)5.13
September	1221.1	1153.4	-67.70	(-)5.54
October	1372.8	1302.9	-69.90	(-)5.09
November	1125.9	1070.4	-55.50	(-)4.93
December	783.9	725.6	-58.30	(-)7.44

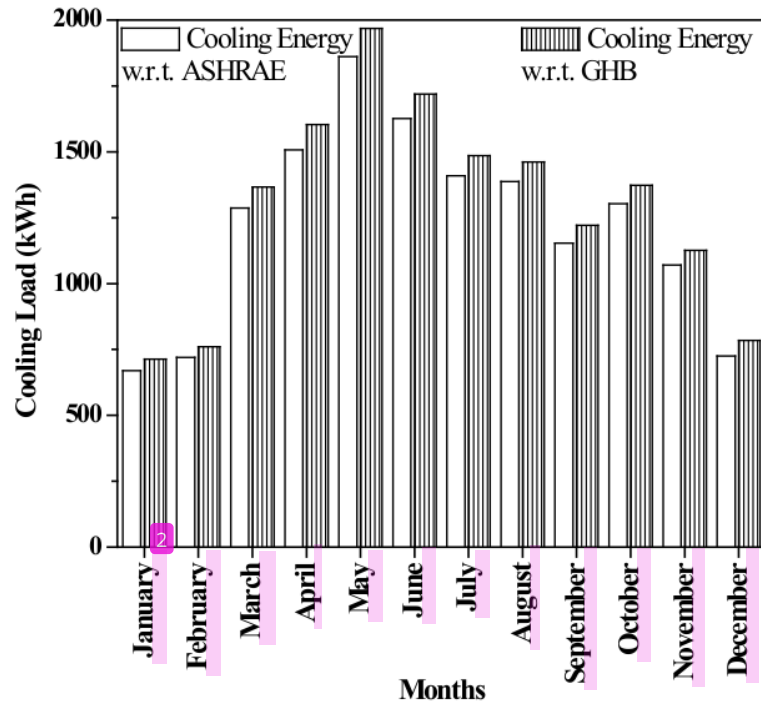


Fig. 4.63 Monthly variation of Cooling Demand for orientation SW30 in ECOTECT

Table 4.29 - Monthly Cooling Demand in kWh for orientation SW45 by Experimental value and ASHRAE value in ECOTECT.

Month	Cooling Energy w.r.t. GHB (kWh)	Cooling Energy w.r.t. ASHRAE (kWh)	Difference (kWh)	Percentage Deviation (%)
January	711.0	674.1	-36.90	(-)5.19
February	765.5	723.3	-42.20	(-)5.51
March	1372.3	1293.8	-78.50	(-)5.72
April	1608.5	1512.8	-95.70	(-)5.95
May	1979.7	1871.9	-107.80	(-)5.45
June	1727.5	1634	-93.50	(-)5.41
July	1490.9	1413.8	-77.10	(-)5.17
August	1467.4	1392.4	-75.00	(-)5.11
September	1223.8	1156.3	-67.50	(-)5.52
October	1370.1	1300.5	-69.60	(-)5.08
November	1116.9	1062	-54.90	(-)4.92
December	780.4	734.1	-46.30	(-)5.93

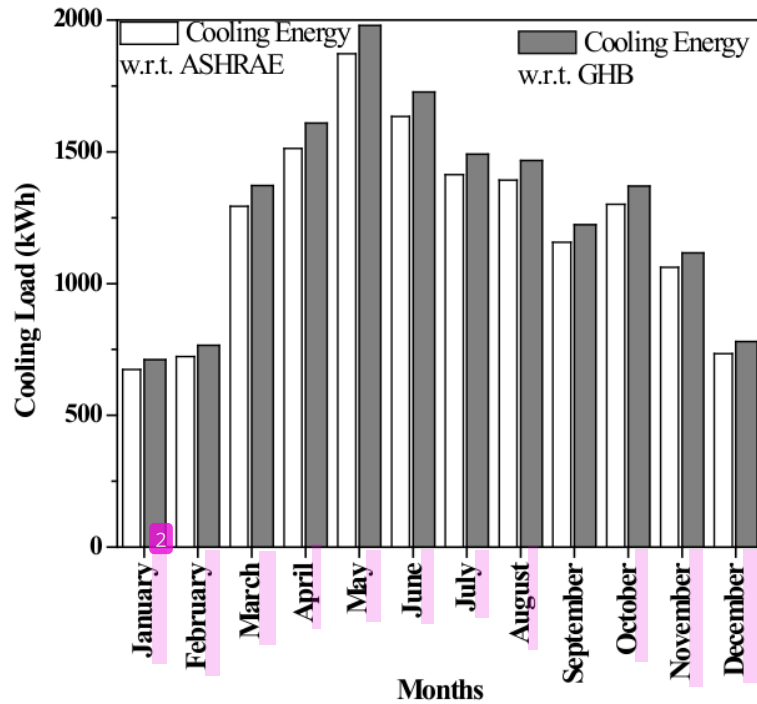


Fig. 4.64 Monthly variation of Cooling Demand for orientation SW45 in ECOTECT.

Table 4.30 - Monthly Cooling Demand in kWh for orientation SW60 by Experimental value and ASHRAE value in ECOTECT.

Month	Cooling Energy w.r.t. GHB (kWh)	Cooling Energy w.r.t. ASHRAE (kWh)	Difference (kWh)	Percentage Deviation (%)
January	708.2	669.7	-38.50	(-5.44)
February	770.5	728.8	-41.70	(-5.41)
March	1376.1	1298	-78.10	(-5.68)
April	1606.5	1510.8	-95.70	(-5.96)
May	1981.8	1873.6	-108.20	(-5.46)
June	1728.7	1634.9	-93.80	(-5.43)
July	1491.2	1413.9	-77.30	(-5.18)
August	1467.6	1392.4	-75.20	(-5.12)
September	1224.6	1157.1	-67.50	(-5.51)
October	1368.7	1299.8	-68.90	(-5.03)
November	1111.9	1058.4	-53.50	(-4.81)
December	779.4	734	-45.40	(-5.82)

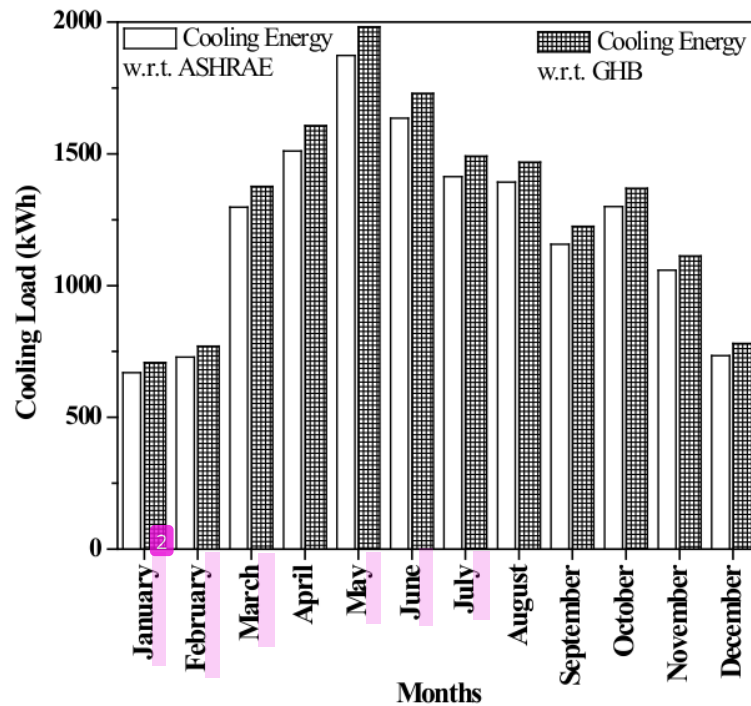


Fig. 4.65 Monthly variation of Cooling Demand for orientation SW60 in ECOTECT

From the tabulated results (Table 4.19 to Table 4.30), it is observed that irrespective of building orientation, the calculated cooling load while using thermos-physical properties of building materials (from ASHRAE Handbook) is always lower than the one where experimentally determined overall heat transfer coefficient values is used. Moreover, the pattern of monthly variation is almost similar for most of the orientations.

U-value of wall as obtained from ECOTECT ($2.720 \text{ W/m}^2\text{K}$) is more than experimentally obtained overall heat transfer coefficient value ($2.549 \text{ W/m}^2\text{K}$) and the U-value of roof is much more in the case of experimental method or guarded hot box testing ($4.332 \text{ W/m}^2\text{K}$) as compared to one obtained from ECOTECT ($3.640 \text{ W/m}^2\text{K}$).

Thus it is evident that difference in U-value of roof is much higher (19%) as compared to difference in U-value of wall (7%). So the cooling load thus calculated (Cooling Energy w.r.t. GHB) is always. As a result, the percent deviation of cooling load difference is always negative irrespective of orientations.

In ECOTECT, CIBSE Admittance method is used for determination of cooling loads. In the software the thermal decrement and thermal lag parameters are not calculated inherently. Instead the software depended on the user to provide the above mentioned parameters or else the software will select them its material database. The time step for simulation in ECOTECT

is one hour. Moreover, the analysis in EOCTECT is sort of steady state analysis the difference in cooling load remains more or less similar for most of the orientations. All these factor might result in a similar trend of deviation in cooling load for all the orientations.

4.4.3 eQUEST Simulation Results

The monthly cooling demands have been tabulated (Table 4.31 to Table 4.42) and presented graphically as well (Fig. 4.66 to Fig. 4.77) for each individual orientation. Here ‘**Cooling Energy w.r.t. ASHRAE**’ refers to the scenario where the simulation was carried out using the thermos-physical properties of the construction materials as per *ASHRAE Handbook Fundamentals, 2017* (Table 4.1). The ‘**Cooling Energy w.r.t. GHB**’ refers to the scenario where the overall heat transfer coefficient values of wall, roof and glazing as obtained from experiment results (Chapter 3) were directly impregnated into eQUEST simulation software. The difference in cooling energy of calculated with respect to the ‘**Cooling Energy w.r.t. GHB**’ scenario has also been calculated and the resultant percentage deviation has also been shown in tables below.

Table 4.31 - Monthly Cooling Demand in kWh for orientation N0 by Experimental value and ASHRAE value in eQUEST (North facing).

Month	Cooling Energy w.r.t. GHB (kWh)	Cooling Energy w.r.t. ASHRAE (kWh)	Difference (kWh)	Percentage Deviation (%)
January	139.3	173.2	33.90	24.34
February	202.4	271.8	69.40	34.29
March	306.1	377.2	71.10	23.23
April	434	487.7	53.70	12.37
May	357.5	399.3	41.80	11.69
June	366.5	409.2	42.70	11.65
July	309.3	344.8	35.50	11.48
August	324.2	363.3	39.10	12.06
September	333.9	371	37.10	11.11
October	271.6	311.9	40.30	14.84
November	223.3	264.8	41.50	18.58
December	178.8	216.4	37.60	21.03

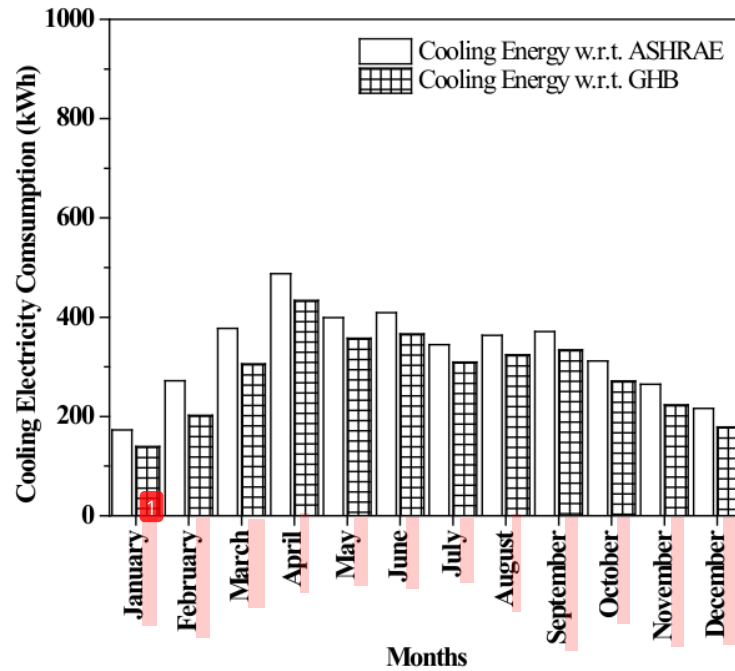


Fig. 4.66 Monthly variation of Cooling Demand for orientation N0 in eQUEST (North facing).

Table 4.32 - Monthly Cooling Demand in kWh for orientation S0 by Experimental value and ASHRAE value in eQUEST (South facing).

Month	Cooling Energy w.r.t. GHB (kWh)	Cooling Energy w.r.t. ASHRAE (kWh)	Difference (kWh)	Percentage Deviation (%)
January	170.2	193.1	22.90	13.45
February	246.9	303.7	56.80	23.01
March	318.4	384.3	65.90	20.70
April	409.6	463.1	53.50	13.06
May	352.3	393.6	41.30	11.72
June	359.3	402.1	42.80	11.91
July	303.5	338.7	35.20	11.60
August	320.5	358.6	38.10	11.89
September	327.9	364.9	37.00	11.28
October	283.2	319.3	36.10	12.75
November	247.2	282.1	34.90	14.12
December	210.4	242.1	31.70	15.07

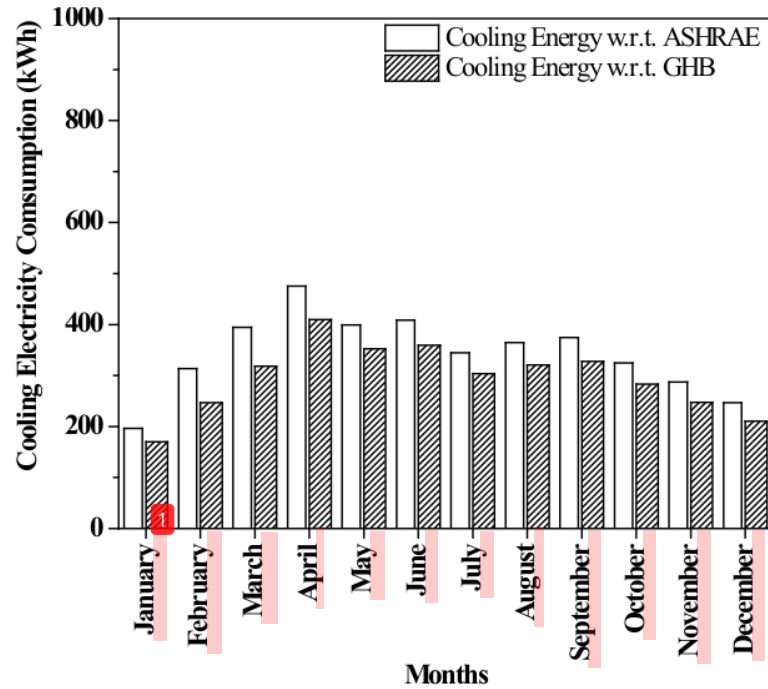


Fig. 4.67 Monthly variation of Cooling Demand for orientation S0 in eQUEST
(South facing).

Table 4.33 - Monthly Cooling Demand in kWh for orientation E0 by Experimental value and ASHRAE value in eQUEST (East facing).

Month	Cooling Energy w.r.t. GHB (kWh)	Cooling Energy w.r.t. ASHRAE (kWh)	Difference (kWh)	Percentage Deviation (%)
January	360	346.4	-13.60	-3.78
February	540	540.6	0.60	0.11
March	680	677.3	-2.70	-0.40
April	860	813.4	-46.60	-5.42
May	610	613.5	3.50	0.57
June	630	638.7	8.70	1.38
July	560	558.5	-1.50	-0.27
August	590	588.6	-1.40	-0.24
September	660	636.4	-23.60	-3.58
October	510	516.3	6.30	1.24
November	460	464.3	4.30	0.93
December	420	425.3	5.30	1.26

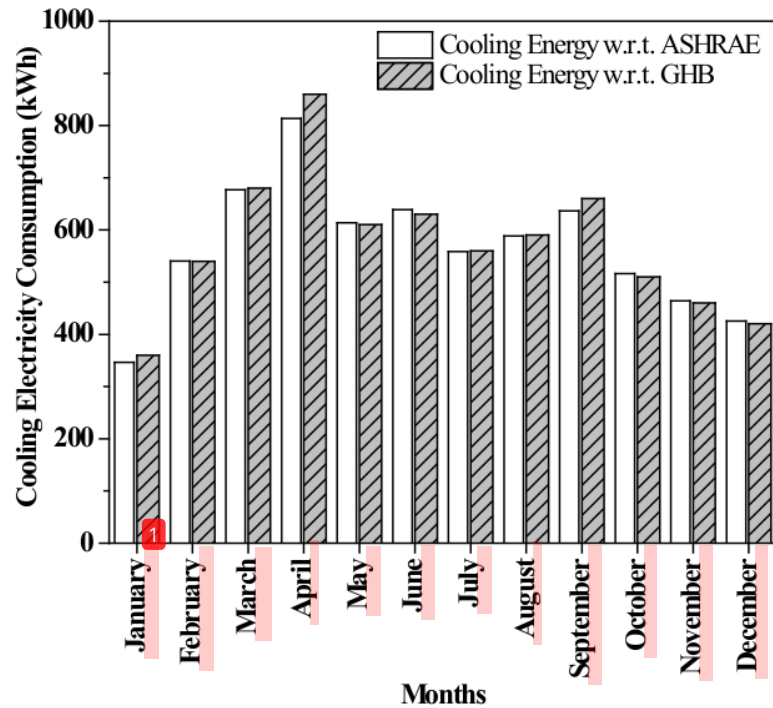


Fig. 4.68 Monthly variation of Cooling Demand for orientation E0 in eQUEST (East facing).

Table 4.34 - Monthly Cooling Demand in kWh for orientation W0 by Experimental value and ASHRAE value in eQUEST (West facing).

Month	Cooling Energy w.r.t. GHB (kWh)	Cooling Energy w.r.t. ASHRAE (kWh)	Difference (kWh)	Percentage Deviation (%)
January	146.9	174.2	27.30	18.58
February	199.1	263.8	64.70	32.50
March	296.8	362.5	65.70	22.14
April	404.3	453.8	49.50	12.24
May	365.3	400	34.70	9.50
June	371.1	406.8	35.70	9.62
July	311.9	340.9	29.00	9.30
August	328.7	360.6	31.90	9.70
September	320	355.5	35.50	11.09
October	277.8	311.1	33.30	11.99
November	230.2	264.5	34.30	14.90
December	185.2	215.8	30.60	16.52

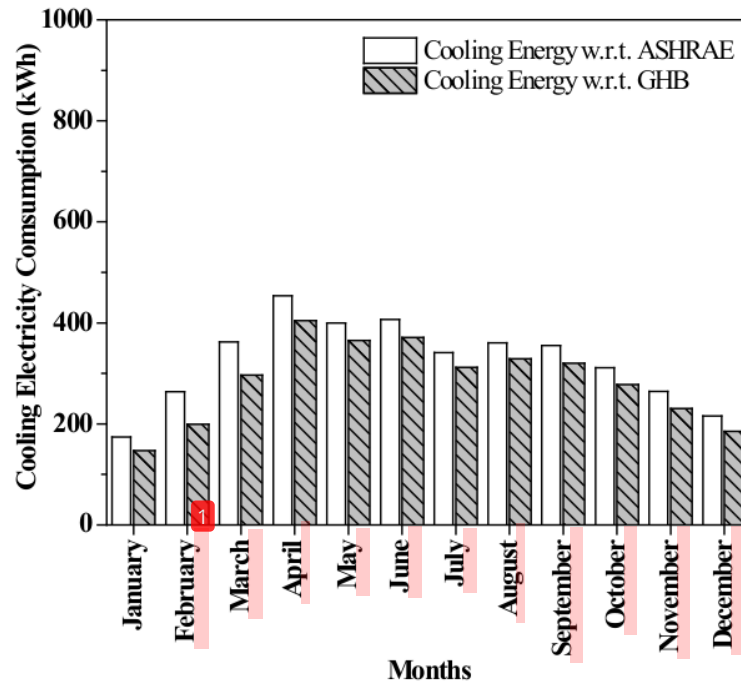


Fig. 4.69 Monthly variation of Cooling Demand for orientation W0 in eQUEST
(West facing).

Table 4.35 - Monthly Cooling Demand in kWh for orientation NE45 by Experimental value and ASHRAE value in eQUEST.

Month	Cooling Energy w.r.t. GHB (kWh)	Cooling Energy w.r.t. ASHRAE (kWh)	Difference (kWh)	Percentage Deviation (%)
January	272.1	272.8	0.70	0.26
February	427.1	455.5	28.40	6.65
March	581.7	606.0	24.30	4.18
April	784.6	748.6	-36.00	-4.59
May	537.3	547.0	9.70	1.81
June	559.0	566.5	7.50	1.34
July	486.6	490.4	3.80	0.78
August	510.2	516.2	6.00	1.18
September	588.1	576.2	-11.90	-2.02
October	432.6	442.7	10.10	2.33
November	376.8	388.8	12.00	3.18
December	333.0	335.7	2.70	0.81

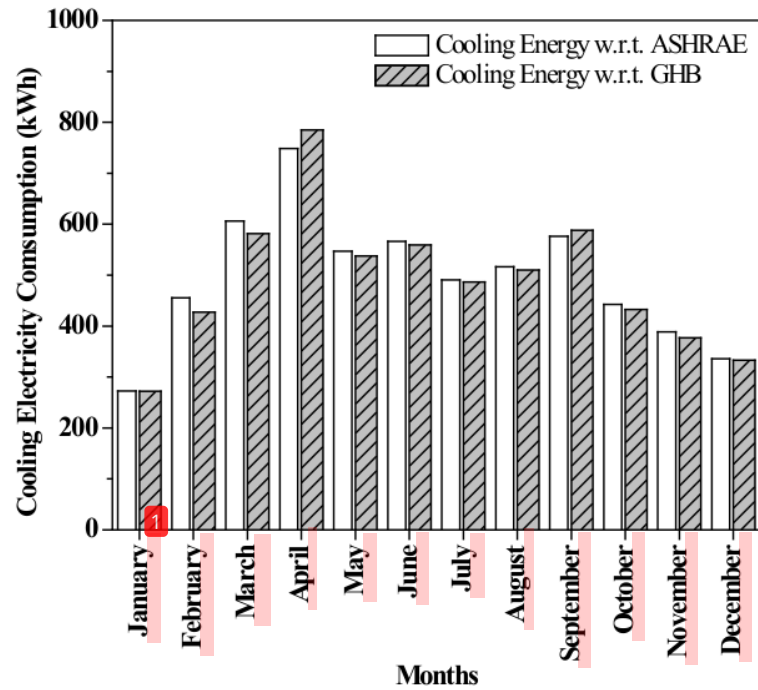


Fig. 4.70 Monthly variation of Cooling Demand for orientation NE45 in eQUEST.

Table 4.36 - Monthly Cooling Demand in kWh for orientation NW45 by Experimental value and ASHRAE value in eQUEST.

Month	Cooling Energy w.r.t. GHB (kWh)	Cooling Energy w.r.t. ASHRAE (kWh)	Difference (kWh)	Percentage Deviation (%)
January	137.4	172.0	34.60	25.18
February	213.5	291.7	78.20	36.63
March	324.7	410.8	86.10	26.52
April	445.3	513.4	68.10	15.29
May	367.6	414.3	46.70	12.70
June	374.0	421.9	47.90	12.81
July	314.5	355.0	40.50	12.88
August	330.7	374.9	44.20	13.37
September	349.5	396.5	47.00	13.45
October	273.2	317.0	43.80	16.03
November	222.0	266.6	44.60	20.09
December	176.7	217.4	40.70	23.03

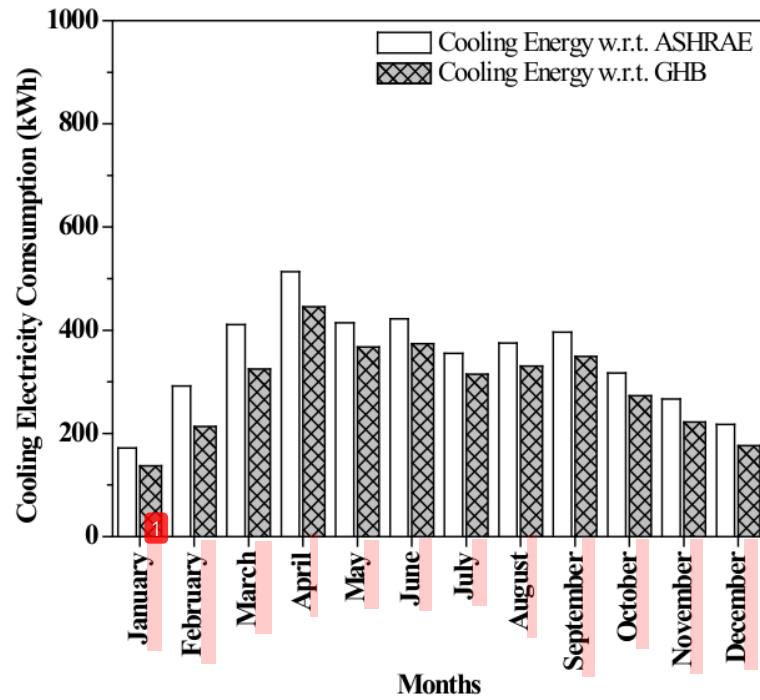


Fig. 4.71 Monthly variation of Cooling Demand for orientation NW45 in eQUEST.

Table 4.37 - Monthly Cooling Demand in kWh for orientation SE30 by Experimental value and ASHRAE value in eQUEST.

Month	Cooling Energy w.r.t. GHB (kWh)	Cooling Energy w.r.t. ASHRAE (kWh)	Difference (kWh)	Percentage Deviation (%)
January	213.4	212.4	1.00	0.47
February	369.7	381.8	-12.10	-3.27
March	455.8	476.5	-20.70	-4.54
April	555.6	558.9	-3.30	-0.59
May	413.3	426.9	-13.60	-3.29
June	422.1	434.1	-12.00	-2.84
July	361.4	368.4	-7.00	-1.94
August	383.9	392.6	-8.70	-2.27
September	440.3	433.7	6.60	1.50
October	337.4	346.5	-9.10	-2.70
November	295.5	303.9	-8.40	-2.84
December	258.8	265.5	-6.70	-2.59

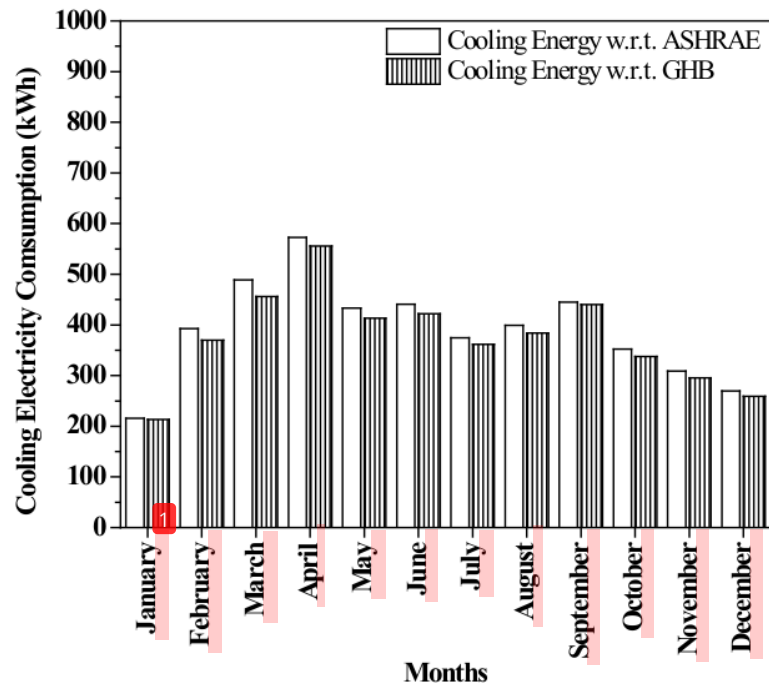


Fig. 4.72 Monthly variation of Cooling Demand for orientation SE30 in eQUEST

Table 4.38 - Monthly Cooling Demand in kWh for orientation SE45 by Experimental value and ASHRAE value in eQUEST.

Month	Cooling Energy w.r.t. GHB (kWh)	Cooling Energy w.r.t. ASHRAE (kWh)	Difference (kWh)	Percentage Deviation (%)
January	254.3	252.20	-2.10	-0.83
February	428.7	434.30	5.60	1.31
March	535.9	550.20	14.30	2.67
April	679	658.10	-20.90	-3.08
May	470.5	482.30	11.80	2.51
June	482.9	493.50	10.60	2.20
July	417.6	423.50	5.90	1.41
August	442.6	449.90	7.30	1.65
September	520.6	506.70	-13.90	-2.67
October	386.3	394.20	7.90	2.05
November	340.3	347.90	7.60	2.23
December	303.7	309.80	6.10	2.01

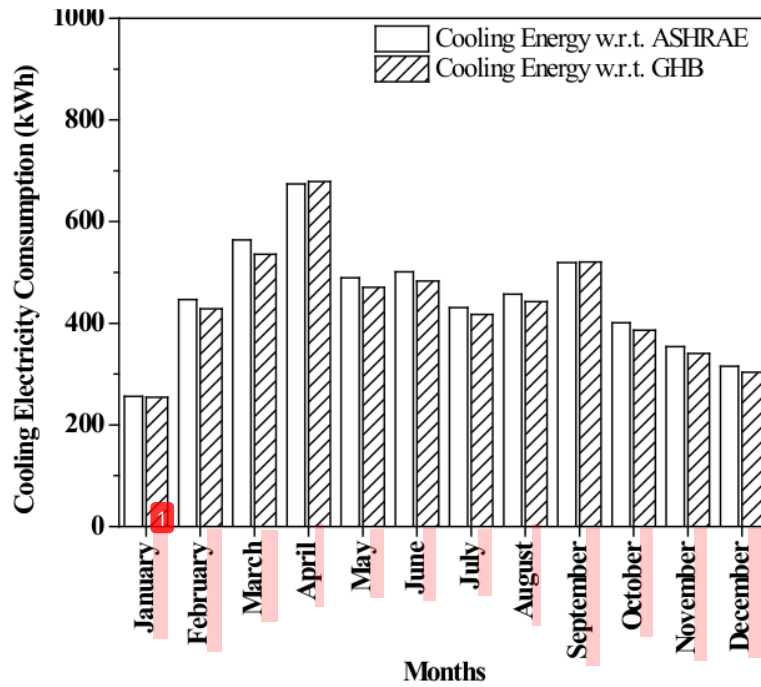


Fig. 4.73 Monthly variation of Cooling Demand for orientation SE45 in eQUEST

Table 4.39 - Monthly Cooling Demand in kWh for orientation SE60 by Experimental value and ASHRAE value in eQUEST.

Month	Cooling Energy w.r.t. GHB (kWh)	Cooling Energy w.r.t. ASHRAE (kWh)	Difference (kWh)	Percentage Deviation (%)
January	306.3	300.90	-5.40	-1.76
February	480.6	477.80	-2.80	-0.58
March	612.3	618.50	6.20	1.01
April	787.9	750.60	-37.30	-4.73
May	538.1	547.40	9.30	1.73
June	556.3	564.60	8.30	1.49
July	485.4	489.50	4.10	0.84
August	512.7	517.90	5.20	1.01
September	598.7	578.80	-19.90	-3.32
October	446.2	452.70	6.50	1.46
November	397	403.80	6.80	1.71
December	360.8	366.40	5.60	1.55

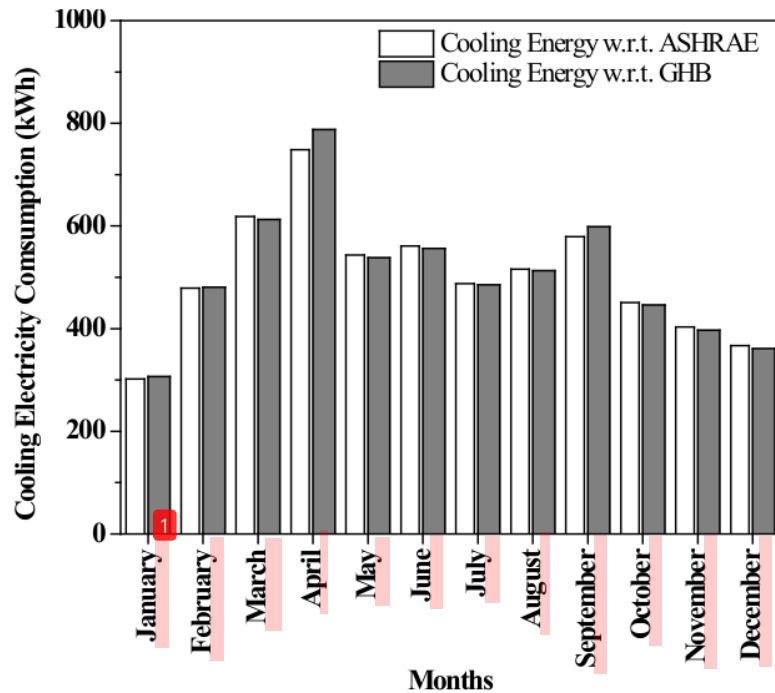


Fig. 4.74 Monthly variation of Cooling Demand for orientation SE60 in eQUEST

Table 4.40 - Monthly Cooling Demand in kWh for orientation SW30 by Experimental value and ASHRAE value in eQUEST.

Month	Cooling Energy w.r.t. GHB (kWh)	Cooling Energy w.r.t. ASHRAE (kWh)	Difference (kWh)	Percentage Deviation (%)
January	161.1	194.20	33.10	20.55
February	203.4	274.30	70.90	34.86
March	317.5	400.20	82.70	26.05
April	447.2	515.40	68.20	15.25
May	364.5	411.70	47.20	12.95
June	369.7	418.50	48.80	13.20
July	312.3	353.30	41.00	13.13
August	330.8	375.00	44.20	13.36
September	346.7	393.40	46.70	13.47
October	284.8	326.40	41.60	14.61
November	243.3	284.10	40.80	16.77
December	202.7	238.20	35.50	17.51

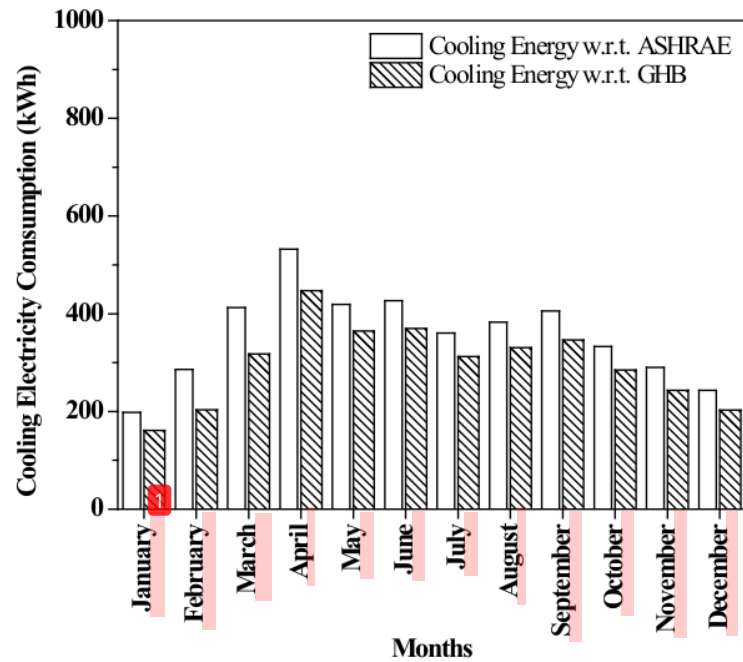


Fig. 4.75 Monthly variation of Cooling Demand for orientation SW30 in eQUEST
 Table 4.41 - Monthly Cooling Demand in kWh for orientation SW45 by Experimental value and ASHRAE value in eQUEST.

Month	Cooling Energy w.r.t. GHB (kWh)	Cooling Energy w.r.t. ASHRAE (kWh)	Difference (kWh)	Percentage Deviation (%)
January	156.6	189.40	32.80	20.95
February	214.7	292.50	77.80	36.24
March	325.5	411.10	85.60	26.30
April	445.9	513.50	67.60	15.16
May	367.1	413.60	46.50	12.67
June	371.3	419.30	48.00	12.93
July	313.3	353.70	40.40	12.89
August	332.2	376.00	43.80	13.18
September	349.9	396.60	46.70	13.35
October	284	325.80	41.80	14.72
November	239.6	280.90	41.30	17.24
December	196.7	233.40	36.70	18.66

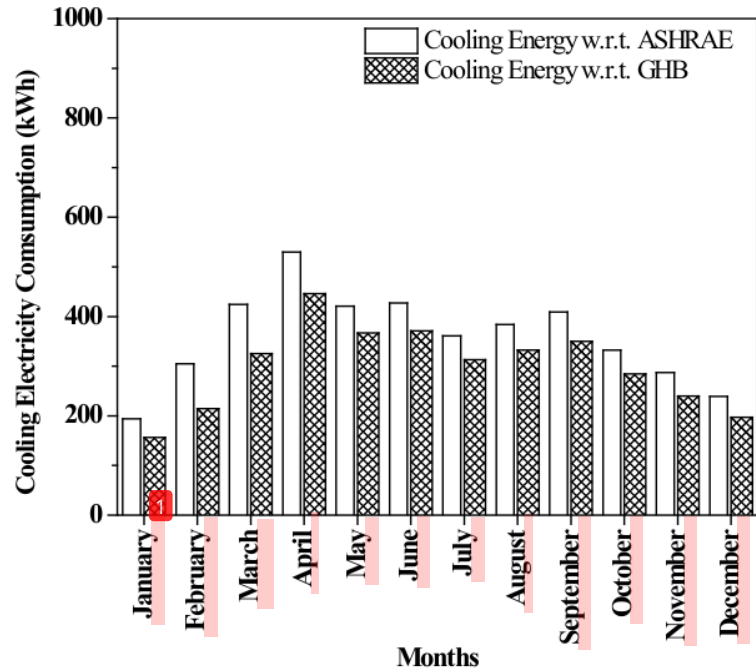


Fig. 4.76 Monthly variation of Cooling Demand for orientation SW45 in eQUEST

Table 4.42 - Monthly Cooling Demand in kWh for orientation SW60 by Experimental value and ASHRAE value in eQUEST.

Month	Cooling Energy w.r.t. GHB (kWh)	Cooling Energy w.r.t. ASHRAE (kWh)	Difference (kWh)	Percentage Deviation (%)
January	150.40	181.60	31.20	17.18
February	218.00	295.30	77.30	26.18
March	319.60	401.30	81.70	20.36
April	421.00	481.90	60.90	12.64
May	363.30	405.90	42.60	10.50
June	366.40	410.50	44.10	10.74
July	308.90	345.20	36.30	10.52
August	327.60	367.30	39.70	10.81
September	338.80	381.40	42.60	11.17
October	278.90	318.00	39.10	12.30
November	233.20	272.30	39.10	14.36
December	189.30	224.50	35.20	15.68

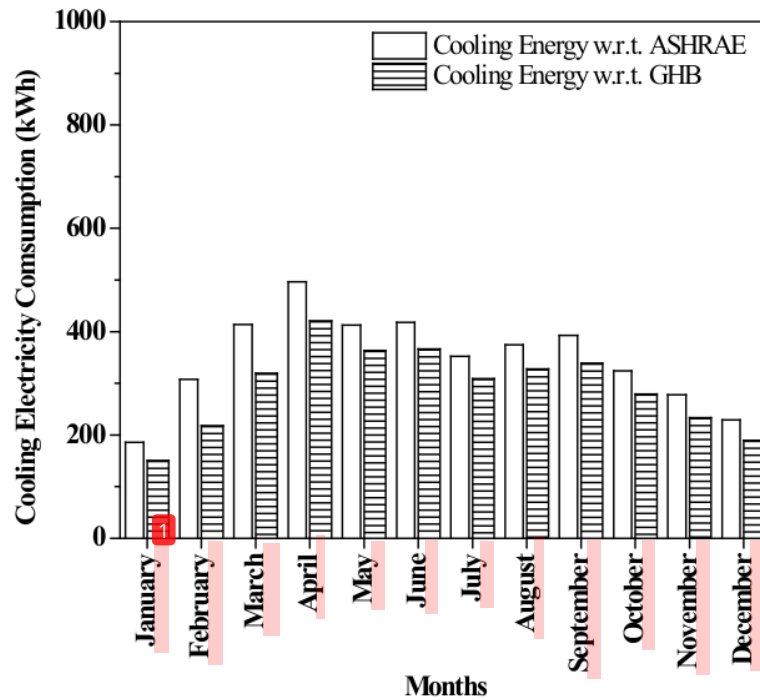


Fig. 4.77 Monthly variation of Cooling Demand for orientation SW60 in eQUEST

From the tabulated results (Table 4.31 to Table 4.42) it is observed that for orientations North, North-West 45°, West, South-West 60°, South-West 45°, South-West 30° and South, the calculated cooling load is higher while using thermos-physical properties of building materials (from ASHRAE Handbook). However, for the orientations North-East 45°, East, South-East 30°, South-East 45° and South-East 60° the difference in cooling load is much lower.

This is due to the fact that wall U-value as obtained from eQUEST ($3.278 \text{ W/m}^2\text{K}$) is higher than the experimentally obtained overall heat transfer coefficient ($2.549 \text{ W/m}^2\text{K}$). Now the U-value of roof is $4.662 \text{ W/m}^2\text{K}$ as calculated in eQUEST compared to the experimentally derived U-value ($4.332 \text{ W/m}^2\text{K}$).

Since both the wall and roof U-values as computed by eQUEST is higher than that obtained from Guarded hot box testing the resultant cooling load obtained by using thermos-physical properties of building materials (from ASHRAE Handbook) is much higher for most of the orientations.

During the night cycle the ambient temperature drops leading to drop in building structural temperature. During the day cycle the structural heat gain by the building system gives rise to the stored heat. This stored heat actually gives rise to the cooling load during the post noon

period. Thus, the cooling load is lower in the early hours of the day compared to the rest of the period.

4.5 Conclusion

The simulation engine in each software calculates the overall heat transfer coefficient using its own algorithm. In eQUEST, the inside air film resistance for calculation of overall heat transfer coefficient is taken from *ASHRAE 90.1*, while that of the external air film resistance is calculated by the LOADS subprogram as a function of surface roughness and wind speed. In DesignBuilder there are six main EnergyPlus convection algorithms and seven main outside convection algorithms. Among them, TARP (Thermal Analysis Research Program) method for inside convective algorithm and DOE-2 convection model is used for outside convective algorithm by default. These pre-selected settings were kept unchanged throughout the analysis. Moreover, in DesignBuilder users are also given an option to input the inside and outside convective transfer coefficients. In such a condition, these fixed values would be used to override the default methods for computation of the surface heat transfer coefficients. In ECOTECT, the internal and film resistances are evaluated according to *CIBSE Guide A*. As a result, the overall heat transfer coefficient values calculated in the simulation software (DesignBuilder, ECOTECT and eQUEST) differs from the values obtained from Guarded Hot Box testing (Table 4.4, 4.5 and 4.6).

The energy consumption of a building system is determined by the following factors: -

- Shape and footprint of the building;
- thermal-physical properties of materials used;
- size and orientation of walls, floors, roofs, windows, and doors;
- shading, lighting schedules, occupancy patterns, equipment operation and ambient conditions.
- operation of primary and secondary HVAC systems.

The CIBSE admittance method based ECOTECT uses mean irradiation values while calculating the cooling load, while the DOE-2.3 based eQUEST and EnergyPlus based DesignBuilder uses peak irradiation values.

The DOE-2 program uses weightage factors for computation of thermal loads and air temperature of room. This is mid-way method between steady state calculation method where the ability of the building mass to store energy is completely ignored or not computed dynamically and complete energy balance calculation methods such as Finite Difference

based solution techniques. Moreover, the calculations are done in hourly basis as compared to DesignBuilder whereby user has the option to quantify the number of time-steps per hour. We can see that each computational algorithm uses its own solution technique to model the heat transfer through the building fabric starting from how the irradiance data is handled to how the heat transfer coefficients are being computed and how heat transfer through the building is being handled. In EnergyPlus based DesignBuilder the different inbuilt module of the simulation process is processed simultaneously and there is feedback among them whereas eQUEST can be said to have a more sequential type analysis approach. All these factors result in variation of the overall heating or cooling loads or energy consumptions.

***CHAPTER 5 – RESULTS &
DISCUSSIONS***

In this chapter all the findings of the overall work done have been summarised. A brief discussion on experimental results is presented below.

5.1 Detailed calibration of Guarded Hot Box Testing Facility

In the present work, the Guarded Hot Box test facility was used for evaluation of overall heat transfer coefficient of masonry samples and warm-edge spacer based air-filled double-glazing samples respectively. Before actual testing of the sample, a detailed calibration of the test set up was done to identify and evaluate the various losses of the system (extraneous heat transfer, \dot{Q}_{Extra} and flanking losses \dot{Q}_{Fl}) and later those were integrated into the calculation procedure to determine the overall heat transfer of the samples with precision.

Detailed air velocity profile of the air space between (a) metering box baffle and surround panel surface and (b) cold box baffle; and surround panel surface were obtained using hot wire anemometer. Air velocity was measured at three different planes in the space between metering box baffle plate and surround panel surface as shown in Fig. 2.15 of Chapter 2. The air velocity was observed to have varied linearly with increase in supply input voltage to the fan (Fig. 2.24 and Fig. 2.25). At any given distance from the baffle, the variation of fan velocity with change in input fan voltage was observed to be smaller in case of metering box as compared to cold box. This was probably due to the fact that vertical distance traversed by air in front of baffle is greater in the cold box as compared to that of metering box.

The extraneous heat transfer was determined by using 300mm thick extruded polystyrene made calibration panel inserted into the surround panel sample aperture and testing conditions were replicated as would be used during actual testing of the samples.

\dot{Q}_{Extra} was observed to have increased with increase in differential air temperature between metering box and cold box in a linear fashion (Fig. 2.27). It was also observed that change in air velocity of metering box and cold box seemed to have little impact on \dot{Q}_{Extra} (Fig. 3.28). This can be due to the fact that with increase in differential air temperature, the total heat flow from metering box to cold box also increased proportionately resulting in an increased extra heat transfer.

For experimental evaluation of flanking losses, extruded polystyrene sheets of thickness 25mm, 50mm and 100mm having dimensions of 500mm by 500mm had been inserted in the sample holding aperture. Firstly, impact of differential air temperature (δt_{air}) on variation of flanking losses (\dot{Q}_{Fl}) was evaluated (Fig. 2.30). It was observed that the flanking losses seemed to vary non-linearly with change in sample thickness. Moreover, from variation of flanking loss with fan velocity, it was observed that the span of the graph is much wider for variation

of flanking loss with cold box air velocity ($u_{CB\text{ Air}}$) as compared to that of metering box air velocity ($u_{MB\text{ Air}}$). It implied that variation of cold side air stream velocity had a more dominant effect on flanking loss heat transfer as compared to metering box air stream velocity. Moreover, with higher differential air temperature, the heat flow from metering box to cold box was also found to be increased resulting in increased flanking losses.

When using 300mm extruded polystyrene insulation, maximum fluctuation of air temperature in metering box was 0.050°C, 0.056 °C and 0.76 °C respectively and that of cold box air temperature was 0.20°C, 0.18°C and 0.23°C respectively for differential air temperature of 40.10°C, 29.99 °C and 20.16 °C between metering box air and cold box air temperature. These results were within the one percent of the air-to-air temperature difference as prescribed in *BS EN ISO 8990:1996* (Table 2.4).

5.2 Preparation of masonry samples for experimental evaluation of overall heat transfer coefficient

Three configurations of masonry wall samples were constructed having dimension of 480mm by 480mm. 125mm thick brick wall made of burnt red clay brick (using stretcher bonds) were constructed in a wooden sample holding frame. Thereafter, 12.5mm thick plaster was applied on both sides of the wall. This was Sample WI (Fig 3.4 of Chapter 3). Sample WII (Fig. 3.6) was constructed upon Sample WI by applying two coats of acrylic cement-based primer on both sides. Sample WIII (Fig. 3.7) was constructed upon Sample WII applying water based magenta coloured plastic paint on the side which would face the metering box.

A traditional reinforced cement concrete (RCC) based roof structure of thickness 100mm and 480mm by 480mm was constructed. After proper curing of the sample, it was placed in sample holding frame. Side that would be facing cold side was plastered and two coats of white coloured cement primer was applied on it while side facing metering box had self-adhesive bituminous layer member placed on it. That was Sample WIV (Fig. 3.17).

5.3 Experimental evaluation of impact of sample holding frame for masonry samples on overall heat transfer coefficient

The impact of wooden sample holding frame on overall heat transfer coefficient was evaluated. This was done by using 300mm thick, 480mm by 480mm extruded polystyrene sheet as sample placed in sample holding frame. The extraneous heat transfer was evaluated and was compared to one where 500mm by 500mm extruded polystyrene insulation sheet was placed in sample holding aperture (i.e., without the sample holding frame). From the results (Table 3.3 of Chapter 3) it was seen that variation in extraneous heat transfer was from 0.76%

to 1.19%. As such it would have very negligible impact on calculation on overall heat transfer coefficient. This was due to fact that area of the wooden frame in the direction of heat flow (from metering box to cold box) was very small. Moreover, the wooden frame locks onto its mid-way position in the surround panel aperture (Fig. 2.7 of Chapter 2) which step like structure. Since the extruded polystyrene insulation has very low thermal conductivity, it acts as an insulation resulting in reduced heat flow through the wooden sample holding frame.

5.4 Determination of spectral properties of opaque coloured surfaces

Three opaque samples were prepared (Fig 3.8 of Chapter 3) having coloured surfaces similar to Sample WI, WII & WIII. Diffuse reflectance spectra (Fig. 3.9) of the surfaces were measured using Perkin Elmer make UV–Vis–NIR spectrophotometer LAMDA 950 over entire solar spectrum using 150mm integrating sphere. From the reflectance characteristic spectra, absorbance spectra was derived. Reflectance and absorbance over visible spectrum (Table 3.2a) and over entire solar spectrum (Table 4.2b) had been calculated as per *ASTM E903-93*. From the results it was evident that, cement plastered sample surface had lowest reflectance and highest absorbance while white coloured sample surface had highest reflectance and lowest absorbance over both visible spectrum and entire solar spectrum respectively.

5.5 Experimental evaluation of impact of varying differential air temperature on overall heat transfer coefficient of masonry samples

The wall samples WI, WII & WIII were placed in the sample holding aperture of surround panel. The air velocity of metering box was kept constant at 0.920 m/s while the cold box air velocity was kept constant at 1.931 m/s throughout the duration of the experiment. Tests were conducted at air temperature differentials of 40°C, 30°C and 20°C. Table 3.4 (of Chapter 3) showed the detailed testing results for Sample WI. Tests were repeated and standard deviation of the results were calculated. Table 3.5 showed that the maximum random air temperature fluctuations were within the limits as per *BS EN ISO 8990:1996*. Fig. 3.10 showed the variation in metering box air temperature, cold box air temperature, surround panel hot side average surface temperature, surround panel cold side average surface temperature, sample surface hot side average surface temperature and sample surface cold side average surface temperature. Similarly, detailed test results for Sample WII and Sample WIII have been shown in Table 3.6, Table 3.7, Table 3.8 and Table 3.9. The maximum random air temperature fluctuations in both metering box air and cold box air were within the permissible limits as per *BS EN ISO 8990:1996*.

The variation in overall heat transfer coefficient with change in differential air temperature has been represented in Fig. 3.14 and Fig. 3.15. From the regression plots, it was observed that variation of overall heat transfer coefficient w.r.t differential air temperature was linear for all the three samples. From these regression equations, the overall heat transfer coefficient for any differential air temperature could be calculated. Moreover, it was also observed that the overall heat transfer coefficient had slightly decreased with increase in differential air temperature for Sample WI & Sample WII while for Sample WIII, the overall heat transfer coefficient had slightly increased with increase in differential air temperature. The reason for such results could be attributed to the fact that the overall moisture content of the sample changed with the change in differential air temperature across the specimen. Lower the differential air temperature, higher was the moisture content of the sample and higher was the overall heat transfer coefficient of the sample. Now Sample WIII had a paint layer on the hot side which has silicon in the paint. As a result, the hygroscopic nature of the sample surface was altered and there was hardly any change in moisture content when exposed to varying differential air temperature. So, the overall heat transfer coefficient increased with increase in differential air temperature due to increase in thermal properties such as thermal conductivity. The roof Sample WIV was also loaded in the sample holding aperture and the effect of differential air temperature on overall heat transfer coefficient was studied. Detailed testing results have been shown in Table 3.11 and Table 3.12. The maximum random air temperature fluctuations in both metering box air and cold box air were within the permissible limits as per *BS EN ISO 8990:1996*. From the regression plot (Fig. 4.20), it was observed that the overall heat transfer coefficient increased slightly with increase in differential air temperature. Here also the bituminous waterproofing membrane acted as a moisture barrier thereby preventing any change in moisture content of the sample. Moreover, the U-value of the roof sample was almost double than that of the wall samples.

The experiments were repeated and the calculated standard deviation values were very low indicating that the results obtained were fairly accurate.

5.6 Experimental evaluation of impact of varying differential air temperature on overall heat transfer coefficient of double-glazing air-filled unit

An air-filled double-glazing unit (Fig. 3.24) incorporating warm-edge spacer (Sample WV) was built in laboratory using 4mm Modiguard clear float glass and 14.5mm spacer. The double-glazing unit was placed in a wooden frame (Fig. 3.25) and properly sealed in place.

Similarly, another air-filled double-glazing unit was constructed with 14.5mm aluminium based spacers for comparison. The testing was conducted at metering air velocity of 0.920 m/s and cold box air velocity of 1.931 m/s. Detailed testing results have been shown in Table 3.13 and Table 3.15. It was observed from the regression plot Fig. 3.27 and Fig. 3.30, that the overall heat transfer coefficient increased with increase in differential air temperature across the specimen. This was probably due to that fact that increased differential air temperature had caused more heat to flow through the sample resulting in an increase in overall heat transfer coefficient.

Moreover a maximum reduction in overall heat transfer coefficient of 7.87% was achieved while using warm edge spacer based air filled double glazing as compared to traditional aluminium based spacer.

5.7 Experimental evaluation of impact of varying air velocity on overall heat transfer coefficient of masonry samples.

The impact of change in air velocity on overall heat transfer coefficient of Sample II (125mm brick wall with 12.5mm cement plaster and white cement primer coat over it on both sides) was studied. Tests with varying metering box air velocity while keeping cold box air velocity constant & vice versa were carried out. The tests were carried out at differential air temperatures of 30°C and 20°C. Details of testing results have been shown in Table 3.10. In all the scenarios (Fig. 3.16), overall heat transfer coefficient of the sample has increased in a linear fashion with increase in air velocity. This was probably due to the fact that with increase in air velocity, the convective heat transfer increased resulting in an increased heat flow through the sample. This resulted in an increased overall heat transfer coefficient of the sample. It was observed that for 30°C differential air temperature, a reduction in U-value by almost 4% occurred when air velocity in metering box was reduced by 33% approximately and by almost 8.2% when air velocity was reduced by 32% in cold box. Moreover, for 20°C differential air temperature, a reduction in U-value by almost 5% occurred when air velocity in metering box was reduced by 33% approximately and by almost 10% when air velocity was reduced by 32% in cold box.

5.8 Comparison between experimentally obtained overall heat transfer coefficient values obtained from Guarded Hot Box and theoretically calculated values.

U-values of walls and roof have also been derived theoretically using the equation below:

$$U = \frac{1}{R_T}, \text{ where,}$$

$$R_T = \text{Total thermal resistance} = R_{se} + R_1 + R_2 + \dots + R_n + R_{si}$$

$$R_1, R_2 \dots R_n = \text{Thermal resistance of individual layers of the sample} = \Delta x_n / k_n$$

$$\Delta x_n = \text{Thickness of } n^{\text{th}} \text{ layer}$$

$$k_n = \text{Thermal conductivity of } n^{\text{th}} \text{ layer}$$

For direction of heat flow being horizontal i.e. for vertical wall systems (*BS EN ISO 6946:2007*):

$$R_{se} = \text{Exterior surface film thermal resistance} = 0.04 \text{ m}^2\text{K/W};$$

$$R_{si} = \text{Interior surface film thermal resistance} = 0.13 \text{ m}^2\text{K/W}$$

For direction of heat flow being upwards i.e. for horizontal roof systems (*BS EN ISO 6946:2007*):

$$R_{se} = \text{Exterior surface film thermal resistance} = 0.04 \text{ m}^2\text{K/W};$$

$$R_{si} = \text{Interior surface film thermal resistance} = 0.10 \text{ m}^2\text{K/W}.$$

Thermal properties of the building materials used have been shown in Table 5.1.

Table 5.1 - Thermal properties of the building materials used:

Building material	Density (kg/m ³)	Thermal Conductivity (W/mK)
Solid Burnt Clay (<i>ECBC, 2017</i>)	1440	0.620
Cement Plaster (<i>ECBC, 2017</i>)	1560	0.630
Reinforced Cement Concrete (<i>BIS, 1987</i>)	2288	1.580

Using the thermal properties of the building materials, U-values were calculated as per *BS EN ISO 6946:2007* (Table 5.2 and Table 5.3).

Table 5.2 – Comparison of U-value of Sample W1

Interior surface film thermal resistance (m^2K/W)	29	0.130
Exterior surface film thermal resistance (m^2K/W)		0.040
Thermal conductivity of brick (W/mK)		0.620
Thickness of brick (m)		0.125
Thermal conductivity of cement plaster (W/mK)		0.630
Thickness of cement plaster (m)		0.012
Total Thermal Resistance (R_T) (m^2/KW)		0.410
Average U-value as obtained from Guarded Hot Box testing (W/m^2K)		2.357
U-value as calculated theoretically (W/m^2K)		2.441
Percentage deviation (%)		3.55

Table 5.3 - Theoretical U-value of RCC roof (Sample WIV)

Interior surface film thermal resistance (m^2K/W)	29	0.100
Exterior surface film thermal resistance (m^2K/W)		0.040
Thermal conductivity of RCC (W/mK)		1.58
Thickness of RCC block (m)		0.100
Thermal conductivity of cement plaster (W/mK)		0.630
Thickness of cement plaster (m)		0.0125
Total Thermal Resistance (R_T) (m^2/KW)		0.223
Average U-value as obtained from Guarded Hot Box testing (W/m^2K)		4.371
U-value as calculated theoretically (W/m^2K)		4.482
Percentage deviation (%)		2.90

The theoretical U-value of both the samples are more than that of experimental values. The reason for these deviations may be due to fact that in practical scenario, thermal conductivity of the bricks, plaster used may be different from that mentioned in the standard. Properties of materials vary widely depending on construction / fabrication and also innate nature of the ingredients itself. Moreover, the surface heat transfer coefficients used in the standard may not be a true representation of that used during testing of guarded hot box.

The experimental values are closer to reality as it covers the entire differential temperature as experienced in various climatic conditions in India.

5.9 Comparison of overall heat transfer coefficient values of building components: Simulation Software derived U-values vs Guarded Hot Box testing based experimental values

For the purpose of simulation, a single zone model plan was prepared in AUTOCAD. Three simulation softwares were used namely DesignBuilder, ECOTECT and eQUEST. An AUTOCAD based plan layout was generated and then it was incorporated into the software, there after a 3-D model of the building was generated. The building HVAC details, operating schedules and internal heat gain details were entered into the model as per Table 2.2. The brick wall considered for study was 125mm brick wall with 12.5mm plaster on either side, glazing considered was a double-glazing unit and roof was considered as 100mm RCC roof with 12.5mm cement plaster on the inside and waterproofing bituminous layer on the outside. The results have been listed in the Table 4.4, 4.5 and 4.6 of Chapter 4. At the time of operating all the three-above softwares, the same thermal properties of the building materials had been entered as input. The deviation of experimentally obtained overall heat transfer coefficient from that obtained from simulation software (while using *ASHRAE Handbook Fundamentals* based materials as input) are highlighted below:

For wall sample, maximum deviation of U-value from experimental results was observed for eQUEST at 28.6% while minimum deviation was at 6.71% for ECOTECT.

For roof sample, maximum deviation of U-value from experimental results was observed for ECOTECT at 19% while minimum deviation was at 2.52% for DesignBuilder.

For warm-edge spacer based double glazing unit, maximum deviation of U-value from experimental results was observed for DesignBuilder at 5.91%, while minimum deviation was at 5% for ECOTECT.

The variation of results may be due to the difference in the way the overall heat transfer coefficient is calculated in each of the software. In eQUEST, the inside air film resistance value is taken from *ASHRAE Handbook Fundamentals 1997*, while the outside air film resistance coefficient is calculated internally depending upon the surface roughness, air temperature and wind speed.

In DesignBuilder, the values of internal and external surface heat transfer coefficients are calculated based upon the selected EnergyPlus convection algorithms. In present scenario Thermal Analysis Research Program has been selected for inside convective algorithm and DOE-2 convection model has been selected for outside connective algorithm.

In ECOTECT, the overall heat transfer coefficient is calculated using *CIBSE Guide A*.

5.10 Comparison of Cooling energy consumptions using DesignBuilder, ECOTECT & eQUEST.

From the results obtained in Chapter 4 (Table 4.7 to Table 4.18, Table 4.19 to Table 4.30 and Table 4.31 to Table 4.42) the following observations have been made.

In case of DesignBuilder, during the summer months the difference in cooling load is very small and sometimes negative while the difference in cooling load in winter seasons is much higher and positive. This could be attributed to the fact that U-value of roof as calculated from DesignBuilder is higher than experimentally obtained value and the U-value of wall is more for guarded hot method or experimental results. Thus, during the winter seasons, we see the ‘Cooling Energy w.r.t GHB’ is much higher but during the summer season the ‘Cooling Energy w.r.t. ASHRAE’ is more or less similar, sometimes slightly negative as well.

Now for ECOTECT, the U-value of roof as obtained from guarded hot box is much higher than results obtained from ECOTECT while the U-value of wall as obtained from ECOTECT is higher. This results in higher cooling load while using experimentally obtained U-value results during simulation (‘Cooling Energy w.r.t. GHB’) for all the orientations.

Lastly for eQUEST the overall heat transfer co-efficient values for both wall and roof as computed by eQUEST is higher resulting in higher cooling load for most of the orientation.

The cooling energy / load deviation range and the annual cooling energy difference with respect to experimental value (i.e. scenario where experimentally obtained overall heat transfer coefficient values were used in simulation software) for the entire year for the three different software are tabulated as below:

Table 5.4 – Cooling energy difference range for entire year.

Orientation	Cooling Energy Deviation range for entire year by DESIGNBUILDER w.r.t. Experimental Value	Cooling Energy Deviation range for entire year by ECOTECT w.r.t. Experimental Value	Cooling Energy Deviation range for entire year by eQUEST w.r.t. Experimental Value
N0	(-)0.07 to (+)4.17	(-)6.12 to (-)4.65	(+)11.11 to (+)34.29
S0	(-)0.07 to (+)2.77	(-)6.11 to (-)4.86	(+)11.28 to (+)23.01
E0	(-)0.33 to (+)2.25	(-)7.05 to (-)4.85	(-)05.42 to (+)01.38
W0	(-)0.30 to (+)4.03	(-)6.12 to (-)4.72	(+)09.30 to (+)32.50
NE45	(-)0.20 to (+)3.42	(-)6.58 to (-)4.76	(-)04.59 to (+)06.65
NW45	(+)0.04 to (+)3.86	(-)6.77 to (-)4.85	(+)12.70 to (+)36.63
SE30	(-)0.11 to (+)2.05	(-)8.10 to (-)5.09	(+)01.50 to (-)04.50

SE45	(-)0.06 to (+)1.69	(-)9.31 to (-)5.13	(+)03.08 to (-)02.67
SE60	(-)0.22 to (+)1.57	(-)8.69 to (-)5.16	(+)04.73 to (-)01.73
SW30	(+)0.03 to (+)3.70	(-)7.44 to (-)4.93	(-)12.95 to (-)34.86
SW45	(+)0.05 to (+)3.94	(-)5.95 to (-)4.92	(-)12.67 to (-)36.24
SW60	(-)0.08 to (+)4.10	(-)5.96 to (-)4.81	(+)26.18 to (+)10.50

Table 5.5 - Annual cooling energy difference w.r.t. experimental value.

Orientation	Annual Cooling Energy Difference in DesignBuilder w.r.t. Experimental Value	Annual Cooling Energy Difference in ECOTECH w.r.t. Experimental Value	Annual Cooling Energy Difference in eQUEST w.r.t. Experimental Value
N0	45.26	-840.38	543.70
S0	26.90	-857.50	496.20
E0	20.64	-873.22	-60.70
W0	37.04	-841.34	472.20
NE45	36.00	-839.78	57.30
NW45	43.92	-838.10	622.40
SE30	23.90	-882.00	-94.00
SE45	19.00	-889.40	40.20
SE60	17.70	-892.50	-13.40
SW30	33.20	-863.50	600.70
SW45	35.80	-845.00	609.00
SW60	37.30	-843.80	569.80

We can see from the results in Table 5.4 that in case of DesignBuilder least difference in Annual cooling energy occurs for South-East 60° orientation (17.70 kWh) and maximum difference occurs for North 0° orientation (45.26 kWh). For South-East 60° orientation, the deviation is within $\pm 0.5\%$ for the months May, June, July, August, October and November. While for the months of January, February, March, April, September and December the absolute deviation varies within $\pm 0.5\%$ to $\pm 2\%$ for the same orientation. For North 0° orientation, the absolute deviation is within $\pm 0.5\%$ for months May, June, July, August while for the months of January, February, March, April, September, October, November and December the absolute deviation varies within $\pm 0.5\%$ to $\pm 5\%$.

For all the orientations, the ‘percentage deviation’ is least for the months of May, June, July and August where it is less than $\pm 0.5\%$. Moreover, for orientations of North, North-East 45° and North-West 45° , the pattern of monthly variation of ‘percentage deviation’ is almost similar.

We can see from the results (Table 5.4) that for ECOTECH the least annual cooling energy difference among the two methods of simulation occur for South-East 60° orientation (-892.50 kWh) and maximum difference occurs for North-West 45° (-838.10 kWh) orientation. For South-East 60° orientation, the absolute deviation is almost within 6% for the months April, May, June, July, August, September, October and November while for the months of January, February, March and December the absolute deviation varies within 7% to 9%. For North 0° orientation, the absolute deviation is within 6% for all months except January (6.77%). Moreover, for the months of May to November the percentage deviation of results is always less than -6% for all the orientations considered.

It is evident from the results that for all the orientations, the annual cooling energy is always lower than ‘Cooling Energy w.r.t. GHB’ scenario. The difference varies from -838 kWh to -893 kWh.

We can see from the results (Table 5.4) that for eQUEST the least difference among the two scenarios occur for South-East 30° orientation (-94.0 kWh) and maximum difference occurs for North-West 45° orientation (622.40 kWh). For South-East 60° orientation, the absolute deviation is within 4%. For North-West 45° orientation, the deviation is within 14% for months May, June, July, August and September.

The monthly deviations for various orientations are within $\pm 5\%$ for South-East 30° , South-East 45° , South-East 60° , East, North-East 45° orientations

Using the cooling energy consumption obtained by directly impregnating the experimentally obtained U-values into the simulation software as reference and comparing it with the scenario where *ASHRAE Handbook Fundamentals* based building materials have been used in the simulation, following observations could be made:

- Cooling energy estimated by using DESIGNBUILDER simulation tool appears to be lesser than that by experimentally obtained impregnated value.
- Cooling energy estimated by using ECOTECH simulation tool appears to be higher than that by experimentally obtained impregnated value.
- Cooling energy estimated by using eQUEST simulation tool appears to be lower to that by experimentally obtained impregnated value.

- Among the three software, the annual cooling energy difference is smallest for EnergyPlus based DesignBuilder (i.e. the cooling energy consumption values for both the cases are very close) followed by eQUEST and maximum for ECOTEECT.
- However, the cooling energy deviation range is maximum for eQUEST, followed by DesignBuilder and minimum for ECOTEECT.
- In case of DesignBuilder, the maximum range of deviation occurs for West orientation from (-)0.30% to (+)4.03% and minimum range of deviation for South East 45° orientation from (-)0.06% to (+)1.69%.
- In case of ECOTEECT, the maximum range of deviation occurs for South East 45° orientation from (-)9.31% to (-)5.13% and minimum range of deviation for South West 60° orientation from (-)5.96% to (-)4.81%.
- Lastly for eQUEST, the maximum range of deviation occurs for North West 45° orientation from (+)12.70% to (+)36.63% and minimum range of deviation for South East 45° orientation from (+)03.08% to (-)02.67 %.

Each software uses its own algorithm or method while calculating the energy performance of cooling and thus the cooling load. Further, it may be mentioned that the CIBSE admittance method used by ECOTEECT uses mean irradiation values of solar radiation while the DOE-2.3 based eQUEST and EnergyPlus based DesignBuilder use peak irradiation values.

DesignBuilder operates simulation, at time steps per hour of 1, 2, 4, 6, 10, 12, 30 or 60 while simulation for eQUEST and ECOTEECT are carried out on hourly interval only.

Heat transfer from soil i.e. ground heat transfer modelling is no considered in ECOTEECT, The DOE-2 program is a sort of quasi steady state analysis while ECOTEECT analysis can be said to more or less a steady state one while Finite Difference based computation analysis in DesignBuilder is of transient nature and each module of the program dynamically interacts with each other at each stage of analysis and there is feedback among them. In eQUEST the approach is more of sequential approach type.

Though the difference in energy consumption seems to be small (as in case of DesignBuilder) but the model used here is a single zone model. Now in real scenario, a building would be composed of number of such zones and complex geometry. As a result, the difference in simulation results would be much higher.

So, it is suggested that overall heat transfer coefficient values obtained from Guarded Hot Box testing as per local climatic conditions could be used as input to simulation software to obtain more accurate modelling results.

***CHAPTER 6 – CONCLUSION & FUTURE
SCOPE OF WORK***

After presenting the research work on detailed simulation study to find the impact of experimentally obtained overall heat transfer values (from guarded hot box testing) in simulation software as compared to conventional method of entering the thermos-physical properties of building component materials as input, the following conclusions can be summarised from the entire work:

Guarded Hot Box test method of experimental determination of overall heat transfer coefficient is the most accurate one. In the present work detailed calibration of the in-house developed Guarded hot box was conducted to quantify the various losses (extraneous heat transfer, flanking losses) associated with the testing setup. The maximum fluctuation of air temperature in metering box and cold box when using 300mm extruded polystyrene insulation were 0.049°C , 0.056°C and 0.076°C for $\delta t_{\text{air}} = 40.10^{\circ}\text{C}$, 29.99°C and 20.16°C respectively. These values are will the prescribed limit of 1% of the air-to-air temperature difference across the specimen as per *BS EN ISO 8990:1996*. It was observed that magnitude of extraneous heat transfer varied increased linearly with increase in differential air temperature whereas change in convective heat transfer coefficients had little impact on the extraneous heat transfer.

Overall heat transfer coefficients of masonry wall and roof samples made from locally available building materials were evaluated experimentally. The U-value of the samples decreased linearly with increase in differential air temperature for five-inch brick wall finished with cement plaster on both sides (Sample WI) and five-inch brick wall with cement plaster and finished with two coats of white cement primer on both sides (Sample WII). The plaster finished surface based wall has a higher absorptivity both in solar range (70.8%) and visible range (68.6%) as compared to white coloured wall (29.2% in solar range and 31.4% in visible range). Hence the U-value of Sample WI was more than that of Sample WII. Overall heat transfer coefficient of Sample WII finished with white colour on one side and silicon based magenta coloured plastic paint (Sample WIII) was also evaluated experimentally. The U-value of the Sample WIII increased linearly with increase in differential air temperature across the specimen.

Overall heat transfer coefficient of reinforced cement concrete with plaster finished with white cement primer on one side and bituminous layer on other side (Sample WIV) was evaluated experimentally. The U-value of the sample increased linearly with increase in

differential air temperature across the specimen (similar to that of Sample WIII). Moreover, the U-value of the roof sample is almost double than that of the wall samples.

The overall heat transfer coefficient of an air filled warm edge spacer based double glazing was evaluated experimentally and the results were compared to that of conventional aluminium spacer based double glazing system. The U-value of the sample increased linearly with increase in differential air temperature across the specimen in both the cases. A maximum reduction of 7.87% (at δt_{air} of 40°C) and a minimum reduction of 7.06% (at δt_{air} of 20°C) in U-value was observed while using warm-edge spacer based double glazing unit.

From the regression plot of variation of overall heat transfer coefficient with respect to air temperature, the overall heat transfer coefficient of the samples can be evaluated experimentally for any particular differential air temperature as suited for any of the five climatic zones of our country.

The impact of impregnating experimentally obtained overall heat transfer coefficient values of common building components (such as wall, roof & glazings) directly into simulation software, and comparing the same with software-based results, based entirely on embedded library of materials, their properties and resultant U-value thereof have been explored. Three simulation software DesignBuilder, ECOTECT and eQUEST have been used. The cooling energy consumption / cooling load in both the scenarios have been evaluated and compared. It was found that for DesignBuilder the annual difference in cooling energy consumption was smallest while it was maximum for ECOTECT.

In case of DesignBuilder, during the summer months the difference in cooling load is very small and sometimes negative while the difference in cooling load in winter seasons is much higher and positive.

Now for ECOTECT higher cooling load while using experimentally obtained U-value results during simulation ('Cooling Energy w.r.t. GHB') for all the orientations.

Lastly for eQUEST the overall heat transfer co-efficient values for both wall and roof as computed by eQUEST is higher resulting in higher cooling load for most of the orientation.

Future scope of work:

- (i) The overall heat transfer coefficient of building walls, roof, glazing used in our country need to be evaluated experimentally with respect to the local boundary conditions to which they belong. The database thus generated, can be used by the Industry and Academia of the country to optimize its building resources and energy

consumption through a close climatic understanding in all the possible areas of application.

- (ii) The impact of relative humidity on the overall heat transfer coefficient of building masonry needs to be evaluated experimentally.
- (iii) The simulation study should also be carried for various types of buildings in real life scenario.

ANNEXURE A

1 CALCULATION PROCEDURE FOR EXTRANEOUS HEAT TRANSFER:

Data set for extra heat transfer

Data Set	Air Temperature Difference between Metering box and cold box (°C)	Extra Heat Transfer (W)
Test 1	44.73	7.55
Test 2	44.72	7.57
Test 3	40.09	6.89
Test 4	39.97	6.26
Test 5	39.95	6.70
Test 6	34.69	5.72
Test 7	34.45	5.40
Test 8	29.99	5.22
Test 9	29.95	5.18
Test 10	19.97	3.00
Test 11	20.18	3.41

Calculation for extra heat transfer for Test 1:

Metering Box Average Air Temperature $(T_{MB\ Air}) = 40.001^{\circ}\text{C}$

Cold Box Average Air Temperature $(T_{CB\ Air}) = -4.731^{\circ}\text{C}$

Differential Air Temperature $(\delta t_{air}) = 44.733^{\circ}\text{C}$
 $(T_{MB\ Air} - T_{CB\ Air})$

Power Input from Heaters in Metering Box $(\dot{Q}_{Heaters}) = 14.463\ \text{W}$

Power Input from Fans in Metering Box $(\dot{Q}_{Fans}) = 7.004\ \text{W}$

Total power input from heaters and fans installed in the metering box $(\dot{Q}_{Heat\ I/P}) = 21.467\ \text{W}$

Total metering box wall loss $(\dot{Q}_{MB\ Avg\ Wall\ Loss}) = 1.098\ \text{W}$

Measured heat flow from metering box to cold box $(\dot{Q}_{MB\ to\ CB,\ measured}) = 20.369\ \text{W}$

Surround panel hot side surface average temperature $(T_{SurPnl\ Temp\ Hot\ Face,\ Avg}) = 39.722^{\circ}\text{C}$

Surround panel cold side surface average temperature $(T_{SurPnl\ Temp\ Cold\ Face,\ Avg}) = -5.110^{\circ}\text{C}$

Differential surface
temperature of surround
panel

$$\Delta T_{SurPnl\ Surface} = 44.832\ ^\circ\text{C}$$

Surround panel surface area

$$A_{SurPnl\ Surface} = 2.360\ \text{m}^2$$

Sample hot side surface
average temperature

$$T_{Samp\ Temp\ Hot\ Face,\ Avg} = 39.594\ ^\circ\text{C}$$

Sample cold side surface
average temperature

$$T_{Samp\ Temp\ Cold\ Face,\ Avg} = -3.517\ ^\circ\text{C}$$

Thickness of Sample

$$\delta x = 300\ \text{mm}$$

Differential surface
temperature of sample

$$\Delta T_{Samp\ Surface} = 43.111\ ^\circ\text{C}$$

Sample surface area

$$A_{Samp\ Surface} = 0.250\ \text{m}^2$$

Calculated heat flow from
metering box to cold box

$$\begin{aligned} \dot{Q}_{MB\ to\ CB,\ calculated} &= k \cdot A \cdot \Delta T / \delta x \\ &= 0.033 * (2.36 * \Delta T_{SurPnl\ Surface} + 0.25 * \Delta T_{Samp\ Surface}) / 0.3 \\ &= 12.824\ \text{W} \end{aligned}$$

Extraneous heat transfer

$$\begin{aligned} \dot{Q}_{extra} &= \dot{Q}_{MB\ to\ CB,\ measured} \\ &\quad - \dot{Q}_{MB\ to\ CB,\ calculated} \\ &= 20.369\ \text{W} - 12.824\ \text{W} \\ &= 7.745\ \text{W} \end{aligned}$$

... P.T.O

2 CALCULATION OF FLANKING LOSS:Data set for flanking loss at δ_{air} equal to 20°C

Sample Thickness (mm)	Flanking Loss at 20°C
25	2.626
50	1.542
100	0.800
300	0.000

$T_{MB Air}$	=	40.009 °C
$T_{CB Air}$	=	19.715 °C
$T_{MB Air} - T_{CB Air}$	=	20.294 °C
$\emptyset_{Heaters}$	=	6.971 W
\emptyset_{Fans}	=	6.937 W
$\emptyset_{Heat IP}$	=	13.909 W
$\emptyset_{MB Avg Wall Loss}$	=	1.052 W
$\emptyset_{MB to CB, measured}$	=	12.857 W
$T_{SurPnl Temp Hot Face, Avg}$	=	39.941 °C
$T_{SurPnl Temp Cold Face, Avg}$	=	19.948 °C
$\Delta T_{SurPnl Surface}$	=	19.944 °C
$A_{SurPnl Surface}$	=	2.360 m ²
$T_{Samp Temp Hot Face, Avg}$	=	38.468 °C
$T_{Samp Temp Cold Face, Avg}$	=	21.337 °C
$\Delta T_{Samp Surface}$	=	17.131 °C
$A_{Samp Surface}$	=	0.250 m ²
δx	=	300 mm
$\emptyset_{Surround Panel}$	=	$k * A_{SurPnl Surface} * \Delta T_{SurPnl Surface} / \delta x$
	=	5.190 W
$T_{Samp Temp Hot Face, Avg}$	=	38.468 °C
$T_{Samp Temp Cold Face, Avg}$	=	21.337 °C
$\Delta T_{Samp Surface}$	=	17.131 °C
$A_{Samp Surface}$	=	0.250 m ²
δx	=	50 mm
$\emptyset_{sample, measured}$	=	$k * A_{Samp Surface} * \Delta T_{Samp Surface} / \delta x$
	=	2.827 W

$$\begin{aligned}\varnothing_{Extra} &= 3.298 \text{ W} \\ \varnothing_{sample, Calc} &= \varnothing_{MB to CB} - \varnothing_{Surround Panel} - \varnothing_{Extra} \\ &= 4.369 \text{ W} \\ \varnothing_{Flanking Loss} &= \varnothing_{sample, measured} - \varnothing_{sample, Calc} \\ &= 1.542 \text{ W}\end{aligned}$$

STUDY ON THE EXPERIMENTAL THERMAL PARAMETERS OF BUILDING ENVELOPE COMPONENTS UNDER THE TROPICAL CLIMATIC CONDITIONS AND COMPARING THE RESULTANT BUILDING COOLING LOAD WITH THOSE OBTAINED FROM GLOBALLY AVAILABLE DIFFERENT SIMULATION TOOLS

ORIGINALITY REPORT

6%

SIMILARITY INDEX

PRIMARY SOURCES

1	quod.lib.umich.edu Internet	254 words — 1%
2	fraser.stlouisfed.org Internet	154 words — < 1%
3	www.centralbank.go.ke Internet	119 words — < 1%
4	www.ipcc.ch Internet	85 words — < 1%
5	www.thehindu.com Internet	85 words — < 1%
6	stacks.stanford.edu Internet	82 words — < 1%
7	fire.nist.gov Internet	77 words — < 1%
8	www.ebd.lth.se Internet	54 words — < 1%

9	www.columbia.k12.mo.us Internet	48 words — < 1%
10	K.Y. Leong, R. Saidur, T.M.I. Mahlia, Y.H. Yau. "Performance investigation of nanofluids as working fluid in a thermosyphon air preheater", International Communications in Heat and Mass Transfer, 2012 Crossref	44 words — < 1%
11	dokumen.tips Internet	43 words — < 1%
12	eprints.nottingham.ac.uk Internet	42 words — < 1%
13	infostore.saiglobal.com Internet	35 words — < 1%
14	core.ac.uk Internet	34 words — < 1%
15	era.ed.ac.uk Internet	34 words — < 1%
16	Kilic, Namik. "Simulation of Construction Materials in a Computer Environment for Uptimum Energy Consumption in Buildings.", Marmara Universitesi (Turkey), 2021 ProQuest	33 words — < 1%
17	eprints.utas.edu.au Internet	33 words — < 1%
18	documents.mx Internet	32 words — < 1%

19	Internet	30 words — < 1%
20	www.meefog.com Internet	30 words — < 1%
21	theconstructor.org Internet	28 words — < 1%
22	Marco Casini. "Building performance simulation tools", Elsevier BV, 2022 Crossref	27 words — < 1%
23	credai.org Internet	26 words — < 1%
24	www.readbag.com Internet	26 words — < 1%
25	Nelson Soares, Cláudio Martins, Margarida Gonçalves, Paulo Santos, Luís Simões da Silva, José J. Costa. "Laboratory and in-situ non-destructive methods to evaluate the thermal transmittance and behaviour of walls, windows, and construction elements with innovative materials: a review", Energy and Buildings, 2018 Crossref	25 words — < 1%
26	www.niti.gov.in Internet	25 words — < 1%
27	scholarspace.manoa.hawaii.edu Internet	24 words — < 1%
28	www.cibse.org Internet	23 words — < 1%

29 Ge, Hua, and Fuad Baba. "Dynamic effect of thermal bridges on the energy performance of a low-rise residential building", *Energy and Buildings*, 2015. 20 words — < 1%

Crossref

30 Lakshman Ravi Teja Pedamallu, Vivek Kumar Singh, Alvaro Peixoto Filipe Gomes. "Quantitative Assessment of Advanced Energy Efficiency Retrofitting for Hospitals in India", Volume 1: Biofuels, Hydrogen, Syngas, and Alternate Fuels; CHP and Hybrid Power and Energy Systems; Concentrating Solar Power; Energy Storage; Environmental, Economic, and Policy Considerations of Advanced Energy Systems; Geothermal, Ocean, and Emerging Energy Technologies; Photovoltaics; Posters; Solar Chemistry; Sustainable Building Energy Systems; Sustainable Infrastructure and Transportation; Thermodynamic Analysis of Energy Systems; Wind Energy Systems and Technologies, 2016 20 words — < 1%

Crossref

31 Min Woo Jeong, Seung Won Jeon, Yongchan Kim. "Optimal thermal design of a horizontal fin heat sink with a modified-opening model mounted on an LED module", *Applied Thermal Engineering*, 2015 20 words — < 1%

Crossref

32 arrow.tudublin.ie 20 words — < 1%

Internet

33 hdl.handle.net 20 words — < 1%

Internet

34 www.gezondheidsaward.nl 20 words — < 1%

Internet

35 Chayan Kumar Basak, Debrudra Mitra, Amrita Ghosh, Gautam Sarkar, Subhasis Neogi. 19 words — < 1%

"Performance Evaluation of a Guarded Hot Box Test Facility Using Fuzzy Logic Controller for Different Building Material Samples", Energy Procedia, 2016

Crossref

36	Kumar, Sumedha. "Interoperability between building information models (BIM) and energy analysis programs", Proquest, 20111108 ProQuest	19 words — < 1%
37	spectrum.library.concordia.ca Internet	19 words — < 1%
38	www.tandfonline.com Internet	19 words — < 1%
39	edepot.wur.nl Internet	18 words — < 1%
40	nagoya.repo.nii.ac.jp Internet	17 words — < 1%
41	discovery.dundee.ac.uk Internet	16 words — < 1%
42	facejpi.net Internet	16 words — < 1%
43	vtechworks.lib.vt.edu Internet	16 words — < 1%
44	acikbilim.yok.gov.tr Internet	15 words — < 1%
45	civiltoday.com Internet	15 words — < 1%

-
- 46 coek.info
Internet 15 words — < 1%
-
- 47 polen.itu.edu.tr
Internet 15 words — < 1%
-
- 48 www.eqmagpro.com
Internet 15 words — < 1%
-
- 49 www.hvac.okstate.edu
Internet 15 words — < 1%
-
- 50 Avijit Ghosh, Arup Ghosh, Subhasis Neogi. "Reuse of fly ash and bottom ash in mortars with improved thermal conductivity performance for buildings", Heliyon, 2018
Crossref 14 words — < 1%
-
- 51 V Ciocan, E F Turcanu, M Verdeş, R S Luciu, M C Bălan, S V Hudişteanu, A Burlacu. "Hygro-thermal monitoring inside Gheorghe Asachi library and their effects on heritage conservation", IOP Conference Series: Materials Science and Engineering, 2019
Crossref 14 words — < 1%
-
- 52 apps1.eere.energy.gov
Internet 14 words — < 1%
-
- 53 ddd.uab.cat
Internet 14 words — < 1%
-
- 54 ethesis.nitrkl.ac.in
Internet 14 words — < 1%
-
- 55 www.nyserda.ny.gov
Internet 14 words — < 1%

56 Byoung-Jun Lee, Stephen Pessiki. "Thermal performance evaluation of precast concrete three-wythe sandwich wall panels", *Energy and Buildings*, 2006
Crossref 13 words — < 1%

57 Ozdemir, M.. "Analysis of color development during roasting of hazelnuts using response surface methodology", *Journal of Food Engineering*, 200007
Crossref 13 words — < 1%

58 Prateek Srivastava, Yasin Khan, Mahabir Bhandari, Jyotirmay Mathur, Ranaveer Pratap. "Calibrated Simulation Analysis for Integration of Evaporative Cooling and Radiant Cooling System for Different Indian Climatic Zones", *Journal of Building Engineering*, 2018
Crossref 13 words — < 1%

59 docshare.tips
Internet 13 words — < 1%

60 ebin.pub
Internet 13 words — < 1%

61 purehost.bath.ac.uk
Internet 13 words — < 1%

62 www.esru.strath.ac.uk
Internet 13 words — < 1%

63 Iole Nardi, Domenica Paoletti, Dario Ambrosini, Tullio de Rubeis, Stefano Sfarra. "U-value assessment by infrared thermography: A comparison of different calculation methods in a Guarded Hot Box", *Energy and Buildings*, 2016
Crossref 12 words — < 1%

64 Somanath Khot, Nitendra Palankar, Archana N. Shagoti, B. M. Mithun. "Chapter 53 Effect of Binder Type on the Properties of Dry Lean Concrete Mixes", Springer Science and Business Media LLC, 2023
Crossref 12 words — < 1%

65 [archive.org](https://www.archive.org)
Internet 12 words — < 1%

66 sreda.portal.gov.bd
Internet 12 words — < 1%

67 www.datumphasechange.com
Internet 12 words — < 1%

68 "International Business, Trade and Institutional Sustainability", Springer Science and Business Media LLC, 2020
Crossref 11 words — < 1%

69 Aldali, Y., T. Muneer, and D. Henderson. "Solar absorber tube analysis: thermal simulation using CFD", International Journal of Low-Carbon Technologies, 2011.
Crossref 11 words — < 1%

70 Debreka Ghosh, Ujjaini Sarkar, Shreyosi De. "Analysis of ambient formaldehyde in the eastern region of India along Indo-Gangetic Plain", Environmental Science and Pollution Research, 2015
Crossref 11 words — < 1%

71 Francesca Stazi. "Experimental Methods to Compare Building Component Alternatives", Elsevier BV, 2019
Crossref 11 words — < 1%

72	Liu Yang, Jingjing Yang, Yan Liu, Yungang An, Jingheng Chen. "Hot box method to investigate U-values for straw bale walls with various structures", Energy and Buildings, 2021 Crossref	11 words — < 1%
73	beeindia.gov.in Internet	11 words — < 1%
74	docplayer.net Internet	11 words — < 1%
75	researchonline.lshtm.ac.uk Internet	11 words — < 1%
76	standards.iteh.ai Internet	11 words — < 1%
77	text-id.123dok.com Internet	11 words — < 1%
78	www.ijeei.org Internet	11 words — < 1%
79	www.orfonline.org Internet	11 words — < 1%
80	www.slideshare.net Internet	11 words — < 1%
81	www.spcmc.ac.in Internet	11 words — < 1%
82	www.ukas.org Internet	11 words — < 1%

83 Aican Daloglu. "Study on overall heat transfer coefficient for a rotating cavity type heat exchanger", International Communications in Heat and Mass Transfer, 1999

10 words — < 1%

Crossref

84 Asbas, Caner. "Design of a C-Band Dual-Polarized Strip-Fed Aperture Coupled Stacked Patch Planar Antenna Array for Point-to-Point Communication", Bilkent Universitesi (Turkey)

10 words — < 1%

ProQuest

85 Chen, Fangzhi, and Stephen K. Wittkopf. "Summer condition thermal transmittance measurement of fenestration systems using calorimetric hot box", Energy and Buildings, 2012.

10 words — < 1%

Crossref

86 Ding Luo, Zerui Liu, Yuying Yan, Ying Li, Ruochen Wang, Lulu Zhang, Xuelin Yang. "Recent advances in modeling and simulation of thermoelectric power generation", Energy Conversion and Management, 2022

10 words — < 1%

Crossref

87 G. Leftheriotis, P. Yianoulis. "Thermal properties of building materials evaluated by a dynamic simulation of a test cell", Solar Energy, 2000

10 words — < 1%

Crossref

88 Haijin Guo, Shanshan Cai, Kun Li, Zhongming Liu, Lizhi Xia, Jiazhuang Xiong. "Simultaneous test and visual identification of heat and moisture transport in several types of thermal insulation", Energy, 2020

10 words — < 1%

Crossref

89 Harold N. Knickle, Vikram Kalthod. "Evaluation of Commercial Thermal Insulation in Vertical

10 words — < 1%

90 Jain, Sachin. "Single Stage Grid Connected Photovoltaic Systems with Maximum Power Point Tracking.", Indian Institute of Technology, Bombay (India), 2021

10 words — < 1%

ProQuest

91 Mavromatidis, Lazaros Elias. "Study of coupled transient radiation-natural convection heat transfer across rectangular cavities in the vicinity of low emissivity thin films for innovative building envelope applications", Energy and Buildings, 2016.

10 words — < 1%

Crossref

92 Muhammad Abdul Mujeebu, Farheen Bano. "Energy-saving potential and cost-effectiveness of active energy-efficiency measures for residential building in Warm-humid climate", Energy for Sustainable Development, 2022

10 words — < 1%

Crossref

93 Test, F.L.. "Parametric study of flat plate solar collectors", Energy Conversion, 1976

10 words — < 1%

Crossref

94 emrlibrary.gov.yk.ca

Internet

10 words — < 1%

95 etd.lib.metu.edu.tr

Internet

10 words — < 1%

96 theses.whiterose.ac.uk

Internet

10 words — < 1%

97 ir.lib.uwo.ca

Internet

10 words — < 1%

98	ogma.newcastle.edu.au Internet	10 words — < 1%
99	scholarbank.nus.edu.sg Internet	10 words — < 1%
100	scholarscompass.vcu.edu Internet	10 words — < 1%
101	southasia.oneworld.net Internet	10 words — < 1%
102	www.irbnet.de Internet	10 words — < 1%
103	www.mace.ac.in Internet	10 words — < 1%

EXCLUDE QUOTES ON

EXCLUDE BIBLIOGRAPHY ON

EXCLUDE SOURCES < 10 WORDS

EXCLUDE MATCHES < 10 WORDS